

VU Research Portal

Towards better understanding of the pathophysiology of aortic aneurysms: the role of smooth muscle cells

Bogunovic, N.

2020

document version

Publisher's PDF, also known as Version of record

[Link to publication in VU Research Portal](#)

citation for published version (APA)

Bogunovic, N. (2020). *Towards better understanding of the pathophysiology of aortic aneurysms: the role of smooth muscle cells*. [PhD-Thesis - Research and graduation internal, Vrije Universiteit Amsterdam].

General rights

Copyright and moral rights for the publications made accessible in the public portal are retained by the authors and/or other copyright owners and it is a condition of accessing publications that users recognise and abide by the legal requirements associated with these rights.

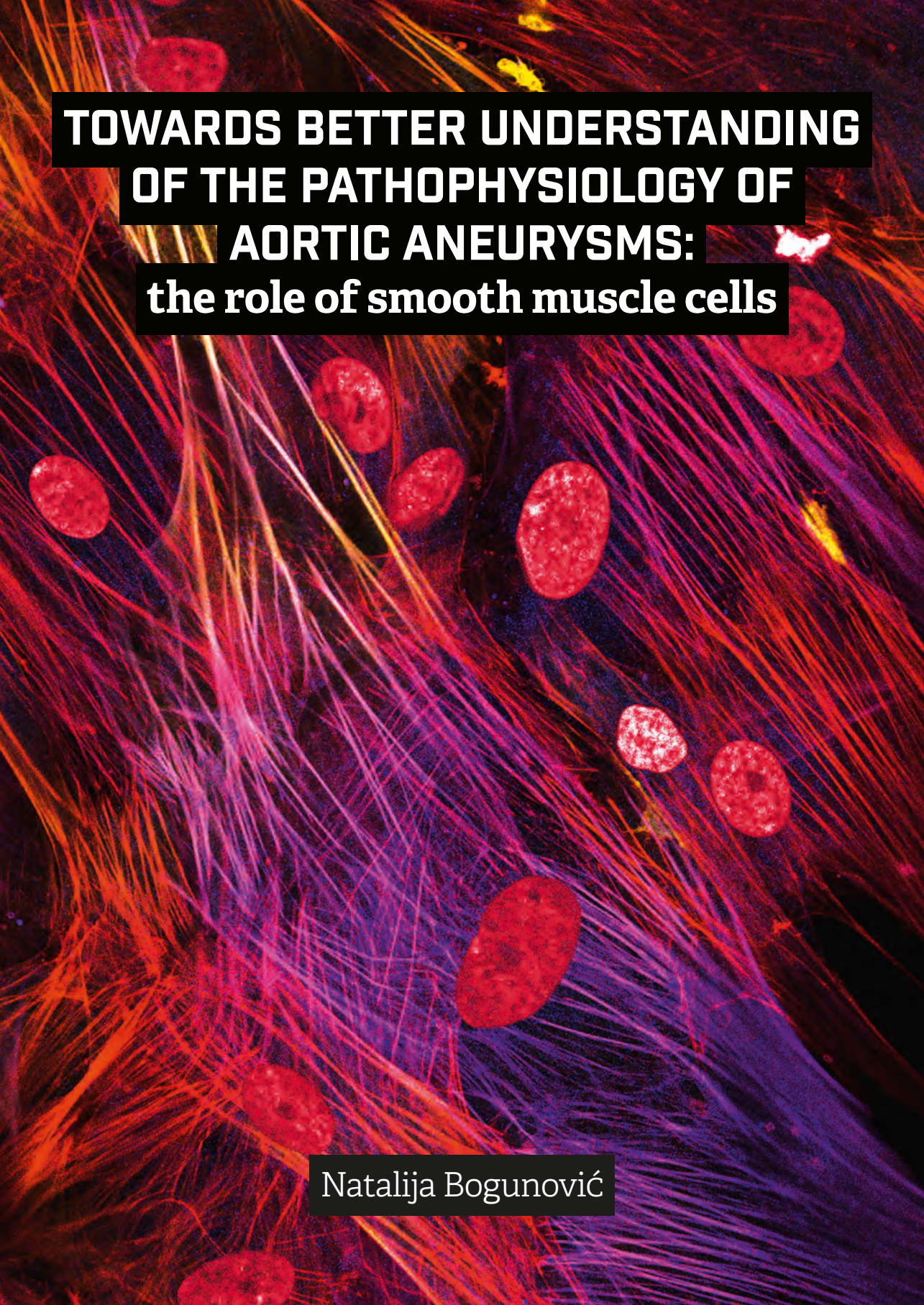
- Users may download and print one copy of any publication from the public portal for the purpose of private study or research.
- You may not further distribute the material or use it for any profit-making activity or commercial gain
- You may freely distribute the URL identifying the publication in the public portal

Take down policy

If you believe that this document breaches copyright please contact us providing details, and we will remove access to the work immediately and investigate your claim.

E-mail address:

vuresearchportal.ub@vu.nl

A fluorescence microscopy image showing smooth muscle cells. The cells are stained with a red dye, likely rhodamine, which highlights the nuclei and the surrounding cytoplasm. The cells are elongated and spindle-shaped, with some showing prominent nuclei. The background is dark, and there are some yellow and orange fibers visible, possibly representing extracellular matrix or other cellular components.

TOWARDS BETTER UNDERSTANDING OF THE PATHOPHYSIOLOGY OF AORTIC ANEURYSMS: the role of smooth muscle cells

Natalija Bogunović

**Towards better understanding of the pathophysiology of
aortic aneurysms: the role of smooth muscle cells.**

Natalija Bogunović

Towards better understanding of the pathophysiology of aortic aneurysms: the role of smooth muscle cells.

ISBN: 978-94-6416-069-7

Financial support by the Dutch Heart Foundation for the publication of this thesis is gratefully acknowledged.

The printing of this thesis was kindly supported by Applied Biophysics. The online app was financially supported by Amsterdam Cardiovascular Sciences.

The research described in this thesis was supported by the ICaR-AIO grant of the Amsterdam Cardiovascular Science Institute [grant number ICAR-VU AIO 2015].

Copyright © Natalija Bogunović 2020. All rights reserved. No part of this thesis may be reproduced, stored or transmitted in any way or by any means without the prior permission of the author, or when applicable, of the publishers of the scientific manuscripts.

Cover image: N. Bogunović

Cover layout, layout and printing: Ridderprint | www.ridderprint.nl.

VRIJE UNIVERSITEIT

**TOWARDS BETTER UNDERSTANDING OF THE PATHOPHYSIOLOGY OF
AORTIC ANEURYSMS: THE ROLE OF SMOOTH MUSCLE CELLS.**

ACADEMISCH PROEFSCHRIFT

ter verkrijging van de graad Doctor of Philosophy aan
de Vrije Universiteit Amsterdam,
op gezag van de rector magnificus
prof.dr. V. Subramaniam,
in het openbaar te verdedigen
ten overstaan van de promotiecommissie
van de Faculteit der Geneeskunde
op woensdag 21 oktober 2020 om 11.45 uur
in de aula van de universiteit,
De Boelelaan 1105

door

Natalija Bogunović

geboren te Beograd, Servië

promotoren:

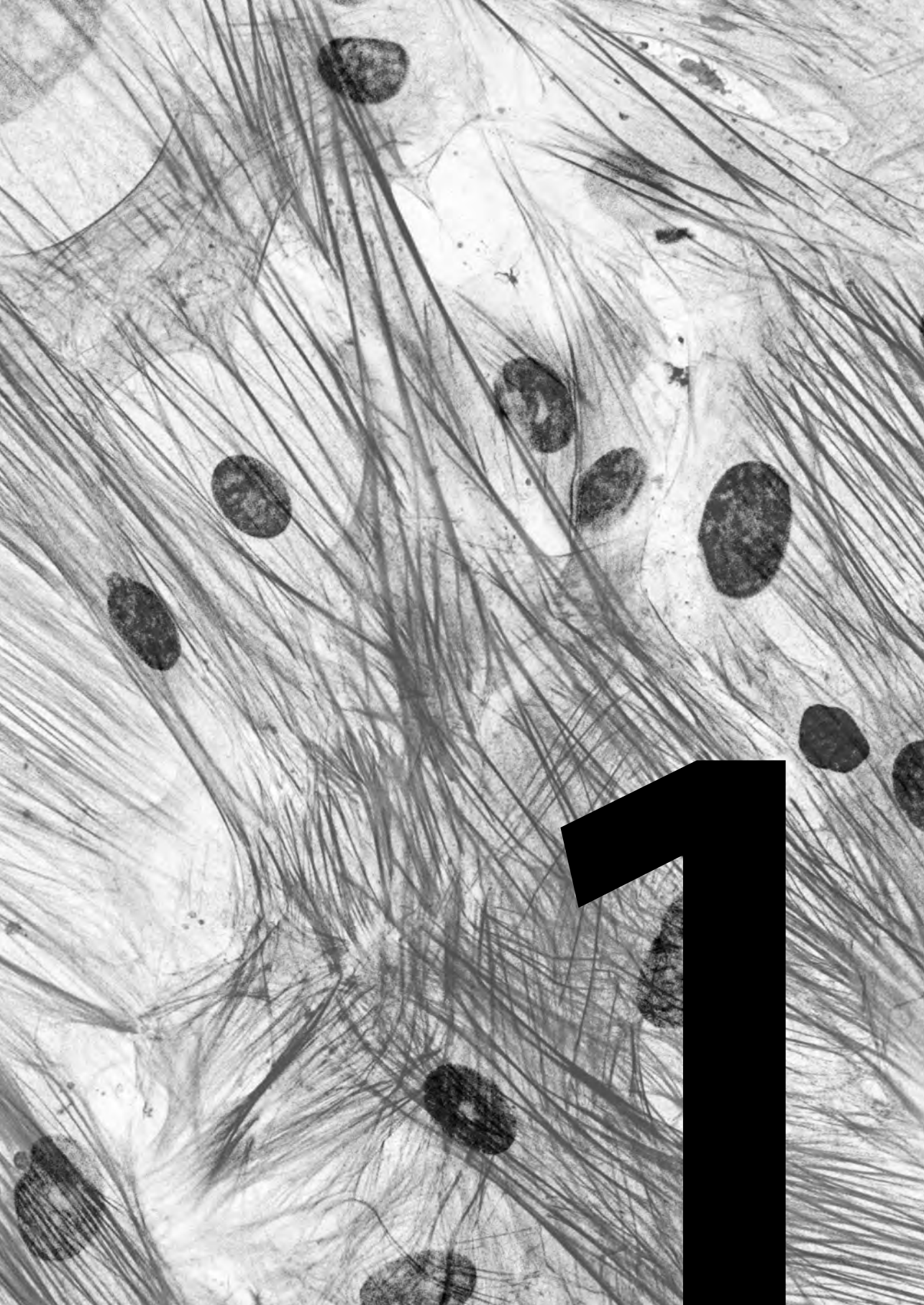
prof.dr. J.D. Blankensteijn
prof.dr. P.L. Hordijk

copromotoren:

dr. K.K. Yeung
dr. D. Micha

TABLE OF CONTENTS

CHAPTER 1	7
Introduction and scope of the thesis	
CHAPTER 2	25
Transdifferentiation of human dermal fibroblasts to smooth muscle-like cells to study the effect of <i>MYH11</i> and <i>ACTA2</i> mutations in aortic aneurysms.	
<i>Human mutation</i> ; 2017; 38(4), 439-450.	
CHAPTER 3	53
Molecular phenotyping and quantitative assessment of effects of pathogenic variants in aneurysm genes <i>ACTA2</i> , <i>MYH11</i> , <i>SMAD3</i> and <i>FBN1</i> .	
Manuscript in Preparation	
CHAPTER 4	89
Betaglycan (TGFBR3) upregulation correlates with increased TGF- β signaling in Marfan patient fibroblasts in vitro.	
Cardiovascular Pathology; 2018; 32, 44-49.	
CHAPTER 5	109
Impaired smooth muscle cell contractility as a novel concept of abdominal aortic aneurysm pathophysiology.	
Scientific reports; 2019; 9(1), 6837.	
CHAPTER 6	145
An in vitro method to keep human aortic tissue sections functionally and structurally intact.	
Scientific reports; 2018; 8(1), 8094.	
CHAPTER 7	173
Bioengineered Patient-Specific 3D Vascular Scaffolds for the Investigation of Smooth Muscle Cell and Extracellular Matrix Dysfunction in Aortic Aneurysms.	
Manuscript Submitted	
CHAPTER 8	203
Summary and Discussion	
APPENDICES	221



Introduction and scope of the thesis

Aortic aneurysms

Aortic aneurysms (AA) are pathological dilations of the aorta. The diameter of a healthy aorta is approximately 2 cm, and a dilation can be considered aneurysmal once it exceeds 3 cm, or 150% of the original diameter¹. Aneurysms occur in both anatomical segments of the aorta; they are thus accordingly named **abdominal aortic aneurysms (AAA)** and **thoracic aortic aneurysms (ThAA)**. Figure 1 depicts a schematic comparison between the infrarenal abdominal region of a healthy aorta (Figure 1a) and an infrarenal AAA (Figure 1b). The natural course of the disease is to grow and rupture.

Ruptured AA are surgical emergencies associated with an overall mortality rate of up to 90%², mainly due to internal bleeding complications. Our knowledge about risk factors leading to and/or indicating rupture are restricted, but the most prominent risk factors are large aneurysm diameter and high growth rates of the aneurysmal sac¹.

AA raises serious concerns in the modern age. AAA affects up to 8% of men above the age of 65¹ and 1.4% of women above the age of 75³. ThAA are less common in the general population, with an incidence of 5-10 individuals per 100.000⁴.

Many risk factors are associated with AA, but a direct causal relationship is still lacking; the most commonly proposed ones include: gender, smoking, old age, cardiovascular comorbidities and genetic causes. Men are reported to have six times higher risks of developing an AAA⁵ than women. That risk further increases 40% every five years above the age of 65⁵. Smoking has a strong clinical association with developing an AA^{6,7}. A study reports that 87% of AAA patients in a cohort of Swedish men were either current or former smokers⁶. Patients suffering from hypertension are reported to have 30-40% more chance of developing an AA. Furthermore, people who were ever treated with antihypertension medication have 80% more risk of developing an AA⁵. It is, however, noted that the prevalence of AA in the Western world is decreasing with increasing emphasis on healthier lifestyle and better medication for cardiovascular comorbidities, emphasizing the role these comorbidities play in AA pathogenesis⁸.

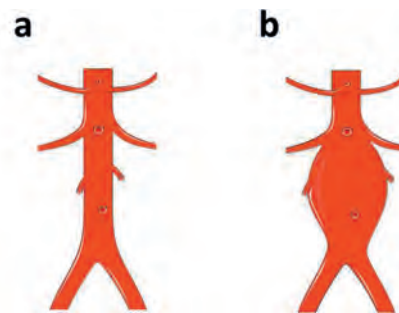


Figure 1. Schematic representation of an abdominal aortic aneurysm before and after repair. a) Healthy aorta. b) Infrarenal abdominal aortic aneurysm. Elements were modified from Servier Medical Art, licensed under a Creative Common Attribution 3.0 Generic License. <https://smart.servier.com/>; <https://creativecommons.org/licenses/by/3.0/>

A subset of patients develops an aneurysm due to genetic mutations, which can manifest as syndromic and non-syndromic. Patients with Marfan, Loeys-Dietz or vascular Ehlers-Danlos type IV syndromes have increased risk of developing an aortic aneurysm or dissection. Marfan syndrome is caused by mutations in the *FBN1* gene encoding for fibrillin-1 and causes a distinguishable phenotype with elongated limbs, altered ratios between body segments and ocular myopia and aortic aneurysms and dissections⁹. Additionally, mutations in genes encoding components of the TGF β signaling pathway (*TGFBR1*, *TGFBR2*, *TGFB2*, *TGFB3*, *SMAD2*, *SMAD3* and *SKI*), genes encoding extracellular matrix (ECM) proteins (*FBN1* and *COL3A1*) and genes encoding components of the smooth muscle cell (SMC) contractile apparatus (*ACTA2*, *MYH11*, *MYLK*, and *PRKG1*)¹⁰ are associated with aneurysm formation.

Molecular pathophysiology of aortic aneurysm formation: what we (do not) know so far

Although certain risk factors are associated with AA formation⁷, the molecular pathways causing aortic dilations remain unknown. It is well documented that AA development is accompanied by degradation and pathological alterations of the aortic connective tissue. The extracellular matrix (ECM), more specifically, the elastic fibers in the medial layer and collagen in the adventitia provide tensile strength and structural integrity to the aortic wall⁷. The loss of elastin fibers occurs as an early step in aneurysm formation, and the fiber fragmentation during aneurysm growth leads to rupture⁷. The loss of collagen due to degradation is the ultimate cause of ruptures, as the imbalance between degradation and synthesis leads to catabolic conditions in the wall¹¹. The degradation of aortic wall components leads to altered force transmissions and increased stiffness of the aneurysmal region¹². It is suggested that the main culprit is the imbalance between MMPs (matrix metalloproteinases), enzymes which specifically degrade components of the ECM and their inhibitors, TIMP (Tissue Inhibitor Of Metalloproteinases)¹³. Earlier studies suggest that MMP-1, -2, -9 -12 seem to be most highly expressed in AAA¹⁴⁻¹⁶. For example, MMP-1, or collagenase-1, has increased activity in human AAA samples. The main producers of MMP-1 in the human aorta are medial SMC and adventitial fibroblasts¹³ and infiltrating immune cells¹⁷. Fibrillin-1 fibers also play a role in AA, proposedly through dysregulation of TGF-beta signaling. The reigning concept is that fibrillin-1 binds the TGF- β in a latent complex, and regulates its activity, which is disbalanced in Marfan syndrome¹³. Progressive ECM reduction in AA is accompanied by decreased ECM protein secretion, most probably induced by SMC apoptosis¹⁸. In this way, SMC dysfunction affects not only SMC but also surrounding tissue, contributing to AA development.

Aortic aneurysm treatment strategies

At present there are no pharmacological treatments available for AA, leaving surgical treatment as the only available option for affected patients (for patients undergoing elective surgery and as treatment for rupture likewise). Traditionally, AA are treated by **open aneurysm repair**. Open repair is an invasive surgical procedure, requiring a large skin incision to suture a prosthetic graft at the aneurysmal site. An alternative minimal invasive repair emerged over time in the form of an **endovascular aneurysm repair (EVAR)**, which is currently the most common therapeutic practice. During EVAR, an endograft is inserted through a small incision in the groin in the femoral artery and deployed at the site of the aneurysm. Randomized clinical trials between both procedures showed that EVAR had a lower 30-day post-operative mortality rate compared to open repair^{19,20}, whereas long-term follow ups report similar outcomes in respect to mortality and higher complication rates in cases of EVAR due to a higher reintervention rate²¹⁻²³.

Attempts have been made to develop or repurpose medication for treatment and prevention of AA, evading aforementioned invasive surgery. Beta-blockers showed promising results in decreasing aneurysm growth and rupture in animal models, but failed to make a difference in growth rate or death rate, decreasing patients 'life quality scores' in the process²⁴. Doxycycline, a non-specific inhibitor of matrix metalloproteinase (MMP), was suggested to prevent MMP mediated extracellular matrix (ECM) degradation in aortic aneurysms, particularly in patients suffering from Marfan syndrome²⁵. Based on promising data in animal models²⁶⁻²⁸, various clinical studies were performed²⁹⁻³¹ but never led to a broadly applicable treatment or innovation in therapeutic guidelines. Statins are a group of lipid-lowering medications which were suggested to prevent AAA expansion³². Findings varied between no effect³³ and decreasing overall cardiovascular mortality³⁴, but the indirect targeting of AA led to no definitive conclusions. A peculiar negative correlation between diabetes mellitus and AAA has been reported,^{35,36} and the notion became that diabetes medication was in fact responsible for the favorable effects. Among those, Metformin (lowers sugar in blood of patients with DM) showed promising results in recent preliminary studies, but is yet to be confirmed in larger cohorts^{37,38}. Losartan, an angiotensin II receptor type 1 (AT1) hindered the excessive TGF- β signaling in an animal model of Marfan syndrome^{39,40}. In combination with doxycycline treatment, they showed encouraging results in patients with Marfan syndrome⁴¹. However, Marfan syndrome affects only a small percentage of AA patients, limiting the prospects for broad use of doxycycline and losartan in AA therapy.

Taken together, the state-of-the-art efforts to develop a pharmaceutical treatment for AA did not yield an effective therapeutic. The underlying reasons might be our inability to grasp the molecular mechanism leading to aortic dilation, and in turn, the causing factors which should be targeted. This emphasizes the

importance of translational research which conveys knowledge from the lab to the clinic. It is possible that no firm conclusions have been made due to the misplaced focus of AA translational research; researchers often focused on systemic issues (such as inflammation) or associated comorbidities (such as hypertension) instead of focusing on more specific cellular and molecular issues, such as SMC dysfunction.

Smooth muscle cells and their role in aortic aneurysm pathogenesis

Smooth muscle cells are the predominant cell type in the aortic wall

The aortic wall consists out of three distinct histological layers, or tunics (Figure 2). Each of the three layers, tunica intima, media and adventitia (inside outwards) plays a distinct role in maintaining the aortic structure and function. The inside layer, tunica intima, consists predominantly out of endothelial cells (EC) forming the endothelial barrier⁴² and lining the vessel lumen. The circumference of this layer is marked by the internal elastic laminae⁴³, leaning onto the aortic media.

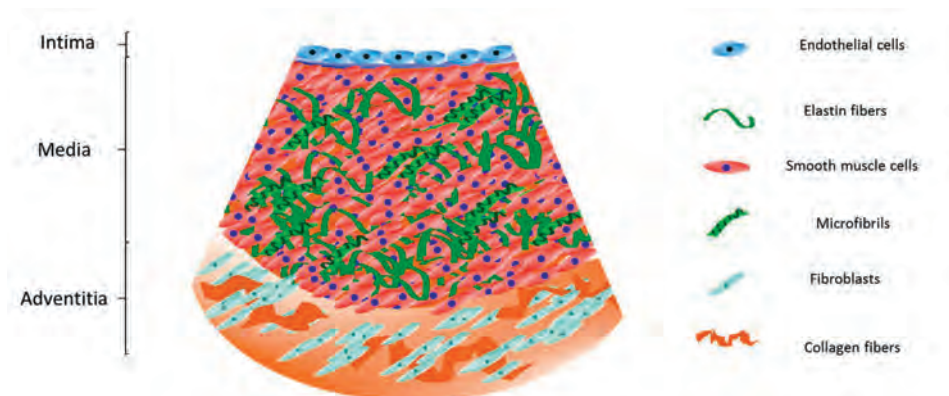


Figure 2. Schematic representation of the aortic wall layers. Top to bottom (inside to outside): Tunica intima, consisting out of a monolayer of endothelial cells (blue). Tunica media, consisting out of smooth muscle cells (red), elastin fibers (green) and microfibrils containing fibrillin-1. Tunica adventitia, consisting out of fibroblasts (cyan) and collagen fibers (brown).

The medial aortic layer, which is concurrently the thickest layer, consists predominantly out of longitudinally oriented vascular SMC, intertwined with multiple layers of elastic laminae. These laminae are composed of elastin filaments, microfibrils and collagen fibers which provide elasticity to the aorta⁴³. Finally, the tunica adventitia, or externa, consists of collagen fibers and fibroblasts, which together provide structural support for the aorta⁴³. As SMC are the predominant cell type in the aorta, their structural and functional integrity plays a paramount role in maintaining the homeostasis of the vessel wall.

Smooth muscle cell contraction and contractile proteins

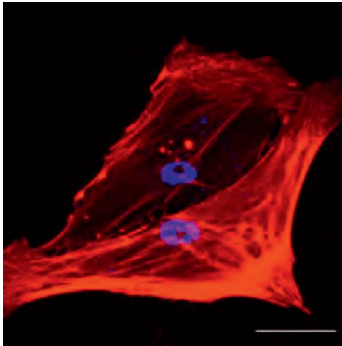


Figure 3. Mature contractile aortic SMC. Immunostained for F-actin (red) and cell nuclei (DAPI, blue). Scale bar 50 μm .

Mature SMC are spindle shaped and abundant in contractile proteins (Figure 3). A unique trait of SMC is that they retain their plasticity, allowing them to drift between a contractile and proliferative phenotype depending on their environment⁴⁴. The primary function of SMC is to regulate blood pressure through their contractile ability (Figure 4a and b)⁴⁴. The circumferential orientation of the SMC around the vessel lumen allows them to contract uniformly and unidirectionally. Therefore, in healthy blood vessels, SMC contraction plays an important role in blood flow regulation, by regulating vasoconstriction and vasodilation⁴⁵.

The SMC contractile cascade starts with an influx of extracellular Ca^{2+} ions through the cell membrane (Figure 4c). Upon the release of Ca^{2+} ions from the sarcoplasmic reticulum, they bind to calmodulin which activates the MLCK. MLCK in turn phosphorylates MLC20, leading to myosin activity and acto-myosin based contraction⁴⁶. As the phosphorylation is reversible, relaxation happens when MLCP dephosphorylates the myosin light chain subunits⁴⁷. Proteins involved in the contractile machinery have their own SMC specific isoforms.

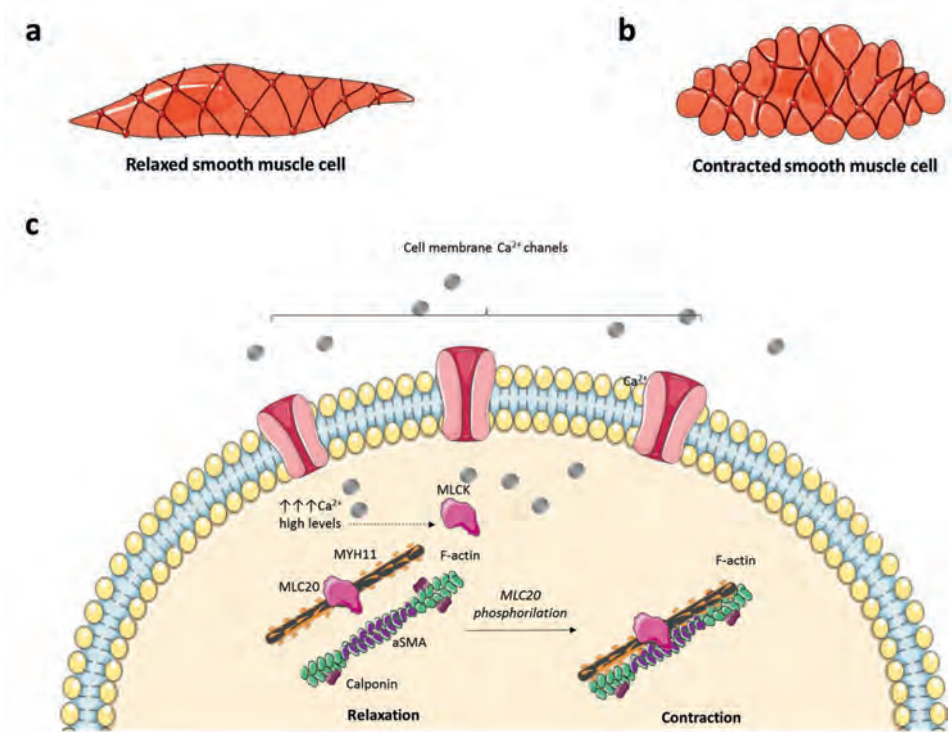


Figure 4. Smooth muscle cell contraction. a) Relaxed spindle shaped SMC. b) Contracted SMC. c) SMC contraction cascade: SMC thick filaments contain SMC specific myosin isophorm MYH11 (grey). SMC specific actin alpha-SMC actin (purple) is part of the actin (green) cytoskeleton. Actin-associated proteins such as Calponin (purple) facilitate the contraction process. Extracellular Ca^{2+} ions (grey) are transported into the cell through Ca^{2+} channels (pink) on the plasma membrane. An increase in Ca^{2+} concentration inside the cell leads to MLCK phosphorylation (pink). MLCK phosphorylates MLC20, which leads to the binding of myosin heads and actin, inducing contraction. Elements were modified from Servier Medical Art, licensed under a Creative Common Attribution 3.0 Generic License. <https://smart.servier.com/>; <https://creativecommons.org/licenses/by/3.0/>

Those include alpha-SMC actin (aSMA), SMC isoform of myosin heavy chain (MYH11), and actin-associated proteins such as SM22, Calponin and Smoothelin (Figure 5)⁴⁸. These proteins can also be used to confidently discriminate SMC from other cell types in the vessel wall⁴⁹, as they contain a unique palette of contractile proteins and signaling molecules. Although SMC contraction in AA seems to be a common feature of AA, both through loss of phenotype and mutations, no studies have been performed to quantify contraction and contractile function in SMC in the context of AA.

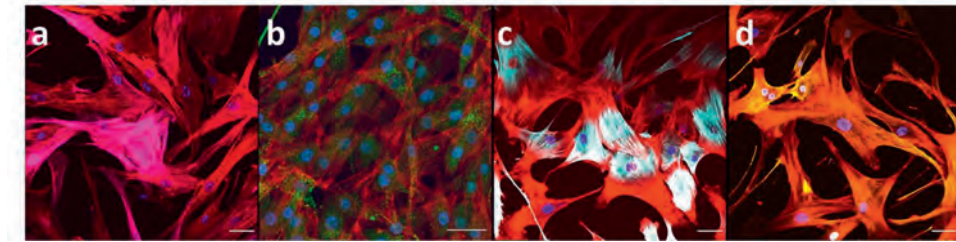


Figure 5. SMC marker proteins. Human primary aortic SMC were immunostained for F-actin (red) and cell nuclei (DAPI, blue). A) alpha smooth muscle actin (aSMA, magenta); b) Myosin heavy chain 11 (MYH11, green); c) Calponin (cyan); d) Smoothelin (gold). Scale bar 50 μ m.

Smooth muscle cells and the extracellular matrix: a functional unit

The aortic media comprises of SMC and elastic fibers of the ECM. They are involved in mechanical resistance, tensile strength and elasticity⁵⁰. Aside from collagen and elastin, fibrillin-1 containing microfibrils play an important role in regulating vasculogenesis and maintaining tissue elasticity by linking SMC to elastin fibrils⁵¹. The link between SMC and ECM is both structural and functional: they form a compact unit which ensures the elastic but also firm structure of the wall and they are responsible for producing the proteins which are linked into ECM fibers (Figure 6)⁵².

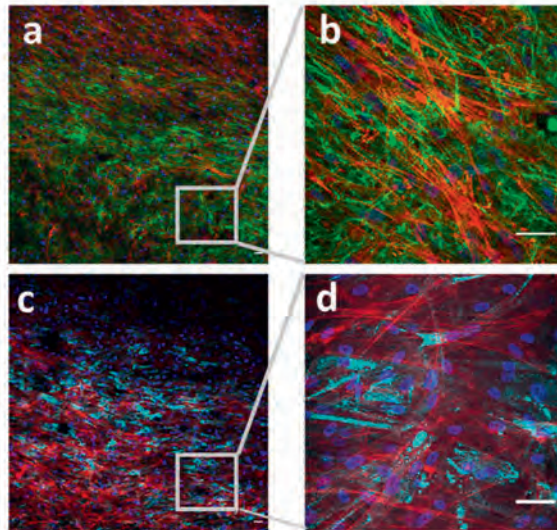


Figure 6. SMC and ECM form a functional unit. Aortic SMC and ECM were immunostained for F-actin (red), cell nuclei (DAPI, blue), fibrillin-1 (green) and collagen type 3 (COL3A1, cyan). Scale bar 50 μ m. a) Stitched image of ECM produced by multiple layers of SMC. b) Close up of fibrillin-1 fibers forming a web surrounding the SMC. c) Stitched image depicting SMC producing ECM. Some of the SMC show positive staining for COL3A1. d) Close up of SMC positive for COL3A1. Scale bar 50 μ m.

The aorta is continuously exposed to cyclic mechanical loads from pulsatile blood pressure⁵³. A multifaceted system comes in place, linking the fibers of the intra and extracellular surroundings. Particularly, SMC interact mechanically with the ECM fibers through transmembrane receptors, integrins. They further interact with signaling molecules and cytoskeletal actin fibers through linker proteins, such as

vinculin and filamin⁵⁴. Vasomotion induced by SMC can contribute to overall mechanoadaptation of the vessel wall, as they govern the mechanical properties by regulating the ECM in the mechanotransduction complex of the media⁵³. Although the general structure is clear, it is difficult to investigate the microarchitecture of the aorta and molecular mechanisms in laboratory conditions, since appropriate models are lacking. SMC play their crucial roles in the aorta through providing structural integrity to the medial layer, regulating vasoconstriction and vasodilation with their contractile abilities, and by synthesizing the ECM which encompasses them. Disturbance of one of more of these processes leads to pathological alterations in the aorta.

Smooth muscle cells in focus: changes associated with aortic aneurysm development

Disrupted homeostasis of SMC is a hallmark and potential cause of AA development (Figure 7). SMC apoptosis has been studied earlier as a major contributor to vessel wall degradation. Studies in human aneurysmal material revealed decreased medial density^{55,56} as demonstrated by a decrease in SMC-marker positive cells and an increase in apoptosis marker expression compared to healthy tissue⁵⁷. These changes are additionally associated with cell cycle arrest⁵². SMC depletion might also play a more circumstantial role in vessel wall weakening: as SMC are capable of producing and repairing the connective tissue of the vessel wall, their decrease makes it more difficult to maintain the surrounding matrix and fight the forthcoming changes⁵².

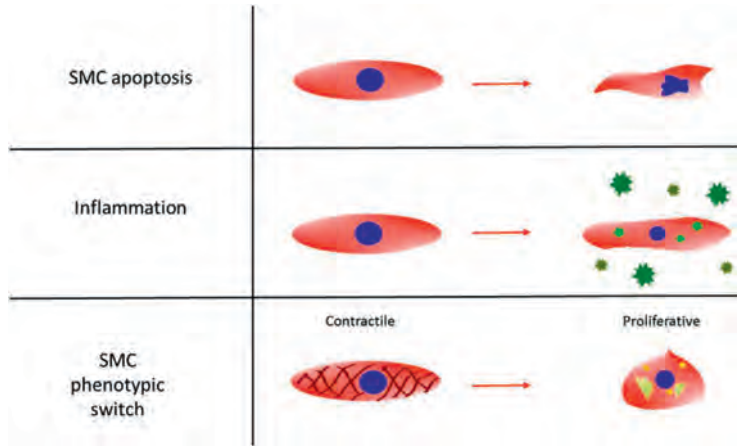


Figure 7. Schematic of current implications of SMC role in AA development. Top to bottom: SMC apoptosis contributing to decreased wall density; Inflammation caused by infiltration of macrophages and lymphocytes into the medial layer (extracellular, dark green) and increased expression of cytokines (intracellular, light green); SMC phenotypic switch from

contractile to proliferative phenotype, accompanied by a loss of SMC-specific contractile protein and change of cell morphology.

Medial SMC apoptosis is closely related to inflammation: inflammatory cells (neutrophils, T cells, B cells, macrophages, etc.) infiltrate all layers of the aortic walls, while secreting proinflammatory cytokines and reactive oxygen species in the process⁵⁸. Studies focused on measuring decreased SMC density and apoptosis markers confirmed a parallel increase in immune cell infiltration. T lymphocytes infiltrate the aortic wall, accompanied by high expression of cytotoxic mediators, which again contribute to the decrease of SMC, which in turn do not produce new and healthy ECM⁵⁷. In addition to lymphocytes, infiltrating macrophages which secrete Prostaglandin E2 can also inhibit SMC proliferation, DNA synthesis and overall viability⁵⁹.

The dynamical balance between contractile and proliferative SMC phenotype is disrupted in AA. It has been reported as an early event in AA pathophysiology that a phenotypic shift takes place from the contractile towards a more proliferative phenotype⁶⁰. Consequently, the compromising of the SMC contractile function can have disruptive consequences on the vessel wall structure⁴⁴. Alongside a phenotypic switch, SMC contractile function can be hindered through AA causing mutations in the SMC contractile apparatus (*ACTA2*, *MYH11*, *MYLK*, and *PRKG1*)¹⁰. These genetic variants tend to decrease actin-myosin interactions through either actin and myosin themselves, or their regulators (*MYLK* and *PRKG1*) and lead to aortic disease¹⁰. Taken together, previous findings indicate the relevance of SMC in maintaining the homeostasis of the aorta and the pathological consequences occurring when their function is disturbed. However, many aspects of supposed SMC dysfunction in AA have never been investigated and we consider that only a small portion of the actual role of SMC in AA is known.

Hypothesis

Aortic aneurysms are a severe cardiovascular disorder with unclear pathophysiology. Smooth muscle cells and disturbances in their function seem to play an important role. **The aim of this thesis is elucidate the role of smooth muscle cell (dys)function in aortic aneurysm pathophysiology and to provide novel in-vitro models and methods to study SMC function.**

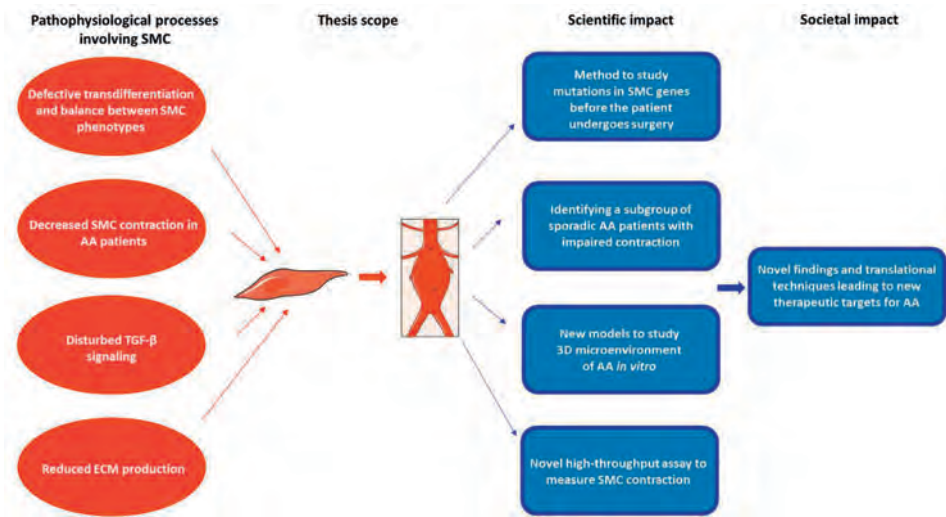


Figure 8. Schematic representation of the thesis scope and potential societal and scientific impact. Smooth muscle cell (SMC); aortic aneurysms (AA); extracellular matrix (ECM). Elements were modified from Servier Medical Art, licensed under a Creative Common Attribution 3.0 Generic License. <https://smart.servier.com/>; <https://creativecommons.org/licenses/by/3.0/>

Defective SMC phenotypic switch and SMC marker expression, decreased SMC contraction in AA patients, disturbed TGF- β signaling cascade and reduced ECM production could all be potential issues affecting SMC function. Once SMC function is threatened, the wall cannot sustain blood pressure and progresses into a pathological dilation. The objective of the thesis is to develop a novel transdifferentiation method, which allows patient-specific analysis before the patient undergoes surgery, to design a novel high-throughput assay to measure SMC contraction and design and use novel models to study the complex microenvironment of the aortic media. All chapters are focused on developing new techniques and uncovering new molecular and cellular perturbations which could one day be targeted therapeutically.

Scope of the thesis

SMC genes and proteins are specifically expressed in SMC, which can only be obtained through aortic surgery. Since AA biopsies are difficult to gain because of invasive surgery, we developed a new method to directly convert mature skin fibroblasts into SMC-like cells without first going through the stage of Induced Pluripotent Stem Cells (iPSC) in **Chapter 2**. We validated our method by confirming the expression of SMC specific markers on RNA and protein level, compared to the skin fibroblasts which do not express them. We performed cDNA sequencing to investigate the effects of the mutations on splicing in the newly expressed SMC

genes. Furthermore, we show that our SMC-like cells can be used to detect splicing errors in patients with mutations in SMC specific genes with potential applications as a prognostic diagnostic tool.

Mutations in genes encoding for proteins in the TGF- β signaling pathway, ECM fibers or SMC contractile apparatus are associated with aneurysm formation. However, the functional implications of these mutations are not known. In **Chapter 3**, we used the method developed in **Chapter 2** to test various functional analyses on transdifferentiated cells of patients with an AA causing mutation. We examined the efficiency of transdifferentiation in patients with mutations in genes encoding for ECM proteins, SMC contractile proteins and TGF- β signaling cascade. We further measured cell contraction and migration, to link the genotype of the mutations with the phenotype which could contribute to AA development.

The aortic media, specifically the SMC and ECM are heavily disturbed in patients with Marfan syndrome, as a result of disturbed TGF- β signaling. In **Chapter 4**, we analyzed TGFBR3 (Betaglycan) expression in context of Marfan syndrome and *FBN1* mutations. We showed changes in betaglycan protein expression and mRNA expression of genes involved in TGF- β signaling in cells of Marfan patients compared to controls. We detected increased TGF- β signaling in patients with a dominant negative mutation compared to those with a haploinsufficient, indicating that beta glycan might play a role in TGF- β signaling in Marfan patients.

To study specific SMC contractile function, and its impairment in the context of AA, we developed a new method to measure SMC contraction *in vitro* using the electric cell-substrate impedance sensor (ECIS) in **Chapter 5**. We measured differences in contraction between SMC derived from healthy individuals and AAA patients. We compared the contraction of SMC derived from both ruptured and non-ruptured patients to healthy controls. We correlated impaired SMC contraction with complications leading to secondary aneurysm surgery and current smoking.

SMC and their environment form a complex dynamical system which is disturbed in AA. To study SMC in their original environment, alongside degrading ECM and infiltrated immune cells, we developed a new method to keep aneurysmal tissues alive in-vitro over 92 days in **Chapter 6**. Using a vibrating microtome, we sectioned the aortic biopsies derived from aneurysm patients and created sections which contain all three layers of the aorta. We further detected the presence of multiple cell types in the sections, validating that it truly contains different segments of the aorta. We stimulated the tissue sections to show future applications of our new model for molecular and cellular translational experiments.

To investigate SMC function and ECM producing capacity in a controlled environment, we developed a patient-specific 3D model to study SMC and ECM interaction *in vitro* in **Chapter 7**. We used a 3D printed biodegradable scaffold to

make a patient-specific segment of the aortic wall, consisting out of SMC and the ECM they produced. We characterized its mechanical properties and confirmed that they correspond to the properties of the aortic wall. We detected differences in SMC alignment and ECM production between scaffolds seeded with SMC derived from healthy controls and AA patients.

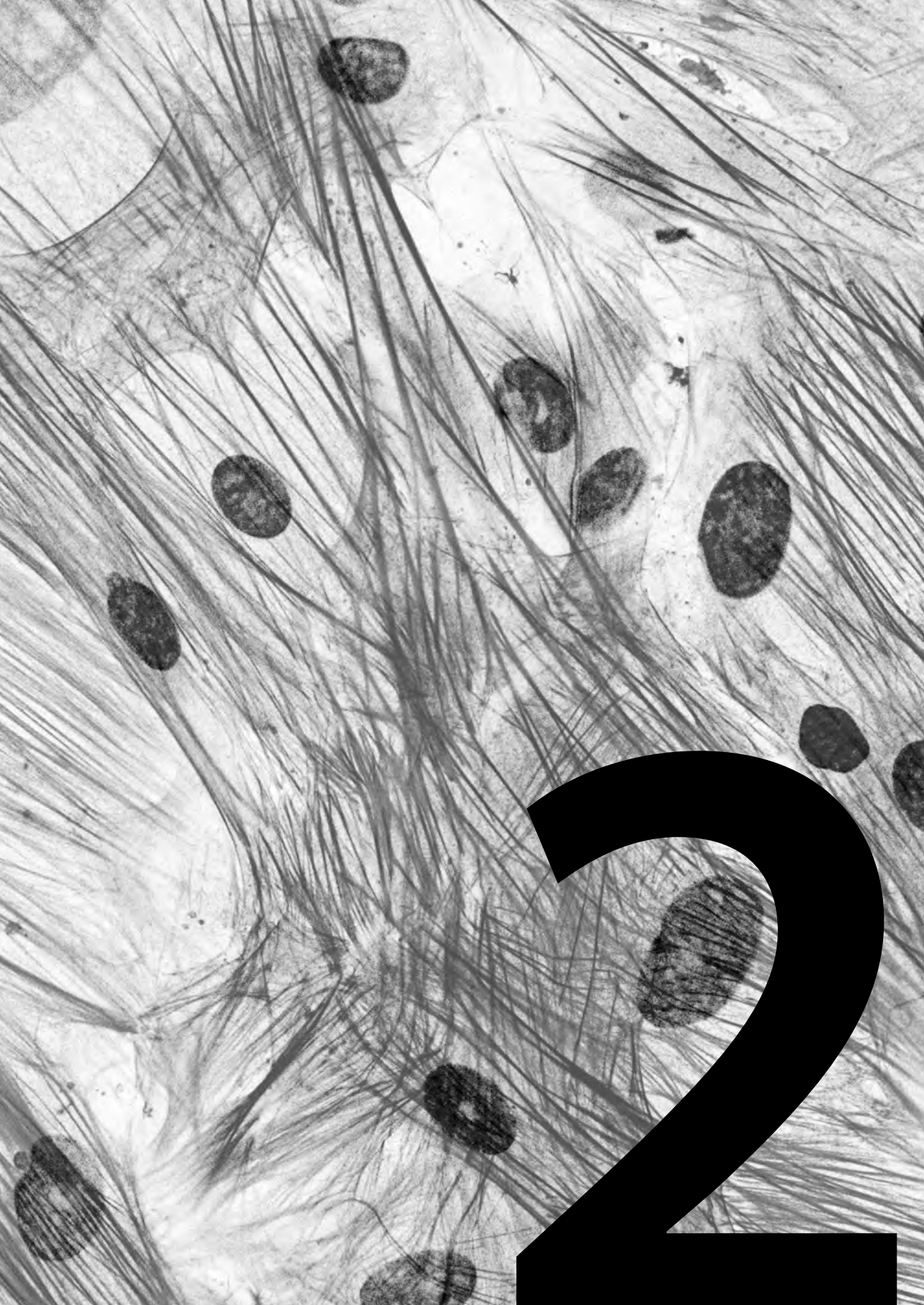
The scientific impact of this thesis is the development of new methods and models which can be used as tools in future translational research into SMC and AA, and findings that hint new potential pathological mechanisms by patient-specific cell analysis. The societal impact of the thesis is a translational effort to answer the question “why does the aorta dilate?”, and to provide novel tools to find this answer.

REFERENCES

- 1 Nordon, I. M., Hinchliffe, R. J., Loftus, I. M. & Thompson, M. M. Pathophysiology and epidemiology of abdominal aortic aneurysms. *Nature Reviews Cardiology* 8, 92, doi:10.1038/nrcardio.2010.180 (2010).
- 2 Assar, A. N. & Zarins, C. K. Ruptured abdominal aortic aneurysm: a surgical emergency with many clinical presentations. *Postgraduate medical journal* 85, 268-273 (2009).
- 3 DeRubertis, B. G. et al. Abdominal aortic aneurysm in women: Prevalence, risk factors, and implications for screening. *Journal of Vascular Surgery* 46, 630-635.e631, doi:https://doi.org/10.1016/j.jvs.2007.06.024 (2007).
- 4 Mathur, A., Mohan, V., Ameta, D., Gaurav, B. & Haranahalli, P. Aortic aneurysm. *Journal of translational internal medicine* 4, 35-41, doi:10.1515/jtim-2016-0008 (2016).
- 5 Vardulaki, K. A. et al. Quantifying the risks of hypertension, age, sex and smoking in patients with abdominal aortic aneurysm. *BJS* 87, 195-200, doi:10.1046/j.1365-2168.2000.01353.x (2000).
- 6 Norman, P. E. & Curci, J. A. Understanding the effects of tobacco smoke on the pathogenesis of aortic aneurysm. *Arteriosclerosis, thrombosis, and vascular biology* 33, 1473-1477 (2013).
- 7 Sakalihasan, N., Limet, R. & Defawe, O. D. Abdominal aortic aneurysm. *The Lancet* 365, 1577-1589 (2005).
- 8 Persson, S.-E., Boman, K., Wanhainen, A., Carlberg, B. & Arnerlöv, C. Decreasing prevalence of abdominal aortic aneurysm and changes in cardiovascular risk factors. *Journal of Vascular Surgery* 65, 651-658, doi:https://doi.org/10.1016/j.jvs.2016.08.091 (2017).
- 9 Pepe, G. et al. Marfan syndrome: current perspectives. *The application of clinical genetics* 9, 55-65, doi:10.2147/TACG.S96233 (2016).
- 10 Isselbacher Eric, M., Lino Cardenas Christian, L. & Lindsay Mark, E. Hereditary Influence in Thoracic Aortic Aneurysm and Dissection. *Circulation* 133, 2516-2528, doi:10.1161/CIRCULATIONAHA.116.009762 (2016).
- 11 Dobrin, P. B. & Mrkvicka, R. Failure of elastin or collagen as possible critical connective tissue alterations underlying aneurysmal dilatation. *Cardiovascular surgery* 2, 484-488 (1994).
- 12 Vorp, D. A. et al. Effect of aneurysm on the tensile strength and biomechanical behavior of the ascending thoracic aorta. *The Annals of thoracic surgery* 75, 1210-1214 (2003).
- 13 Quintana Raymundo, A. & Taylor, W. R. Cellular Mechanisms of Aortic Aneurysm Formation. *Circulation Research* 124, 607-618, doi:10.1161/CIRCRESAHA.118.313187 (2019).
- 14 Annabi, B. et al. Differential regulation of matrix metalloproteinase activities in abdominal aortic aneurysms. *Journal of Vascular Surgery* 35, 539-546, doi:https://doi.org/10.1067/mva.2002.121124 (2002).
- 15 Tamarina, N. A., McMillan, W. D., Shively, V. P. & Pearce, W. H. Expression of matrix metalloproteinases and their inhibitors in aneurysms and normal aorta. *Surgery* 122, 264-272, doi:https://doi.org/10.1016/S0039-6060(97)90017-9 (1997).
- 16 Nosoudi, N. et al. Prevention of Abdominal Aortic Aneurysm Progression by Targeted Inhibition of Matrix Metalloproteinase Activity With Batimastat-Loaded Nanoparticles. *Circulation Research* 117, e80-e89, doi:10.1161/CIRCRESAHA.115.307207 (2015).
- 17 Jacob, M. P. Extracellular matrix remodeling and matrix metalloproteinases in the vascular wall during aging and in pathological conditions. *Biomedicine & Pharmacotherapy* 57, 195-202, doi:https://doi.org/10.1016/S0753-3322(03)00065-9(2003).
- 18 Lopez-Candales, A. et al. Decreased vascular smooth muscle cell density in medial degeneration of human abdominal aortic aneurysms. *Am J Pathol* 150, 993 (1997).
- 19 Greenhalgh, R. M. Comparison of endovascular aneurysm repair with open repair in patients with abdominal aortic aneurysm (EVAR trial 1), 30-day operative mortality results: randomised controlled trial. *The Lancet* 364, 843-848, doi:https://doi.org/10.1016/S0140-6736(04)16979-1 (2004).
- 20 Prinssen, M. et al. A Randomized Trial Comparing Conventional and Endovascular Repair of Abdominal Aortic Aneurysms. *New England Journal of Medicine* 351, 1607-1618, doi:10.1056/NEJMoa042002 (2004).

- 21 De Bruin, J. L. et al. Long-Term Outcome of Open or Endovascular Repair of Abdominal Aortic Aneurysm. *New England Journal of Medicine* 362, 1881-1889, doi:10.1056/NEJMoa0909499 (2010).
- 22 Endovascular versus Open Repair of Abdominal Aortic Aneurysm. *New England Journal of Medicine* 362, 1863-1871, doi:10.1056/NEJMoa0909305 (2010).
- 23 Lederle, F. A. et al. Long-Term Comparison of Endovascular and Open Repair of Abdominal Aortic Aneurysm. *New England Journal of Medicine* 367, 1988-1997, doi:10.1056/NEJMoa1207481 (2012).
- 24 The Propranolol Aneurysm Trial, I. Propranolol for small abdominal aortic aneurysms: Results of a randomized trial. *Journal of Vascular Surgery* 35, 72-79, doi:https://doi.org/10.1067/mva.2002.121308(2002).
- 25 Chung Ada, W. Y., Yang, H. H. C., Radomski Marek, W. & van Breemen, C. Long-Term Doxycycline Is More Effective Than Atenolol to Prevent Thoracic Aortic Aneurysms in Marfan Syndrome Through the Inhibition of Matrix Metalloproteinase-2 and -9. *Circulation Research* 102, e73-e85, doi:10.1161/CIRCRESAHA.108.174367 (2008).
- 26 Petrincec, D. et al. Doxycycline inhibition of aneurysmal degeneration in an elastase-induced rat model of abdominal aortic aneurysm: Preservation of aortic elastin associated with suppressed production of 92 kD gelatinase. *Journal of Vascular Surgery* 23, 336-346, doi:https://doi.org/10.1016/S0741-5214(96)70279-3 (1996).
- 27 Yu, M., Chen, C., Cao, Y. & Qi, R. Inhibitory effects of doxycycline on the onset and progression of abdominal aortic aneurysm and its related mechanisms. *European Journal of Pharmacology* 811, 101-109, doi:https://doi.org/10.1016/j.ejphar.2017.05.041 (2017).
- 28 de Waard, V. et al. Abstract 656: Doxycycline Inhibits Mitochondrial and Cellular Function in Aorta Smooth Muscle Cells. *Arteriosclerosis, Thrombosis, and Vascular Biology* 39, A656-A656, doi:10.1161/atvb.39.suppl_1.656 (2019).
- 29 Mosorin, M. et al. Use of doxycycline to decrease the growth rate of abdominal aortic aneurysms: A randomized, double-blind, placebo-controlled pilot study. *Journal of Vascular Surgery* 34, 606-610, doi:https://doi.org/10.1067/mva.2001.117891 (2001).
- 30 Curci, J. A. et al. Preoperative treatment with doxycycline reduces aortic wall expression and activation of matrix metalloproteinases in patients with abdominal aortic aneurysms. *Journal of Vascular Surgery* 31, 325-342, doi:https://doi.org/10.1016/S0741-5214(00)90163-0 (2000).
- 31 Baxter, B. T. et al. Prolonged administration of doxycycline in patients with small asymptomatic abdominal aortic aneurysms: Report of a prospective (Phase II) multicenter study. *Journal of Vascular Surgery* 36, 1-12, doi:https://doi.org/10.1067/mva.2002.125018 (2002).
- 32 Schouten, O. et al. Statins are Associated with a Reduced Infrarenal Abdominal Aortic Aneurysm Growth. *European Journal of Vascular and Endovascular Surgery* 32, 21-26, doi:https://doi.org/10.1016/j.ejvs.2005.12.024 (2006).
- 33 Ferguson, C. D. et al. Association of statin prescription with small abdominal aortic aneurysm progression. *American Heart Journal* 159, 307-313, doi:https://doi.org/10.1016/j.ahj.2009.11.016 (2010).
- 34 Kertai, M. D. et al. Association between long-term statin use and mortality after successful abdominal aortic aneurysm surgery. *The American Journal of Medicine* 116, 96-103, doi:https://doi.org/10.1016/j.amjmed.2003.08.029 (2004).
- 35 Lederle, F. A. The Strange Relationship between Diabetes and Abdominal Aortic Aneurysm. *European Journal of Vascular and Endovascular Surgery* 43, 254-256, doi:https://doi.org/10.1016/j.ejvs.2011.12.026 (2012).
- 36 Shantikumar, S., Ajjan, R., Porter, K. E. & Scott, D. J. A. Diabetes and the Abdominal Aortic Aneurysm. *European Journal of Vascular and Endovascular Surgery* 39, 200-207, doi:https://doi.org/10.1016/j.ejvs.2009.10.014 (2010).
- 37 Fujimura, N. et al. Metformin treatment status and abdominal aortic aneurysm disease progression. *Journal of Vascular Surgery* 64, 46-54.e48, doi:https://doi.org/10.1016/j.jvs.2016.02.020 (2016).
- 38 Golledge, J. et al. Association between metformin prescription and growth rates of abdominal aortic aneurysms. *BJS* 104, 1486-1493, doi:10.1002/bjs.10587 (2017).
- 39 Habashi, J. P. et al. Losartan, an AT1 Antagonist, Prevents Aortic Aneurysm in a Mouse Model of Marfan Syndrome. *Science* 312, 117, doi:10.1126/science.1124287 (2006).

- 40 Habashi, J. P. et al. Angiotensin II Type 2 Receptor Signaling Attenuates Aortic Aneurysm in Mice Through ERK Antagonism. *Science* 332, 361, doi:10.1126/science.1192152 (2011).
- 41 Yang, H. H. C., Kim, J. M., Chum, E., van Breemen, C. & Chung, A. W. Y. Effectiveness of combination of losartan potassium and doxycycline versus single-drug treatments in the secondary prevention of thoracic aortic aneurysm in Marfan syndrome. *The Journal of Thoracic and Cardiovascular Surgery* 140, 305-312.e302, doi:https://doi.org/10.1016/j.jtcvs.2009.10.039 (2010).
- 42 Lum, H. & Malik, A. B. Regulation of vascular endothelial barrier function. *American Journal of Physiology-Lung Cellular and Molecular Physiology* 267, L223-L241, doi:10.1152/ajplung.1994.267.3.L223 (1994).
- 43 Ladich, E., Butany, J. & Virmani, R. in *Cardiovascular Pathology (Fourth Edition)* (eds L. Maximilian Buja & Jagdish Butany) 169-211 (Academic Press, 2016).
- 44 Liu, R., Leslie, K. L. & Martin, K. A. Epigenetic regulation of smooth muscle cell plasticity. *Biochimica et Biophysica Acta (BBA)-Gene Regulatory Mechanisms* 1849, 448-453 (2015).
- 45 Bacakova, L. et al. in *Muscle Cell and Tissue-Current Status of Research Field* (IntechOpen, 2018).
- 46 Touyz, R. M. et al. Vascular smooth muscle contraction in hypertension. *Cardiovasc Res* 114, 529-539, doi:10.1093/cvr/cvy023 (2018).
- 47 Winder, S. J. & Walsh, M. P. Calponin: thin filament-linked regulation of smooth muscle contraction. *Cellular signalling* 5, 677-686 (1993).
- 48 Harris, L. J. et al. Differentiation of Adult Stem Cells into Smooth Muscle for Vascular Tissue Engineering. *Journal of Surgical Research* 168, 306-314, doi:https://doi.org/10.1016/j.jss.2009.08.001 (2011).
- 49 Owens, G. K. Regulation of differentiation of vascular smooth muscle cells. *Physiological Reviews* 75, 487-517, doi:10.1152/physrev.1995.75.3.487 (1995).
- 50 Carmo, M. et al. Alteration of Elastin, Collagen and their Cross-links in Abdominal Aortic Aneurysms. *European Journal of Vascular and Endovascular Surgery* 23, 543-549, doi:https://doi.org/10.1053/ejvs.2002.1620 (2002).
- 51 Fedak, P. W. M. et al. Vascular matrix remodeling in patients with bicuspid aortic valve malformations: implications for aortic dilatation. *The Journal of Thoracic and Cardiovascular Surgery* 126, 797-805, doi:https://doi.org/10.1016/S0022-5223(03)00398-2 (2003).
- 52 López-Candales, A. et al. Decreased vascular smooth muscle cell density in medial degeneration of human abdominal aortic aneurysms. *Am J Pathol* 150, 993-1007 (1997).
- 53 Humphrey Jay, D., Schwartz Martin, A., Tellides, G. & Milewicz Dianna, M. Role of Mechanotransduction in Vascular Biology. *Circulation Research* 116, 1448-1461, doi:10.1161/CIRCRESAHA.114.304936 (2015).
- 54 Humphrey, J. D., Dufresne, E. R. & Schwartz, M. A. Mechanotransduction and extracellular matrix homeostasis. *Nature reviews. Molecular cell biology* 15, 802-812, doi:10.1038/nrm3896 (2014).
- 55 Rowe, V. L. et al. Vascular smooth muscle cell apoptosis in aneurysmal, occlusive, and normal human aortas. *Journal of Vascular Surgery* 31, 567-576, doi:https://doi.org/10.1067/mva.2000.102847 (2000).
- 56 Thompson, R. W., Liao, S. & Curci, J. A. Vascular smooth muscle cell apoptosis in abdominal aortic aneurysms. *Coronary artery disease* 8, 623-631 (1997).
- 57 Henderson, E. L. et al. Death of smooth muscle cells and expression of mediators of apoptosis by T lymphocytes in human abdominal aortic aneurysms. *Circulation* 99, 96-104 (1999).
- 58 Shimizu, K., Mitchell Richard, N. & Libby, P. Inflammation and Cellular Immune Responses in Abdominal Aortic Aneurysms. *Arteriosclerosis, Thrombosis, and Vascular Biology* 26, 987-994, doi:10.1161/01.ATV.0000214999.12921.4f (2006).
- 59 Walton Lesley, J. et al. Inhibition of Prostaglandin E2 Synthesis in Abdominal Aortic Aneurysms. *Circulation* 100, 48-54, doi:10.1161/01.CIR.100.1.48 (1999).
- 60 Ailawadi, G. et al. Smooth muscle phenotypic modulation is an early event in aortic aneurysms. *The Journal of thoracic and cardiovascular surgery* 138, 1392-1399, doi:10.1016/j.jtcvs.2009.07.075 (2009).



Transdifferentiation of human dermal fibroblasts to smooth muscle-like cells to study the effect of MYH11 and ACTA2 mutations in aortic aneurysms.

Kak K. Yeung, Natalija Bogunovic, Niels Keekstra,
Adriaan A.M. Beunders, Jorrit Pals, Kim van der Kuij,
Eline Overwater, Willem Wisselink, Jan D. Blankensteijn,
Victor W.M. van Hinsbergh, Rene J.P. Musters, Gerard Pals,
Dimitra Micha*, Behrouz Zandieh-Doulabi,*

* These authors contributed equally.

Human mutation; 2017; 38(4), 439-450.

ABSTRACT

Mutations in genes encoding proteins of the smooth muscle cell (SMC) contractile apparatus contribute to familial aortic aneurysms. To investigate the pathogenicity of these mutations, SMC are required. We demonstrate a novel method to generate SMC-like cells from human dermal fibroblasts by transdifferentiation to study the effect of variants in genes encoding proteins of the SMC contractile apparatus (*ACTA2* and *MYH11*) in patients with aortic aneurysms.

Dermal fibroblasts from 7 healthy donors and cells from 7 patients with *MYH11* or *ACTA2* variants were transdifferentiated into SMC-like cells within a 2-week duration using 5ng/mL TGFβ1 on a scaffold containing collagen and elastin. The induced SMC were comparable to primary human aortic SMC in mRNA expression of SMC markers which was confirmed on the protein level by immunofluorescence quantification analysis and western blotting. In patients with *MYH11* or *ACTA2* variants, the effect of intronic variants on splicing was demonstrated on mRNA level in the induced SMC, allowing classification into pathogenic or non-pathogenic variants.

In conclusion, direct conversion of human dermal fibroblasts into SMC-like cells is a highly efficient method to investigate the pathogenicity of variants in proteins of the SMC contractile apparatus.

INTRODUCTION

Thoracic aortic aneurysms (AA) can lead to aortic dissections and ruptures, which are associated with high mortality rates.¹⁻³ Susceptibility of thoracic AA can be inherited in isolation or in association with genetic syndromes, such as Marfan syndrome,^{4,5} and Loeys-Dietz syndrome.^{6,7} When thoracic AA occurs in the absence of syndromic features, it is inherited in an autosomal dominant manner with decreased penetrance and variable expression, and it is referred to as familial thoracic AA.⁸ Approximately 20% of thoracic aneurysms are familial and the majority of familial thoracic AA presents as isolated aneurysms with mutations often present in the vascular SMC-specific β -myosin (*MYH11*) or α -actin (*ACTA2*).⁸⁻¹⁰ *MYH11* (myosin heavy chain 11) and *ACTA2* (smooth muscle actin alpha 2) are proteins that compose the contractile apparatus of the aortic SMC.⁸⁻¹⁰ They are involved in SMC contraction and mutations in these proteins may decrease SMC contractile function. Under these conditions the aortic wall is unable to withstand biomechanical forces, which leads to the formation of aneurysms on areas where the biomechanical forces are the greatest.⁸ Genetic diagnosis of these hereditary conditions remains inconclusive, because it is difficult to interpret and validate the results of DNA analysis. Moreover, in silico predictions are insufficient to establish whether specific variants are pathogenic or not. In particular since many variants are novel. Given the tissue-specific expression of SMC-specific transcripts, functional assays to test the hypothesis of pathogenicity are complicated. The disease affects the aorta, which is not easily accessible for biopsy. Since the majority of aortic aneurysms are nowadays repaired by endovascular procedures, it is difficult to have access to aneurysmatic aortic wall from patients for functional assays. Therefore, an alternative approach to study gene expression in SMC is necessary. Although the differentiation of fibroblasts into induced pluripotent stem cells (iPSC) and SMC derivatives has been reported,^{11, 12} it remains time-consuming and expensive. Direct conversion or transdifferentiation enables the cells to bypass the pluripotency state of cell differentiation,¹³⁻¹⁴ allowing the direct conversion of mature tissue-specific cells into another of a different cell lineage, as described by Waddington's epigenetic landscape model.¹⁵ Transforming Growth Factor- β 1 (TGF β 1) is known to induce differentiation of cardiac fibroblasts from mice to myofibroblasts.^{16,17} However, direct TGF β 1-mediated transdifferentiation has not been performed in human cells before.

We developed a novel protocol of myogenic transdifferentiation of human dermal fibroblasts into SMC-like cells based on TGF β 1 stimulation of cells seeded on matrigel (Matrigel, Corning, Billerbeck, Germany), a skin equivalent scaffold containing collagen and elastin. The effect of variants was studied in SMC of AA patients by generating transdifferentiated SMC directly from their own dermal fibroblasts. SMC properties were validated by the expression of SMC markers and contractile properties. The expression of SMC-specific genes and morphological changes in the transdifferentiation process of the fibroblasts from healthy volunteers

and from patients with a *MYH11* (MIM# 160745) or *ACTA2* (MIM# 102620) variant were examined. The expression of *MYH11* and *ACTA2* in the transdifferentiated SMC-like cells allowed assessment of the pathogenic effect of the variants by investigating the effect on splicing.

MATERIAL AND METHODS

Patients and healthy volunteers

The study was approved by the Medical Ethical Committee of the VU University Medical Center (VUmc) Amsterdam.

Primary fibroblasts were cultured from skin biopsies taken from the upper arm from seven different patients with either a familial aortic aneurysm or dissection. These patients were tested for variants by targeted next generation sequencing for the following AA genes: *ACTA2*, *COL3A1*, *EFEMP2*, *ELN*, *FBN1*, *FBN2*, *MYH11*, *MYLK*, *NOTCH1*, *PLOD1*, *PRKG1*, *SCARF2*, *SKI*, *SLC2A10*, *SMAD2*, *SMAD3*, *SMAD4*, *TGFB2*, *TGFB3*, *TGFBR1*, *TGFBR2*. The presence of variants was confirmed by Sanger sequencing. The presence of an *ACTA2* or *MYH11* variant was confirmed in the seven AA-patients used in this experiment (*ACTA2*: Cytogenetic location: 10q23.31, genomic coordinates (GRCh38): 10:88,935,073-88,991,396; *MYH11*: Cytogenetic location: 16p13.11, genomic coordinates (GRCh38): 16:15,703,134-15,857,031). Patient cells were compared to fibroblasts of 7 healthy donors without an aortic aneurysm or variants in these genes. The latter donors were healthy volunteers without a medical history and DNA testing was performed on AA genes to confirm that they have no variants in these genes. We also compared the transdifferentiated SMC to primary cells established from aortic aneurysm tissue during open aortic aneurysm repair and the primary human SMC cell line HASMC (Thermo Fisher Scientific, Waltham, MA, USA; Cat# C0075C). *Table 1* shows the information of the patients and healthy volunteers. All experiments were conducted in triplicate, i.e. the transdifferentiation process and confirmation of the SMC-like cells with qPCR, staining and contraction experiments. Western blotting was performed in duplo.

Table 1. Characteristics of patients with an aortic aneurysm with a variant in *MYH11* and/or *ACTA2*, healthy volunteers and primary smooth muscle cells. The predicted or possible effect of the mutations and the evidence from RNA studies with transdifferentiated smooth muscle cells (SMC) are shown. Cells were cultured with cycloheximide to prevent nonsense mediated decay (NMD) of mRNA. Numbering of *MYH11* cDNA is according to transcript NM_001041113.1 and of *ACTA2* cDNA is according to transcript NM_001141945. ACTA2: LRG_781; MYH11: ENSG00000133392 (no LRG number is available).

*Exon 42 of transcript NM_001040114.1 NOT detectable in mRNA from healthy controls. The longest transcript of MYH11, NM_001041114.1 is not relevant in familial thoracic aortic aneurysms. ** Human aortic smooth muscle cells (HASMC; Thermo Fischer Scientific)*** SMC from aortic aneurysm patient without a known AA-causing mutation; ESE= exonic splice enhancer; F: Female, M: Male, NA: not applicable.

Patient	Age	Gender	Gene	Mutation	Predicted effect of mutation	Evidence from mRNA	Conclusion
1	62	F	MYH11	c.3879+2dup	Possible splice error exon 29	Use of cryptic splice site at c.3802, p.Val1268_Gln1293del	Pathogenic
2	65	M	MYH11	c.2881-14C>G	Possible splice error exon 24	No effect on splicing	Not pathogenic
3	40	F	MYH11	c.419C>T (p.T139T)	Silent mutation, Possible exon skipping due to loss of ESE	No effect on splicing	Not pathogenic
4	35	F	ACTA2	c.455-74C>T	Possible splice error	No effect on splicing	Not pathogenic
5	45	M	MYH11	c.988G>A (p.D330N)	Misense; possible exon skip (loss of ESE)	No effect on splicing	Likely pathogenic (conserved amino acid; loss of charge)
			ACTA2	c.369+93C>T	Possible splice error	No effect on splicing	Not pathogenic
6	55	M	MYH11	c.5819C>A (p.P1940Q)	Misense in alternate transcript	Alternate transcript not found in cDNA from patient AMD controls *	Not pathogenic*
7	67	F	MYH11	c.3787-3789del	Inframe deletion	No effect on splicing. Mutation is present in cDNA. Loss of conserved amino acid	Likely pathogenic (conserved sequence; loss of charge)
Healthy volunteers (n=7)	47 (28-57)	3 M, 4F	NA	NA	NA		
Primary SMC from aorta **	31	M	NA	NA	NA		
Primary SMC from AA***	63	M	NA	NA	NA		
Primary SMC from AA***	66	M	NA	NA	NA		

Transdifferentiation protocol

Before starting the transdifferentiation we confirmed that the dermal fibroblasts used in this experiment have the immunophenotype of mesenchymal stem cells (MSCs). The cells tested with FACS analysis positive for the adhesion molecule markers CD90, CD105, CD166, CD54, CD73, CD29 and HLA-ABC, which are markers of MSCs. The cells were weakly positive for the Lin-1 cocktail of hematopoietic cell markers CD3, CD14, CD16, CD19, CD20 and CD56, and negative for the hematopoietic stem cell markers: CD117 and CD34 and for the endothelial surface marker CD31 and HLA-DR.

Cells were maintained in a humidified incubator at 37°C and 5% CO₂ in basal medium (Ham's F10 Nutrient Mix (Thermo Fisher Scientific) containing 10% fetal bovine serum (Thermo Fisher Scientific), 100 units/mL Penicillin and 100 µg/mL Streptomycin (Thermo Fisher Scientific). We considered that a gel of only collagen type I does not adequately imitate the matrix of the aorta, which also contains elastin and other collagen types. The role of elastin in SMC differentiation is exemplified by the fact that shortage of elastin provokes cell proliferation instead of differentiation.¹⁸ Thus, we identified matrigel as a suitable cell growth scaffold (Corning/Costar). Matrigel is a collagen- and elastin-containing matrix and it was initially designed as a dermal equivalent for skin burns.¹⁹ 2.5 million cells/mL were seeded in basal media on matrigel sections of 1 cm² in 6-well plates. Cells were evenly seeded on matrigel on the four corners and centrally. After overnight incubation on the matrigel allowing the cells to attach, they were treated with differentiation medium: DMEM (Thermo Fisher Scientific) with 2% heat-inactivated horse serum (HS) (Thermo Fisher Scientific) and 5 ng/mL TGFβ1 (BioVision, Milpitas, CA) to induce fibroblast transdifferentiation into SMC-like cells. The cells were harvested on days 0, 4, and 14 for RNA isolation or fixed with 4% formaldehyde in phosphate-buffered-saline (PBS) for immunofluorescence analysis. We induced transdifferentiation of dermal fibroblasts of 7 healthy volunteers and 7 patients with a variant in *MYH11* or *ACTA2* into SMC-like cells (Table 1). Fibroblasts in medium with HS only, were used as a control of the transdifferentiation process. The transdifferentiated cells were compared to primary smooth muscle cells established from aortic aneurysm tissue during open aortic aneurysm repair and commercially available SMC (HASMC: Human aortic smooth muscle cells from Thermo Fisher Scientific). Primary SMC were cultured in 231 medium (Thermo Fisher Scientific), supplemented with Smooth Muscle Growth Supplement (SMGS; Thermo Fisher Scientific) and 100 units/mL Penicillin and 100 µg/mL Streptomycin (Thermo Fisher Scientific), according to manufacturer's instructions.

RNA isolation and quantitative PCR (qPCR)

Total RNA was extracted from the cells using the NucleoSpin TriPrep kit (Macherey-Nagel, Düren, Germany). First strand cDNA synthesis was performed in a 20 µl reverse transcription reaction containing total RNA depending on the concentration, according to the instructions of the VILO kit (Thermo Fisher Scientific). qPCR analysis was performed to analyse mRNA expression of SMC marker genes (*SMTN* (XM_005261708), *TAGLN* (NM_001001522), *CNN1* (HQ448227), *ACTA2* (NM_001141945), *MYH11* (NM_001040113.1). We examined the gene expression of *ACTN1,2* (NM_001102) a gene involved in the formation of actin bundles. *YWHAZ* (NM_003406), *HPRT* (NM_000194) and *UBC* (NM_021009) were used as housekeeping genes and determined by the LightCycler 480 Instrument II, using the Light Cycler SYBR Green I Master (Roche Applied Science, Penzberg, Germany).

qPCR reactions were prepared in 10 µl total volume with 2 µl PCR grade H₂O, 1 µl forward primer (10 pM), 1 µl reverse primer (10 pM), 5 µl Light Cycler Mastermix (Light Cycler 480 SYBR Green I Master; Roche Applied Science), to which 2 µl of 5 times diluted cDNA was added as PCR template. With the LightCycler software, the absolute values of each sample were assessed from a standard curve of 5 serial dilutions ranging from 10 ng to 1.6 pg of cDNA derived from cDNA obtained from human reference RNA (Agilent Technologies, Santa Clara, CA) which was used as reference cDNA. PCR efficiency was automatically calculated using the fit point method and gene expression data were used only if the PCR efficiency was within a 1.85-2.0 range. For each gene absolute values of mRNA expression were normalized based on the normalization factor derived from *YWHAZ*, *HPRT* and *UBC* housekeeping genes in order to calculate relative gene expression. Cells were additionally cultured with and without cycloheximide treatment at 0.25 mg/mL for 4.5 hours, to inhibit translation and nonsense mediated decay, prior to isolation of RNA and synthesis of cDNA.

Genetic analyses

Splice site prediction software (Alamut® v.2.7.1, Interactive Biosoftware, Rouen, France) was used to predict variants to have a likely or possible effect on RNA splicing, either by affecting the nearby splice site or by loss of exonic splice enhancer sequences. After production of cDNA, as described above, qPCR was performed with primer positions in exons around the exon containing the mutation and products were analyzed with electrophoresis on 1.5% agarose gel. Sequence analysis was performed using BigDye vs. 3 and a ABI 3730 genetic analyzer (Applied Biosystems, Torrance, CA, USA).

Western blot analysis

Cells were washed with Earle's Balanced Salt Solution (EBSS; Thermo Fisher Scientific) and lysed in 120 μ l M-PER mammalian extraction reagent with 1% Halt Protease Inhibitor Cocktail EDTA-free (Thermo Fisher Scientific). Cell lysates were incubated in ice for 15 minutes on a shaking platform. Then, 12 μ l of cell lysate was mixed with 4 μ l of NuPAGE® LDS Sample Buffer containing NuPage Sample reducing agent (Thermo Fisher Scientific). Gel electrophoresis was performed in NuPAGE 4-12% BT gels with NuPAGE MOPS SDS Running Buffer (20x) or NuPAGE 3-8% TA gels with NuPAGE Tris-Acetate running buffer (Thermo Fisher Scientific). Proteins were transferred to nitrocellulose membrane by using the iBlot dry blotting system (Thermo Fisher Scientific). The membrane was blocked by incubating in Odyssey blocking buffer (LI-COR Biosciences, Lincoln, NE, USA) for 1 hour at room temperature on a rocking platform. Primary antibody incubation was performed overnight at 4°C with gentle agitation in Odyssey blocking buffer with 1:1000 Tween 20 (Sigma Aldrich, St. Louis, MO, USA). Primary antibodies against smooth muscle actin (Dako, Glostrup, Denmark), calponin (Abcam, Cambridge, UK), MYH11 (Abcam), SM22 (Abcam), tubulin (Abcam) and actin (Abcam) were used. Secondary antibody incubation was performed at room temperature for 1h with IRDye® 800CW Goat anti-Rabbit IgG and IRDye® 680CW Goat anti-Mouse IgG (LI-COR Biosciences). Signal was visualized using the Odyssey Infrared Imaging System (Odyssey version 4 software; LI-COR Biosciences).

Quantitative 3D immunofluorescence microscopy and confocal scanning laser microscopy

On days 0, 4, and 14, we compared the cell morphology of the converted fibroblasts in the differentiation medium with TGF β 1, with fibroblasts in the control medium with only HS and primary SMC. The seeded cells on matrigel were fixed in 4% formaldehyde solution with PBS for 10 minutes at room temperature. After fixation the sections were washed three times in PBS with 0.05% Tween (Sigma) for 5 minutes. Blocking buffer, consisting of 0.5% BSA (EMD Millipore Corp., Billerica, MA) and 0.1% Triton x-100 (Sigma) in PBS, was added to the cells for 15 minutes. Then the cells were incubated with the primary antibody for one hour, 1:100 diluted α SMA antibody (Dako) in blocking buffer without Triton. After this incubation the sections were washed three times with PBS-Tween (PBST) for 5 minutes at room temperature and were incubated with Alexa 647 labeled secondary antibody Goat-anti-mouse (Thermo Fisher Scientific) for 30 minutes at room temperature at a dilution of 1:100 in PBS. Subsequently, the cells were incubated with 1:50 diluted Smoothelin (Santa Cruz Biotechnology, Dallas, TX, USA) antibody for one hour, followed by 30 minutes incubation with Alexa 488 labeled secondary antibody Donkey-anti-rabbit (Thermo Fisher Scientific) for 30 minutes at room temperature at a dilution of 1:100 in PBS. Negative control sections were treated in the same way,

but did not receive the primary antibody. After incubation with the secondary antibody, the sections were washed three times in PBST for 3 minutes and stained for 20 minutes with rhodamine-phalloidin (Thermo Fisher Scientific) at a dilution of 1:50 in PBS. Next the sections were washed two times with PBST and one time with PBS for 3 minutes at room temperature. Finally, the sections were mounted with DAPI (Thermo Fisher Scientific) and sealed with a cover.

The slides were examined using a Zeiss Axiovert 200M Marianas™ digital imaging inverted microscope system, equipped with a non-stepper-motor (z-axis increments: 0.1 μm) and a turret containing four epifluorescence filtercubes (fluorescein isothiocyanate [FITC], cyanine dyes [Cy-5 and Cy-3], aminomethylcoumarin acetate [AMCA] as well as a differential interference contrast [DIC] brightfield cube). Images were captured with a cooled charge-coupled device (CCD) camera (Cooke Sensicam SVGA [Cooke Co., Tonawanda, NY] 1.280 x 1.024 pixels) with true 16-bit capability. The Marianas™ digital imaging system was controlled by Slidebook™ (Slidebook version 6.1.0.10 software [Intelligent Imaging Innovations, Inc, Denver, CO, USA]). For each fluorescent channel, being the blue (DAPI; i.e. cell nuclei), green (FITC; i.e. smoothelin), near infrared (CY5; i.e. αSMA) and red (Cy3; i.e. rhodamine-phalloidin), images were made using either a Zeiss 10X air objective lens (for low-magnification overviews) or a Zeiss 40X air objective lens (for high-magnification 3D-stacks of 10 micrometer thick optical sections). The acquisition protocol also included whole matriderm (MedSkin Solutions), montage-images (stitching). Images were processed and analyzed by using Slidebook's masking and statistical functions (Slidebook™ 4.1.0.10 software). Correction for non-specific background was done by adjusting the immunofluorescence levels of the positive samples with those of the negative controls. For quantification of fluorescence intensity levels the sum intensity of fluorescence of all voxels in the selected area was used and corrected for the total area. We quantified the fluorescence levels of αSMA , smoothelin, rhodamine-phalloidin and the area of co-localization of αSMA and smoothelin. Values were corrected for the amount of cells. The total amount of cells and the cells positive for staining with αSMA was counted by two independent individuals, which represented the percentage of transdifferentiated cells. Flow cytometry and fluorescence-activated cell sorting (FACS) analysis was not possible, because the cells invaded the matriderm and could not be extracted from the matriderm.

To study the morphology of the cells more extensively, we used the Leica TCS SP8 confocal scanning laser microscope system (Leica Microsystems, Mannheim, Germany) equipped with a white-light excitation laser (WLL) and multiple ultrasensitive photon detectors (PMT and HyD). Leica LAS-X software was used to acquire and analyze multicolor high-magnification 3D-stacks of the cells. For these 3D images Leica 40X and 63X oil-immersion lenses were used. However, in these higher magnification images, the elastin-collagen scaffold of the matriderm blurred

the image of the cells. Thus, we extracted the cells from the matriderm and seeded the cells on round glass coverslips (13mm, #1) (Thermo Fisher Scientific). We studied F-actin, α SMA- and calponin fibers (stained with 1:100 diluted antibody from Abcam and labeled with Alexa 488 secondary antibody Donkey-anti-rabbit, at a dilution 1:100) according to the above protocol in closer detail.

Contraction assay

The folding of the matriderm sections (MedSkin Solutions) due to cell contraction of SMC was used as a contraction assay.¹⁷ Photographic recording of the cell contraction was performed daily. Quantification of contraction images was performed with Image J (version 1.51e, NIH, Bethesda, MA) and numbers are presented here as percentage of area after contraction (100% being no contraction of matriderm).

Statistical evaluation

Data were analysed with SPSS (IBM Statistics v20, Chicago, IL, USA). For multiple groups the Kruskal–Wallis was used first to compare continuous variables with non-parametric distribution, subsequently the Mann–Whitney U test was used for comparing two groups. Fisher's exact test was used for categorical variables in two groups. Correlations were tested with Spearman's Rank Correlation (R_s). Raw data are given as median with range and presented graphically as boxplots (showing median and quartiles) with outliers (according to Tukey's criteria) indicated separately. Tests were considered statistically significant at $p \leq 0.05$.

RESULTS

Conversion of dermal fibroblasts into SMC-like cells in healthy volunteers

Dermal fibroblasts of the 7 healthy volunteers were subjected to myogenic conversion. After 14 days, mRNA expression of *ACTA2*, *SMTN*, *CNN1*, *MYH11* and *TAGLN* (SM22) were upregulated in the converted fibroblasts (Table 2, upper section). Increased expression of MYH11, α SMA, calponin and SM22 was demonstrated in the transdifferentiated cells by western blot analysis, which was comparable to levels observed in HASMC cells (Fig.1a). Treatment with TGF β 1 did not lead to differences in cell proliferation, as total cell counts remained similar on day 0 and day 14 ($p=0.95$). 50,000 cells were seeded per matriderm section to quantify α SMA and smoothelin expression by immunofluorescence. We stained the cells on day 0 before conversion, and at day 4 and 14. After 14 days, α SMA and smoothelin levels as well as F-actin cytoskeleton, as shown by phalloidin staining, were more increased in the cells treated with TGF β 1 than in medium with HS only ($p<0.05$; Fig.1b and c). 84% (range: 76-100) of the dermal fibroblasts were converted to SMC-like cells. Furthermore, the morphology of the cells changed from fibroblasts into SMC-like cells with long fibers containing F-actin and colocalization of α SMA

and smoothelin (Fig.1b and c; example in higher magnification in Fig. 2). To study spontaneous contraction of the cells, we seeded 250,000 dermal fibroblasts per 1 cm² matrigel. Contraction of cells was observed as folding of the matrigel sections, which started around day 5 and maximised on day 14 ($p=0.001$; Fig.1d,e). Furthermore, SMC converted from fibroblasts showed similar SMC gene expression (Table 2) and histological similarities in expression of α SMA and calponin as primary SMC established from aortic aneurysm tissue and commercial primary SMC (Fig. 2).

Table 2. Relative gene expression in smooth muscle cell genes in healthy volunteers and patients with an aortic aneurysm (AA). $p<0.05$ is considered statistically significant. Healthy volunteers (n=7), AA-patients (n=7), AA=aortic aneurysm, TGF β 1 = Transforming Growth Factor β 1, HS = Horse serum, SMC = smooth muscle cells, HASMC=human aortic SMC from Thermo Fischer Scientific; *SMTN* (XM_005261708), *TAGLN* (NM_001001522), *CNN1* (HQ448227), *ACTA2* (NM_001141945), *ACTN1* (NM_001102), *MYH11* (NM_001040113.1)

	day 0	day 4 TGFβ	day 4 HS	day 14 TGFβ	day 14 HS	AA biopsy I	AA biopsy II	BASMC	P-value day 14 TGFβ vs. HS	P-value day 14 TGFβ healthy volunteers vs. AA patients
ACTA2										
healthy volunteers	0.25 (0.15-0.38)	2.84 (1.78-4.88)	0.55 (0.49-2.41)	4.02 (0.54-5.58)	0.77 (0.42-1.17)	1.46	2.24	6.47	0.013	0.338
AA patients	0.25 (0.20-0.41)	2.22 (0.76-5.72)	0.64 (0.44-0.79)	4.21 (2.12-9.06)	0.81 (0.70-1.07)				0.002	
CNN1										
healthy volunteers	0.11 (0.04-0.18)	0.42 (0.14-0.75)	0.05 (0.03-0.21)	0.62 (0.21-0.80)	0.10 (0.02-0.25)	1.05	18.38	2.41	0.003	0.18
AA patients	0.09 (0.00-0.42)	0.49 (0.21-1.06)	0.11 (0.06-0.14)	0.79 (0.37-1.35)	0.10 (0.07-0.22)				0.002	
ACTN1										
healthy volunteers	6.45 (4.65-8.82)	19.24 (16.45-23.46)	8.17 (6.85-23.97)	27.83 (24.55-29.13)	11.16 (9.30-13.44)	38.66	13.90	133.44	0.002	0.009
AA patients	7.52 (0.00-9.77)	17.18 (12.11-21.26)	7.51 (6.26-8.24)	31.68 (27.49-36.71)	11.73 (10.08-14.77)				0.002	
TAGLN										
healthy volunteers	0.35 (0.17-0.96)	4.58 (3.70-5.52)	1.26 (0.68-3.59)	6.28 (4.73-7.07)	1.44 (0.85-1.73)	5.59	9.85	22.10	0.002	0.013
AA patients	0.62 (0.00-3.27)	4.07 (2.36-4.99)	1.36 (0.76-1.65)	7.54 (6.22-12.01)	1.77 (1.10-2.38)				0.002	
SMTN										
healthy volunteers	1.77 (1.48-3.61)	1.88 (1.40-3.07)	1.13 (0.85-1.65)	2.16 (1.33-2.47)	1.77 (1.17-2.98)	0.20	4.32	1.94	0.086	0.002
AA patients	2.14 (0.00-2.65)	2.92 (2.01-3.31)	1.53 (0.91-1.61)	2.86 (2.57-3.29)	2.06 (1.77-3.04)				0.013	
MYH11										
healthy volunteers	0.18 (0.13-0.33)	0.18 (0.08-0.46)	0.18 (0.06-0.33)	0.37 (0.07-0.58)	0.16 (0.07-0.47)	1.97	1.57		0.085	0.940
AA patients	0.15 (0.03-0.26)	0.17 (0.10-0.44)	0.10 (0.05-0.16)	0.29 (0.19-0.49)	0.13 (0.09-0.41)				0.013	

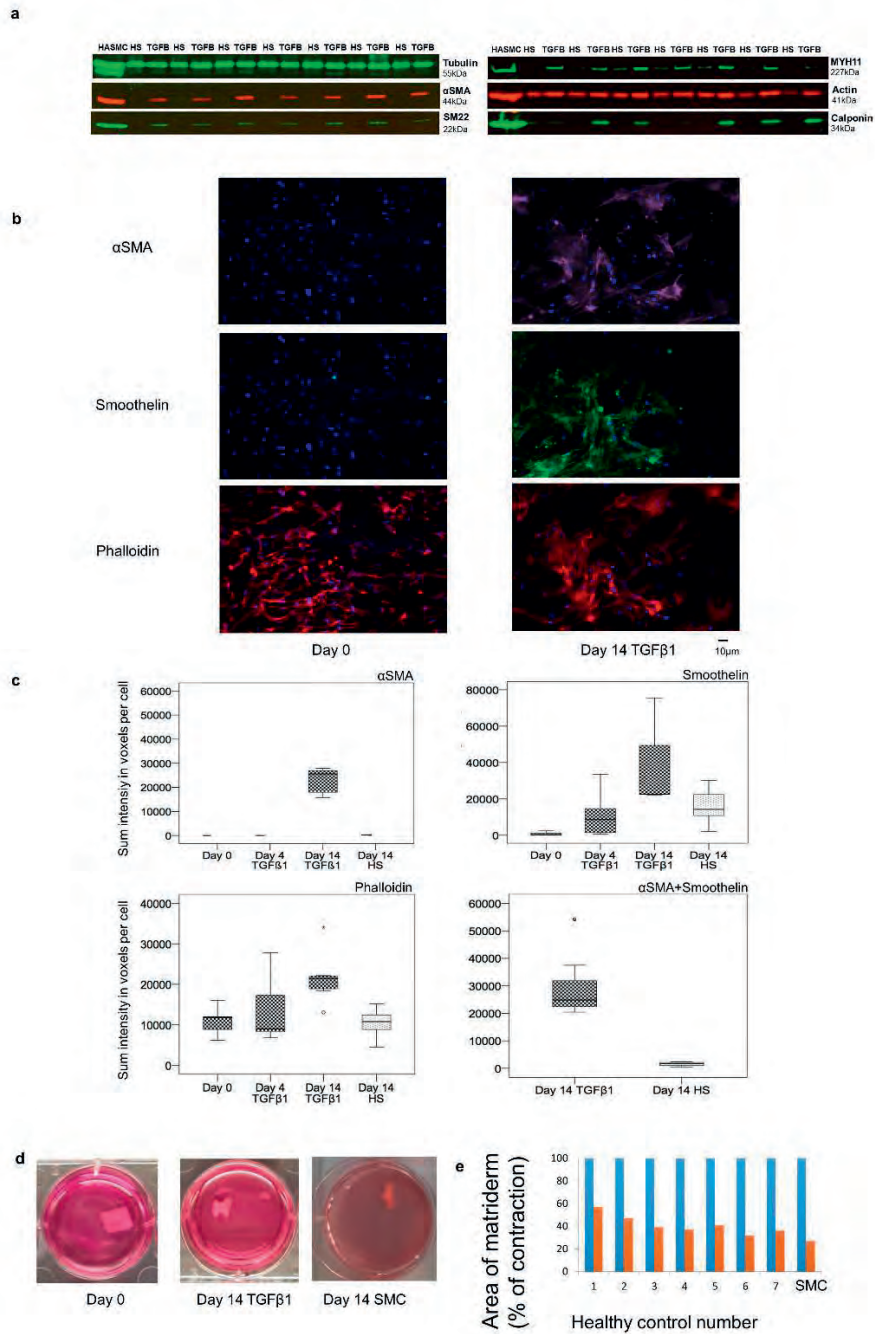


Figure 1. Transdifferentiation of dermal fibroblast to SMC in cells obtained from healthy volunteers. (a) Western blot analysis of α SMA (upper left image), SM22 (lower left image), MYH11 (upper right image) and Calponin (lower right image). HS=dermal fibroblasts in horse serum (HS) after 14 days, TGF β = transdifferentiated SMC-like cells in TGF β 1 after 14 days. HASMC = human aortic smooth muscle cells. Upregulation of α SMA, Calponin, SM22 and MYH11 on day 14 in the transdifferentiated SMC-like cells. (b) Representative images of quantitative immunofluorescence analysis. Images of α SMA (Cy5;purple), Smoothelin (FITC;green), Phalloidin (Cy3;red) and DAPI (blue;nuclei) of dermal fibroblasts after 14 days in HS (left image) and of transdifferentiated SMC-like cells after 14 days in TGF β 1 (right image). Left to right: note the higher levels of α SMA, Smoothelin, Phalloidin of the transdifferentiated SMC-like cells. (c) Quantitative immunofluorescence analysis of the dermal fibroblast differentiation process to SMC-like cells (n=7) on day 0, 4 and 14 in TGF β 1 compared to day 14 in HS. Y-axes represent sum intensity voxels per cell. Upper two panels: left: α SMA (day 14 TGF β 1 vs. day 14 HS;p=0.002), right: smoothelin (p=0.048). Lower two panels: left: F-actin formation (phalloidin;p=0.004), right: colocalization of α SMA and smoothelin (p=0.002). (d) Images of a matrigel in a well-plate. Left: day 0, middle: contraction of the matrigel of the transdifferentiated cells, right: contraction of primary SMC observed as curling of the matrigel on day 14. (e) Area of the matrigel (y-axes;100 = normal not curled matrigel) at day 0 (blue bars) and day 14 (orange bars) of transdifferentiated SMC-like cells of the 7 healthy volunteers (median: 36/100 (28-39/100;p=0.001) and of the commercially available SMC from Thermo Fisher Scientific.

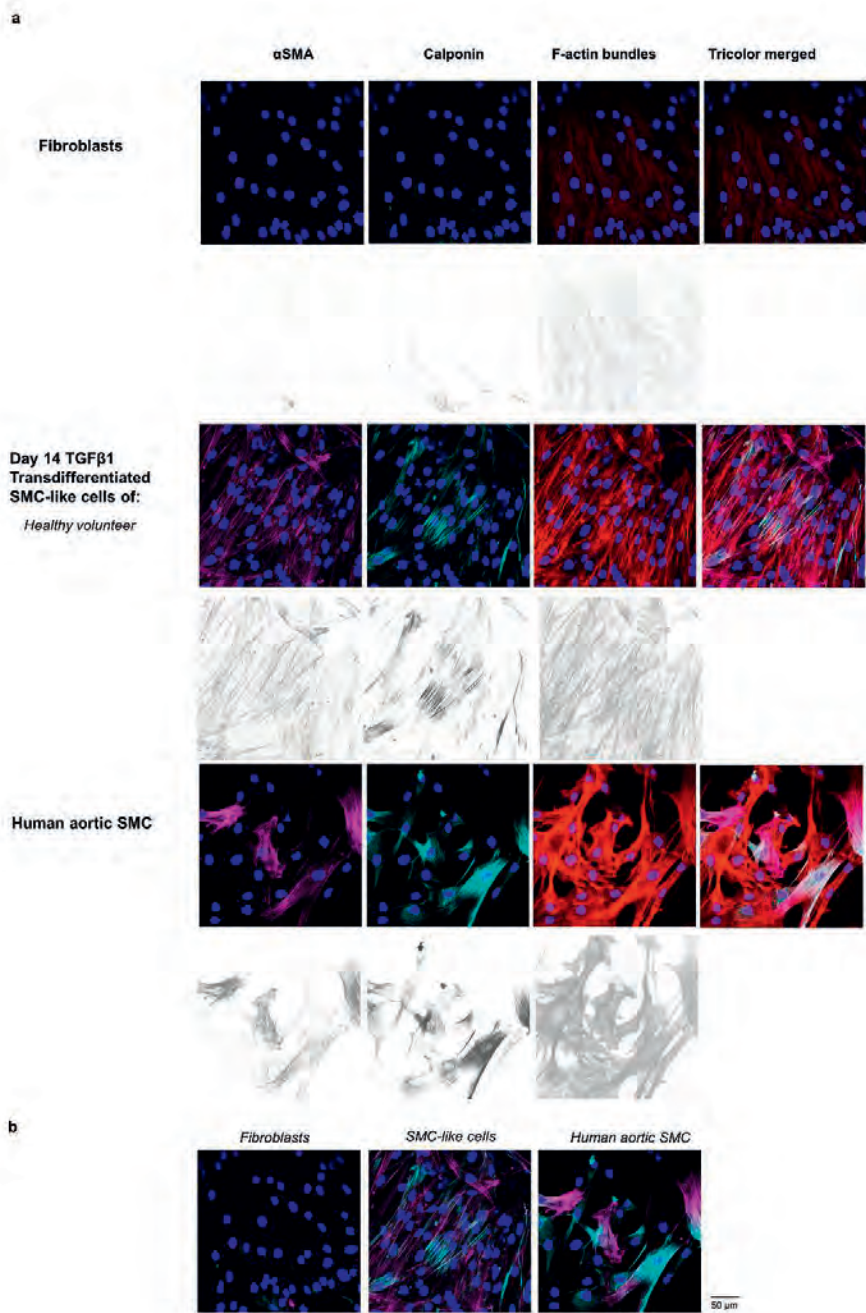


Figure 2. Images in higher magnification using a Leica TCS SP8 confocal scanning laser microscope system. (a) From left to right: Magenta channel (Cy5) = α SMA, Cyan channel (FITC) = calponin, red channel (Cy3) = phalloidin, representing F-actin fibers. Blue is DAPI, representing the nuclei. Most right image: tricolor merged image with DAPI. Under the color images, α SMA, calponin and phalloidin are presented in black respectively (without the nuclei). The first-row images represent dermal fibroblasts after 14 days in horse serum (HS). The second-row images show the transdifferentiated smooth muscle cells (SMC)-like cells of healthy volunteers after 14 days, with long F-actin fiber forming and high levels of α SMA and calponin. The third row primary SMC shows images of primary SMC from a healthy aorta (commercially available from Thermo Fischer Scientific). (b) Colocalisation of Calponin (Magenta) and α SMA (purple) in fibroblasts, transdifferentiated SMC-like cells and primary human SMCs.

Effect of ACTA2 and MYH11 variants on the myogenic conversion of dermal fibroblasts

Subsequently, we examined if the conversion process of fibroblasts into SMC differs between healthy donor cells and cells with a variant in the proteins of the SMC contractile apparatus *MYH11* or *ACTA2*. We therefore investigated fibroblast to SMC conversion of 7 cell lines from AA patients with a variant in *MYH11* or *ACTA2* (Table 1). After 14 days of treatment with differentiation medium with TGF β 1, median 97% (range: 72-100) of the dermal fibroblasts were converted into SMC-like cells in the AA patients. The expression of SMC genes *ACTA2*, *SMTN*, *CNN1* and *TAGLN* were higher in all AA patient cells after 14 days in the differentiation medium with TGF β 1 compared to the control medium with only HS (Table 2). Furthermore, Western blotting analysis confirmed the upregulation of proteins α SMA, MYH11, SM22 and calponin in the transdifferentiated AA patient cells (Fig. 3a). Quantitative immunofluorescence analysis also showed higher levels of α SMA and smoothelin in the transdifferentiated cells when compared to the fibroblasts in the control medium with only HS (Fig. 3b and c; Example in higher magnification in Fig. 4). However, when compared to the data of the healthy volunteers, differences were observed in the transdifferentiated SMC. After 14 days in the differentiation medium with TGF β 1, transdifferentiated SMC of AA-patients showed higher expressions of SMC marker genes *ACTA2*, *CNN1*, *TAGL*, *SMTN* and *ACTN1* when compared to the healthy donor group (Table 2). In addition, immunofluorescence quantification analysis showed that in the aneurysm group the colocalization of smoothelin and α SMA was lower than in the healthy volunteers, which could indicate less stress fibers formation ($p=0.006$; Fig. 3c). Differences in myogenic conversion were not related to age, gender or cell passage number. We hypothesized that the converted fibroblasts with a variant in *MYH11* or *ACTA2* have decreased ability to contract on matrigel. In the contraction experiment, similar matrigel contraction was observed between the transdifferentiated SMC-like cells from AA patients and the healthy volunteers ($p=0.95$). However, we noticed that the contraction force was lower, which became evident when stretching the matrigel. In the healthy volunteer group, the matrigel

rapidly contracted again, while in the AA group it did not. We are currently developing tests to study contraction differences more accurately.

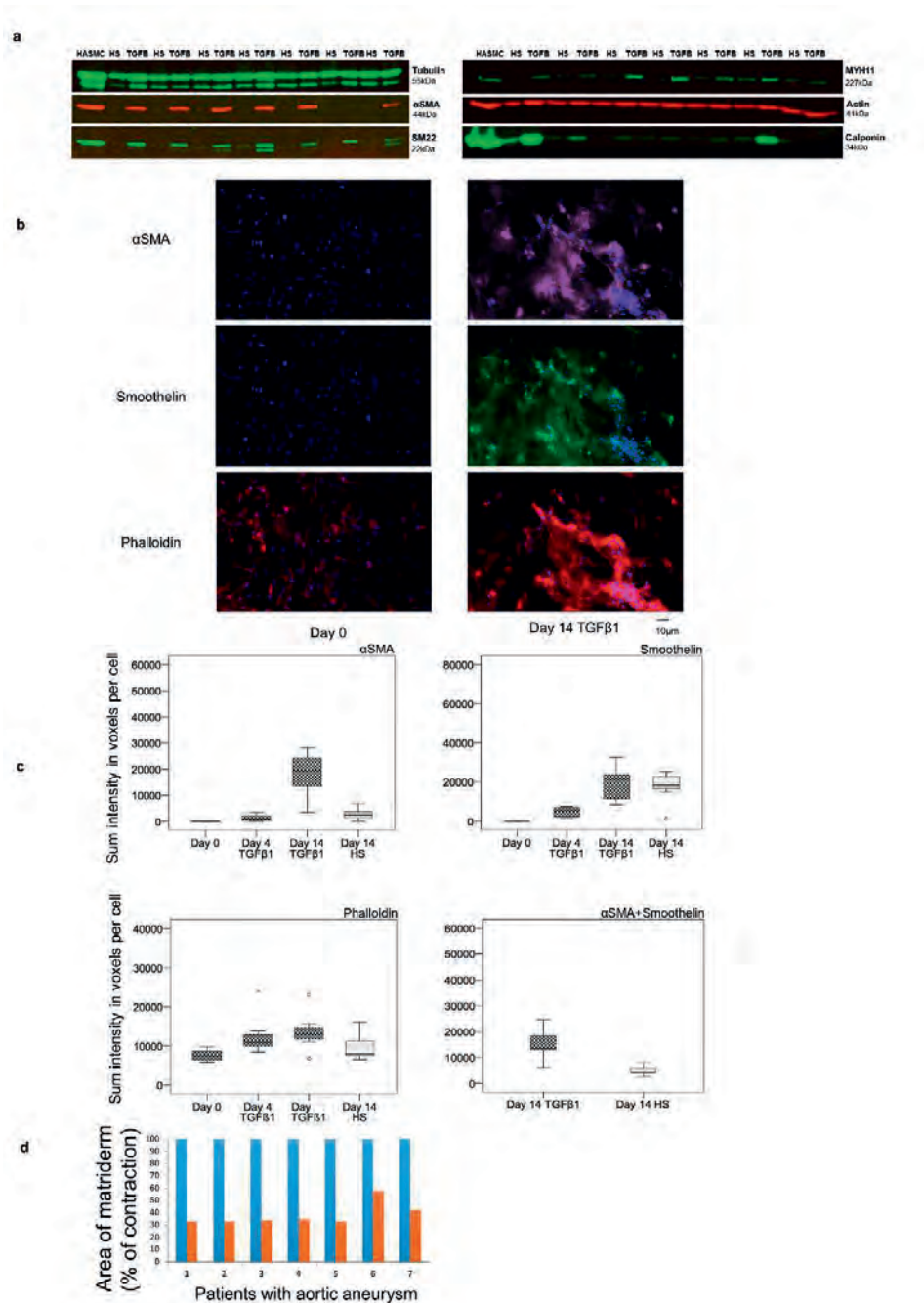


Figure 3. Transdifferentiation of dermal fibroblasts to SMC in fibroblasts obtained from aneurysm patients with a mutation in *MYH11* or *ACTA2*. (a) Western blot analysis of α SMA in the following patients from left to right: 3,5,4,6,1,2,7 (upper left image), SM22 (lower left image), MYH11 (upper right image) and Calponin (lower right image). HS=dermal fibroblasts in horse serum (HS) after 14 days, TGF β = transdifferentiated SMC-like cells in TGF β 1 after 14 days. HASMC = human aortic smooth muscle cells. High levels of α SMA and Calponin were seen on western blot after 14 days in the transdifferentiated SMC-like cells. (b) Representative images of quantitative immunofluorescence analysis. Images of α SMA (Cy5;purple), Smoothelin (FITC;green), Phalloidin (Cy3;red) and DAPI (blue;nuclei) of dermal fibroblasts after 14 days in HS (left image) and of transdifferentiated SMC-like cells after 14 days (right image). Note the higher levels of α SMA, Smoothelin, Phalloidin of the transdifferentiated SMC-like cells. (c) Quantitative immunofluorescence analysis of the dermal fibroblast differentiation process to SMC-like cells (n=7) on day 0,4 and 14 in TGF β 1 compared to day 14 in HS. Y-axes represent sum intensity voxels per cell. Upper two panels: left: α SMA (day 14 TGF β 1 vs. day 14 HS;p=0.004), right: smoothelin (p=0.95). Lower two panels: left: F-actin formation (phalloidin;p=0.14), right: co-expression of α SMA and smoothelin (p=0.003). Only α SMA expression was significantly increased in transdifferentiated SMC-like cells after 14 days in TGF β 1. Also, the sum intensity of the voxels of Phalloidin and co-expression α SMA and smoothelin were lower in these transdifferentiated SMC-like cells of aneurysm patients if compared to the cells of the healthy controls (p=0.035 and p=0.006 respectively). (d) Area of the matriderm (y-axes;100 = normal not curled matriderm) at day 0 (blue bars) and day 14 (orange bars) of transdifferentiated SMC-like cells of the 7 patients with aortic aneurysm.

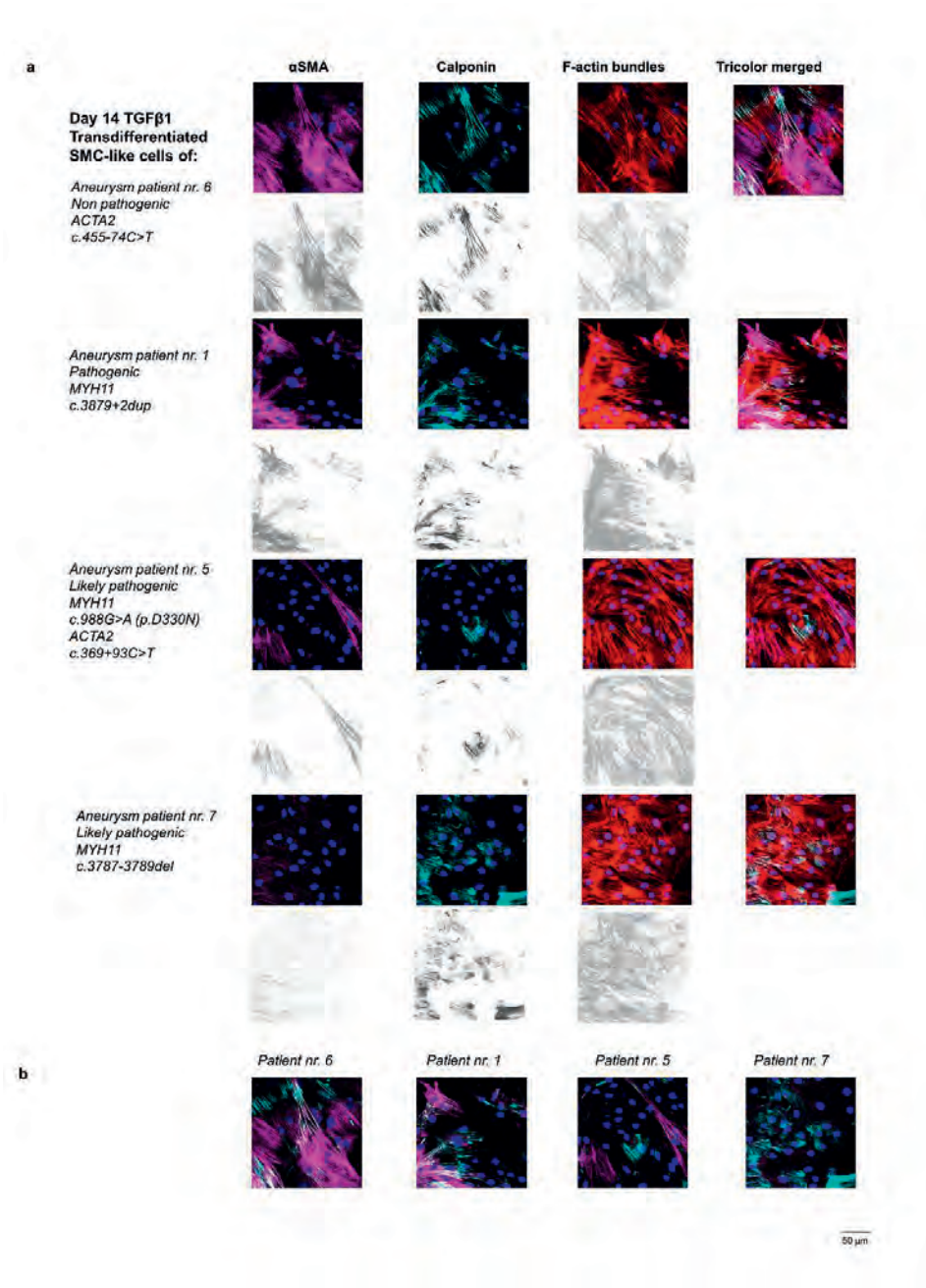


Figure 4. Images of cells from patients with an aortic aneurysm using a Leica TCS SP8 confocal scanning laser microscope system. (a) From left to right: Magenta channel (Cy5) = α SMA, Cyan channel (FITC) = calponin, red channel (Cy3) = phalloidin, representing F-actin fibers. Blue is DAPI, representing the nuclei. Most right image: tricolor merged image with DAPI. Under the color images, α SMA, calponin and phalloidin are presented in black respectively (without DAPI). (b) Colocalisation of Calponin (Magenta) and α SMA (purple). Note that in patient nr. 6 a higher amount of α SMA with Calponin was present when compared to the patients with a pathogenic (1) or likely pathogenic mutation (5 & 7).

Pathogenic and not pathogenic variants

After the transdifferentiation process of fibroblasts into SMC-like cells, the putative pathogenic effect of the variant was analysed by examining RNA splicing. We studied seven patients with variants in *MYH11* and/or *ACTA2*. In five patients (# 1-5) the variants were predicted by splice site prediction software programs (Alamut®) to have a likely or possible effect on RNA splicing, either by affecting the nearby splice site or by loss of exonic splice enhancer sequences (ESEs; Table 1). Patient #5 has two variants: a missense variant in *MYH11*, with loss of ESEs, and an intronic variant in *ACTA2* that creates a possible new splice donor site. Two patients (#6 and 7) have variants that are predicted to may have an effect on splicing affecting protein function.

The SMC-like cells were cultured with cycloheximide to inhibit nonsense mediated decay of mutant mRNA that may contain premature stop codons. The results of qPCR and sequence analysis of cDNA from mRNA of these cell cultures showed no effect on RNA splicing in patients 2-5 and 7. In patient 1 the qPCR product showed a double band on agarose electrophoresis (Fig. 5). Sequence analysis confirmed use of a cryptic splice donor site in exon 29, at position c.3802, resulting in an in frame deletion: p.Val1268_Gln1293del. This removes 26 amino acids from an evolutionary highly conserved sequence in the myosin tail domain. The extremely high content of charged amino acids in this region suggests an important function in protein-protein interactions. Moreover, the loss of 26 amino acid residues will yield a shorter protein that will hamper fibril formation. We therefore conclude that this variant has a pathogenic effect, most likely on fibril assembly.

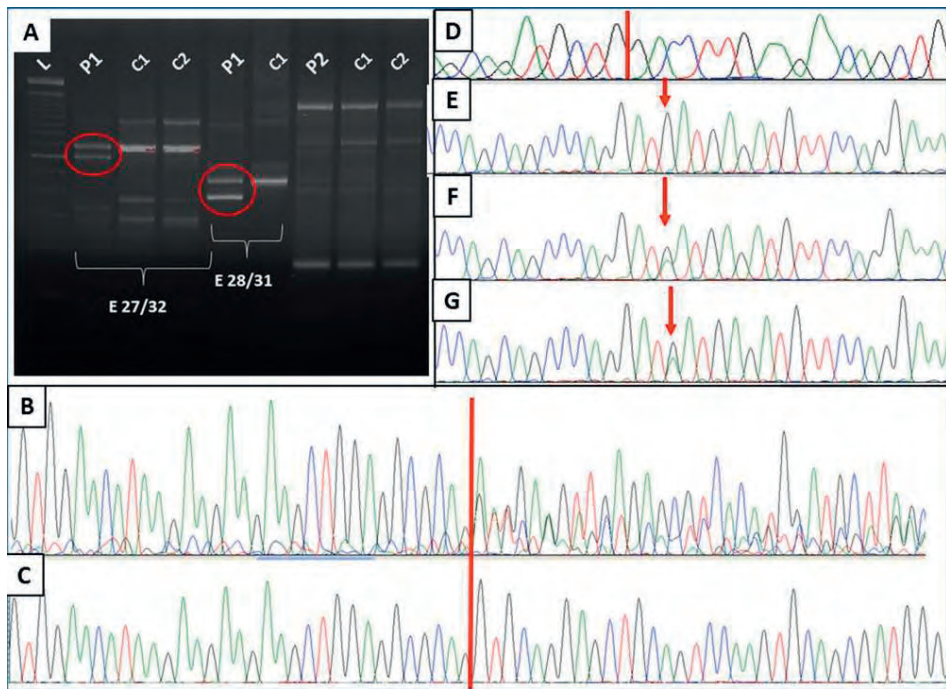


Figure 5. Predicted splice errors in *MYH11*. The possible effect of intronic as well as exonic mutations on splicing was studied in qPCR products of cDNA from cells cultured with cycloheximide. The possible effect of the mutations was predicted with Alamut® software. Agarose gel electrophoresis (A) shows double bands for patient 1 (P1) and not for controls (C1, C2).

The prediction score for the donor splice site of P1 is reduced with the intronic mutation c.3879+2dup in *MYH11*. Sequence analysis (B=P1; C=C1) shows a double sequence after position c.3803 (red line), representing sequence of exons 29 and 30. This confirms use of a cryptic splice site at position c.3803 in exon 29, resulting in p. Val1268_Gln1293del. This mutation can be classified as pathogenic. The background on the left side of the line (B) is caused by partial retention of intron 29. The c.2881-14C>G in *MYH11* (patient 2) was predicted to give a minor reduction in the already very low score for the splice acceptor site. The sequence of cDNA from cells cultured with cycloheximide (D; line indicates border of exon 23/24) showed no evidence of erroneous splicing, so this mutation can be classified as not pathogenic. E shows cDNA sequence of a control; F and G of patient 5 with and without cycloheximide. The mutation c.988G>A can be detected (arrows) and shows no difference with cycloheximide, so it has no effect on splicing or NMD.

The variants in patients 2, 3, 4 and 5 (*ACTA2*) can only have a pathogenic effect if they affect splicing of RNA. Because analysis of cDNA reveals no effect of these variants on RNA splicing, we conclude that these variants are not pathogenic.

The variant in patient 6, c.5819C>A (p.P1940Q), is a special case, because it is found in an exon that is subject to alternative splicing. Transcript NM_001040114.1 encodes the longest protein chain, but lacks exon 42, whereas transcripts NM_022844.2 and NM_001041113.1 both contain exon 42 and encode larger transcripts, but shorter proteins. From our cDNA analysis, it is clear that transcripts containing exon 42 are not expressed in SMC-like cells or primary SMC. We therefore concluded that the variant c.5819C>A in *MYH11* is not pathogenic and that variants in exon 42 are not relevant for familial thoracic AA.

The exonic *MYH11* variant, c.998G>A, in patient 5 has no effect on splicing, but is likely to have an effect on the protein. The variant is not found in the human variant databases and is predicted to be deleterious by prediction programs SIFT and Mutation taster, but not by Polyphen, because the latter only looks at polarity. The aspartic acid residue involved is evolutionary highly conserved and resides in the highly conserved myosin motor head domain with a high content of negatively charged amino acids (aspartic acid and glutamic acid) that are likely to be involved in protein-protein interactions. We consider this variant to be likely pathogenic.

The exonic *MYH11* in frame deletion variant, c.3787-3789del, in patient 7 has no effect on splicing, but is likely to have an effect on the protein. The variant is not found in the human variant databases. The current versions of mutation prediction software cannot handle inframe deletions; however, replacing the last lysine in the stretch of 5 lysines residues by the small uncharged glycine, is predicted to be deleterious by prediction programs SIFT and Mutation taster, and as probably damaging by Polyphen. The lysine residue involved is part of an evolutionary highly conserved stretch of 5 lysine residues and resides in the highly conserved myosin tail domain, which as described above is likely to have an important function in protein-protein interactions. We conclude that this variant is highly likely to be pathogenic.

Further analysis of the AA patients (number 1,5,7): with a determined and likely pathogenic *MYH11* variant showed high expression of *ACTN1* and SMC marker genes, when compared to the other AA patients. The high expression of these SMC markers may affect the contractile cytoskeleton organisation. When we examined the cells in higher magnification (Fig. 4), we only noticed slight differences of shorter or interrupted α SMA and calponin in the transdifferentiated SMC-like cells (AA patients number 1,5,7) when compared to the other AA-patients with a not proven pathogenic variant in *MYH11* or *ACTA2* and the transdifferentiated SMC-like cells from healthy controls.

DISCUSSION

We demonstrate a novel method for direct conversion of dermal fibroblasts into SMC-like cells within a two-week period. Interestingly, the converted cells can be used to investigate pathogenic variants on erroneous splicing in genes encoding proteins that build up the contractile apparatus of aortic SMC. This cannot be shown in fibroblasts, as these variants can only be investigated in cells expressing proteins that build up the SMC apparatus. From analyzing eight variants in *MYH11* or *ACTA2* in SMC-like cells, transdifferentiated from dermal fibroblasts from AA patients, we were able to classify five variants as definitely NOT pathogenic and three variants as (likely) pathogenic in 7 patients. Moreover, the pathogenic *MYH11* variants showed overexpression of contractile proteins accompanied by defective cytoskeleton formation with less contractile fibers in the transdifferentiated SMC. These results are important for diagnostic testing as well as research purposes.

With our presented protocol dermal fibroblasts of healthy volunteers and AA-patients were successfully transdifferentiated in SMC-like cells which expressed α SMA.²⁰ We confirmed that the converted cells also showed expression of the late SMC marker^{21,21} gene *CNN1* and upregulation of the late marker calponin and smoothelin by immunofluorescence staining.²² Our transdifferentiation protocol shows that TGF β 1 stimulation can induce myogenic transdifferentiation on matrigel which provides the proper microenvironment with elastin and collagen to allow nearly 90% transdifferentiation of dermal fibroblasts into SMC-like cells during which they invade the matrigel scaffold.

The results of qPCR and sequence analysis of cDNA of the SMC-like cells showed evidence of erroneous splicing for the *MYH11* variant c.3879+2dup. This variant does not affect the canonical splice donor site, but is predicted to give reduced efficiency. The qPCR and sequencing results show use of a cryptic splice site in exon 29 at position c.3802. This leads to an inframe deletion: c.3802_3879del (p. Val1268_Gln1293del). Although the variant c.2881-14C>G in *MYH11* is predicted to give a reduction of the efficacy of the splice acceptor site, qPCR and sequence analysis of cDNA after cycloheximide treatment showed no evidence of aberrant splicing. This shows that the transdifferentiated cells enable us to distinguish intronic variants as “definitely pathogenic” (c.3879+2dup) or “definitely not pathogenic” (c.2881-14C>G). Moreover, in two other AA patients a likely pathogenic effect on *MYH11* variant was observed: an effect on the protein-protein interaction and an effect of the variant of the deletion of one amino acid in an evolutionary conserved sequence. These pathogenic variants showed overexpression of contractile proteins and *ACTN*, but at the same time an abnormal contractile cytoskeleton formation. This could result in aortic aneurysm formation by defective SMC.²³ The actin-based modifications can lead to disturbance of the mechano-transduction complex. In previous studies Marfan patients showed more robust actin stress fiber formation,

which can increase the stiffness of tissues and can lead to aortic rigidity resulting in aortic aneurysm formation or dissections.²⁴ Our patient with a pathogenic *MYH11* variant also showed shorter calponin and α SMA fibers, resulting in a defective contractile cytoskeleton. The various identified mutations in the SMC contractile apparatus are predicted to disrupt SMC contractile function, leading to the hypothesis that disturbed SMC contractility may be the underlying cause of the disease.⁸ Disturbed SMC contractile function can lead to the weakening of the aortic wall by reducing its resilience to biomechanical forces consequently leading to aneurysm and rupture. Our results also show upregulation of the SMC gene expression in the RNA of the transdifferentiated SMC-like cells of patients with a *MYH11* variant, which can be the result of stimulation of the TGF β signaling pathway by TGF β 1. Transdifferentiation can be altered in patients with a *MYH11* or *ACTA2* variant, since stimulation of TGF β can activate stretch pathways and cause SMC disturbance. TGF β dysregulation has been associated with SMC contractility alterations as the SMC contractile apparatus is linked through the intermediate filaments to the cell surface integrins, which are known as regulators of TGF β activity.²⁵

The variant in *MYH11* or *ACTA2* was not proven pathogenic in 4 of the 7 patients in our study. No remarkable defective cytoskeleton was observed in SMC of these patients, however less co-localization of smoothelin and α SMA was still observed with a lower speed of contraction. This suggests that other, yet unidentified genetic variants in AA patients may contribute to the SMC contractility. We are currently developing more specific tests to investigate SMC contraction. If an (un)known mutation affects the mechanotransduction complex or the mechanical properties of the ECM, an aneurysm can develop.^{8,25} Transdifferentiated SMC-like cells provide perspectives for investigation in SMC morphology and contraction. It is possible to investigate SMC contraction and AA behavior without primary aortic SMC, which is of high significance since most patients currently undergo endovascular AA repair and aortic biopsy is a highly invasive procedure. In addition to investigating the functional impact of mutations and the role of SMC in aortic aneurysm development, transdifferentiated SMC-like cells also provide the possibility to perform mechanistic studies in other vascular diseases. In conclusion, we have shown that direct differentiation of human skin fibroblasts into SMCs is a suitable method for analysis on the mRNA level of unclassified variants in genes that are only expressed in SMC. For missense variants we need to develop additional functional tests.

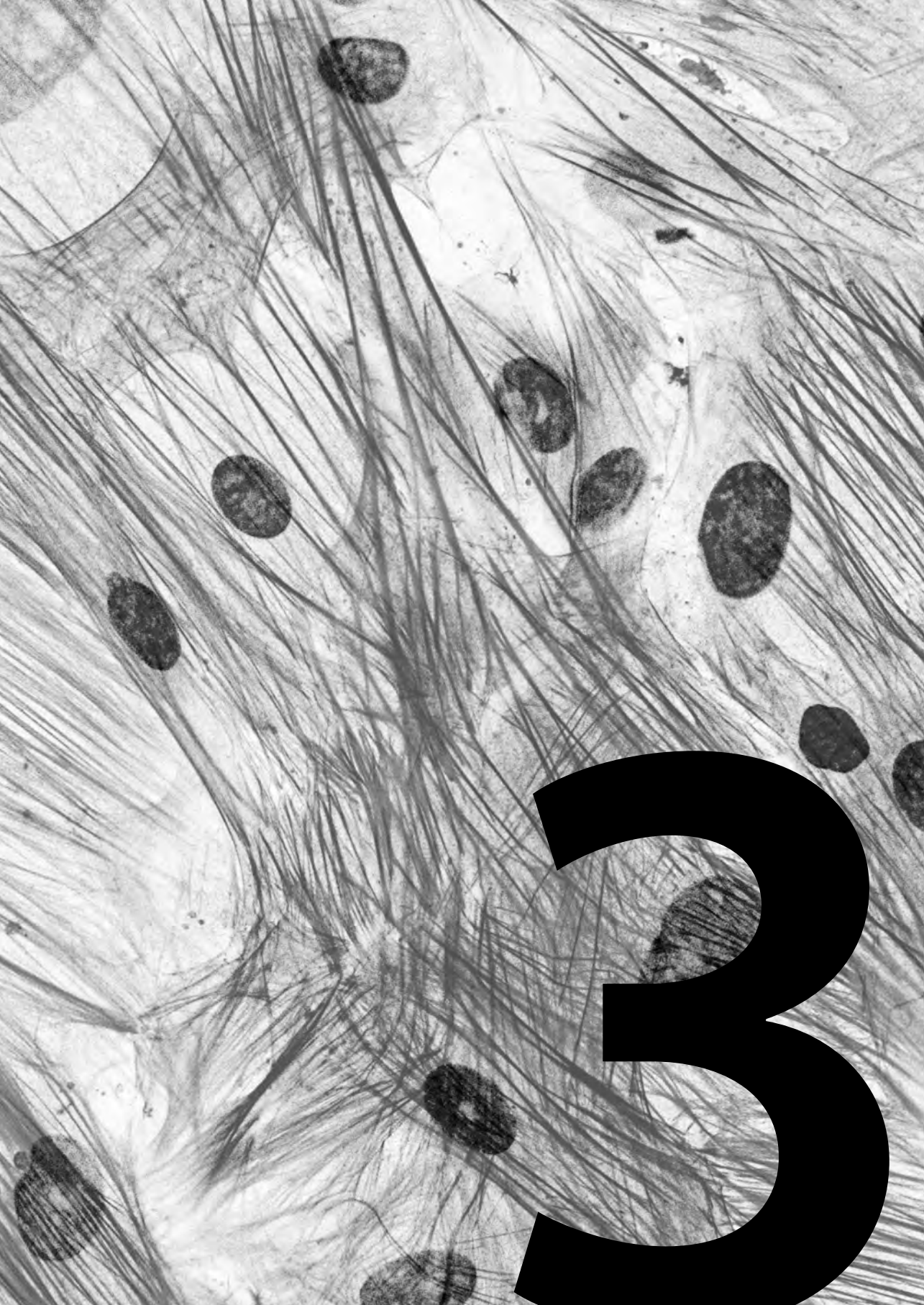
ACKNOWLEDGEMENTS

We like to show our appreciation for Jeroen Kole for his assistance in the use of the confocal microscope. We thank Youssef Moutaouakil for setting up the cell cultures.

REFERENCES

1. Gaudino M, Lau C, Munjal M, Girardi LN. Open repair of ruptured descending thoracic and thoracoabdominal aortic aneurysms. *J. Thorac Cardiovasc Surg* 2015; 150: 814-23.
2. Piffaretti G, Menegolo M, Kahlberg A, Mariscalco G, Rinaldi E, Castelli P, Grego F, Chiesa R, Antonello M. Hemothorax Management After Endovascular Treatment For Thoracic Aortic Rupture. *Eur J Vasc Endovasc Surg* 2015; Sep 8.
3. Eleftheriades JA, Farkas EA. Thoracic aortic aneurysm clinically pertinent controversies and uncertainties. *J Am Coll Cardiol* 2010; 55:841-57.
4. Robinson PN, Godfrey M. The molecular genetics of Marfan syndrome and related microfibrilopathies. *J Med Genet* 2000; 37:9-25.
5. van Dijk FS, Meijers-Heijboer H, Pals G. Angiotensin II blockade in Marfan's syndrome. *N Engl J Med* 2008; 358: 2787-95.
6. MacCarrick G, Black JH 3rd, Bowdin S, El-Hamamsy I, Frischmeyer-Guerrerio PA, Guerrerio AL, Sponseller PD, Loeys B, Dietz HC 3rd. Loeys-Dietz syndrome: a primer for diagnosis and management. *Genet Med* 2014; 16:576-87.
7. Cancrinus E, Hoksbergen AW, Pals GJ, Wisselink W, Yeung KK. Loeys-Dietz syndrome: aortic dissections and aneurysms. *Ned Tijdschr Geneesk* 2015; 159:A8342.
8. Milewicz DM, Guo DC, Tran-Fadulu CL, Inamoto S, Kwartler Genetic basis of thoracic aortic aneurysms and dissections: focus on smooth muscle cell contractile dysfunction. *Annu Rev Genomics Hum Genet* 2008; 9:283-302.
9. Pannu H, Tran-Fadulu V, Papke CL, Scherer S, Liu Y, Presley C, Guo D, Estrera AL, Safi HJ, Brasier AR, Vick GW, Marian AJ, et al. MYH11 mutations result in a distinct vascular pathology driven by insulin-like growth factor 1 and angiotensin II. *Hum Mol Genet* 2007; 16:2453-2462.
10. Guo DC, Pannu H, Tran-Fadulu V, Papke CL, Yu RK, Avidan N, Bourgeois S, Estrera AL, Safi HJ, Sparks E, Amor D, Ades L, et al. Mutations in smooth muscle alpha-actin (ACTA2) lead to thoracic aortic aneurysms and dissections. *Nat Genet* 2007; 39: 1488-93.
11. Dash BC, Jiang Z, Suh C, Qyang Y. Induced pluripotent stem cell-derived vascular smooth muscle cells: methods and application. *Biochem J* 2015; 465:185-94.
12. Polo, J. M. & Hochedlinger, K. When fibroblasts MET iPSCs. *Cell Stem Cell* 2010;
13. Nawy T. Transdifferentiation from the top. *Nat Methods* 2015;12:701.
14. Kurian L, Sancho-Martinez I, Nivet E, Aguirre A, Moon K, Pendaries C, Volle-Challier C, Bono F, Herbert JM, Pulecio J, Xia Y, Li M, et al. Conversion of human fibroblasts to angioblast-like progenitor cells. *Nat Methods* 2013;10:77-83.
15. Ladewig J, Koch P, Brüstle O. Leveling Waddington: the emergence of direct programming and the loss of cell fate hierarchies. *Nat Rev Mol Cell Biol* 2013; 14:225-36.
16. Lawson MA, Purslow PP. Differentiation of Myoblasts in Serum-Free Media: Effects of Modified Media Are Cell Line-Specific. *Cells Tissues Organs* 2000; 167:130-7.
17. Lijnen P, Petrov V, Rumilla K, Fagard R. Transforming growth factor-beta 1 promotes contraction of collagen gel by cardiac fibroblasts through their differentiation into myofibroblasts. *Methods Find Ex. Clin Pharmacol* 2003; 25:79-86.
18. Lannoy M, Slove S, Jacob MP. The function of elastic fibers in the arteries: beyond elasticity. *Pathol Biol* 2014; 62:79-83.
19. Hur GY, Seo DK, Lee JW. Contracture of skin graft in human burns: effect of artificial dermis. *Burns* 2014; 40:1497-503.
20. Arciniegas E, Sutton AB, Allen TD, Schor AM. Transforming growth factor beta 1 promotes the differentiation of endothelial cells into smooth muscle-like cells in vitro. *J Cell Sci* 1992. 103:521-529.
21. Hungerford JE, Little CD. Developmental biology of the vascular smooth muscle cell: building a multilayered vessel wall. *J Vasc Res* 1999; 36:2-27.
22. Hautmann MB, Adam PJ, Owens GK. Similarities and differences in smooth muscle alpha-actin induction by TGF-beta in smooth muscle versus non-smooth muscle cells. *Arterioscler Thromb Vasc Biol* 1999; 19:2049-58.
23. Wang L, Guo DC, Cao J, Gong L, Kamm KE, Regalado E, Li L, Shete S, He WQ, Zhu MS, Offermanns S, Gilchrist D, et al. Mutations in myosin light chain kinase cause familial aortic dissections. *Am J Hum Genet* 2010; 87:701-707.
24. Crosas-Molist E, Meirelles T, Lopez-Luque J, Serra-Peinado C, Selva J, Caja L, Gorbenco del Blanco D, Jose Uriarte J, Bertran E, Mendizabal Y, Hernandez V, Garcia-

- Calero C, Busnadiago O, et al. *Arterioscler Thromb Vasc Biol* 2015; 35:960-72.
25. Gillis E, Van Laer L, Loeys BL. Genetics of thoracic aortic aneurysm: at the crossroad of transforming growth factor- β signaling and vascular smooth muscle cell contractility. *Circ Res* 2013; 113:327-40.



Molecular phenotyping and quantitative assessment of effects of pathogenic variants in aneurysm genes ACTA2, MYH11, SMAD3 and FBN1.

Natalija Bogunovic+, Joyce Burger+, Hiu Liu, Arne Ijpma,
Timo ten Hagen, Dimitra Micha, Danielle Majoor-Krakauer,
Ingrid van der Pluijm, Jeroen Essers*, Kak K. Yeung*

+ These authors contributed equally.

* These authors contributed equally.

Manuscript in Preparation

ABSTRACT

Aortic aneurysms (AA) are pathological dilatations of the aortic wall. The natural course of the disease is to grow and rupture; ruptured AA are associated with a mortality rate of up to 80% due to life threatening internal bleeding. Certain patients develop an aneurysm due to genetic mutations, often associated with the functioning of vascular smooth muscle cells (VSMC). A number of genes associated with AA development has been identified, primarily encoding proteins that are involved in TGF β signaling, contractile machinery and proper organization of the extracellular matrix (ECM). However, only a small proportion of variants in causes a pathogenic variant in the protein, and subsequently aortic aneurysm formation. Our goal was to identify a robust functional assay to confirm the effects of (pathogenic) variants in aneurysm causing genes associated with thoracic and abdominal aortic aneurysms. Since VSMC can only be obtained during invasive surgery, we used a transdifferentiation protocol previously developed by our group. We performed TGF β induced transdifferentiation of skin fibroblasts of controls and patients with a mutation in cytoskeleton contractility (ACTA2, MYH11), TGF β signaling (SMAD3) and a dominant negative (DN) and missense variants (HI) in the extracellular matrix (FBN1). We analyzed the transdifferentiation potential, structural integrity of the cytoskeleton, TGF β signaling profile as well as migration velocity and maximum contraction. TGF β induced transdifferentiation was strongly reduced in the SMAD3 and FBN1 DN cells. ACTA2 and FBN1 DN patient cells showed a decrease in Smad2 phosphorylation. Migration velocity was impaired for ACTA2 and MYH11 patient cells. Additionally, ACTA2 cells showed reduced contractility. Concluding, transdifferentiation potential is a clear first readout as cells with a pathogenic SMAD3 or FBN1 DN variant do not produce SMA after TGF β stimulation. Assays based on functionality, e.g. migration or contractility, could distinguish cells with pathogenic variants in ACTA2 and MYH11 from controls. Therefore, we conclude that effects from pathogenic variants in cytoskeleton, TGF β pathway and ECM aneurysm genes can be identified based on functional readouts.

INTRODUCTION

Aortic aneurysms are pathological dilatations of the aorta that are life-threatening in case of rupture. Aortic aneurysms can occur in the thoracic as well as the abdominal aorta and both show a clear genetic predisposition {Ziganshin, 2015 #21}{van de Lijtgaarden, 2015 #6}. Aortic aneurysms may arise from a variety of pathogenic gene variants encoding structural components of ECM, cytoskeletal/smooth muscle contraction proteins, and proteins associated with TGF β pathway. Pathogenic variants in the cytoskeleton/contractile proteins may lead to altered contractility of vascular smooth muscle cells (VSMCs), caused by structural defects or imbalance of regulatory proteins. Known affected proteins in this group are α -smooth muscle actin (ACTA2), myosin heavy chain 11 (MYH11), myosin light chain kinase (MYLK) and cGMP-dependent protein kinase 1 α isozyme (PRKG1) {Guo, 2007 #16;Zhu, 2006 #27;Wang, 2010 #17;Guo, 2013 #51}. The TGF β signaling group consists of proteins that are involved in the TGF β pathway. Pathogenic variations in genes encoding these proteins will lead to either increased or decreased signaling of this pathway. Altered TGF β pathway genes related to aneurysm formation are TGFBR1, TGFBR2, TGFB2, TGFB3, SMAD2 and SMAD3 {Loeys, 2005 #38;Loeys, 2006 #39;Mizuguchi, 2004 #40;Lindsay, 2012 #11;Boileau, 2012 #43;Rienhoff, 2013 #44;Matyas, 2014 #45;Bertoli-Avella, 2015 #12;van de Laar, 2011 #10;van de Laar, 2012 #42}. Pathogenic variants in proteins associated with the extracellular matrix (ECM) lead to improper assembly of the ECM. This results in aneurysm formation due to loss of cell attachment, loss of elasticity and strength, and the inability to retain latent TGF β . Known proteins in this group include fibrillin-1 (FBN1), collagen type 3 α 1 (COL3A1), elastin (ELN), fibulin-4 (EFEMP2) and lysyl oxidase (LOX) {Dietz, 1991 #9;Milewicz, 1994 #13;Pepin, 2000 #31;Schwarze, 2001 #32;Plancke, 2009 #33;Zhang, 1999 #28;Tassabehji, 1998 #29;Szabo, 2006 #30}{Huchtagowder, 2006 #22;Dasouki, 2007 #23;Lee, 2016 #151;Guo, 2016 #152}.

VSMCs are embedded between elastic laminae in the medial layer of the aorta. Both the VSMCs and elastic laminae are important components in maintaining of the elasticity and contractility of the aorta. During aneurysm formation the medial layer is often degraded which leads to reduced elasticity and contractility {Thompson, 1997 #419}. To study biological and molecular consequences of aneurysm formation, VSMCs can be isolated from aortic tissue retrieved from open surgery. However, this cannot be performed purely for research purposes. To research aneurysm related VSMC defects, dermal fibroblasts from can be transdifferentiated into VSMC-like cells within a 2-week duration using 5 ng/ml TGF β 1 on a scaffold containing collagen and elastin or coverslips. The induced VSMC-like cells are comparable to primary human aortic SMC in mRNA expression of SMC markers α -SMA, SM22 and Calponin {Yeung, 2017 #149}.

A number of variants in aneurysm causing genes cannot be classified based on existing classification systems{Plon, 2008 #420}{Li, 2017 #407}{Richards, 2015 #408}{den Dunnen, 2016 #409} and remain a variant of unknown clinical significance (VUS). To assess VUS, a set of functional assays is needed to identify the (pathogenic) effect of causative gene variants for aortic aneurysms. The aim of this study is to develop these novel functional assays with robust read outs for the effects of pathogenic variants in four aneurysm genes (ACTA2, MYH11, SMAD3, FBN1 haploinsufficient and dominant negative) based on transdifferentiation of skin fibroblasts of aneurysm patients. These functional assays could help to reclassify VUS into nonpathogenic and pathogenic, based on their effect on the protein they encode. This could be a valuable diagnostic tool used to predict the effect of these genes on aneurysm formation in patients who have not yet undergone surgery.

MATERIALS AND METHODS

Patient cells and characteristics

Primary dermal fibroblasts of aneurysm patients from the biobanks of the departments of Clinical Genetics (Amsterdam University Medical Center - location VU and Erasmus University Medical Center) were used for all experiments. Fibroblasts were cultured in Dulbecco's Modified Eagle's Medium (DMEM, Lonza BioWhittaker) supplemented with 10% fetal calf serum (FCS) and 1% penicillin/streptomycin (PS) at 37°C with 5% CO₂. Human fibroblasts of healthy controls and aneurysm patients with heterozygous mutations in ACTA2 (cytoskeleton), MYH11 (cytoskeleton), SMAD3 (TGFβ signaling) and FBN1 (extracellular matrix) were used for all experiments (see Table 1 for patient mutations). These mutations were all class 5 mutations and predicted pathogenic by Alamut Visual, a decision-support software for genomic variant diagnostics.

Table 1. Gene, cell line, pathogenic variant and location of the affected protein.

Gene	Cell line	Pathogenic variant	Expected effect on protein	Cellular process
<i>ACTA2</i>	ACTA2 #1	c.445C>T, p.R149C	Missense mutation, could affect the binding sites of the protein due to the disappearance of a positive amino acid load	Cytoskeleton contractility
<i>MYH11</i>	MYH11 #1	c.3879+2dup, p.1260 of 1945 amino acids present	Frameshift, premature stop codon. Effects on the protein are currently unknown but could include reduced protein levels	Cytoskeleton contractility
<i>SMAD3</i>	SMAD3 #1	c.859C>T, p.R287W	Missense mutation, potential loss of H-bridges at interacting site that leads to reduced SMAD3/SMAD4 complex stability	TGF β signaling
<i>FBN1</i>	FBN1 #1	c.2369insC, p.717 of 2872 amino acids present	Frameshift, premature stop codon resulting in haploinsufficiency	Extracellular matrix organization
	FBN1 #2	c.2851insG, p.846 of 2872 amino acids present	Frameshift, premature stop codon resulting in haploinsufficiency	Extracellular matrix organization
	FBN1 #3	c.2132G>A, p.C711Y	Missense mutation in the TGF β binding protein like domain that could affect binding to fibrillin-1 and results in a dominant negative effect on the protein	Extracellular matrix organization

Transdifferentiation

Fibroblasts were seeded at a density of 2,5 million cells/ml, as previously described {Yeung, 2017 #149}. Fibroblasts were seeded in DMEM with 10% FCS and 1% penicillin/streptomycin at a density of 2,5 million cells/ml on the corners of a 1cm² piece of matrigel (Matrigel, Corning). Two days after seeding, the medium was changed to DMEM supplemented with 2% heat-inactivated fetal calf serum, 1% PS and 5ng/ml human recombinant TGF β 1 (4342-5, Biovision). Heat-inactivation was performed by placing the FCS in a 56°C water bath for 30 minutes and mixing

regularly. Medium supplemented with TGF β 1 was changed every 4 days. After 14 days, the cells were enzymatically extracted from the matriderm with the use of a collagenase solution in complete medium (2000IU/ml, Worthington) at 37°C on a shaker for 3 hours. Centrifugation was performed to remove remainders of the collagenase and cells were transferred to new flasks and cultured for further experiments. After transdifferentiation cells will further referred to as VSMC-like cells. Passage number after transdifferentiation was kept below 5 to prevent loss of transdifferentiation markers, and cells were kept in DMEM with 10% FCS and 1% penicillin/streptomycin.

RNA isolation and real-time PCR

Fibroblasts were seeded in triplicate per condition in 12-well plates at a density of 100.000 cells/well. After two days day 0 samples were taken and medium was changed to DMEM supplemented with 2% heat-inactivated fetal calf serum, 1% PS and 5ng/ml human recombinant TGF β 1 (4342-5, Biovision) for the transdifferentiation samples. TGF β supplemented medium was changed every 4 days and after 14 days RNA was isolated.

RNA was isolated with the RNeasy mini kit (Qiagen). cDNA was made with iScript cDNA synthesis kit (Biorad) according to manufacturing protocol. q-PCR was performed with 200 nM forward and reverse primers and iQTM SYBR® Green Supermix (Biorad) on the CFX96 system (Biorad); denaturation at 95°C for 3min, 40 cycles denaturation at 95°C for 15 s, annealing/extension at 55°C for 30 s. TBP was used as reference gene. Relative gene expression levels were determined with the comparative Ct (also referred to as $\Delta\Delta$ Ct) method according to the MIQE guidelines. See Table 2 for primers used to detect gene of interest expression.

Table 2. Primer sequences for qPCR.

Gene name	RefSeq	Fw and rev primer seq
<i>YWHAZ</i>	NM_145690	GATGAAGCCATTGCTGAACCTG CTATTTGTGGGACAGCATGGA
<i>TBP</i>	NM_003194	AGTTCTGGGATTGTACCGCA TCCTCATGATTACCGCAGCA
<i>ACTA2</i>	NM_001141945	ACTGGGACGACATGGAAGAAG CATACATGGCTGGGACATTG
<i>CNN1</i>	NM_001308341	GCCCAGAAGTATGACCACCA TGATGAAGTTGCCGATGTTG
<i>SMTN</i>	NM_001207018	TGGAGGAATTGACTGCACTG GAAACCTCTGCCTGCTGTTG
<i>TAGLN/SM22</i>	NM_001001522	AAGAATGATGGGCACTACCG AGCCCTCTCCGCTCTAACTG

Immunofluorescent staining

Dermal fibroblasts were seeded on 18mm coverslips in 12-well plates with a density of 100.000 cells/well in DMEM with 10% FCS and 1%PS. Two days after seeding the medium was changed to DMEM supplemented with 2% heat-inactivated fetal calf serum, 1% PS and 5ng/ml human recombinant TGF β 1 (4342-5, Biovision). TGF β supplemented medium was changed every 4 days and after 14 days cells were fixed with 2% paraformaldehyde in PBS for 15 minutes. After fixation cells were washed with PBS supplemented with 0,1% Triton X-100 and blocked with PBS+ (0,5% BSA and 0,15% glycine in PBS) for 30 minutes. Primary antibodies were incubated overnight at 4°C in PBS+; mouse monoclonal anti-smooth muscle actin (SMA) (1:1000, ab7817, Abcam) and rabbit polyclonal anti-SM22 (1:400 ab14106, Abcam). Cells were washed with PBS supplemented with Triton-X100 and incubated shortly with PBS+ prior to incubation with the secondary antibody in PBS+ (1:1000, anti-mouse Alexa Fluor 488 and anti-rabbit Alexa Fluor 594, Molecular Probes) for 1 hour at room temperature. Simultaneously, actin filaments were stained with SiR-Actin (1:1000, Cytoskeleton). After incubation coverslips were mounted on glass slides with Vectashield supplemented with DAPI (H-1200, Vector laboratories) and sealed with nail polish. Images were recorded on a wide field epifluorescent microscope (Axio Imager D2, Zeiss).

Quantification of the immunofluorescent signal was performed by calculating the corrected total cell fluorescence (CTCF) of SMA and actin. The CTCF of actin and SMA was determined by setting a color threshold to select the fibers in the image with Fiji image analyzing software {Schindelin, 2012 #133} and determining the integrated density of this area (intensity of the fluorescence). This measurement was corrected for the background fluorescence and the total area of the fibers and results in the CTCF. The percentage of fluorescence is then calculated by dividing the SMA CTCF and actin CTCF to determine what percentage of the actin cytoskeleton is positive for SMA compared to the total actin cytoskeleton.

Cytoskeletal fiber organization was assessed by measuring anisotropy on microscopic images using FibrilTool plug-in in Fiji {Boudaoud, 2014 #403}. The anisotropy coefficient ranges from zero to one; parallel lines result in an anisotropy coefficient of one, whereas nonparallel structures have an anisotropy coefficient close to zero. The alignment of F-actin and SMA fibers was assessed in confocal images of transdifferentiated cells of controls and patients with a mutation. According to the published protocol, X-Y fields of view were marked as regions of interest (ROI), and anisotropy was quantified within those regions.

Western blotting

VSMC-like cells were seeded at 100.000 cells/6-well and allowed to attach for 48 hours. Cells were scraped in PBS supplemented with protease inhibitor cocktail (1:100, 11836145001, Roche applied science) and phosphatase inhibitor cocktail (1:100, P0044, Sigma) and lysed in equal volumes of 2x Laemmli buffer (4% SDS, 20% glycerol, 120mM Tris pH 6,8) supplemented with protease inhibitor cocktail and phosphatase inhibitor. Lysates were cleared of large DNA by passing through a 25G needle and then heated to 65°C for 10 minutes. Protein concentrations were measured with the Lowry protein assay {Lowry, 1951 #135}. Equal amounts of protein were size separated by SDS-PAGE and separated proteins were then transferred to a PVDF membrane (1hour, 100V, Immobilon). Membranes were blocked for 1 hour at room temperature by either 5% BSA or 3% milk in PBS supplemented with 0,1% Tween-20. Membranes were incubated 45 minutes at room temperature with primary antibody (see Table 3 for primary antibodies). Membranes were washed 5 times with 0.1% Tween-20 in PBS and then incubated with horseradish peroxidase-conjugated secondary antibodies (1:2,000, Jackson ImmunoResearch) for 1 hour at room temperature. Bound secondary antibodies were detected with an Amersham Imager 600 (GE Healthcare Life Sciences) using chemiluminescence. Band intensity was quantified using Fiji image analyzing software {Schindelin, 2012 #133}. Number of replicates is specified in the figure legends. Results are presented as mean \pm SD, figures also include the mean of the controls (dashed grey line) and the 2xSD range of the controls (dotted black line).

Table 3. Primary antibodies.

Primary antibody	Predicted kDa	Dilution	Manufacturer	Catalog number
Rabbit α -SM22 IgG	23	1:2000	Abcam	Ab14106
Mouse α -SMA IgG2a	40	1:10.000	Abcam	Ab7817
Rabbit α -pSMAD2 IgG	55-60	1:400	Merck Millipore	04-953
Rabbit α -SMAD2 IgG	60	1:1000	Cell signaling	5339S
Mouse α - β catenin IgG1	92	1:2000	BD Bioscience	610153

TGF β stimulation

TGF β stimulation was performed to determine the sensitivity of control and patient fibroblasts to TGF β . Fibroblasts were seeded in DMEM supplemented with 10% FCS and 1% PS in 6-well plates to reach confluence and were allowed to attach for 24 hours. The following day, medium was changed to DMEM supplemented with 1% PS and fibroblasts were serum deprived for 24 hours prior to TGF β stimulation. Protein samples were collected after 0 minutes, 15 minutes, 30 minutes, 1 hour and

4 hours of stimulation with TGFβ1 (5 ng/ml; 4342-5, Biovision). Lysis of cells and western blotting was performed as previously described. Membranes were incubated overnight at 4°C with primary antibody (see Table 3 for primary antibodies).

Ring barrier migration assay

To measure the migration length and efficiency, a ring barrier migration assay was performed [Das, 2015 #155]. In this assay a barrier is placed in a cell culture chamber that prevents cells from entering the cell-free area. VSMC-like cells are seeded outside of this barrier and form a monolayer prior to the removal of the barrier. Upon removal of the barrier VSMC-like cells can migrate into the cell-free area and migration can be monitored. Migration parameters such as total and effective migration can be monitored. Migration velocity can be calculated based on total migration and the duration of the experiment. 50.000 VSMC-like cells were seeded in the outer ring of the set-up and were allowed to attach for 24 hours. After removing the ring barrier, cells were washed twice with DMEM supplemented with 1% PS (serum free) and were left in this medium during migration to prevent cell division. Multiple locations at the migration front were selected to monitor movement. Every 10 minutes pictures were taken at the selected locations for 24 hours. Data was analyzed with the axiovision software (version 4.5.0.0) by measuring the total migration length of multiple cells and calculating the migration velocity.

Measuring cell contraction

Cell contraction was measured and calculated according to previously published protocol [Bogunovic, 2019 #256]. VSMC-like cells were seeded in duplicate in the array at a density of 30.000 cells/well in a sterile 96 well plate array well (96w10; Ibidi, Planegg, Germany). Cells were cultured for 48 hours prior to stimulation. The impedance was recorded at a frequency of 4000 Hz.

VSMC-like cells were stimulated with 10 µg/ml ionomycin (Sigma Aldrich, Darmstadt, Germany). Contractile responses were measured in duplicate in each experiment. Contraction (C) of each well equals one minus the ratio between the resistance post- (Pos) and pre-stimulation (PrS) post empty well value subtraction, as depicted in equation 1:

$$C = \left(1 - \frac{(Pos[\Omega] - 290[\Omega])}{(PrS[\Omega] - 290[\Omega])}\right) \cdot 100$$

Equation 1: Formula for the calculation of VSMC-like cells contractile response.

The change in contraction was recorded and expressed as maximum contraction. To characterize the contractile output of the patients, the mean response of the

control group was used as a reference. Contraction of the patient VSMC-like cells was compared to a range between 2xSD above and below the mean contractile response of the control group.

Statistics

Number of experiment replicates and independent samples are stated in the figure legends. Data were corrected for outliers with the Grubbs' test for outliers. Statistical analysis was performed with a non-parametric Mann-Whitney test. Significance was tested 2-tailed against the mean of the controls. Significance in gene expression analysis of stimulated controls was tested 2-tailed against unstimulated controls. A p-value <0,05 was considered to indicate a significant difference between groups. In the figures p<0,05 is shown with *, p<0,01 with **, p<0,001 with #. Results are expressed as mean \pm SD, real-time PCR results are expressed as geometric mean \pm geometric SD. All analyses were performed using Graphpad, version 7.03.

RESULTS

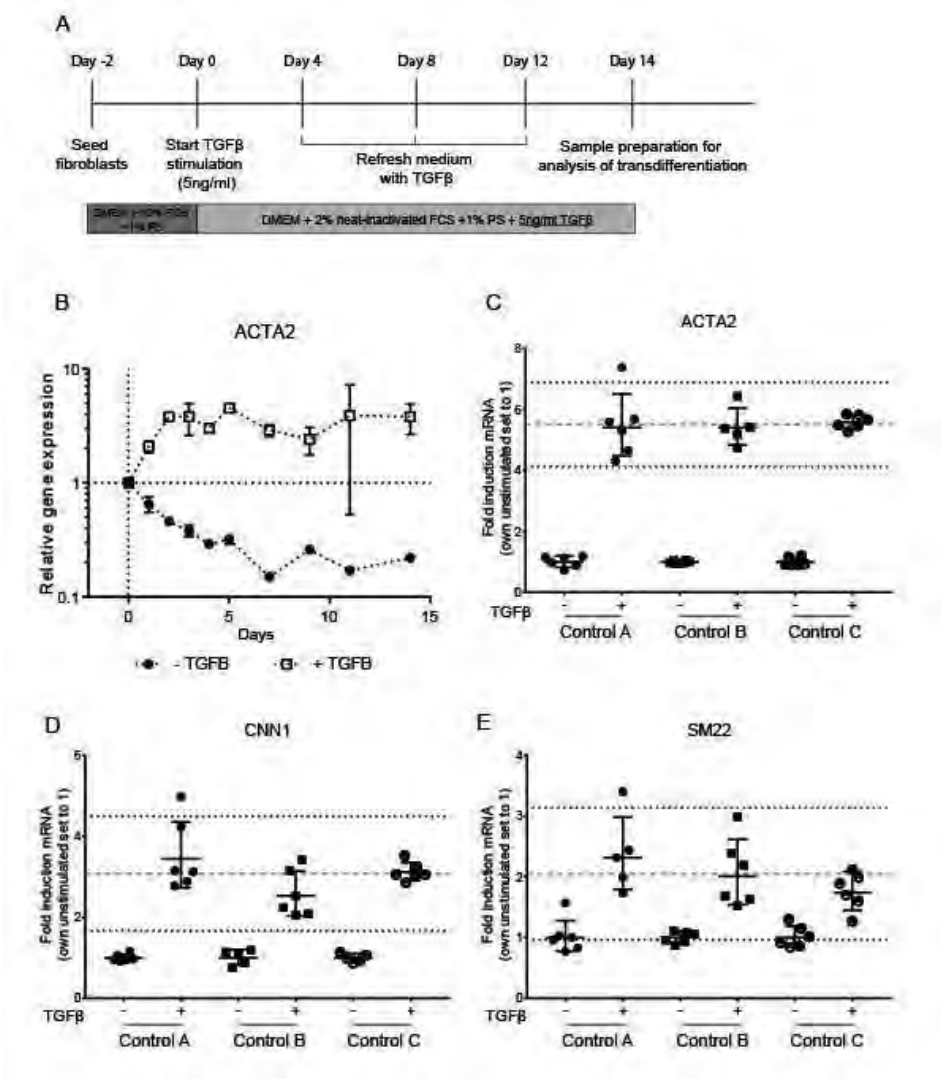
Assessment of baseline measurements for control VSMC-like cells

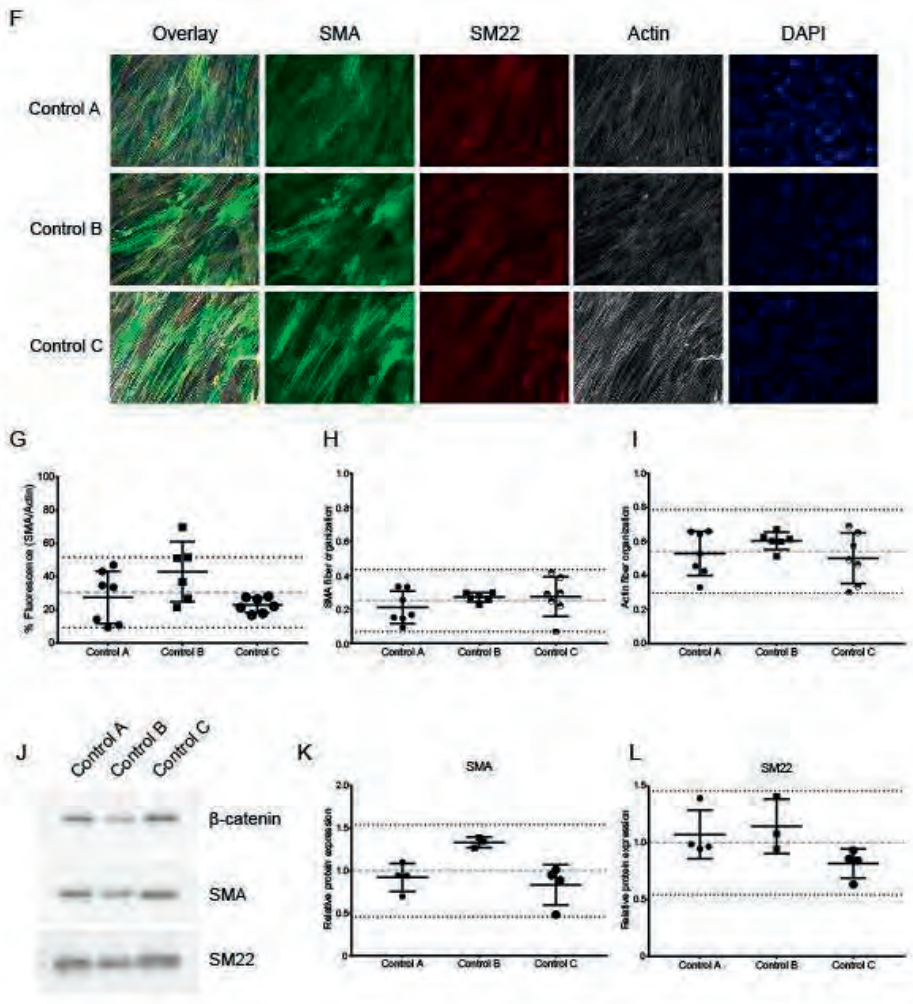
A schematic overview of the transdifferentiation protocol is given in figure 1A. Transdifferentiation was initiated by replacing the culture medium from DMEM supplemented with 10% FCS and 1% PS with DMEM supplemented with 2% heat-inactivated serum, 1% PS and 5ng/ml TGF β 1. According to previous protocols {Yeung, 2017 #149}, medium was refreshed every 4 days and TGF β stimulation was performed for 14 days. Efficiency of transdifferentiation was determined by analyzing the RNA expression level of genes that are specifically expressed in vascular smooth muscle cells (VSMCs, Table 2). A 4,5-fold increased expression of ACTA2 was measured within 5 days after addition of TGF β 1 and expression levels continued to rise until the end of the experiment (14 days) (Fig. 1B).

We determined the induction of ACTA2 gene expression in three healthy control fibroblast cell lines to analyze the variability in fold change expression and determine a baseline for comparison with the patients. On average, a consistent 5,5-fold induction of ACTA2 gene expression was measured in all controls after 14 days of TGF β stimulation (Fig 1C). CNN1 gene expression was 2,5-3,5 fold and SM22 1,8-2,2 fold increased after 14 days of TGF β stimulation. The expression of both genes showed considerably more variation compared to ACTA2 upregulation (Fig. 1D and E).

Subsequently we determined the transdifferentiation potential by analyzing the protein expression level of SMA and SM22 by immunofluorescence and western blot analysis. Supplementary figure 1 shows a comparison of fibroblasts prior to stimulation and VSMC-like cells after TGF β stimulation for 14 days.

Immunofluorescence staining after 14 days of transdifferentiation showed that all control fibroblast cell lines are positive for SMA which is organized in elongated cytoplasmic SMA fibers stretched throughout the cell. Induction of SMA shows variability between the control cell lines (Fig. 1F). Positive staining for SM22 and actin was observed in all control cell lines. To quantify the amount of SMA fiber fluorescence intensity, we determined the ratio between SMA fibers to the total actin content in the cytoplasm. The transdifferentiated controls showed an overlay of approximately 30% of SMA fiber fluorescence with total actin, with the 2xSD range running from 9% to 51% (Fig. 1G). Anisotropy, and thereby organization, of the SMA fibers was quantified in control VSMC-like cells. The anisotropy coefficient ranges from zero to one; parallel lines result in an anisotropy coefficient of one, whereas nonparallel structures have an anisotropy coefficient close to zero. Control VSMC-like cells showed a mean anisotropy coefficient of 0,25, with a range from 0,07 to 0,43 (Fig. 1H). Analysis of actin organization showed a mean a of 0,54 in control VSMC-like cells with a range from 0,29 to 0,79 (Fig. 1I).





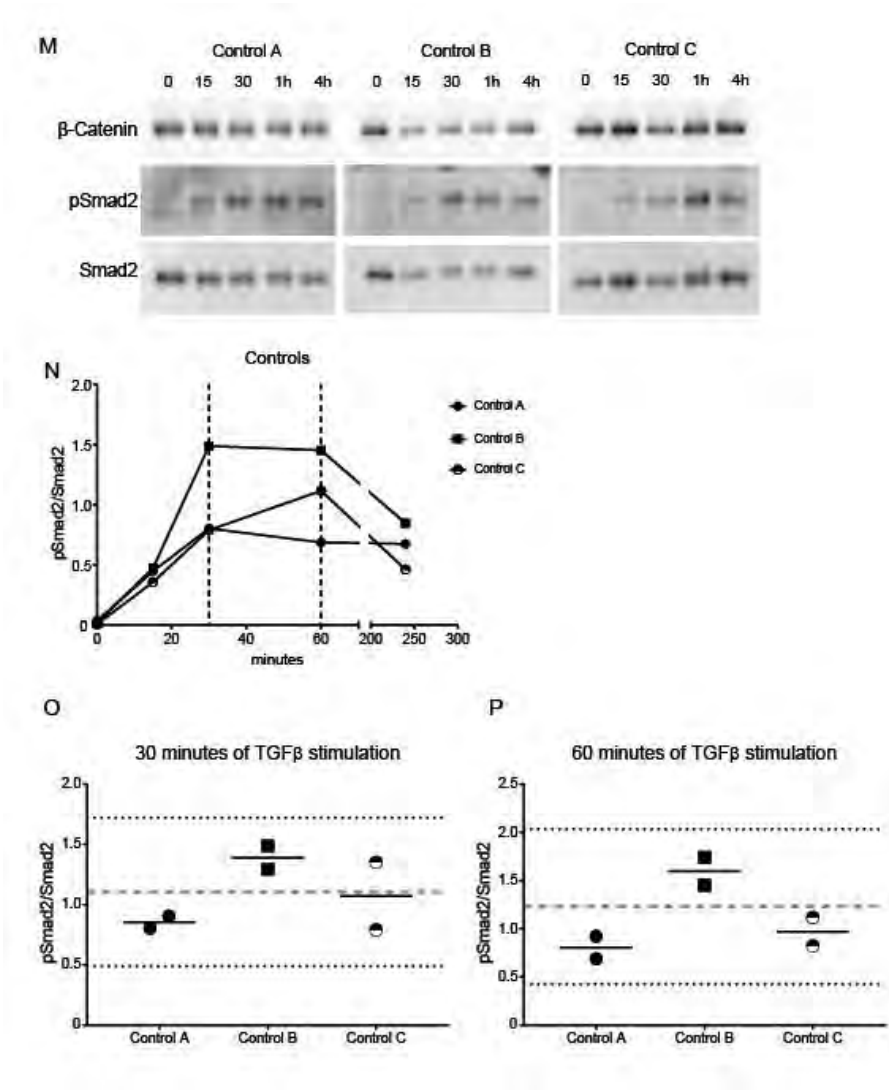


Figure 1. Assessment of baseline measurements for control VSMC-like cells. A) Time line of transdifferentiation. B) Gene expression of ACTA2 during 14 days of TGF β stimulation. C) ACTA2 gene expression in controls after 14 days of stimulation with TGF β . D) CNN1 gene expression in controls after 14 days of stimulation with TGF β . E) SM22 gene expression in controls after 14 days of stimulation with TGF β . Unstimulated samples are set to one to compare the fold induction and determine the variability in controls. Results are presented as geometric mean \pm geometric SD, figures also include the geometric mean of the controls (dashed grey line) and the 2x geometric SD range of the controls (dotted black line). 3 samples, n=2. F) Immunofluorescent staining of SMA (green), SM22 (red), actin (gray) and DAPI (blue) after 14 days of transdifferentiation. Scale bar represent 100 μ m. G) Quantification

of the fluorescent signal of SMA set out against the fluorescent signal of actin. Quantified 7 representative images per cell line. H) Quantification of SMA fiber organization in control VSMC-like cells. Alignment of SMA fibers was analyzed for 7 representative images per cell line. I) Quantification of actin fiber organization in control VSMC-like cells. Alignment of actin fibers was analyzed for 7 representative images per cell line. J) Western blots detecting SMA and SM22 in VSMC-like cells. β -catenin levels serve as a loading control. K) Quantification of SMA levels as shown in panel J. L) Quantification of SM22 levels as shown in panel J. 2 independent samples, $n=3$. M) Western blots detecting pSmad2 and Smad2 in control fibroblasts upon stimulation with TGF β (15 min, 30 min, 1 hour and 4 hours) after serum deprivation. β -catenin levels serve as a loading control. N) pSmad2/Smad2 ratio visualized over time in controls. O) Quantification of pSmad2/Smad2 ratio at 30 minutes of stimulation, $n=2$. Results are presented as mean \pm SD. Grey dashed line represents mean of the controls and the black dotted line represents 2xSD range of controls.

Western blot analysis of SMA and SM22 expression showed the presence of both proteins in all controls after transdifferentiation (Fig. 1J). Quantification of SMA and SM22 protein levels revealed variability between the controls. The variability in relative protein expression of SMA in the controls ranged from 0,46 to 1,54. For SM22 the variability in relative protein expression ranged between 0,54 to 1,45 in the controls (Fig. 1K and L).

To determine TGF β signaling activity the phosphorylation of Smad2 was analyzed over time. The response of non-transdifferentiated control fibroblasts to TGF β in time was determined as the ratio of activated (phosphorylated) Smad2 compared to total Smad2 protein after TGF β stimulation (Fig. 1M and N). Overall, phosphorylated Smad2 was already detected 15 minutes after TGF β stimulation. The amount of phosphorylated Smad2 reached a maximum level between 30 and 60 minutes, after which it decreased. As the controls almost reached their measured maximum at 30 minutes after TGF β stimulation we used the expression level at this time point as a reference for TGF β activation. At the 30-minute time point the mean pSmad2/Smad2 ratio is approximately 1,1 and ranged from 0,49 to 1,72 (Fig. 1O)

Taken together, these data show that all controls can be transdifferentiated to VSMC-like cells upon stimulation with TGF β , assessed by the RNA and protein expression of SMA, SM22 and CNN1 as well as SMA fiber organization and pSmad2 mediated TGF β signaling upon TGF β stimulation.

Transdifferentiation of fibroblasts of aneurysm patients

The goal of our study is to use these parameters to determine aberrant phenotypes in aneurysmal patient cells. We used the mean and 2xSD range of the control cell lines to determine if patient cells were outside of this range they were deemed significantly aberrant from controls.

The differentiation potential of fibroblasts of aneurysmal patient was assessed by quantitative analysis of SMA fibers after transdifferentiation. ACTA2 #1 and MYH11 #1 VSMC-like-cells both showed SMA and SM22 fibers after transdifferentiation. However, MYH11 #1 VSMC-like cells visually showed elongated SMA fibers that stretched throughout the cell whereas ACTA2 #1 VSMC-like cells showed disorganization of SMA fibers (Fig. 2A). Quantification of SMA fiber fluorescence, normalized for total actin, showed that both ACTA2 #1 and MYH11 #1 VSMC-like cells have a similar SMA fluorescence as the controls, 30% and 29% respectively (Fig. 2B). Analysis of anisotropy confirmed decreased organization of SMA (0,099) and actin (0,32) in ACTA2 #1 VSMC-like cells compared to controls (Fig. 2C and D, $p < 0,001$). MYH11 #1 VSMC-like cells showed a similar anisotropy for SMA (0,23) and actin (0,46) as controls (Fig. 2C and D).

SMAD3 #1 fibroblasts did not appear to form SMA fibers after TGF β stimulation, while SM22 was present (Fig. 2A). Quantification of SMA fluorescence levels revealed that SMA fluorescence levels (6,5%) were significantly reduced in SMAD3 #1 VSMC-like cells (Fig. 2B, $p < 0,001$). SMA fibers that were present in SMAD3 #1 VSMC-like cells after TGF β stimulation furthermore showed a significantly decreased SMA anisotropy (0,12) compared to controls (Fig. 2C, $p < 0,01$). Actin fiber organization (0,51) was similar to controls (Fig. 2D).

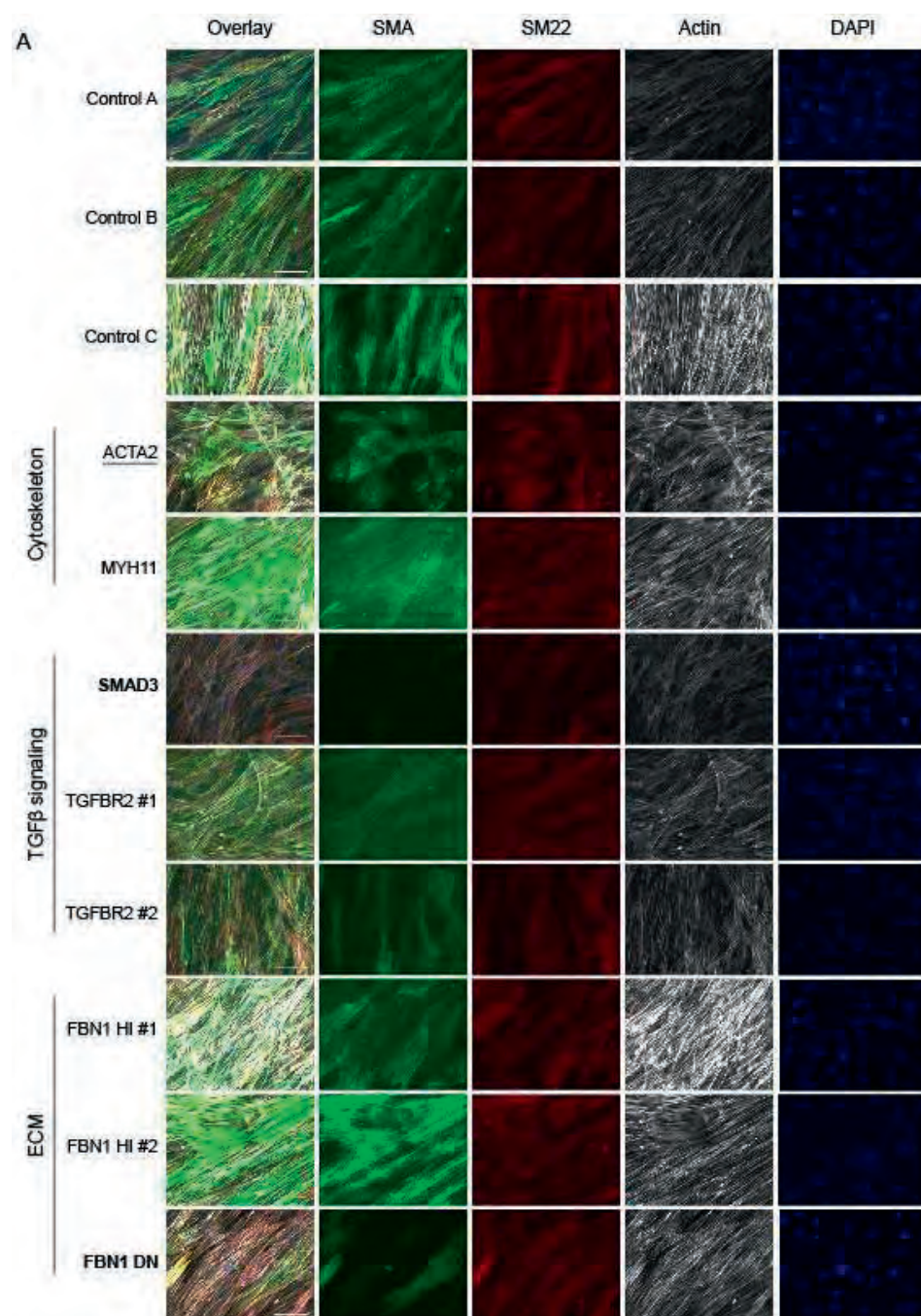
Analysis of FBN1 #1 and FBN1 #2 VSMC-like cells revealed elongated SMA and SM22 fibers after TGF β stimulation (Fig. 2A). Both FBN1 #1 and FBN1 #2 VSMC-like cells showed similar SMA fluorescence, 22% and 26% respectively, compared to controls (Fig. 2B). Quantification of anisotropy for SMA (0,22 and 0,30) and actin (0,52 and 0,46) in FBN1 #1 and FBN1 #2 VSMC-like cells revealed no aberrations in the fiber organization compared to controls (Fig. 2C and D). After TGF β stimulation FBN1 #3 VSMC-like cells showed a very low presence of SMA positive cells compared to controls. Quantification of SMA fluorescence showed a significant decrease in intensity (8,9%) compared to controls, suggesting reduced transdifferentiation potential (Fig. 2A and B, $p < 0,001$). The SMA fibers that were present in FBN1 #3 VSMC-like cells showed no aberrations in SMA anisotropy (0,20) compared to controls (Fig. 2C). Actin fiber anisotropy of FBN1 #3 VSMC-like cells showed similar organization (0,58) as controls (Fig. 2D).

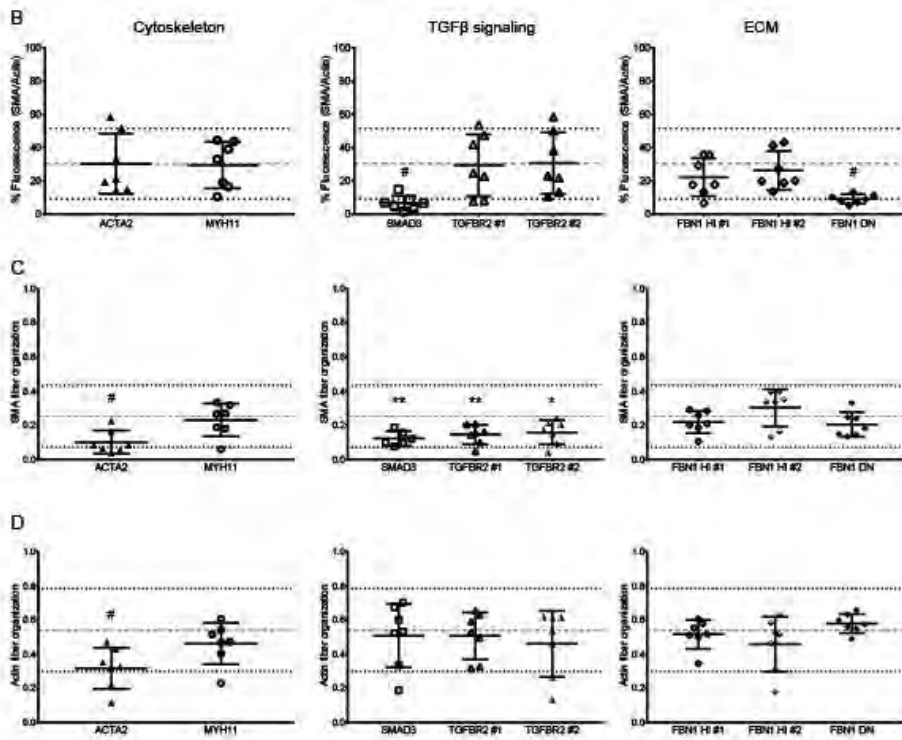
Differentiation potential was further determined by western blot analysis of SMA and SM22 protein levels after stimulation with TGF β . SMA and SM22 was present after transdifferentiation in both ACTA2 #1 and MYH11 #1 VSMC-like cells (Fig. 2E). Quantification revealed increased SMA protein levels (1,59) in ACTA2 #1 VSMC-like cells (Fig. 2F, $p < 0,01$), whereas SM22 protein levels (1,03) were comparable to controls (Fig. 2G). MYH11 #1 VSMC-like cells showed increased SMA protein levels (1,37) compared to controls, yet this does not suggest altered transdifferentiation as SMA is present after TGF β stimulation (Fig. 2F, $p < 0,05$). SM22 was significantly

decreased (0,69) in MYH11 #1 VSMC-like cells compared to controls, but was also remained in the control range (Fig. 2G, $p<0,05$).

After TGF β stimulation SMA remained almost absent (0,08) in SMAD3 #1 VSMC-like cells compared to controls and SM22 protein levels (0,51) were decreased (Fig. 2E, F and G, $p<0,001$). FBN1 #1 and FBN1 #2 VSMC-like cells showed similar SMA (0,92 and 1,47 respectively) and SM22 (0,94 and 0,95 respectively) protein levels to controls after transdifferentiation (Fig. 2E, F and G). FBN1 #3 VSMC-like cells showed decreased SMA protein levels (0,39) compared to controls (Fig. 2E and F, $p<0,01$), while having comparable SM22 protein levels (1,06) (Fig. 2E and G).

In conclusion, SMA and SM22 immunostaining and western blot indicate that SMAD3 #1 and FBN1 #3 cells have decreased transdifferentiation potential. ACTA2 #1 VSMC-like cells showed disorganized SMA fibers, while SMAD3 #1 and FBN1 #3 VSMC-like cells did not show SMA fibers. This suggests that SMAD3 #1 and FBN1 #3 VSMC-like cells show reduced transdifferentiation after TGF β stimulation. A summary of the data in the results section can be found in figure 6.





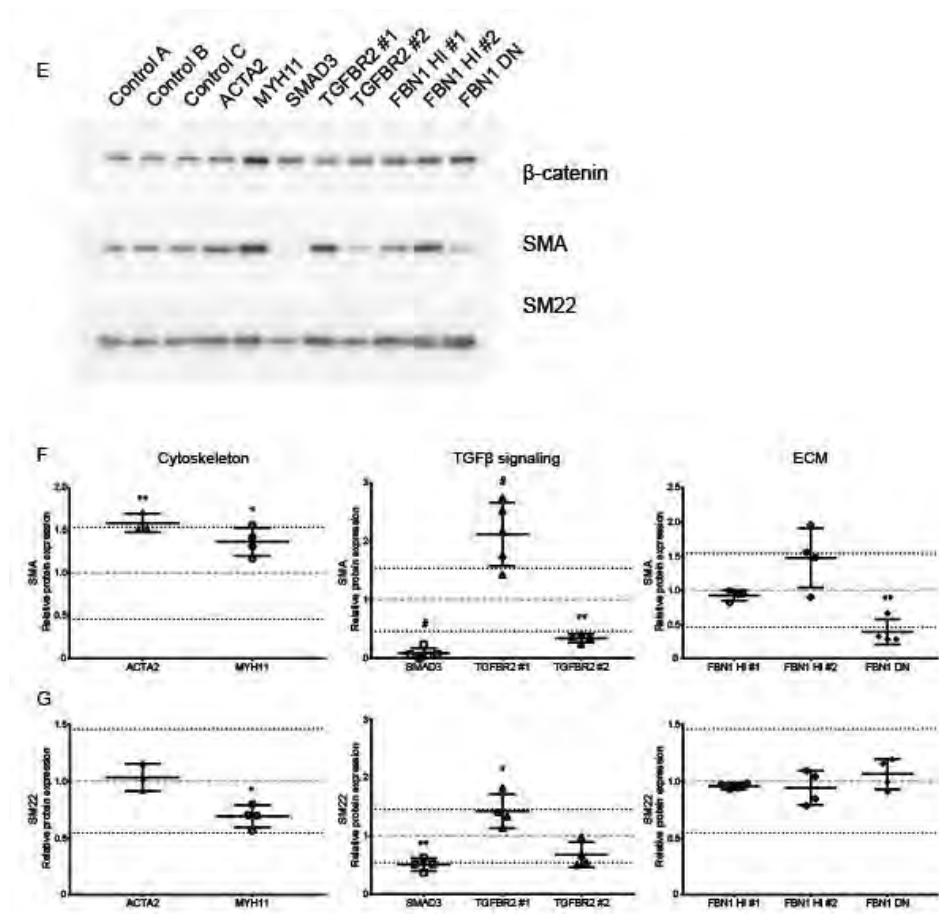


Figure 2. Transdifferentiation of fibroblasts of aneurysm patients. A) Immunofluorescent staining of SMA (green), SM22 (red), actin (gray) and DAPI (blue) after 14 days of transdifferentiation. Scale bar represent 100 μ m. Underlined cell lines visually showed disorganization of the cytoskeleton. Bold cell lines visually showed decreased presence of SMA fibers. B) Quantification of the fluorescent signal of SMA set out against the fluorescent signal of actin. Quantified 7 representative images per cell line. C) Quantification of SMA fiber organization in pathogenic variant VSMC-like cells. Alignment of SMA fibers was analyzed for 7 representative images per cell line. D) Quantification of actin fiber organization in pathogenic variant VSMC-like cells. Alignment of actin fibers was analyzed for 7 representative images per cell line. E) Western blots detecting SMA and SM22 in pathogenic variant VSMC-like cells. β -catenin levels serve as a loading control. F) Quantification of SMA levels as shown in panels E. G) Quantification of SM22 levels as shown in panels E. 2 independent samples, $n=3$. Grey dashed line represents mean of the controls and black dotted line represents 2xSD range of controls. * $p<0,05$, ** $p<0,01$, # $p<0,001$.

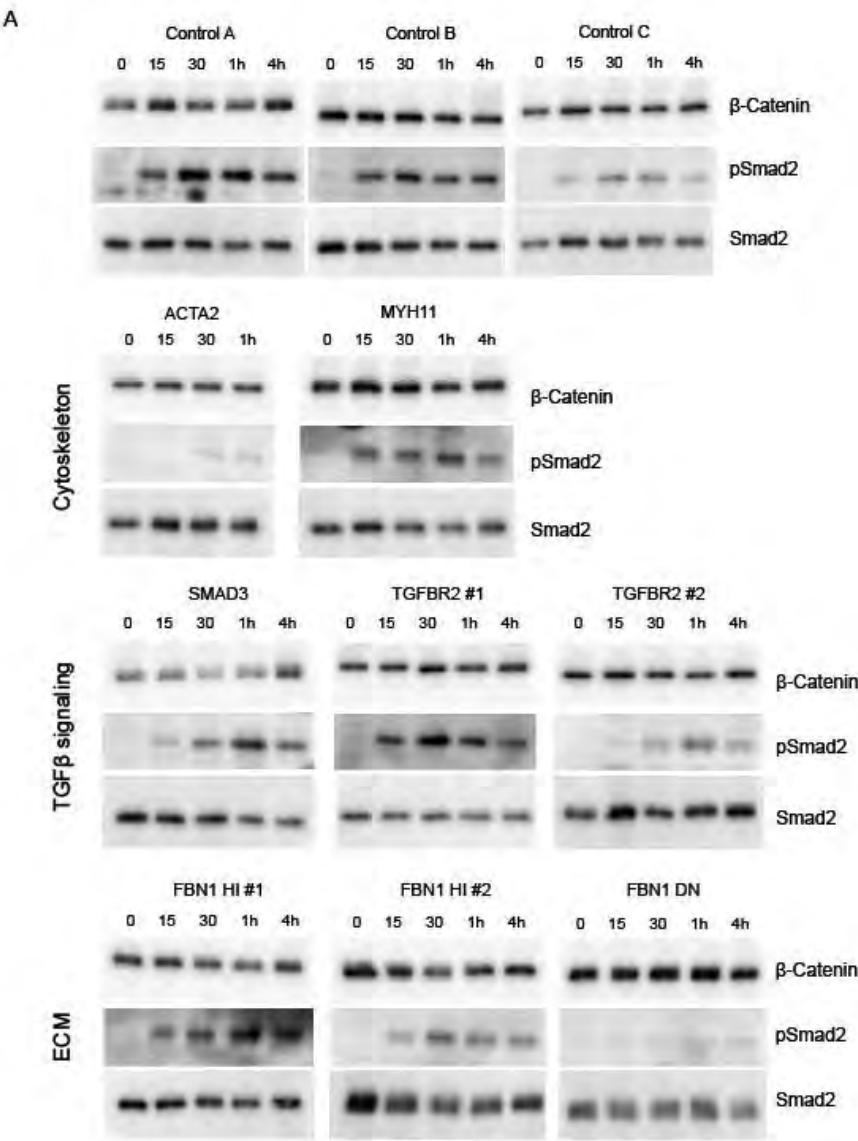
Kinetics of pSmad2 activation of fibroblasts of aneurysm patients

TGF β signaling activity was analyzed by examining the ratio of phosphorylated Smad2 to total Smad2 over time as a measure of TGF β responsiveness. ACTA2 #1 fibroblasts showed reduced induction of Smad2 phosphorylation after TGF β stimulation. When quantified, ACTA2 #1 fibroblasts showed a pSmad2/Smad2 ratio of 0,44 after 30 minutes of TGF β stimulation which was below the 2xSD range of the controls (Fig. 3A and B). MYH11 #1 fibroblasts showed comparable phosphorylation of Smad2 to control fibroblasts (Fig. 3A). Quantification also indicated a normal pSmad2/Smad2 ratio of 0,98 for MYH11 #1 fibroblasts compared to controls (Fig. 3B).

Phosphorylation of Smad2 was comparable to controls for SMAD3 #1 fibroblasts, the pSmad2/Smad2 ratio at 30 minutes of 1,35 and was therefore similar to the controls (Fig. 3A and C).

Smad2 phosphorylation in FBN1 #1 and FBN1 #2 fibroblasts showed similar pSmad2/Smad2 ratios, 0,72 and 1,08 respectively, compared to controls after 30 minutes of TGF β stimulation (Fig. 3A and D). FBN1 #3 fibroblasts showed reduced phosphorylation of Smad2 after TGF β stimulation (Fig. 3A). The pSmad2/Smad2 ratio of 0,46 for FBN1 #3 fibroblasts after 30 minutes of TGF β stimulation remained below the 2xSD range of the controls (Fig. 3D).

Taken together, these data show that pSmad2 activation is highly dynamic. In non-transdifferentiated cells we detected differences in ACTA2#1 and FBN#3 cells compared to controls although there is a large range for the readouts. A summary of the data in this results section can also be found in figure 6.



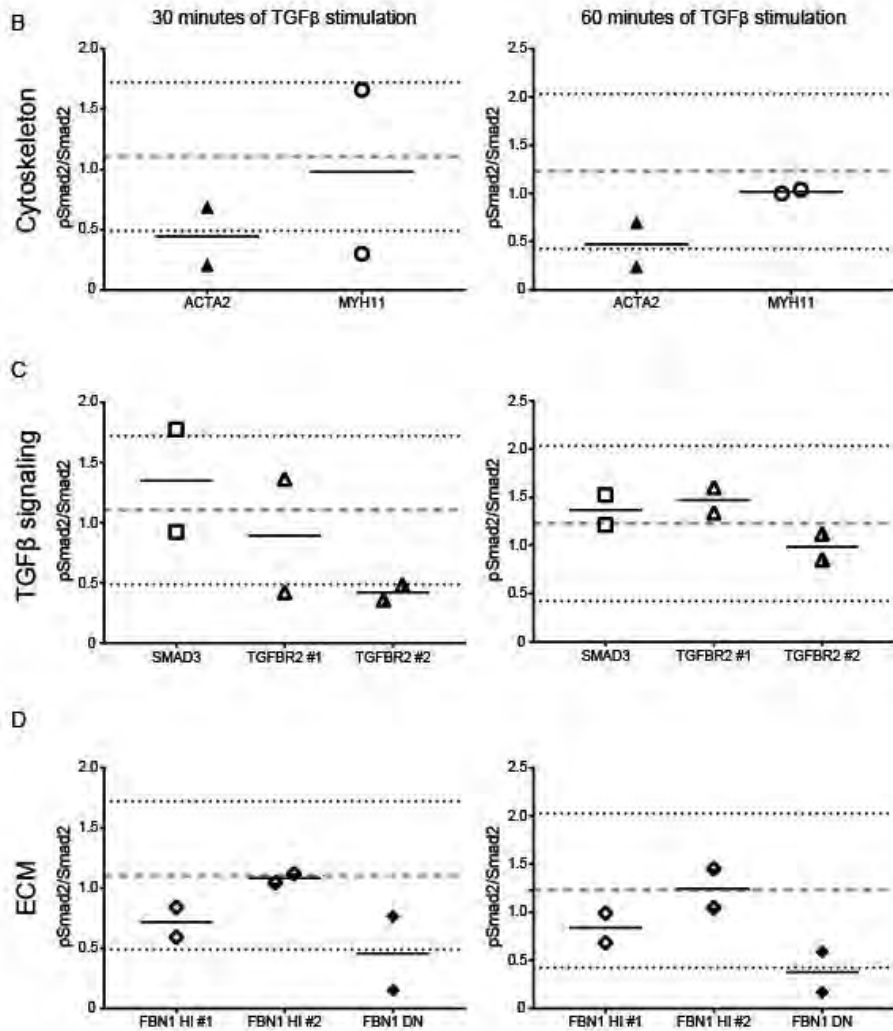


Figure 3. TGF β responsiveness over time of fibroblasts of aneurysm patients. A) Western blots detecting pSmad2 and Smad2 in TAA mutant fibroblasts upon stimulation with TGF β (15 min, 30 min, 1 hour and 4 hours) after serum deprivation. β -catenin levels serve as a loading control. B) Quantification of pSmad2/Smad2 ratio at 30 minutes of stimulation in ACTA2 and MYH11 variant fibroblasts. C) Quantification of pSmad2/Smad2 ratio at 30 minutes stimulation in SMAD3 variant fibroblasts. D) Quantification of pSmad2/Smad2 ratio at 30 minutes of stimulation in FBN1 variant fibroblasts. 2 independent samples, n=2. Grey dashed line represents mean of the controls and black dotted line represents 2xSD range of controls.

Migration capacity of pathogenic variant and control VSMC-like cells

The migration capacity of the induced VSMC-like cells was analyzed by performing a ring barrier migration assay. Migration velocity of ACTA2 #1 VSMC-like cells (5,0 $\mu\text{m/hr}$) was decreased compared to the migration velocity of controls (9,0 $\mu\text{m/hr}$) ($p < 0,001$, Fig. 4A). Interestingly, MYH11 #1 VSMC-like cells also showed decreased migration velocity (3,5 $\mu\text{m/hr}$) compared to controls (9,4 $\mu\text{m/hr}$) ($p < 0,001$, Fig. 4B). SMAD3 #1 VSMC-like cells displayed a comparable velocity to the control migration velocity (Fig. 4C). FBN1 #1, #2 and #3 VSMC-like cells all did not differ in migration velocity from controls (Fig. 4D and E).

These data indicate that both cytoskeleton mutations, ACTA2 #1 and MYH11 #1 VSMC-like cells, display reduced migration after transdifferentiation compared to controls. A summary of the data in this results section can also be found in figure 6.

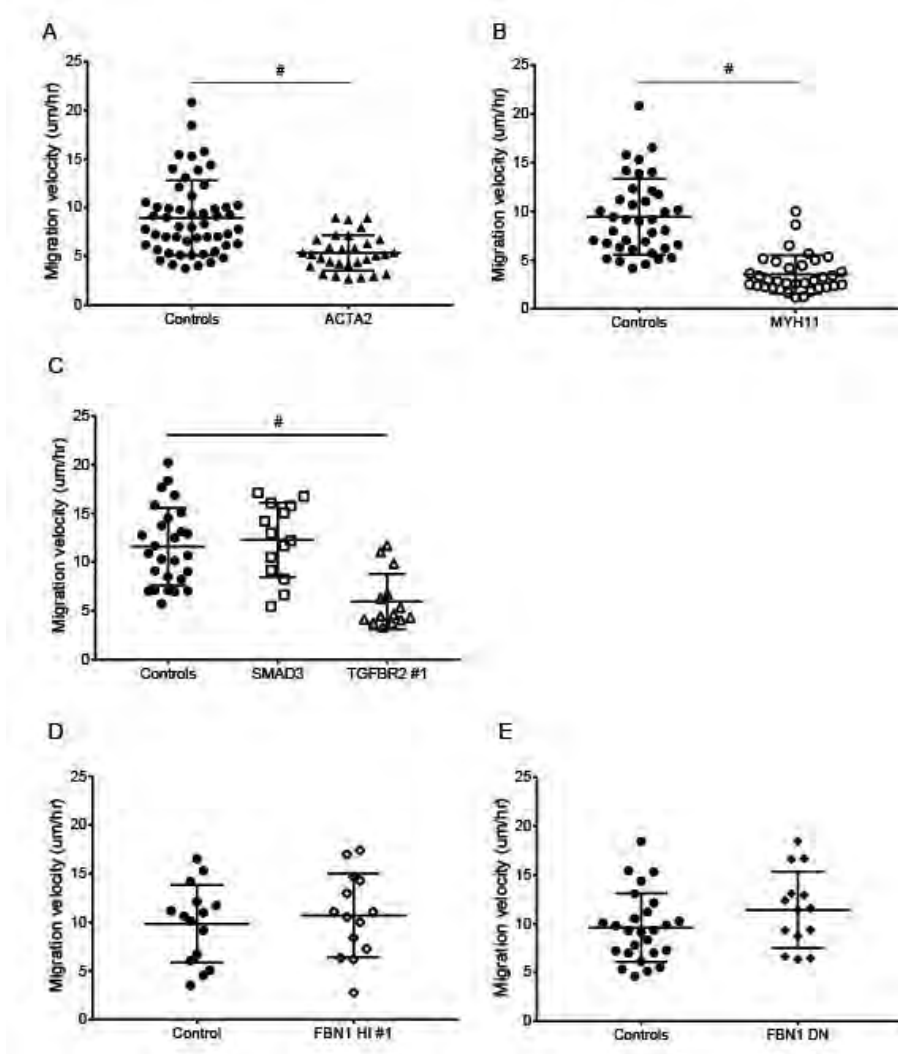


Figure 4. Migration potential of pathogenic variant and control VSMC-like cells.

Migration velocity of pathogenic variant VSMC-like cells compared to controls. A) ACTA2, B) MYH11, C) SMAD3, D) FBN1 #1, and E) FBN1 #3 VSMC-like cells. n=2, # p<0,001

Contractility of pathogenic variant and control VSMC-like cells

Contractility was determined to analyze the effects that pathogenic variants. The maximum contraction of control VSMC-like cells was on average 49,7% with a 2xSD ranging from 23,3 to 76,1% (Fig. 5A). The maximum contraction of ACTA2 #1 VSMC-like cells was 16,3% and thereby below the 2xSD range of the controls. MYH11 #1 VSMC-like cells showed a maximum contraction of 42,1% and did not differ from

controls (Fig. 5B). SMAD3 #1 VSMC-like cells displayed a maximum contraction of 70,4% and showed a relatively high contractility, however, the maximum contraction did not differ from the controls (Fig. 5C). FBN1 #1 and FBN1 #2 VSMC-like cells presented with a maximum contractility of 47,8 and 47,2% respectively and were thereby comparable to the controls. FBN1 #3 VSMC-like cells also did not differ from the controls with a maximum contraction of 46,5%. (Fig. 5D).

From these data we can conclude that ACTA2 #1 VSMC-like cells show reduced contractility compared to controls. A summary of the data in this results section can also be found in Figure 6.

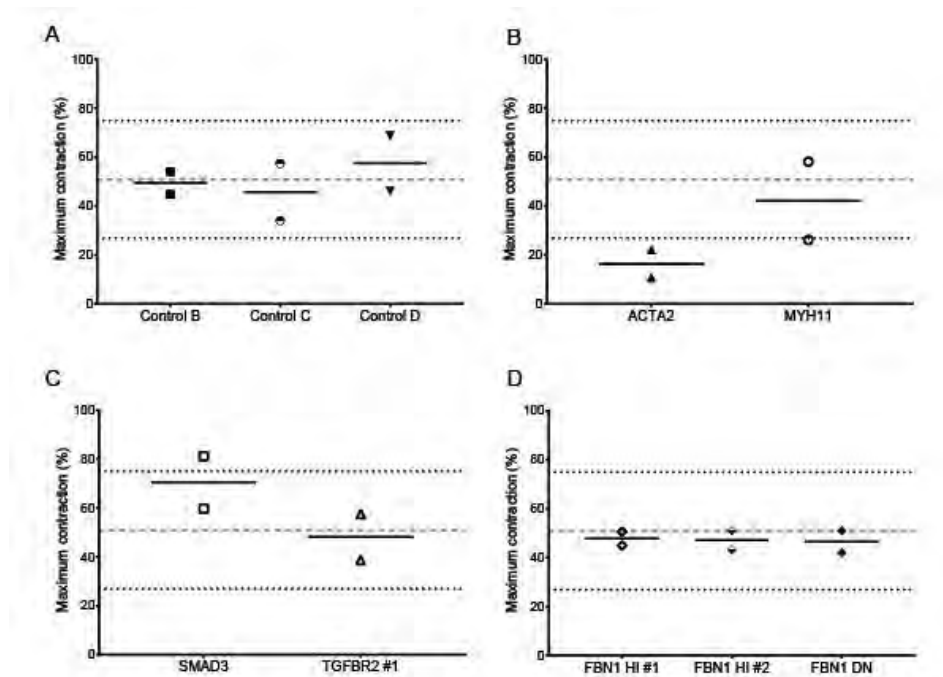


Figure 5. Contractility of patient and control VSMC-like cells. Maximum contraction of pathogenic variant VSMC-like cells compared to controls. A) Maximum contraction of controls VSMC-like cells. B) Maximum contraction of ACTA2 and MYH11 variant VSMC-like cells. C) Maximum contraction of SMAD3 variant VSMC-like cells. D) Maximum contraction of FBN1 variant VSMC-like cells. Grey dashed line represents mean of the controls and black dotted line represents 2xSD range of controls. n=2.

		Immunofluorescence						Western blotting				TGFβ response		Migration	Contractility
SMA fibers visually	% SMA	SMA organization		Actin organization		SMA		SM22		30 min	60 min	Average controls	Average controls		
		Average controls	Outside 2xSD	Average controls	Outside 2xSD	Average controls	Outside 2xSD	Average controls	Outside 2xSD						
Mutation															
ACTA2	Disorganized	~	~	~	↓	~	↑	~	~	↓	↓~	↓	↓	↓	
MYH11	Normal	~	~	~	~	~	↑	~	~	~	~	~	~	~	
SMAAD3	Almost absent	↓	~	↓	~	~	↓	↓	↓	~	~	~	↓	~	
TGFBR2 #1	Normal	~	~	~	~	~	↑	~	~	~	~	~	~	~	
TGFBR2 #2	Normal	~	~	↓	~	~	↓	~	~	↓	~	~	~	~	
FBN1 HI #1	Normal	~	~	~	~	~	~	~	~	~	~	~	~	~	
FBN1 HI #2	Normal	~	~	~	~	~	~	~	~	~	~	~	~	~	
FBN1 DN	Almost absent	↓	↓	~	~	~	↓	↓	~	↓	↓	~	~	~	

Figure 6. Summary of functional assay results of transdifferentiated fibroblasts of aneurysm patients with a pathogenic variant in aneurysm genes. Overview of results per pathogenic variant and experiment. Significant differences compared to the mean of the controls are noted as decreased (↓) or increased (↑) in the “compared to controls” column. If

the mean of the samples of the patient cell line was within the 2xSD control range the arrow is marked with an *. No difference compared to the controls is visualized as ~.

DISCUSSION

Variants in aneurysm related genes are often associated with aneurysm formation. However, the effect of these mutations on the protein is not always clear, and thus, the clinical relevance is hard to assess. In this study, we used cells of aneurysm patient with six different pathogenic variants to evaluate the clinical robustness of novel functional assays to determine the pathogenic effects of variants. Such assays are needed since VUS are being identified in a diagnostic settings but can currently not be assessed for their potential functional pathogenicity. In the present study, we measured a decrease in SMA protein expression as an indicator of reduced transdifferentiation potential in SMAD3 and FBN1 dominant negative (FBN1 #3) patients. VSMC-like cells of ACTA2 and FBN1 dominant negative patients also showed a decrease in pSmad2 activation. Migration velocity was impaired for ACTA2 and MYH11. While only ACTA2 showed reduced contractility. Our data suggests that TGF β induced transdifferentiation of fibroblasts allowed the distinguishing of pathogenic variants in the cytoskeleton, TGF β pathway and ECM aneurysm genes for ACTA2, MYH11, SMAD3, FBN1 dominant negative, but not for FBN1 haploinsufficient variants compared to control. A limitation of our study is that only one cell line was used per mutation as proof of concept. In order to draw more significant conclusions on the role of mutations of these genes in AA formation, replication of the functional experiments using larger numbers of cell lines carrying these and other aneurysm genes are needed. Below, we will discuss these results per aneurysm causing gene analyzed. A summary of the data can also be found in figure 6.

ACTA2

ACTA2 #1 VSMC-like cells produced SMA protein after TGF β stimulation and showed similar transdifferentiation potential as controls. However, the SMA fibers appeared fragmented and disorganized. Guo et al. previously showed lack of SMA fibers in VSMCs of patient with ACTA2 variants (p.R118Q and p.T353N) {Guo, 2007 #16}. Our data shows that the p.R149C variant of ACTA2 #1 resembles other known ACTA2 pathogenic variants with its disorganized SMA fibers after transdifferentiation. Clinical data on ACTA2 p.R149C, p.R256H and p.T353N aortic sections confirmed that SMA protein is produced, but that VSMCs appear to be disorganized and lack structure {Malloy, 2012 #194}. Complications with the assembly of mutant SMA (p.R256H) is further confirmed by analysis of mutant ACTA2 in yeast {Malloy, 2012 #194}. Analysis of SMA fiber assembly by Malloy et al. showed decreased SMA polymerization and elongated assembly times in ACTA2 p.R256H mutant yeast compared to wild-type yeast. Studies on ACTA2 mutations

(p.R118Q, p.R256H and p.T353N) show overall disorganization of SMA fibers that is caused by dysfunctional assembly of SMA. Our results confirmed the overall disorganization of SMA for an additional ACTA2 pathogenic variant (p.R149C) in VSMC-like cells.

Additionally, ACTA2 #1 VSMC-like cells showed decreased migration and contractility. During migration the cytoskeleton is polymerized in the direction of movement, while depolymerization occurs at the rear-end of cells. Variants in proteins that constitute the cytoskeleton, such as ACTA2 and MYH11, can be explanatory for the observed defective migration. Literature revealed that ACTA2 is induced during migration as well as during metastasis, suggesting that ACTA2 is essential for migration {Rockey, 2013 #240}{Lee, 2013 #241}. Decreased contractility of multiple ACTA2 pathogenic variant VSMCs was previously found by Lu et al. (2015) by performing a one-bead laser trap experiment to analyze force-output. Our data on the reduced contractility of ACTA2 #1 VSMC-like cells is in line with this finding and indicates the importance of ACTA2 for the contractility of VSMCs.

MYH11

MYH11 #1 VSMC-like cells showed decreased SM22 protein levels on western blot. Overexpression of MYH11 has been reported to induce degradation and turnover of thick filament associated proteins and cytoskeleton proteins like SM22 but not SMA {Kwartler, 2014 #239}. Since MYH11 c.3879+2dup (MYH11 #1) is a relatively unknown variant, it is unclear whether this variant could lead to a gain-of-function of MYH11 and thereby inducing the degradation of specific cytoskeleton proteins or that this pathogenic variant leads to reduced levels or function of MYH11. Our finding that SMA is not degraded is in line with the results of Kwartler et al. and suggests that this MYH11 pathogenic variant could indeed induce the described unfolded protein response that induces degradation of specific cytoskeleton proteins.

Although the MYH11 #1 VSMC-like cells were able to transdifferentiate, migration velocity was decreased in MYH11 variant VSMC-like cells, similar to the ACTA2 #1 VSMC-like cells. MYH11 pathogenic variants have been predicted to decrease SMC contractility as well as compromising migration, which is in line with our results {Kuang, 2012 #201}{Pannu, 2007 #50}.

SMAD3

SMAD3 #1 VSMC-like cells lacked induction of SMA fibers upon TGF β stimulation, which suggests reduced induction of transdifferentiation. This lack of SMA can be explained by disturbance in the TGF β signaling pathway caused by the SMAD3 pathogenic variant. Induction of SMA by TGF β was shown to occur via SMAD3 {Hu, 2003 #232}{Vardouli, 2008 #233}, suggesting that induction will not occur when

SMAD3 is mutated. Like SMA, SM22 is induced via activation of the TGF β pathway, specifically via SMAD3 {Qiu, 2003 #234}. This also explains the reduced SM22 protein levels of SMAD3 pathogenic variant VSMC-like cells.

The TGF β signaling pathway is often deemed physiological when Smad2 is phosphorylated upon TGF β stimulation, yet, for SMAD3 variants resulting in absent or defective Smad3 proteins, this is not necessarily true {van der Pluijm, 2016 #130}. Although, the initial response to TGF β stimulation is intact in SMAD3 knock-out cells, downstream signaling is impaired due to absence of Smad3 protein. This hampers induction of target genes, thereby leading to impaired induction of SMA and SM22 and thus diminished transdifferentiation.

FBN1

VSMC-like cells with a FBN1 dominant negative pathogenic variant (FBN1 #3) express less SMA protein as well as SMA fibers after transdifferentiation. This could be caused by defective ECM build-up resulting from the FBN1 variant. A lack of anchoring points in the ECM can lead to reduced binding sites for the cytoskeleton via integrins. The rigidity of the ECM is also important for the development of the cytoskeleton as, for example, a soft matrix results in a less well-defined cytoskeleton {Choquet, 1997 #236}{Lo, 2000 #237}{Saez, 2005 #238}. The effect of a defective matrix on the cytoskeleton has recently also been shown in the Fibulin-4 VSMC specific knock-out mouse model in which absence of fibulin-4 led to absence of SMA protein and fibers {Burger, 2019 #235}.

Transdifferentiation of FBN1 dominant negative and haploinsufficient patient fibroblasts reveals different results between two (predicted) types of FBN1 pathogenic variants. While the dominant negative FBN1 #3 VSMC-like cells show decreased induction of SMA and SM22, results from FBN1 #1 and #2 haploinsufficient fibroblasts appear quite similar to controls. Clinical data previously also suggested differences between FBN1 dominant negative and haploinsufficient variant in responsiveness to losartan treatment {Franken, 2015 #164}{den Hartog, 2016 #247}. Patients with an FBN1 haploinsufficient pathogenic variant that received losartan treatment were responsive to the inhibition of aortic root dilation by losartan, while FBN1 dominant negative patients did not respond to treatment {Franken, 2015 #164}. Furthermore, patients with an FBN1 haploinsufficient variant showed improvement in biventricular end diastolic volume and stroke volume upon losartan treatment. This effect was not found in FBN1 dominant negative patients that received losartan treatment {den Hartog, 2016 #247}. This indicates that mutations in one gene can lead to different outcomes and could result in different clinical consequences for patients. The nature of the FBN1 variants and their effects are in line with this as haploinsufficient variants result in half of the normal protein levels while dominant negative variants interfere with the normal protein and can result in

nonfunctional protein levels. Our functional assays proved to be able to distinguish between FBN1 haploinsufficient and dominant negative mutations and could potentially simplify the identification of haploinsufficient and dominant negative patients. In particular, the presence or absence of SMA and potentially the pSmad2/Smad2 ratio after TGF β stimulation can distinguish FBN1 dominant negative VSMC-like cells from FBN1 haploinsufficient VSMC-like cells.

CONCLUSION

The assays we have chosen are suitable to determine the effect of the mutation on the functionality of the protein. We detected reduced transdifferentiation potential in SMAD3 #1 and FBN1 #3, the defective migration in MYH11 #1 and ACTA2 #1 and the defective contractility ACTA2 #1. Our results suggests a potential application for these novel functional assays in assessing the functionality of a larger number of patients with mutations in the same genes. We are one step closer in to analyze the potential pathogenic effect of VUS in aneurysm gene and thereby enhance genetic diagnosis and family screening for aneurysms.

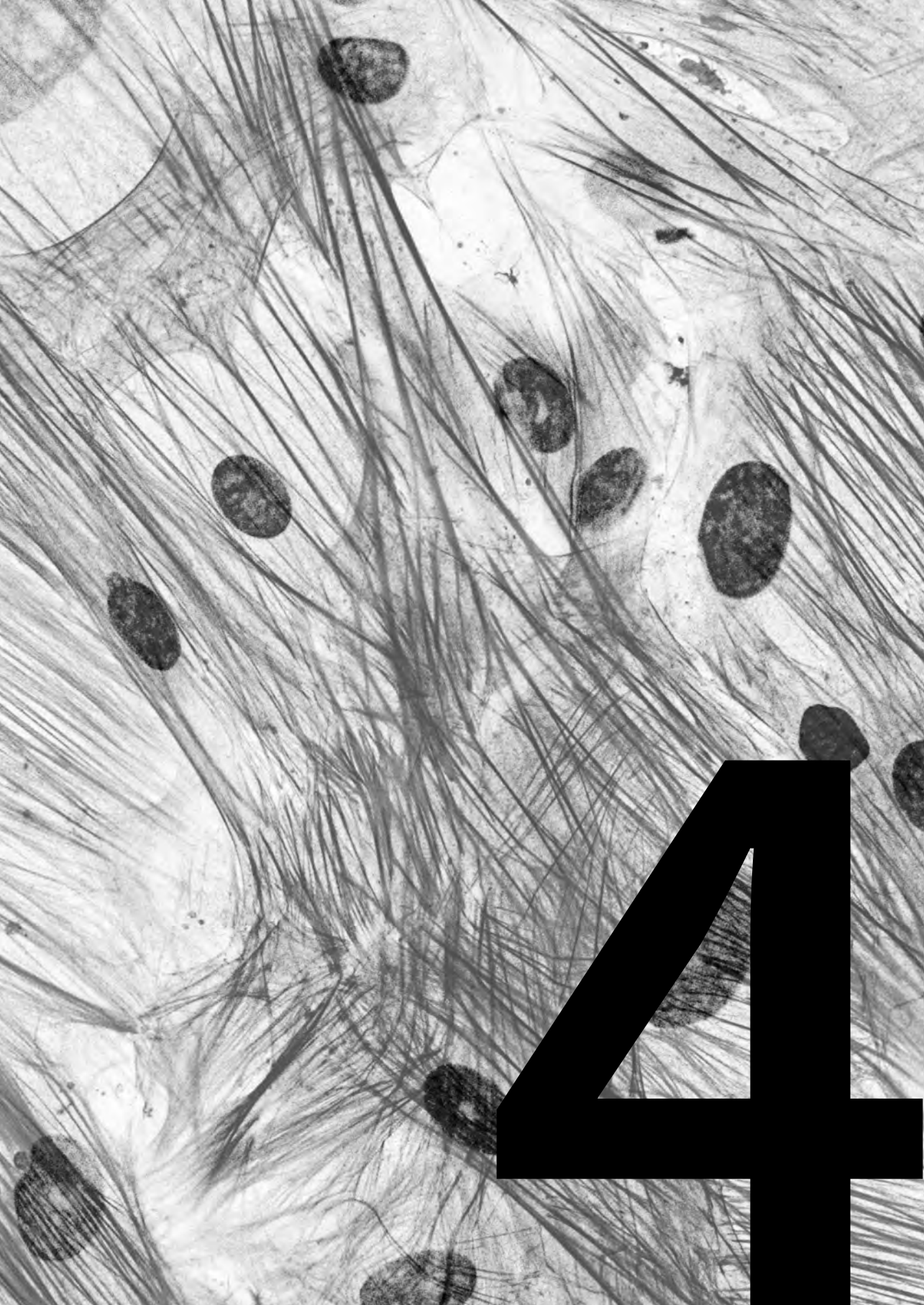
REFERENCES

- 1 Ziganshin, B. A. et al. Routine Genetic Testing for Thoracic Aortic Aneurysm and Dissection in a Clinical Setting. *Ann Thorac Surg* 100, 1604-1611, doi:S0003-4975(15)00735-3 [pii] 10.1016/j.athoracsur.2015.04.106 (2015).
- 2 van de Lijngaarden, K. M. et al. First genetic analysis of aneurysm genes in familial and sporadic abdominal aortic aneurysm. *Hum Genet* 134, 881-893, doi:10.1007/s00439-015-1567-0 (2015).
- 3 Guo, D. C. et al. Mutations in smooth muscle alpha-actin (ACTA2) lead to thoracic aortic aneurysms and dissections. *Nat Genet* 39, 1488-1493, doi:ng.2007.6 [pii]10.1038/ng.2007.6 (2007).
- 4 Zhu, L. et al. Mutations in myosin heavy chain 11 cause a syndrome associating thoracic aortic aneurysm/aortic dissection and patent ductus arteriosus. *Nat Genet* 38, 343-349, doi:ng1721 [pii]10.1038/ng1721 (2006).
- 5 Wang, L. et al. Mutations in myosin light chain kinase cause familial aortic dissections. *Am J Hum Genet* 87, 701-707, doi:S0002-9297(10)00522-7 [pii]10.1016/j.ajhg.2010.10.006 (2010).
- 6 Guo, D. C. et al. Recurrent gain-of-function mutation in PRKG1 causes thoracic aortic aneurysms and acute aortic dissections. *Am J Hum Genet* 93, 398-404, doi:S0002-9297(13)00288-7 [pii] 10.1016/j.ajhg.2013.06.019 (2013).
- 7 Loeys, B. L. et al. A syndrome of altered cardiovascular, craniofacial, neurocognitive and skeletal development caused by mutations in TGFBR1 or TGFBR2. *Nat Genet* 37, 275-281, doi:ng1511 [pii] 10.1038/ng1511 (2005).
- 8 Loeys, B. L. et al. Aneurysm syndromes caused by mutations in the TGF-beta receptor. *N Engl J Med* 355, 788-798, doi:355/8/788 [pii]10.1056/NEJMoa055695 (2006).
- 9 Mizuguchi, T. et al. Heterozygous TGFBR2 mutations in Marfan syndrome. *Nat Genet* 36, 855-860, doi:10.1038/ng1392 ng1392 [pii] (2004).
- 10 Lindsay, M. E. et al. Loss-of-function mutations in TGFB2 cause a syndromic presentation of thoracic aortic aneurysm. *Nat Genet* 44, 922-927, doi:ng.2349 [pii]10.1038/ng.2349 (2012).
- 11 Boileau, C. et al. TGFB2 mutations cause familial thoracic aortic aneurysms and dissections associated with mild systemic features of Marfan syndrome. *Nat Genet* 44, 916-921, doi:ng.2348 [pii] 10.1038/ng.2348 (2012).
- 12 Rienhoff, H. Y., Jr. et al. A mutation in TGFB3 associated with a syndrome of low muscle mass, growth retardation, distal arthrogryposis and clinical features overlapping with Marfan and Loeys-Dietz syndrome. *Am J Med Genet A* 161A, 2040-2046, doi:10.1002/ajmg.a.36056 (2013).
- 13 Matyas, G., Naef, P., Tollens, M. & Oexle, K. De novo mutation of the latency-associated peptide domain of TGFB3 in a patient with overgrowth and Loeys-Dietz syndrome features. *Am J Med Genet A* 164A, 2141-2143, doi:10.1002/ajmg.a.36593 (2014).
- 14 Bertoli-Avella, A. M. et al. Mutations in a TGF-beta ligand, TGFB3, cause syndromic aortic aneurysms and dissections. *J Am Coll Cardiol* 65, 1324-1336, doi:S0735-1097(15)00403-9 [pii] 10.1016/j.jacc.2015.01.040 (2015).
- 15 van de Laar, I. M. et al. Mutations in SMAD3 cause a syndromic form of aortic aneurysms and dissections with early-onset osteoarthritis. *Nat Genet* 43, 121-126, doi:ng.744 [pii] 10.1038/ng.744 (2011).

- 16 van de Laar, I. M. et al. Phenotypic spectrum of the SMAD3-related aneurysms-osteoarthritis syndrome. *J Med Genet* 49, 47-57, doi:jmedgenet-2011-100382 [pii]10.1136/jmedgenet-2011-100382 (2012).
- 17 Dietz, H. C. et al. The Marfan syndrome locus: confirmation of assignment to chromosome 15 and identification of tightly linked markers at 15q15-q21.3. *Genomics* 9, 355-361, doi:0888-7543(91)90264-F [pii] (1991).
- 18 Milewicz, D. M. Identification of defects in the fibrillin gene and protein in individuals with the Marfan syndrome and related disorders. *Tex Heart Inst J* 21, 22-29 (1994).
- 19 Pepin, M., Schwarze, U., Superti-Furga, A. & Byers, P. H. Clinical and genetic features of Ehlers-Danlos syndrome type IV, the vascular type. *N Engl J Med* 342, 673-680, doi:MJBA-421001 [pii] 10.1056/NEJM200003093421001 (2000).
- 20 Schwarze, U. et al. Haploinsufficiency for one COL3A1 allele of type III procollagen results in a phenotype similar to the vascular form of Ehlers-Danlos syndrome, Ehlers-Danlos syndrome type IV. *Am J Hum Genet* 69, 989-1001, doi:S0002-9297(07)61315-9 [pii] 10.1086/324123 (2001).
- 21 Plancke, A. et al. Homozygosity for a null allele of COL3A1 results in recessive Ehlers-Danlos syndrome. *Eur J Hum Genet* 17, 1411-1416, doi:ejhg200976 [pii] 10.1038/ejhg.2009.76 (2009).
- 22 Zhang, M. C. et al. Cutis laxa arising from frameshift mutations in exon 30 of the elastin gene (ELN). *J Biol Chem* 274, 981-986 (1999).
- 23 Tassabehji, M. et al. An elastin gene mutation producing abnormal tropoelastin and abnormal elastic fibres in a patient with autosomal dominant cutis laxa. *Hum Mol Genet* 7, 1021-1028, doi:ddb125 [pii] (1998).
- 24 Szabo, Z. et al. Aortic aneurysmal disease and cutis laxa caused by defects in the elastin gene. *J Med Genet* 43, 255-258, doi:jmg.2005.034157 [pii]10.1136/jmg.2005.034157 (2006).
- 25 Huchtagowder, V. et al. Fibulin-4: a novel gene for an autosomal recessive cutis laxa syndrome. *Am J Hum Genet* 78, 1075-1080, doi:S0002-9297(07)63929-9 [pii] 10.1086/504304 (2006).
- 26 Dasouki, M. et al. Compound heterozygous mutations in fibulin-4 causing neonatal lethal pulmonary artery occlusion, aortic aneurysm, arachnodactyly, and mild cutis laxa. *Am J Med Genet A* 143A, 2635-2641, doi:10.1002/ajmg.a.31980 (2007).
- 27 Lee, V. S. et al. Loss of function mutation in LOX causes thoracic aortic aneurysm and dissection in humans. *Proc Natl Acad Sci U S A* 113, 8759-8764, doi:1601442113 [pii] 10.1073/pnas.1601442113 (2016).
- 28 Guo, D. C. et al. LOX Mutations Predispose to Thoracic Aortic Aneurysms and Dissections. *Circ Res* 118, 928-934, doi:CIRCRESAHA.115.307130 [pii]10.1161/CIRCRESAHA.115.307130 (2016).
- 29 Yeung, K. K. et al. Transdifferentiation of Human Dermal Fibroblasts to Smooth Muscle-Like Cells to Study the Effect of MYH11 and ACTA2 Mutations in Aortic Aneurysms. *Hum Mutat* 38, 439-450, doi:10.1002/humu.23174 (2017).
- 30 Schindelin, J. et al. Fiji: an open-source platform for biological-image analysis. *Nat Methods* 9, 676-682, doi:nmeth.2019 [pii]10.1038/nmeth.2019 (2012).
- 31 Lowry, O. H., Rosebrough, N. J., Farr, A. L. & Randall, R. J. Protein measurement with the Folin phenol reagent. *J Biol Chem* 193, 265-275 (1951).
- 32 Das, A. M., Eggermont, A. M. & ten Hagen, T. L. A ring barrier-based migration assay to assess cell migration in vitro. *Nat Protoc* 10, 904-915, doi:nprot.2015.056 [pii]10.1038/nprot.2015.056 (2015).

- 33 Bogunovic, N. et al. Impaired smooth muscle cell contractility as a novel concept of abdominal aortic aneurysm pathophysiology. *Sci Rep* 9, 6837, doi:10.1038/s41598-019-43322-310.1038/s41598-019-43322-3 [pii] (2019).
- 34 Malloy, L. E. et al. Thoracic aortic aneurysm (TAAD)-causing mutation in actin affects formin regulation of polymerization. *J Biol Chem* 287, 28398-28408, doi:M112.371914 [pii]10.1074/jbc.M112.371914 (2012).
- 35 Rockey, D. C., Weymouth, N. & Shi, Z. Smooth muscle alpha actin (Acta2) and myofibroblast function during hepatic wound healing. *PLoS One* 8, e77166, doi:10.1371/journal.pone.0077166PONE-D-13-11692 [pii] (2013).
- 36 Lee, H. W. et al. Alpha-smooth muscle actin (ACTA2) is required for metastatic potential of human lung adenocarcinoma. *Clin Cancer Res* 19, 5879-5889, doi:1078-0432.CCR-13-1181 [pii]10.1158/1078-0432.CCR-13-1181 (2013).
- 37 Kwartler, C. S. et al. Overexpression of smooth muscle myosin heavy chain leads to activation of the unfolded protein response and autophagic turnover of thick filament-associated proteins in vascular smooth muscle cells. *J Biol Chem* 289, 14075-14088, doi:M113.499277 [pii]10.1074/jbc.M113.499277 (2014).
- 38 Kuang, S. Q. et al. Rare, nonsynonymous variant in the smooth muscle-specific isoform of myosin heavy chain, MYH11, R247C, alters force generation in the aorta and phenotype of smooth muscle cells. *Circ Res* 110, 1411-1422, doi:CIRCRESAHA.111.261743 [pii]10.1161/CIRCRESAHA.111.261743 (2012).
- 39 Pannu, H. et al. MYH11 mutations result in a distinct vascular pathology driven by insulin-like growth factor 1 and angiotensin II. *Hum Mol Genet* 16, 2453-2462, doi:ddm201 [pii]10.1093/hmg/ddm201 (2007).
- 40 Hu, B., Wu, Z. & Phan, S. H. Smad3 mediates transforming growth factor-beta-induced alpha-smooth muscle actin expression. *Am J Respir Cell Mol Biol* 29, 397-404, doi:10.1165/rcmb.2003-0063OC 2003-0063OC [pii] (2003).
- 41 Vardoulis, L., Vasilaki, E., Papadimitriou, E., Kardassis, D. & Stournaras, C. A novel mechanism of TGFbeta-induced actin reorganization mediated by Smad proteins and Rho GTPases. *FEBS J* 275, 4074-4087, doi:EJB6549 [pii]10.1111/j.1742-4658.2008.06549.x (2008).
- 42 Qiu, P., Feng, X. H. & Li, L. Interaction of Smad3 and SRF-associated complex mediates TGF-beta1 signals to regulate SM22 transcription during myofibroblast differentiation. *J Mol Cell Cardiol* 35, 1407-1420, doi:S0022282803002839 [pii] (2003).
- 43 van der Pluijm, I. et al. Defective Connective Tissue Remodeling in Smad3 Mice Leads to Accelerated Aneurysmal Growth Through Disturbed Downstream TGF-beta Signaling. *EBioMedicine* 12, 280-294, doi:S2352-3964(16)30413-3 [pii]10.1016/j.ebiom.2016.09.006 (2016).
- 44 Choquet, D., Felsenfeld, D. P. & Sheetz, M. P. Extracellular matrix rigidity causes strengthening of integrin-cytoskeleton linkages. *Cell* 88, 39-48, doi:S0092-8674(00)81856-5 [pii] (1997).
- 45 Lo, C. M., Wang, H. B., Dembo, M. & Wang, Y. L. Cell movement is guided by the rigidity of the substrate. *Biophys J* 79, 144-152, doi:S0006-3495(00)76279-5 [pii]10.1016/S0006-3495(00)76279-5 (2000).
- 46 Saez, A., Buguin, A., Silberzan, P. & Ladoux, B. Is the mechanical activity of epithelial cells controlled by deformations or forces? *Biophys J* 89, L52-54, doi:S0006-3495(05)73006-X [pii]10.1529/biophysj.105.071217 (2005).

- 47 Burger, J. et al. Fibulin-4 deficiency differentially affects cytoskeleton structure and dynamics as well as TGFbeta signaling. *Cell Signal* 58, 65-78, doi:S0898-6568(19)30037-3 [pii]10.1016/j.cellsig.2019.02.008 (2019).
- 48 Franken, R. et al. Beneficial Outcome of Losartan Therapy Depends on Type of FBN1 Mutation in Marfan Syndrome. *Circ Cardiovasc Genet* 8, 383-388, doi:CIRCGENETICS.114.000950 [pii] 10.1161/CIRCGENETICS.114.000950 (2015).
- 49 den Hartog, A. W. et al. The effect of losartan therapy on ventricular function in Marfan patients with haploinsufficient or dominant negative FBN1 mutations. *Neth Heart J* 24, 675-681, doi:10.1007/s12471-016-0905-8 10.1007/s12471-016-0905-8 [pii] (2016).



Betaglycan (TGFB β 3)
upregulation correlates
with increased TGF- β
signaling in Marfan patient
fibroblasts in vitro.

Natalija Bogunovic*, Menno E. Groeneveld*, René J. P. Musters,
Geert Jan Tangelder, Gerard Pals, Willem Wisselink,
Dimitra Micha, Kak K. Yeung

* These authors contributed equally.

ABSTRACT

Marfan syndrome (MFS), a congenital connective tissue disorder leading to aortic aneurysm development, is caused by fibrillin-1 (FBN1) gene mutations. Transforming growth factor beta (TGF- β) might play a role in the pathogenesis. It is still a matter of discussion if and how TGF- β up-regulates the intracellular down-stream pathway, although TGF- β receptor 3 (TGFB3 or Betaglycan) is thought to be involved. We aimed to elucidate the role of TGFB3 protein in TGF- β signaling in Marfan patients.

Dermal fibroblasts of MFS patients with haploinsufficient (HI; n=9) or dominant negative (DN; n=4) FBN1 gene mutations, leading to insufficient or malfunctioning fibrillin-1, respectively, were used. Control cells (n=10) were from healthy volunteers. We quantified TGFB3 protein expression by immunofluorescence microscopy and gene expression of FBN1, TGFB1, its receptors, and downstream transcriptional target genes by quantitative polymerase chain reaction.

Betaglycan protein expression in FBN1 mutants pooled was higher than in controls (P=.004) and in DN higher than in HI (P=.015). In DN, significantly higher mRNA expression of FBN1 (P=.014), SMAD7 (P=.019), HSP47 (P=.023), and SERPINE1 (P=.008), but a lower HSPA5 expression (P=.029), was observed than in HI. A pattern of higher expression was noted for TGFB1 (P=.059), FN1 (P=.089), and COL1A1 (P=.089) in DN as compared to HI. TGFB3 protein expression in cells, both presence in the endoplasmic reticulum and amount of vesicles per cell, correlated positively with TGFB1 mRNA expression ($R_s=0.60, P=.017$; $R_s=0.55, P=.029$; respectively). TGFB3 gene expression did not differ between groups.

We demonstrated that activation of TGF- β signaling is higher in patients with a DN than an HI FBN1 gene mutation. Also, TGFB3 protein expression is increased in the DN group and correlates positively with TGFB1 expression in groups pooled. We suggest that TGFB3 protein expression is involved in up-regulated TGF- β signaling in MFS patients with a DN FBN1 gene mutation.

INTRODUCTION

Marfan syndrome (MFS) is a connective tissue disorder that is characterized by abnormalities in the skeletal, ocular, pulmonary, nervous and cardiovascular system.¹⁻³ The most severe cardiovascular manifestation of MFS is the development of aortic aneurysms (AA), predominantly thoracic AA, which can lead to rupture associated with high mortality.^{4,5} The syndrome is caused by mutations in the fibrillin-1 gene (*FBN1*). Fibrillin-1 constitutes the core of microfibrils, which provide structural stability to extracellular matrix (ECM) and are also responsible for the elastic properties of the vessel wall.^{6,7} Mutations can be classified as dominant negative (DN) or as haploinsufficient (HI), depending on the effect that the mutation has on the fibrillin-1 protein.⁸ DN mutations lead to a malformed or malfunctioning fibrillin-1 protein and thus a disturbed ECM.^{9,10} HI mutations are caused by the deletion of one copy of the whole gene, degradation of the mutant protein, or nonsense-mediated decay by degradation of fibrillin-1 mRNA.¹⁰⁻¹² The latter mutation will lead to reduced level of wild type fibrillin-1 protein, and thus compromised functionality.^{9,10} In the ECM, fibrillin-1, together with fibrillin-2, also regulates the bioavailability of transforming growth factor β (TGF- β) by binding this growth factor in a latent complex.¹³ TGF- β signaling is responsible for the expression of connective tissue components in the ECM.^{4,13} In MFS, excessive TGF- β signaling is observed as a result of mutated fibrillin-1 in the ECM, which is thought to be responsible for AA development.¹⁴ Malformed fibrillin-1 proteins, may be subjected to degradation in the endoplasmic reticulum (ER) mediated by heat shock proteins A5 (HSPA5) and 47 (HSP47).^{15,16}

TGF- β isoforms regulate transcription of ECM components such as collagen and fibrin.^{4,13,17-19} By binding to cell surface TGF- β receptors (TGFB1, -2 and -3; TGFB3 is also known as Betaglycan), their downstream intracellular pathway is activated by SMADS, the intracellular effectors of TGF- β signaling.^{13,19-23} SMADS are recruited to the activated receptor complex and after phosphorylation they form a complex, which is transported into the nucleus.²³ This results in the transcription of their target genes collagen type 1 alpha 1 (*COL1A1*), fibronectin (*FN1*), *SERPINE1* and connective tissue growth factor (*CTGF*).²⁴⁻²⁷ A negative feedback loop on the expression of TGF- β itself is provided by the transcriptional TGF- β target SMAD7.^{19,28} TGF- β has long been acknowledged as a major factor of MFS development, however, in the past years more studies question whether such a role can be attributed to TGF- β .²⁹

TGFB3 is a co-receptor of the TGF- β superfamily that increases the binding of TGF- β to TGFB1 and TGFB2. In recent years however, more functions of TGFB3 have been identified, expanding its role from a simple co-receptor to a broader and more complex receptor. It has been suggested to influence cellular processes such as TGF- β receptor trafficking and regulation of signaling output.³⁰

We hypothesized that the expression TGFBR3 may modulate TGF- β signaling. In the current work we aimed to elucidate the role of TGFBR3 in the TGF- β signaling pathway of MFS patients. This was investigated by the quantification of mRNA expression of *TGFBR3* and *TGFB*, as well as a panel of TGF- β signaling-associated target genes in primary dermal fibroblasts of MFS patients. TGFBR3 expression was studied at the protein level by immunofluorescence staining in MFS fibroblasts. As the type of mutation modulates the effect on a protein level, a differentiation was made for patients with a DN and a HI *FBN1* gene mutation.⁸

MATERIALS AND METHODS

Patients and healthy volunteers

The study was approved by the Medical Ethical Committee of the VU University Medical Center (VUmc) Amsterdam. Primary dermal fibroblasts were cultured from skin biopsies taken from the upper arm of thirteen patients (7 men) with a median age (with range) of 37 years (9 – 64), all with a known mutation in the *FBN1* gene (4 DN and 9 HI mutations). As control fibroblasts of 10 healthy volunteers were used (7 men) with median age 34 (0 – 56). Controls were gender-matched healthy volunteers without a medical history of cardiovascular disease. Table 1 shows the characteristics and *FBN1* mutations of the patients and controls.

Cell culture preparation

Primary human dermal fibroblasts were cultured in Ham's F10 Nutrient Mix Medium (Thermo Fischer Scientific; catalog number 31550031) supplemented with 10% fetal bovine serum (Thermo Fischer Scientific; catalog number 10270106), 100 units/mL penicillin and 100 μ g/mL streptomycin (Thermo Fischer Scientific; catalog number 15070063). The cells were maintained in a humidified incubator at 37°C and 5% CO₂. Cells were seeded in chamber slides (Thermo Fischer Scientific; catalog number 154534) and were left to attach and establish a monolayer during five days prior to immunofluorescence.

Table 1. Genotypic characteristics of all 13 included patients are presented. The *FBN1* mutation type is given as haploinsufficient (HI) or dominant negative (DN).

Mutants	Age	Gender	Type	Domain	Mutation	Effect
1	37	M	HI	8Cys-4	4605T>A	Y1535X
2	17	F	HI	INTRON	1468+2T>C	retention intron 11
3	20	M	HI	NA	0-allele	NA
4	39	F	HI	INTRON	3464-6C>A	splice error insACAG and NMD
5	9	M	HI	cb-EGF45	7732C>T	Q2578X and 0-allele
6	27	M	HI	cb-EGF25	4428C>A	Y1476X
7	43	F	HI	Proline-rich	1285C>T	R429X
8	64	M	HI	cb-EGF29	5368C>T	R1790X
9	24	M	HI	cb-EGF6	1387G>T	G463X
10	50	M	DN	cb-EGF24	4291T>C	C1431R
11	56	F	DN	8Cys-4	4588C>T	R1530C
12	40	F	DN	8Cys-3	2946 C>G	C982W
13	33	F	DN	cb-EGF8	1701G>T leads to 1700_1714del	G567_Q571del

Quantification of protein expression by immunofluorescence microscopy

Cells were rinsed with phosphate buffered saline (PBS) (3 times 3 minutes at 37°C), then fixed in 4% formaldehyde containing PBS and rinsed again in 0.05% Tween (PBST) for 3 minutes. After cell membrane permeabilization by 0.2% Triton for 10 minutes, the cells were rinsed, and incubated overnight at 4°C with the primary antibody for TGFB3 (dilution 1:100; sc-75411, Santa Cruz, USA). After washing, cells were incubated with the secondary antibody (dilution 1:100; Molecular Probes, USA) for 30 minutes at room temperature. Additionally, samples were incubated for 20 minutes in wheat-germ-agglutinin (WGA) Alexa 555 fluorescent probes, targeting the cell membrane glycocalyx (dilution 1:50 in PBS; Molecular Probes, USA). After staining, samples were rinsed and mounted on a glass slide using VectashieldTM mounting medium containing DAPI nuclear stain (Vector Laboratories Inc., USA) and sealed using a cover glass.

Sections were examined with a Zeiss Axiovert 200M MarianasTM inverted microscope, equipped with a motorized stage (stepper-motor) z-axis increments 0.1µm, and a turret with a DIC brightfield cube and four epifluorescence cubes,

having emission in blue (DAPI for cell nuclei), green (FITC for TGFB3), red (Cy3 for cell membrane). A cooled CCD camera (Cooke Sensicam SVGA (Cooke Co., USA), 1280 x 1024 pixels), linear over its full dynamic range, recorded images with true 16-bit capability. The microscope, camera, and data processing were controlled by SlideBookTM software (version 5.0.1.8, Intelligent Imaging Innovations, Denver, U.S.). Fifteen images covering the whole slide per patient were taken with a 63X oil-immersion objectives (CARL ZEISS, The Netherlands).

Analysis of images was conducted by a manual operator-dependent count of TGFB3 positive vesicles and cells, which was performed by two independent researchers (representative images are seen in figure 1A-D). Vesicles were defined as spherical structures that demonstrate staining for both TGFB3 and glycocalyx from the cell membrane. Vesicles were characterized as large (>6µm) or small. Furthermore, cells were counted and distinguished into positive and negative for the presence of intracellular TGFB3. Vesicles per cell and the ratio between TGFB3 positive cells and total cell counts were calculated after automatic nuclei counts (performed by SlideBookTM software). No interobserver variability was found in the measurements (vesicles: $p=0.69$; TGFB3 positive cells: $p=1.0$).

Quantification of gene expression by quantitative polymerase chain reaction

Total RNA was isolated using the NucleoSpin Triprep Kit (Macherey-Nagel, Düren, Germany). Complementary DNA synthesis was performed using the VILO kit (Macherey-Nagel, Düren, Germany), in a 20µL reverse transcription reaction, according to manufacturer's instructions. Quantitative PCR (qPCR) was performed to show the effect of the mutations on mRNA level in *FBN1* (NM_000138), and to analyze the potential effect of the mutation on the expression of related and target genes: *FBN2* (NM_001999), *FBN3* (NM_032447), *FN1* (NM_002026), *SERPINE1* (NM_000602), *SMAD7* (NM_005904), *TGFB1* (NM_000660), *TGFB1* (NM_004612), *TGFB2* (NM_003242), *TGFB3* (NM_003243), *COL1A1* (NM_000088), *CTGF* (NM_001901) *HSP47* (NM_001207014) and *HSPA5* (NM_005347). As housekeeping genes for the normalization of the acquired data *YWHAZ* (NM_003406), *HPRT* (NM_000194) and *UBC* (NM_021009) were used. The analysis was performed using the using the Light Cycler SYBR Green I Master (Roche Applied Science, Penzberg, Germany) in the LightCycler 480 Instrument II (Roche Applied Science, Penzberg, Germany), as described before in more detail.³¹

Each qPCR reaction was prepared in a total volume of 10µL, consisting of 2µL PCR grade water, 1µL forward primer (10pM), 1µL reverse primer (10pM) and 5µL Light Cycler Mastermix (Light Cycler 480 SYBR Green I Master; Roche Applied Science), to which 2µL of the synthesized cDNA was added. Using absolute quantification, all values were determined based on standard curve of four serial dilutions ranging from 10ng until 0.08ng of human reference cDNA (Agilent Technologies, Santa Clara,

CA). qPCR efficiency was assessed using the fit points method, and gene expression data was analyzed with the efficiency ranging between 1.7-2.0. Moreover, mRNA expression of the investigated genes was normalized by a normalization factor derived from the expression of three housekeeping genes (*YWHAZ*, *HPRT* and *UBC*).

Statistical analysis

Data were analyzed with SPSS (IBM Statistics v24, Chicago, IL). For multiple groups, the Kruskal–Wallis was used first to compare continuous variables with nonparametric distribution; subsequently, the Mann–Whitney U test was used for comparing two groups. Fisher's exact test was used for categorical variables in two groups. Raw data are given in the text as median with ranges in between brackets and data are presented graphically as boxplots (showing median and quartiles) with outliers (according to Tukey's criteria) indicated separately. Correlations between two continuous variables were calculated by Spearman rank. Tests were considered statistically significant at $P < 0.05$. In case of multiple testing, corrected p-values are used according to Bonferroni.

RESULTS

Protein expression in cell lines

By immunofluorescence microscopy, a significantly higher ratio of TGFB3 positive cells was observed in the cell cultures of both DN and HI groups pooled (median 0.35 [0.11 - 0.80]) as compared to controls (median 0.00 [0.00 - 0.37]; $p = 0.004$). DN patients had higher ratios of TGFB3 positive cells (median 0.47 [0.14 - 0.80]) than HI patients (median 0.33 [0.11 - 0.80]; $p = 0.015$). No differences were found in the expression of TGFB3 vesicles between *FBN1* mutant cells and controls or between DN and HI patients (table 2 and figure 1).

Table 2. TGF- β receptor 3 protein expression was demonstrated by immunofluorescence microscopy in membrane-encapsulated vesicles or in the endoplasmic reticulum. Vesicles were classified as small ($\leq 6\mu\text{m}$) or large. The ratio of vesicles per nucleus is given, as well as the ratio of cells positive for TGF- β receptor 3 in the endoplasmic reticulum per total cell count. Median ratios are given with ranges in between brackets. Genetic expressions were measured by quantitative polymerase chain reaction and presented in arbitrary units. Statistical differences between *FBN1* mutants pooled and controls are given by p-values, as well as between DN and HI *FBN1* mutations. P-values < 0.05 were considered significant and are indicated by an asterisk.

Immunofluorescence microscopy	Mutants (total)	Control	p-value	DN	HI	p-value
	<i>n</i> = 13	<i>n</i> = 10		<i>n</i> = 4	<i>n</i> = 9	
Small vesicles (per nucleus)	0.14 (0.03 - 0.60)	0.14 (0.03 - 0.30)	0.419	0.26 (0.07 - 0.41)	0.12 (0.03 - 0.60)	0.643
Large vesicles (per nucleus)	0.02 (0.00 - 0.07)	0.01 (0.00 - 0.04)	0.651	0.01 (0.00 - 0.07)	0.02 (0.00 - 0.04)	1.000
Total vesicles (per nucleus)	0.16 (0.04 - 0.61)	0.16 (0.03 - 0.30)	0.420	0.30 (0.07 - 0.41)	0.14 (0.04 - 0.61)	0.643
β-glycan positive cells (of total)	0.35 (0.11 - 0.80)	0.00 (0.00 - 0.37)	0.004*	0.47 (0.14 - 0.80)	0.33 (0.11 - 0.80)	0.015*
Quantitative PCR	<i>n</i> = 10	<i>n</i> = 6		<i>n</i> = 4	<i>n</i> = 6	
<i>TGFB1</i>	7.23 (4.55 - 11.1)	4.64 (2.76 - 6.97)	0.027*	7.59 (7.19 - 11.06)	6.17 (4.55 - 7.83)	0.059
<i>TGFBR1</i>	1.09 (0.71 - 2.01)	1.39 (0.79 - 1.96)	0.615	1.04 (0.84 - 1.70)	1.21 (0.71 - 2.01)	0.05
<i>TGFBR2</i>	2.25 (1.14 - 7.95)	1.59 (0.62 - 3.75)	0.191	2.45 (1.85 - 7.95)	2.25 (1.14 - 3.11)	0.345
<i>TGFBR3</i>	3.65 (1.78 - 7.69)	4.33 (0.41 - 7.03)	0.688	3.21 (2.5 - 4.01)	4.74 (1.78 - 7.69)	0.257
<i>SMAD7</i>	7.29 (4.77 - 15.5)	5.61 (3.03 - 6.73)	0.044*	9.24 (7.09 - 15.47)	6.43 (4.77 - 11.7)	0.019*
<i>FBN1 P1</i>	2.08 (0.74 - 6.20)	1.83 (0.88 - 5.04)	0.546	3.48 (2.10 - 6.20)	1.93 (0.74 - 2.59)	0.014*
<i>FBN1 P2</i>	0.66 (0.34 - 1.25)	0.79 (0.34 - 2.12)	0.315	0.79 (0.63 - 1.25)	0.51 (0.34 - 1.21)	0.089
<i>FBN2</i>	8.13 (0.49 - 52.4)	11.28 (7.81 - 101.3)	0.228	8.13 (4.68 - 34.4)	8.72 (0.49 - 52.4)	0.450
<i>HSP47</i>	41.2 (27.9 - 75.5)	29.8 (4.56 - 50.3)	0.070	53.6 (37.5 - 75.5)	34.1 (27.9 - 51.2)	0.023*
<i>HSPA5</i>	2.77 (1.99 - 4.20)	2.48 (1.62 - 3.28)	0.131	2.49 (1.99 - 2.89)	3.18 (2.58 - 4.20)	0.029*
<i>SERPINE1</i>	42.7 (24.8 - 71.5)	35.2 (13.24 - 87.5)	0.688	51.8 (46.6 - 71.5)	39.5 (24.8 - 45.0)	0.008*
<i>FN1</i>	21.1 (10.4 - 64.6)	22.7 (7.61 - 33.9)	0.688	37.2 (17.5 - 64.6)	19.1 (10.4 - 27.0)	0.089
<i>CTGF</i>	39.5 (4.40 - 163.9)	23.6 (16.5 - 44.0)	0.615	48.5 (11.1 - 163.9)	30.2 (4.40 - 78.6)	0.571
<i>COL1A1</i>	1898.0 (939.0 - 2689.4)	1137.8 (406.1 - 1589.5)	0.088	2314.2 (1894.1 - 2360.0)	1269.3 (939.0 - 2689.4)	0.089

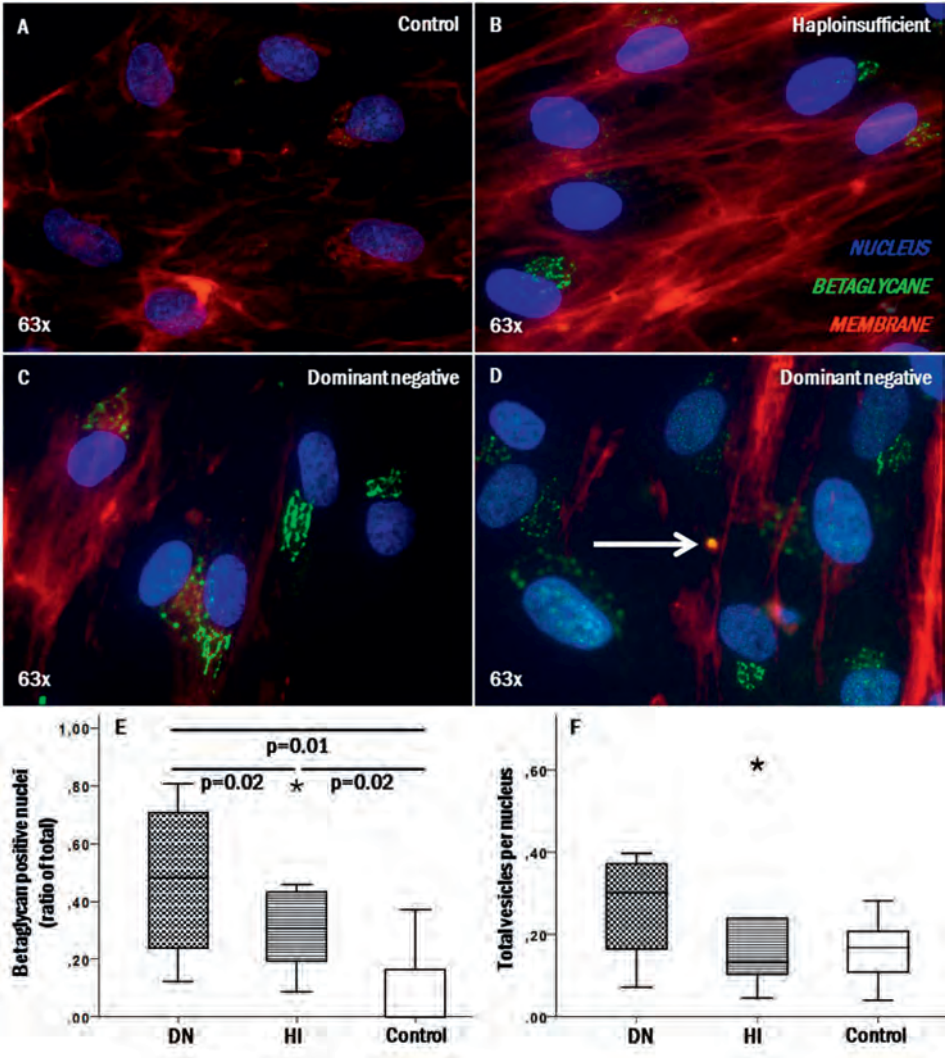


Figure 1. Representative immunofluorescence microscopy images of Betaglycan expression in fibroblast cell cultures of a control (A), a haploinsufficient (B) and dominant negative (C) FBN1 gene mutation. Betaglycan was seen in the endoplasmic reticulum or in membrane encapsulated vesicles as indicated by the arrow in image D. Ratios of Betaglycan positive cells per total cell count (E) and vesicles per nucleus (F) are given as median with interquartile ranges in the boxplots. Significant differences ($P \leq 0.05$) are highlighted by a horizontal line and outliers are indicated separately by an asterisk.

Gene expression in cell cultures

By qPCR, a significantly higher gene expression was measured in *FBN1* mutant cells than in controls for both *TGFB1* (median 7.23 [4.55 - 11.1] versus 4.64 [2.76 - 6.97]; $p=0.027$; respectively) and *SMAD7* (median 7.29 [4.77 - 15.5] versus 5.61 [3.03 - 6.73]; $p=0.044$; respectively). *COL1A1* had a tendency to be higher (median 1898.0 [939.0 - 2689.4]) than in controls (median 1137.8 [406.1 - 1589.5]; $p=0.088$), as well *HSP47* (median 41.2 [27.9 - 75.5] versus 29.8 [4.56 - 50.3]; $p=0.070$, respectively). No differences were found in *TGFR1*, -2 and -3 expression between groups, or in downstream proteins *FBN1* and *FBN2*, *HSPA5*, *FN1*, *SERPIN1* and *CTGF*. See figure 2 for boxplots of a selection of gene expressions.

Subgroup analysis showed higher gene expressions in DN as compared to HI of *SMAD7* (median 9.24 [7.09 - 15.47] versus 6.43 [4.77 - 11.7]; $p=0.019$; respectively), *FBN1* P1 (median 3.48 [2.10 - 6.20] versus 1.93 [0.74 - 2.59]; $p=0.014$; respectively), *HSP47* (median 53.6 [37.5 - 75.5] versus 34.1 [27.9 - 51.2]; $p=0.023$; respectively) and *SERPIN1* (median 51.8 [46.6 - 71.5] versus 39.5 [24.8 - 45.0]; $p=0.008$; respectively). DN had lower gene expression of *HSPA5* than HI (median 2.49 [1.99 - 2.89] versus 3.18 [2.58 - 4.20]; $p=0.029$; respectively). DN tended to have higher gene expressions than HI of *TGFB1* (median 7.59 [7.19 - 11.06] versus 6.17 [4.55 - 7.83]; $p=0.059$; respectively), *FBN1* P2 (median 0.79 [0.63 - 1.25] versus 0.51 [0.34 - 1.21]; $p=0.089$; respectively) *FN1* (median 37.2 [17.5 - 64.6] versus 19.1 [10.4 - 27.0]; $p=0.089$; respectively) and *COL1A1* (median 2314.2 [1894.1 - 2360.0] versus 1269.3 [939.0 - 2689.4]; $p=0.089$; respectively).

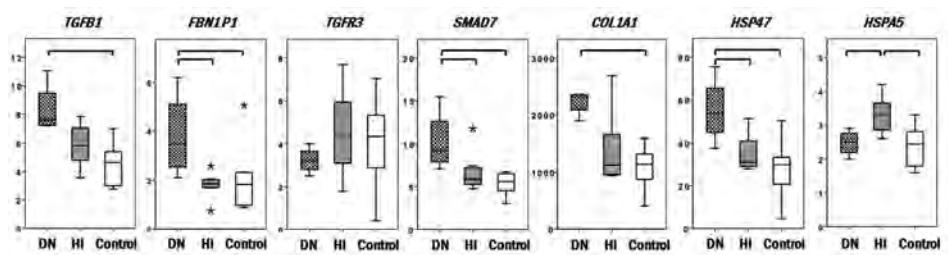


Figure 2. In this figure a selection of the results of quantitative polymerase chain reaction in arbitrary units in dominant negative and haploinsufficient *FBN1* mutations and controls are graphically represented as boxplots with interquartile ranges.

Significant differences between groups ($P \leq 0.05$) are highlighted by an accolade. Outliers are separately indicated by an asterisk.

Correlations between protein and mRNA expression

The correlation between *TGFB1* mRNA expression with *TGFB3* mRNA and TGFB3 positive cells (both ratio and total positive cells) was tested (significance level after Bonferroni correction for multiple testing is $p \leq 0.017$). *TGFB1* mRNA expression was positively correlated with the ratio of TGFB3 positive cells ($R_s=0.60$, $p=0.017$; figure 3). No correlation was found between TGFB3 protein expression and *TGFB3* mRNA expression.

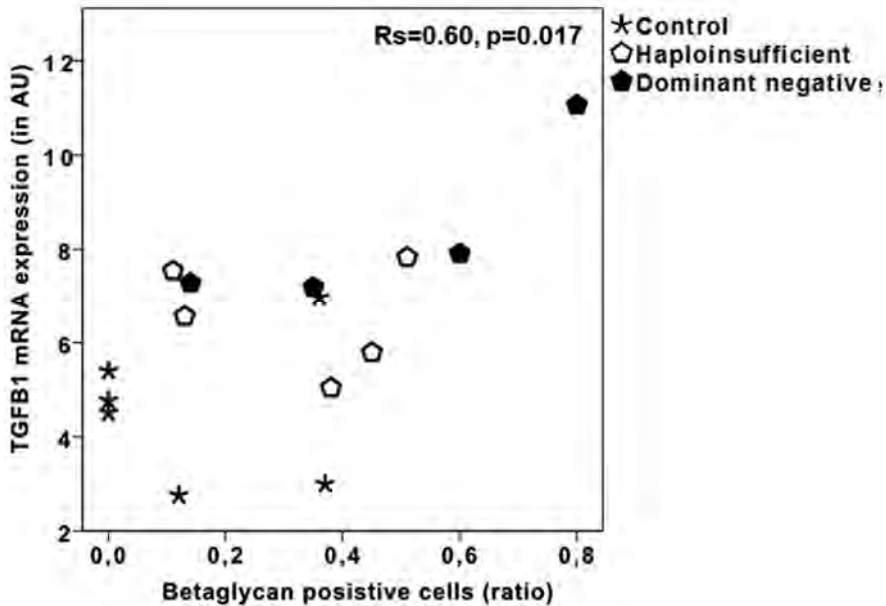


Figure 3. Correlations between TGFB3 protein expression and TGFB1mRNA expression. The ratio of TGFB3 positive cells to the total cell count is given on the x-axis, TGFB1 mRNA expression on the Y-axis (in AU). Correlations are given in Spearman rank (R_s) correlation with p-value.

DISCUSSION

The major findings of the present study are: i) in patients with a DN *FBN1* gene mutation, fibroblasts have upregulated *TGFB1* and associated downstream signaling activation as compared to controls. Also, DN *FBN1* gene mutants have a tendency of upregulated *TGFB1* and associated signaling activation as compared to HI *FBN1* gene mutants; ii) TGFBR3 protein expression in patients with a DN *FBN1* gene mutation is higher than in the HI group; iii) *TGFB1* expression is positively correlated with TGFBR3 protein expression.

The intracellular downstream pathway of TGF- β involves, among others, SMAD7 activation as well as transcription of COL1A1 and FN1.^{20–27} In figure 4 we graphically represented the investigated part of the pathway in DN mutants. We demonstrated upregulated TGF- β activation and downstream signaling. On a protein level we observed more TGFBR3 expression in DN *FBN1* gene mutants than in HI patients. It has been suggested that TGFBR3 is able to inhibit as well as enhance downstream TGF- β signaling.³⁰ However, it remains a matter of debate how TGFBR3 provides the downstream TGF- β signaling in MFS.³⁰ It has been acknowledged that TGFBR3 stimulates downstream signaling by presenting TGF- β to TGFBR2.¹⁸ Recently, however, two studies suggested that TGFBR3 regulates the signaling turnover by adjusting the ratio of soluble to membrane bound receptors.^{32,33} In the current study we demonstrated a positive correlation between TGFBR3 protein expression and TGF- β signaling. We acknowledge that no knock-out or over-expression experiments have been performed, which hinders providing causative correlations. However, our data suggest that increased expression of TGFBR3 in MFS patients with DN mutation enhances activation of the TGF- β signaling pathway. Our study warrants further investigation of the role of TGFBR3.

TGFBR3 protein expression was observed in two distinct locations in the cell, either in the ER or in intracellular membrane encapsulated vesicles. We observed higher expressions of TGFBR3 in MFS patients with a DN than a HI mutation. However, no differences were found in gene expression of *TGFBR3* between mutants and controls or between DN and HI. We hypothesize that the encapsulated TGFBR3 is stored in vesicles in order to regulate the total amount of receptors that are expressed on the cell membrane. By doing so, as described above, TGFBR3 might adjust the ratio of soluble to membrane bound receptors and influence TGF- β signaling.³³ This hypothesis could explain the discrepancy between *TGFBR3* mRNA and TGFBR3 protein expression in fibroblasts. However, one must realize that we investigated cell cultures of skin fibroblasts that lack an ECM like in the aortic wall. The lack of ECM might alter the stimulation and direction of the TGFBR3 filled vesicles.

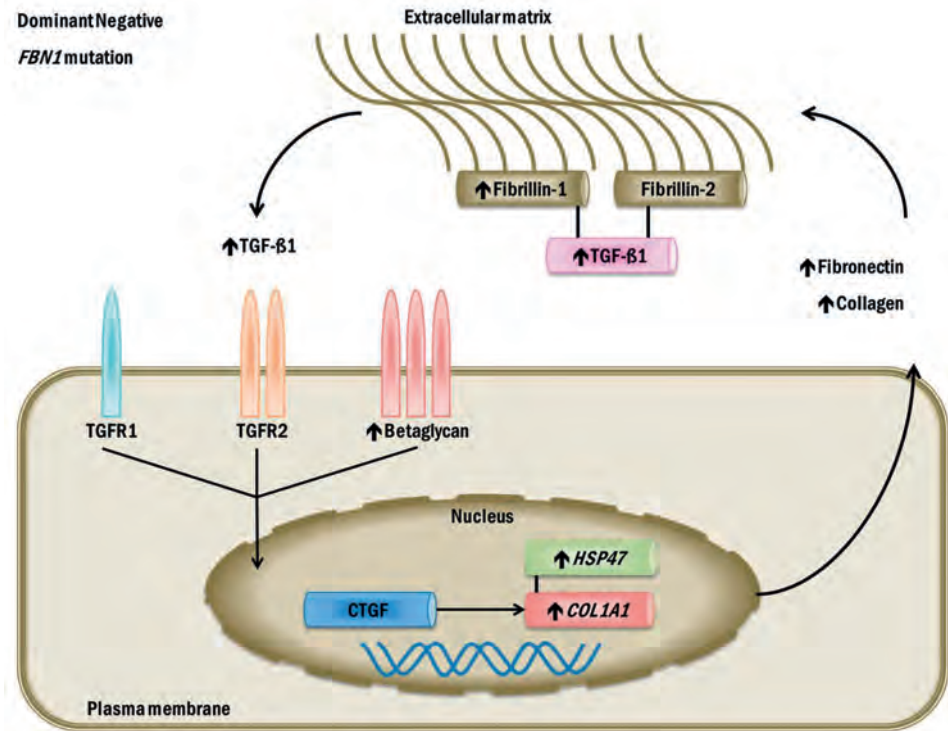


Figure 4. TGF- β signaling and its partially downstream pathways in dominant negative *FBN1* mutations. Upward pointing arrows indicate increased expression as compared to healthy controls. In the extracellular matrix fibrillin-1 expression is up-regulated, though it partly concerns wild type but also malformed proteins. Therefore its binding capacity to TGF- β 1 is affected, resulting in high levels of free TGF- β 1 in the extracellular matrix. The intracellular downstream pathway of TGF- β 1 is consequently activated in higher amounts. Interestingly, increased downstream activation occurs while the amount of TGF- β receptors are similar to controls. Eventually, intranuclear transcription of COL1A1 and its chaperone protein HSP47 are up-regulated resulting in increased collagen expression and the tendency of higher fibronectin expression.

As discussed earlier, fibrillin-1 protein is involved in the regulation of TGF- β bioavailability in the ECM by binding to complexes of latent TGF- β .¹³ In patients with a DN *FBN1* mutation we observed upregulated *FBN1* gene expressions as compared to controls and a tendency of higher expressions in the DN than in the HI group. In MFS patients with a DN mutation this will lead to malfunctioning fibrillin-1 protein, with less capacity to bind latent TGF- β in the ECM.⁹ We suggest that in DN *FBN1* gene mutants this might be the cause of increased free TGF- β in the ECM of diseased vessel walls, as was earlier demonstrated.³⁴ Fibrillin-2 protein has also

been acknowledged to have a role in the regulation of free TGF- β in the ECM.¹³ However, we found that TGF- β and its downstream signaling was increased in DN mutants, despite similar *FBN2* gene expression. Therefore, we suggest that fibrillin-2 has only a limited role in the level of TGF- β expression.

A remarkable contradiction was the finding of upregulated expression of *HSP47* in the DN group as compared to HI patients, versus downregulated expression of *HSPA5* in the DN group as compared to HI patients. Both genes are acknowledged as ER stress markers, more specifically as markers of activated unfolded protein response.^{35,36} Furthermore, TGF- β has been demonstrated to upregulate the expression of *HSP47*.³⁷ Therefore, increased *HSP47* expression was expected in the DN group, as DN *FBN1* mutations lead to malformed fibrillin-1 proteins and consequently to activation of the unfolded protein response. We did not expect *HSPA5* expression to be increased in the HI group as compared to the DN group and controls. This could be explained by the fact that *HSPA5* also functions as a chaperone protein, transporting newly synthesized polypeptides and facilitates their assembly into proteins. This process may be disturbed in DN mutants.^{15,16}

The use of fibroblasts may be regarded as a limitation of this study, as it possibly does not fully reflect aortic cell pathology. These cells have the genotype but not the phenotype. However, it has been demonstrated that patients with enhanced TGF- β signaling in dermal fibroblasts also are associated with multiple syndromic presentations of aortic aneurysms.³⁸ We therefore consider these cells to be representative for this part of the investigated pathway. Furthermore, in the current work we have mainly focused on the genetically stimulation. Therefore, at this time our data lack clinical information. Therefore, our model does not take into account the potential impact of aspects such as phenotypic variation between patients and pharmacological treatments.

The implication of the present work is that it emphasizes important differences in patients between the effects of DN versus HI mutations of the *FBN1* gene. A recent study showed that MFS patients with HI *FBN1* mutations had higher therapeutic benefit from Losartan treatment compared to patients with DN *FBN1* mutations which indicates a distinct pathological mechanism.⁸ Thus, the different types of *FBN1* mutations must be approached in a different manner in the search for therapeutic options.

In conclusion, we demonstrated an increased activation of TGF- β and its downstream signaling pathway in patients with a DN *FBN1* gene mutation as compared to patients with a HI *FBN1* mutation and to control groups. Also, TGFB3 protein expressions are increased in the DN group and correlate positively with *TGFB1* expressions in groups pooled. We suggest that TGFB3 expression is

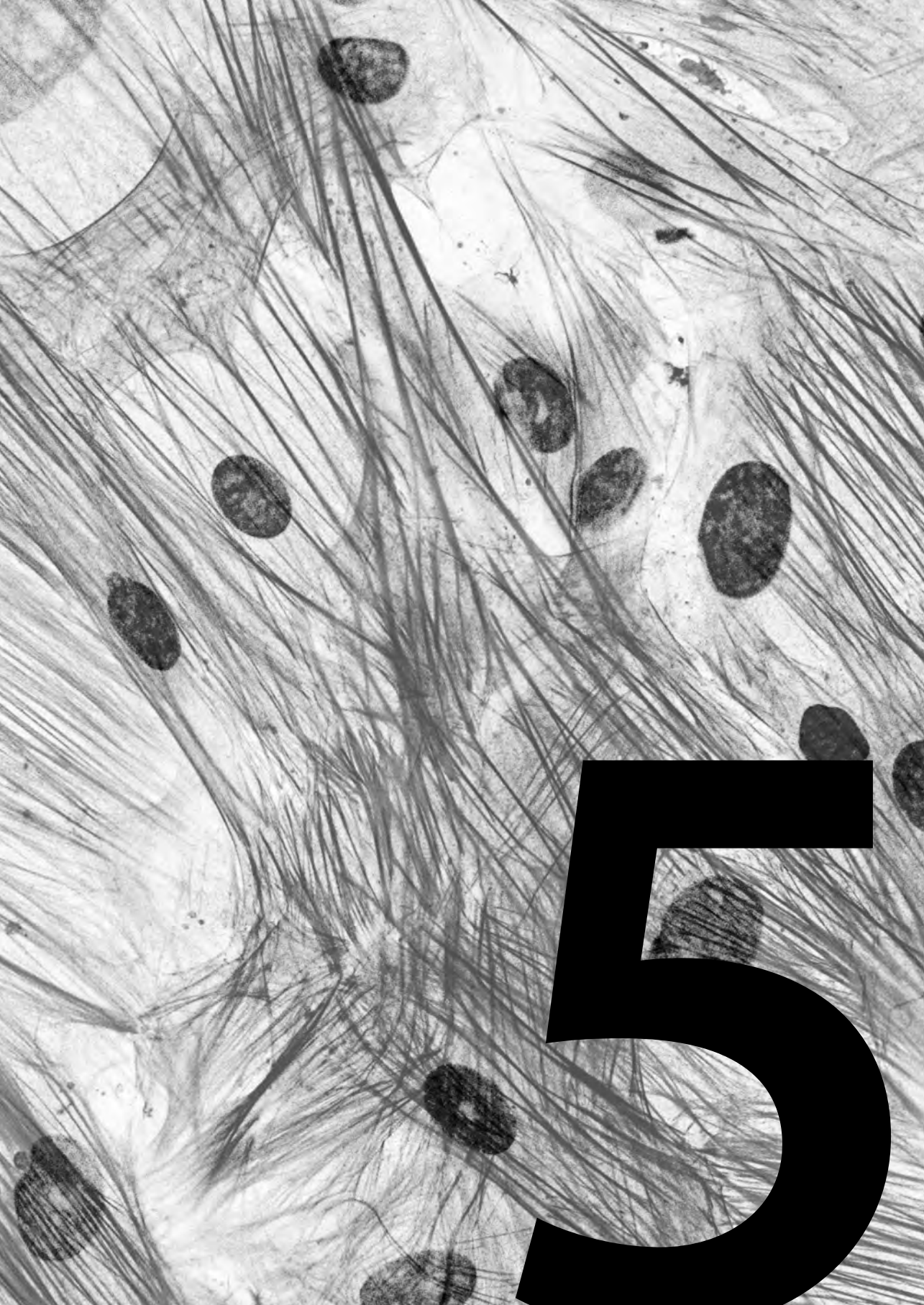
involved in upregulated TGF- β signaling in MFS patients with a DN *FBN1* gene mutation.

REFERENCES

1. Dietz HC. Marfan syndrome. In: Marfan Syndrome. 2001 Apr 18 [Updated 2017 Feb 2]. In: Pagon RA, Adam MP, Ardinger HH, et Al., Editors. GeneReviews® [Internet]. Seattle (WA): University of Washington, Seattle; 1993-2017. <https://www.ncbi.nlm.nih.gov/books/NBK1335/>.
2. Takeda N, Yagi H, Hara H, et al. Pathophysiology and Management of Cardiovascular Manifestations in Marfan and Loeys-Dietz Syndromes. *Int Heart J*. 2016;271-277. doi:10.1536/ihj.16-094.
3. Sakai LY, Keene DR, Renard M, De Backer J. FBN1: The disease-causing gene for Marfan syndrome and other genetic disorders. *Gene*. 2016;591(1):279-291. doi:10.1016/j.gene.2016.07.033.
4. Gillis E, Van Laer L, Loeys BL. Genetics of thoracic aortic aneurysm: At the crossroad of transforming growth factor- β signaling and vascular smooth muscle cell contractility. *Circ Res*. 2013;113(3):327-340. doi:10.1161/CIRCRESAHA.113.300675.
5. Attenhofer Jost CH, Greutmann M, Connolly HM, et al. Medical treatment of aortic aneurysms in Marfan syndrome and other heritable conditions. *Curr Cardiol Rev*. 2014;10(2):161-171. doi:10.2174/1573403X1002140506124902.
6. Zeyer KA, Reinhardt DP. Engineered mutations in fibrillin-1 leading to Marfan syndrome act at the protein, cellular and organismal levels. *Mutat Res - Rev Mutat Res*. 2015;765:7-18. doi:10.1016/j.mrrev.2015.04.002.
7. Jensen S, Handford P. New insights into the structure, assembly and biological roles of 10-12 nm connective tissue microfibrils from fibrillin-1 studies. *Biochem Journal*. 2016;473(7):827-838. doi:10.1042/BJ20151108.
8. Franken R, Den Hartog AW, Radonic T, et al. Beneficial Outcome of Losartan Therapy Depends on Type of FBN1 Mutation in Marfan Syndrome. *Circ Cardiovasc Genet*. 2015;8(2):383-388. doi:10.1161/CIRCGENETICS.114.000950.
9. Faivre L, Collod-Beroud G, Loeys BL, et al. Effect of Mutation Type and Location on Clinical Outcome in 1,013 Proband with Marfan Syndrome or Related Phenotypes and FBN1 Mutations: An International Study. *Am J Hum Genet*. 2007;81(3):454-466. doi:10.1086/520125.
10. Hilhorst-Hofstee Y, Hamel BCJ, Verheij JBGM, et al. The clinical spectrum of complete FBN1 allele deletions. *Eur J Hum Genet*. 2011;19(3):247-252. doi:10.1038/ejhg.2010.174.
11. Schrijver I, Liu W, Odom R, et al. Premature Termination Mutations in FBN1: Distinct Effects on Differential Allelic Expression and on Protein and Clinical Phenotypes. *Am J Hum Genet*. 2002;71(2):223-237. doi:10.1086/341581.
12. Schrijver I, Liu W, Brenn T, Furthmayr H, Francke U. Cysteine substitutions in epidermal growth factor-like domains of fibrillin-1: distinct effects on biochemical and clinical phenotypes. *Am J Hum Genet*. 1999;65(4):1007-1020. doi:10.1086/302582.
13. Ten Dijke P, Arthur HM. Extracellular control of TGF β signalling in vascular development and disease. *Nat Rev Mol Cell Biol*. 2007;8(11):857-869. doi:10.1038/nrm2262.
14. Habashi JP, Judge DP, Holm TM, et al. Losartan, an AT1 antagonist, prevents aortic aneurysm in a mouse model of Marfan syndrome. *Science* (80-). 2006;312(5770):117-121. doi:10.1126/science.1124287.
15. Zhu G, Lee AS. Role of the unfolded protein response, GRP78 and GRP94 in organ

- homeostasis. *J Cell Physiol.* 2015;230(7):1413-1420. doi:10.1002/jcp.24923.
16. Morry J, Ngamcherdtrakul W, Gu S, et al. Dermal delivery of HSP47 siRNA with NOX4-modulating mesoporous silica-based nanoparticles for treating fibrosis. *Biomaterials.* 2015;66:41-52. doi:10.1016/j.biomaterials.2015.07.005.
17. López-Casillas F, Payne HM, Andres JL, Massagué J. Betaglycan can act as a dual modulator of TGF- β access to signaling receptors: Mapping of ligand binding and GAG attachment sites. *J Cell Biol.* 1994;124(4):557-568. doi:10.1083/jcb.124.4.557.
18. López-Casillas F, Wrana JL, Massagué J. Betaglycan presents ligand to the TGF β signaling receptor. *Cell.* 1993;73(7):1435-1444. doi:10.1016/0092-8674(93)90368-Z.
19. Massagué J, Gomis RR. The logic of TGF β signaling. *FEBS Lett.* 2006;580(12):2811-2820. doi:10.1016/j.febslet.2006.04.033.
20. Hill CS. Nucleocytoplasmic shuttling of Smad proteins. *Cell Res.* 2009;19(1):36-46. doi:10.1038/cr.2008.325.
21. Heldin C, Moustakas A. Signaling Receptors for TGF- β Family Members. *Cold Spring Harb Perspect Biol.* 2016;8(8). doi:10.1101/cshperspect.a022053.
22. Xie S, Sukkar MB, Issa R, Oltmanns U, Nicholson AG, Chung KF. Regulation of TGF- β 1-induced connective tissue growth factor expression in airway smooth muscle cells. *Am J Physiol Lung Cell Mol Physiol.* 2005;288:68-76. doi:10.1152/ajplung.00156.2004.
23. Feng X-H, Derynck R. Specificity and Versatility in Tgf-B Signaling Through Smads. *Annu Rev Cell Dev Biol.* 2005;21(1):659-693. doi:10.1146/annurev.cellbio.21.022404.142018.
24. Lindahl GE, Chambers RC, Papakrivopoulou J, et al. Activation of fibroblast procollagen α 1(I) transcription by mechanical strain is transforming growth factor- β -dependent and involves increased binding of CCAAT-binding factor (CBF/NF-Y) at the proximal promoter. *J Biol Chem.* 2002;277(8):6153-6161. doi:10.1074/jbc.M108966200.
25. Pan X, Chen Z, Huang R, Yao Y, Ma G. Transforming Growth Factor β 1 Induces the Expression of Collagen Type I by DNA Methylation in Cardiac Fibroblasts. *PLoS One.* 2013;8(4). doi:10.1371/journal.pone.0060335.
26. Igotz RA, Massagué J. Transforming growth factor-beta stimulates the expression of fibronectin and collagen and their incorporation into the extracellular matrix. *J Biol Chem.* 1986;261(9):4337-4345. <http://www.ncbi.nlm.nih.gov/pubmed/3456347>.
27. Dallas SL, Sivakumar P, Jones CJP, et al. Fibronectin regulates latent transforming growth factor- β (TGF β) by controlling matrix assembly of latent TGF β -binding protein-1. *J Biol Chem.* 2005;280(19):18871-18880. doi:10.1074/jbc.M410762200.
28. Yan X, Liu Z, Chen Y. Regulation of TGF-beta signaling by Smad7. *Acta Biochim Biophys Sin (Shanghai).* 2009;41(4):263-272. doi:10.1093/abbs/gmp018.Review.
29. Akhurst RJ. The paradoxical TGF- β vasculopathies. *Nat Genet.* 2013;44(8):838-839. doi:10.1002/ana.22528.Toll-like.
30. Bilandzic M, Stenvers KL. Betaglycan: A multifunctional accessory. *Mol Cell Endocrinol.* 2012;359(1-2):13-22. doi:10.1016/j.mce.2012.03.020.
31. Yeung KK, Bogunovic N, Keekstra N, et al. Transdifferentiation of Human Dermal Fibroblasts to Smooth Muscle-Like Cells to Study the Effect of MYH11 and ACTA2 Mutations in Aortic Aneurysms. *Hum Mutat.* 2017. doi:10.1002/humu.23174.
32. Derynck R, Zhang YE. Smad-dependent and Smad-independent pathways in TGF- β family

- signalling. *Nature*. 2003;425(6958):577-584. doi:10.1038/nature02006.
33. Elderbroom JL, Huang JJ, Gatza CE, et al. Ectodomain shedding of T β RIII is required for T β RIII-mediated suppression of TGF- β signaling and breast cancer migration and invasion. *Mol Biol Cell*. 2014;25(16):2320-2332. doi:10.1091/mbc.E13-09-0524.
 34. Chaudhry SS, Cain SA, Morgan A, Dallas SL, Shuttleworth CA, Kielty CM. Fibrillin-1 regulates the bioavailability of TGF β 1. *J Cell Biol*. 2007;176(3):355-367. doi:10.1083/jcb.200608167.
 35. Wang J, Lee J, Liem D, Ping P. HSPA5 Gene encoding Hsp70 chaperone BiP in the endoplasmic reticulum. *Gene*. 2017;618:14-23. doi:10.1016/j.gene.2017.03.005.
 36. Kawasaki K, Ushioda R, Ito S, Ikeda K, Masago Y, Nagata K. Deletion of the collagen-specific molecular chaperone Hsp47 causes endoplasmic reticulum stress-mediated apoptosis of hepatic stellate cells. *J Biol Chem*. 2015;290(6):3639-3646. doi:10.1074/jbc.M114.592139.
 37. Martelli-Junior H, Cotrim P, Graner E, Sauk JJ, Coletta RD. Effect of Transforming Growth Factor- β 1, Interleukin-6, and Interferon- γ on the Expression of Type I Collagen, Heat Shock Protein 47, Matrix Metalloproteinase (MMP)-1 and MMP-2 by Fibroblasts from Normal Gingiva and Hereditary Gingival Fibromatosis. *J Periodontol*. 2003;74(3):296-306.
 38. Doyle AJ, Doyle JJ, Bessling SL, et al. Mutations in the TGF- β Repressor SKI Cause Shprintzen- Goldberg Syndrome with Aortic Aneurysm. *Nat Genet*. 2013;44(11):1249-1254. doi:10.1038/ng.2421.Mutations.



Impaired smooth muscle cell contractility as a novel concept of abdominal aortic aneurysm pathophysiology.

Natalija Bogunovic, Jorn P. Meekel, Dimitra Micha,
Jan D. Blankensteijn, Peter L. Hordijk, Kak K. Yeung

Scientific reports; 2019; 9(1), 6837.

ABSTRACT

Ruptured abdominal aortic aneurysms (AAA) are associated with overall mortality rates up to 90%. Despite extensive research, mechanisms leading to AAA formation and advancement are still poorly understood. Smooth muscle cells (SMC) are predominant in the aortic medial layer and maintain the wall structure. Apoptosis of SMC is a well-known phenomenon in the pathophysiology of AAA. However, remaining SMC function is less extensively studied. The aim of this study is to assess the in vitro contractility of human AAA and non-pathologic aortic SMC. Biopsies were perioperatively harvested from AAA patients (n=21) and controls (n=6) and clinical data were collected. Contractility was measured using Electric Cell-substrate Impedance Sensing (ECIS) upon ionomycin stimulation. Additionally, SMC of 23 % (5 out of 21) of AAA patients showed impaired maximum contraction compared to controls. Also, SMC from patients who underwent open repair after earlier endovascular repair and SMC from current smokers showed decreased maximum contraction vs. controls ($p=0.050$ and $p=0.030$, respectively). Our application of ECIS can be used to study contractility in other vascular diseases. We present quantifiable. Finally, our study provides with first proof that impaired SMC contractility might play a role in AAA pathophysiology.

INTRODUCTION

Abdominal aortic aneurysms (AAA) are considered among the most severe surgical emergencies due to the overall mortality rate of 90% in case of rupture ¹. The chance of rupture increases with a larger AAA size and/or high growth rate ^{2,3}. Given that AAA cases mostly are not consequences of a specific traumatic event, infection or a genetic connective-tissue disorder, the majority of AAA cases are considered non-specific or sporadic ³. Even though the pathophysiology of aortic aneurysms remains unclear, the disease is associated with atherosclerosis, tobacco smoking and male gender ³. The lack of a known molecular mechanism increases the difficulties of finding targets for pharmacological therapies, which leaves surgical intervention as the only available treatment option ⁴. Smooth muscle cells (SMC) are the predominant cell type in the aortic media, which represents the thickest layer of the aorta. SMCs are oriented radial and, using their contractile properties, regulate blood flow and pulse pressure in the aorta ⁵. Furthermore, SMC contractile units contribute to force distribution in the aorta by regulating the mechanical properties through their link with the extracellular matrix ⁶. Mutations in genes encoding for contractile proteins, such as smooth muscle myosin heavy chain (*MYH11*) and smooth muscle actin (*ACTA2*) have been associated with cases of hereditary thoracic aortic aneurysms and dissections ^{5,6}. This underscores a potential role of SMC contractile elements in aortic aneurysmal pathology ⁶⁻⁸. However, little is known regarding the SMC function, especially the role of SMC contraction in sporadic AAA.

Measuring SMC contraction is challenging. *In vitro* SMC contractility and associated signaling have so far mostly been measured indirectly by traction force microscopy ^{9,10}, quantification of Fura-2 fluorescence intracellular calcium fluxes ¹¹ and collagen wrinkling assays ¹². Although indispensable for the gain of knowledge of SMC function in culture, most available assays are low throughput and therefore not optimal for screening of patient SMC biobanks. To overcome this problem, we chose to use a new method: the electric cell-substrate impedance sensing (ECIS). ECIS is a real-time, medium throughput assay, widely used to quantify adherent cell behavior and contraction ¹³⁻¹⁶. ECIS has been used previously to study SMC growth and behavior in wound-healing and migration assays ¹⁷⁻¹⁹. We thus opted to use ECIS as a novel, quantitative strategy to analyze the contractile responses of vascular SMC.

To examine the role of SMC contractility in AAA pathophysiology, we measured the contractile properties of SMC isolated from aortic biopsies of controls and sporadic AAA patients. Using the ECIS, we compared the contractile properties of SMC derived from biopsies of both non-ruptured and ruptured AAA and correlated our findings with clinical characteristics and SMC-marker expression profile of the patients. The aim of this study is to evaluate SMC contractility in patients with sporadic AAA.

METHODS

Patient population

Aortic biopsies were obtained during open aneurysm repair in Amsterdam University Medical Centers, location VU University Medical center, Amsterdam and Westfriesgasthuis, Hoorn, the Netherlands. All patients signed an informed consent to participate in the study. Twenty-one AAA patient was included, of which thirteen with non-ruptured AAA (NRAAA1-13) and eight with ruptured (RAAA1-8). Tissue of patients RAAA4 and NRAAA1-3 was collected after open repair after earlier endovascular repair and are marked † (Table S1). Control aortic biopsies used in this study were obtained from non-dilated aorta of post-mortem kidney donors anonymously. All material was collected in accordance to regulations of the WMA Declaration of Helsinki and institutional guidelines of the Medical Ethical Committee of the VU Medical Center. All the experiments and experimental protocols were performed in accordance with institutional guidelines and approved by the Medical Ethical Committee of the VU Medical Center. Clinical information of controls and patients are shown in Table 1. Age and gender of the control and patient group were reported. Additionally, patient characteristics were reported as follows: aneurysm size, known genetic causes of aneurysms, related comorbidities and medication use.

Aortic biopsy explant protocol and SMC cell culture

Perioperatively harvested human aortic wall was transported from the operating room to the laboratory in ice cold sterile Custodiol ® (Dr. Franz Köhler Chemie GmbH, Alsbach-Hähnlein, Germany). All AAA biopsies were taken during open surgical repair of the aorta, usually at the ventral site of the aneurysm. Control aortic tissue was obtained from heart-beating donors during the kidney transplantation procedure. The non-dilated aorta was attached to the renal artery of the kidney used for transplant. The aortic tissue was afterwards transported in custodial, a tissue preservation medium, which made sure that both the kidney and aorta remain viable and we transported them in a similar way as the AAA patient biopsies. The biopsies were sliced with sterilized surgical instruments in a sterile Petri dish. From the initial biopsy, the intima (in AAA patients often including atherosclerotic plaque and calcification) and the adventitia layer with the attached perivascular adipose tissue and fibers were removed, leaving solely a compact and uniform medial layer. The tissue slice was further cut into pieces of roughly 1 mm², and 15 pieces of tissue were placed on the top bottom quarter of a culture flask (25 cm²) containing 1.5 ml culture medium. All biopsies were cultured in 231 medium (Thermo Fisher Scientific, Waltham, MA, USA), supplemented with Smooth Muscle Growth Supplement (Thermo Fisher Scientific), and 100 units/ml penicillin and 100 µg/ml streptomycin (Thermo Fischer Scientific), to provide optimal vascular SMC growth. Cells were cultured in a humidified incubator 37 °C, 5% CO₂. After 10 days of incubation, cell

growth could be observed in the form of cell colonies growing around the tissue sections. The culture medium was refreshed two times per week until the cell population became subconfluent. Subsequently, cells were transferred into a larger culture flask of 80 cm². A confluent population of cells was established in approximately 6 weeks from the day the initial aortic biopsy was collected. Primary SMC were used between passage 1-8 in all experiments.

Measuring SMC contraction

Electric cell-substrate impedance sensor (ECIS; Applied Biophysics, Troy, NY, USA) is a technique used to quantify the attachment and behavior of adherent cells in real time ³⁵. Cells are seeded on gold-coated electrodes embedded in special culture plates (Figure 1a). An alternating current is applied to the cells. As a function of the surface covered by attached cells, the system generates an impedance value. The baseline impedance value generated by cell adhesion is derived from changes in voltage between the measuring and counter electrodes ¹⁴. Data on contraction derived from the ECIS are recorded in a well with a monolayer consisting of several tens of thousands of cells. Cell behavior is detected by ten electrodes on the bottom of the well. The contractile output is derived as a mean of the recording of the ten electrodes at the time of the stimulation. In this way, the data are averaged in the whole well.

Sterile 96 well plate arrays with 10 electrodes per well (96w10; Ibidi, Planegg, Germany) were coated with L- cysteine and subsequently gelatin, according to a previously described array preparation protocol ¹⁴. SMC were seeded in duplicate in the array at a density of 30000 cells/well on a surface of 0.3 cm² in a cell suspension of 200 µl in complete medium. Cells were cultured for 48 hours prior to stimulation, allowing cells to attach and establish a monolayer. By the time of the stimulation experiment, the cells formed a subconfluent monolayer, allowing for cell migration and contraction as shown in Figure 1b. The attachment and spreading of cells on the electrodes generates a baseline resistance value, composed of cell-cell and cell-matrix contact ³⁶. The impedance was recorded at a frequency of 4000 Hz.

Cells were stimulated with 10 µg/ml ionomycin (Sigma Aldrich, Darmstadt, Germany), a Ca²⁺ ionophore which induces a contractile response in adherent vascular SMC induced by the influx of extracellular Ca²⁺ ¹⁷. Cell recovery upon ionomycin stimulation was tested by tracking the impedance after washing out the stimulus and replacing it with ordinary culture medium.

Contractile responses were measured in duplicate in each experiment, and the measurement was repeated two- or three times per cell line in independent experiments. Mean contractile values thus derived from the means of the 4-6 measurements performed for each cell line. Maximum Contractile values represent the highest noted contractile strength for each cell line among all the experiments.

As shown in equation (1), the value of a well filled with culture medium without attached cells (290 Ω) was subtracted from all the results in the final calculation. Individual contractile outputs per well were calculated according to the formula below, where C indicates contraction (expressed in % of change compared to baseline) and prestimulation (PrS) and poststimulation (PoS) resistance values respectively (expressed in Ω). Contraction of each well thus equals one minus the ratio between the resistance post- and pre-stimulation post empty well value subtraction. The final values thus represent a ratio between the value post- and pre-stimulation and are expressed as percentages of change.

$$C = \left(1 - \frac{(PoS[\Omega] - 290[\Omega])}{(PrS[\Omega] - 290[\Omega])}\right) \cdot 100$$

Equation (1)

Reproducibility and variation were assessed intra- and inter-experimentally. Interexperimental ECIS contraction measurement reproducibility was tested using a difference Bland-Altman plot³⁷. Each data point shows the deviation from the mean among two independent measurements of the same cell line. Data points are shown within or outside the 95% confidence interval.

Due to the novelty of our method in the study of AAA pathology, no published references for expected SMC contractility *in vitro* were available. To characterize the contractile output of the patients, the mean response of the control group was used as a reference point for healthy SMC behavior. Deviant contractility was defined as outcomes more than two standard deviations compared to the mean contractile response of the control group.

RNA isolation and quantitative PCR

To assess differences between the contractile phenotypes of SMC from controls and patients, the mRNA expression level of SMC-specific markers was performed. Using quantitative PCR (qPCR), the expression of early (*ACTA2*, *TAGLN* and *VIM*) and late (*CNN1* and *SMTN*) SMC-specific-marker genes was measured. The proliferative capacity of SMC cell lines was assessed by quantification of *MKi67* gene expression. Firstly, total RNA was isolated using the NucleoSpin RNA kit (Macherey Nagel, Duren, Germany) according to manufacturer's instructions. Next, first strand cDNA synthesis was performed in a 20 μ l reverse transcription reaction using the VILO kit (Thermo Fisher Scientific), adjusted to the concentration of total isolated RNA and according to the instructions provided by the manufacturer. qPCR was then performed to quantify the expression of SMC markers *ACTA2*, *CNN1*, *SMTN*, *TAGLN*, *VIM* and mammalian proliferation marker *MKi67*. *YWHAZ* and *TBP* were

used as housekeeping genes to normalize for the amount of total RNA per sample. All data were normalized using a normalization factor derived from the expression of housekeeping genes. RefSeq gene numbers and primer sequences are provided in Supplementary Table 1. Gene expression was determined by the LightCycler 480 Instrument II (Roche Applied Science, Penzberg, Germany), and the reactions were prepared using Light Cycler SYBR Green I Master (Roche Applied Science), as previously described ³⁸.

Immunostaining and confocal microscopy

To examine overall cell morphology and contractile cytoskeletal properties, immunostainings on representative samples of both the control and patient group were performed. Cells were seeded on glass coverslips (#1, Ø 13 mm; Thermo Fisher Scientific) in a seeding density of 100000 cells/ml. The cells were cultured overnight, washed with EBSS and fixed for 10 minutes on room temperature in 4% paraformaldehyde. Next, coverslips were washed 3x with PBS-Tween (PBST) and the cells were subsequently permeabilized for 10 minutes in 0.2% Triton in PBS. Consequently, samples were incubated in blocking solution, consisting of 1% BSA solution in PBST for 1h at room temperature. Primary antibody against smoothelin (Thermo Fisher Scientific) was incubated overnight on 4 °C, diluted 1:100 in blocking solution. Samples were washed five times using PBST the next day. Secondary antibody (1:100; Thermo Fisher Scientific), DAPI (1:200; Thermo Fisher Scientific), and Phalloidin (1:200; Thermo Fisher Scientific), were incubated for 1 hour on room temperature in the dark. Slides were closed with Mowiol mounting medium (Sigma Aldrich). Images were acquired using the Nikon A1R (Nikon, Tokyo, Japan) microscope and the corresponding software Nis-Elements C Software (Nikon). Representative images were analyzed and adjusted using Fiji ³⁹.

To obtain representative images of SMC contraction in real time, cells were seeded in 35mm glass bottom dishes (Thermo Fisher Scientific) coated with gelatin. After overnight incubation, the cells were placed in an incubation chamber at 37 °C, 5% CO₂. Cells were stimulated with ionomycin and imaged using Nikon A1R (Nikon) in intervals of 10s for 1h.

Western Blot

SMC marker proteins in control and patient cell lines were quantified using western blot. Cells were seeded in 6 well plates at a seeding density of 150.000 cells/well and incubated overnight. The next day, they were washed with Earl's Balanced Salt Solution (EBSS; Thermo Fisher Scientific) and each well was lysed in 100ul of Nu Page Sample buffer and reducing agent (9:1) (Thermo Fisher Scientific. After boiling, 8ul of each sample was loaded onto either NuPAGE 4-12% Bis-Tris or NuPAGE 3-8% TA gels depending on the size of the protein in question. Western blotting was

performed as previously published³⁸. Primary antibodies were incubated overnight at 4°C. Primary antibodies against tubulin (1:8000) was used as loading control. Primary antibodies against Calponin (1:4000; Abcam), Smooth muscle actin (1:4000; Dako), SM22 (1:4000; Abcam) were incubated overnight at 4°C. Secondary antibodies IRDye® 800CW Goat anti-Rabbit IgG and IRDye® 680CW Goat anti-Mouse IgG (1:5000; LI-COR Biosciences) The fluorescent signal was visualized using the Odyssey Infrared Imaging System (Odyssey version 4 software; LI-COR Biosciences). Intensity of bands was quantified using Fiji³⁹.

Correlation of contraction and clinical characteristics

To elucidate SMC contractile function, contractility was correlated with gender and age of patients and controls (Table 1). In AAA patients, contractility was correlated with maximum aneurysm size, smoking, diabetes, hypertension, hyperlipidemia and pre-surgery statin use. Additionally, we compared the contractility of SMC obtained during primary surgery and SMC obtained during open conversion after endovascular aneurysm repair (EVAR) because of endoleak causing the aneurysm to grow (i.e. endoleak repair).

Statistics and Graphs

Data were analyzed with SPSS (version 22, IBM Statistics, Armonk, NY, USA). The datasets were not normally distributed and were thus compared using non-parametric tests. Two groups were compared using the Mann-Whitney U test and multiple groups were compared with Kruskal-Wallis test, using the Mann-Whitney U test as post-hoc analysis. Correlations were tested with Spearman's Rank correlations. Correlation output was corrected using the Bonferroni correction. Data are presented as box plots with median and range. Tests were considered statistically significant at $p < 0.05$. Representative curves and difference plots, boxplots and scatterplots were constructed using GraphPad Prism7 (GraphPad. La Jolla, CA, USA).

RESULTS

Smooth muscle cell contraction

Contractility of aortic smooth muscle cells could be quantified using the ECIS. Adherent SMC, seeded on gold plated electrodes (Figure 1a), were stimulated with ionomycin to induce a contractile response within a few seconds. As depicted in Figure 1c, the stimulated cells contracted and lost cell-cell contact post stimulation, compared to the same monolayer in Figure 1b. The consequent reduction in surface coverage is measured by ECIS as a drop in impedance. This way, SMC contraction can be quantified using ECIS, as deduced from the almost immediate and significant decrease of impedance post stimulation. The same process can be observed in

Figure 1d, where a monolayer of SMC shows contraction in a time-lapse recording. The marked cell outlines of five representative cells indicates the change in cell shape during contraction. The full time-lapse video is available as Supplementary Video 1. Intraexperimental reproducibility is shown on Figure 2a, where the two curves represent two stimulated wells of control 1. Vertical dotted line marks the time point on the x axes which indicates stimulation with ionomycin and consequent reduction of resistance which corresponds to contraction. A representative interexperimental difference plot (Bland-Altman) shows the reproducibility between independent contraction measurements in control and patient SMC. As depicted in Figure 2b, there are two outliers in the combined group of 27 controls and patients. The vast majority of contractility measurements post stimulation are within the 95% confidence interval. Cell recovery post stimulation of contraction is depicted in Figure 2c. Black thick line represents the unstimulated resistance value of a control smooth muscle cell line. Dotted line represents the stimulated resistance value of the same cell line. Resistance values were normalized to the values pre stimulation to monitor the behavior of cells post stimulation. Vertical dotted line marks the time point on the x-axes, which indicates stimulation with ionomycin and consequent reduction of resistance which corresponds to contraction. After approximately 1h post stimulation, the medium was refreshed to remove the stimulus (vertical dotted grey line) and the recovery of the cells was tracked for the next few hours.

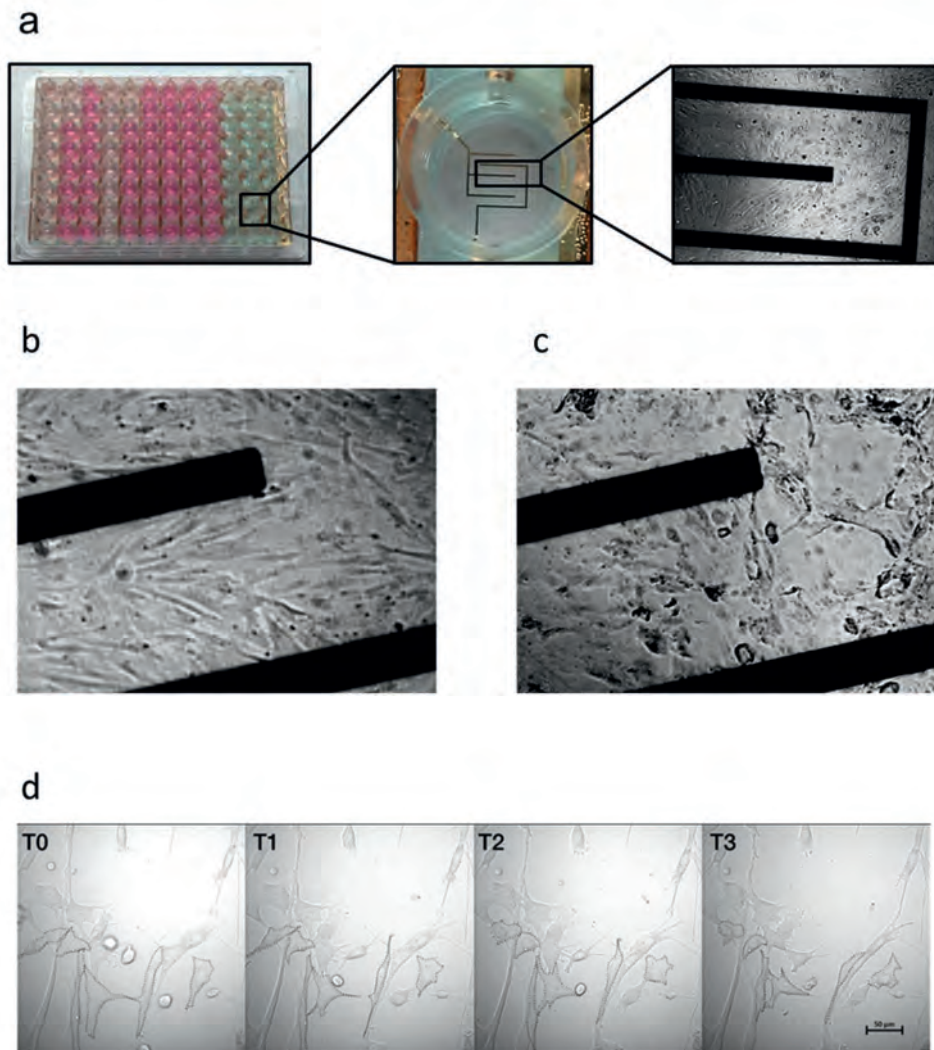


Figure 1. Graphic representation of aortic SMC contraction. a) Left; ECIS 96e10e cultureware plate. Middle; magnified picture of a single well within the plate with a detailed view of the ten electrodes on the bottom of the well. Right; light microscope image of SMC seeded on the plate. b) Representative images of a monolayer of control SMC. Left; cells prior to stimulation of contraction. Right; cells post stimulation. c) Representative images of control SMC contraction captured by time-lapse microscopy. T0 image depicts cells prior to stimulation, and T1-3 depict time points post stimulation. The outline of five representative cells is marked with dotted lines to represent the change in cell shape during contraction. Scale bar: 50 μ m.

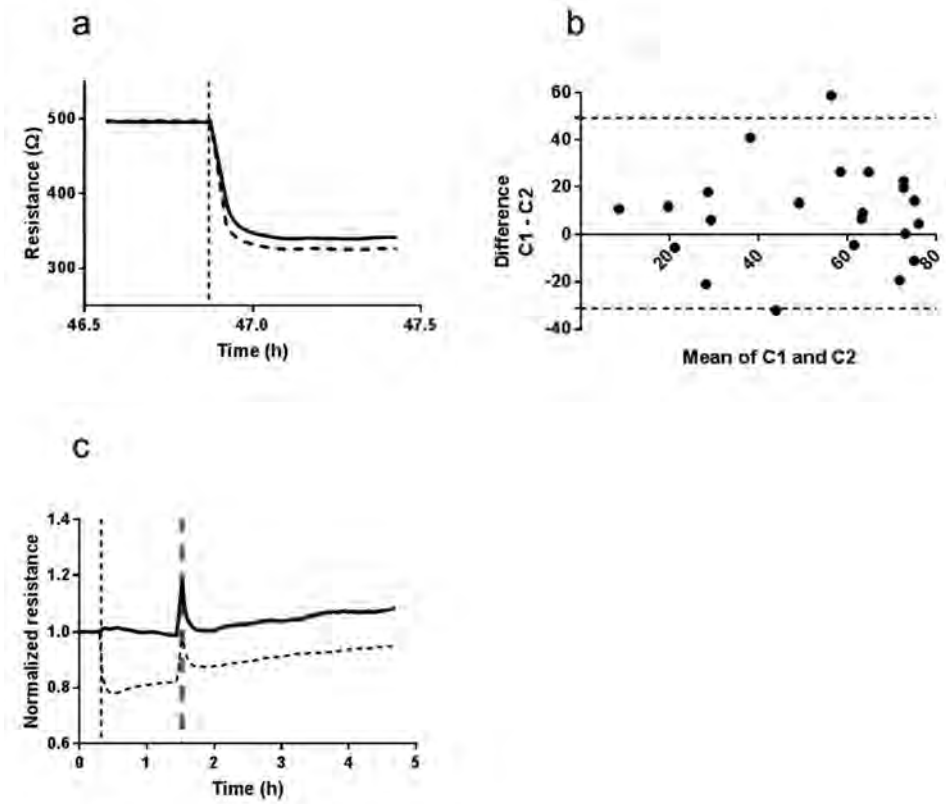


Figure 2. Measuring SMC contraction using ECIS. a) Representative intraexperimental reproducibility of ECIS contraction measurements. Resistance curves generated by SMC of control 1 seeded in two wells. Vertical dotted line marks the stimulation. b) Difference plot demonstrating interexperimental measurement reproducibility between two separate contraction measurements. Dotted lines represent the 95% confidence interval and thick medial line represents the mean of two interexperimental measurements. Each data point represents the deviation from the mean of two independent measurements. c) Cell recovery post stimulation of contraction. Black thick line represents the unstimulated resistance value of a control smooth muscle cell line. Dotted line represents the stimulated resistance value of the same cell line. Resistance values were normalized to the values pre stimulation to monitor the behavior of cells post stimulation. Vertical dotted line marks the time of stimulation. After approximately 1h post stimulation, the medium was refreshed to remove the stimulus (vertical dotted grey line) and the recovery of the cells was tracked for a few hours longer.

Contractile response of control and AAA patient' SMC

Contractility of SMC isolated from the aortic biopsies of controls and sporadic AAA patients was quantified using the ECIS. Resistance curves of control 1 and patient 1 are depicted in Figure 3a, representing exemplary normal contraction in the control and impaired contraction in the patient group. The dotted line marks the ionomycin stimulation. Resistance values decrease post stimulation and a steeper curve can be noted in the control compared to the patient cell line. The median of the average contractile response of the control group (n=6) was 61% (46-77%) of the initial value pre-stimulation vs. 52% (15-75%) for the patient group (Figure 3b). The median of the maximum contractile response of the control group (n=6) was 76% (59-86%) of the pre-stimulation value vs. 67% (26-83%) for the patient group (Figure 3c).

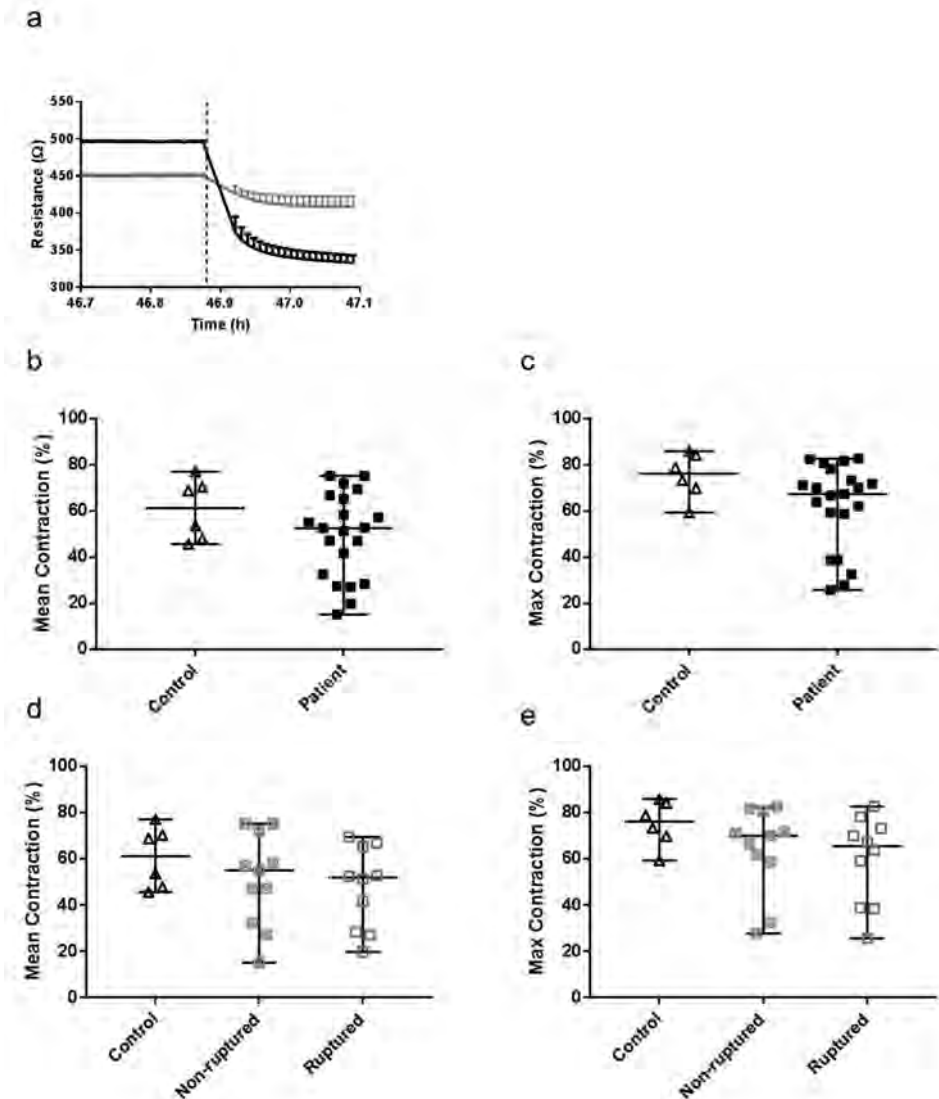


Figure 3. Contraction of control and AAA patient SMC upon ionomycin stimulation. a) Representative resistance curves generated by control 1 (black) and patient 1 (grey) SMC before and after stimulation of contraction. Resistance values were measured in duplicate and represented as mean with SD. Vertical dotted line marks the stimulation with ionomycin. b) Mean contractile response of control (▲; n=6) and AAA patient (■; n=21) SMC upon ionomycin stimulation derived from multiple experiments. c) Maximum contractile response of control (▲; n=6) and AAA patients' (■; n=21) SMC upon ionomycin stimulation. d) Mean contractile response of control (▲; n=6), non-ruptured AAA patients' (☒; n=13) and ruptured AAA patients' (□; n=7) SMC multiple experiments. e) Maximum contractile response of control

(▲; n=6), non-ruptured AAA patients' (⊠; n=13) and ruptured AAA patients' (□; n=7) SMC. Contraction is expressed in percentages of decrease compared to baseline value. Boxplots are shown as median with range.

The contractile response of the patients' cells exhibited larger variability. We could not detect a significant difference between all AAA patient and the control group, neither in mean ($p=0.235$) nor in maximum contraction ($p=0.085$). No significant difference was found between the mean contractile response of the cells from patients with non-ruptured aneurysms (median response 54%, range: 15-75%, $p=0.525$) vs cells from those with ruptured aneurysms (median response 51%, range: 20-69%; $p=0.417$; Figure 3d). In addition, no significant differences in maximum contraction were found between controls vs SMC derived from non-ruptured aneurysms (median response 69%, range: 28-82%, $p=0.216$) vs cells from those with ruptured aneurysms (median response 65%, range: 26-83%; $p=0.73$; Figure 3e). The median responses of both non-ruptured and ruptured AAA groups were almost identical and heterogeneous like the response spread of the cells from all AAA patients. Mean and maximum contraction of all 27 cell lines was significantly correlated ($R = .853$, $p < 0.001$).

Using the control group as a reference for normal SMC contractility *in vitro*, the patient group was divided into low and high contracting groups. Patient cell lines exhibiting contractility lower than two standard deviations below the mean of the controls, i.e. a mean contractile response lower than 34% and a maximum contractile response lower than 57%, were categorized as low contracting. Upon screening both ruptured and non-ruptured patient SMC, 28% of the AAA-patients (ruptured and non-ruptured) SMC contractile response showed repeatedly lower contractility (Low contracting; $n=6/21$, Figure 4a). The low contracting AAA patients' cells thus showed a median contractile response of 35% (26-59%). The same trend could be observed in the measurements of maximum contraction; where 23% of all AAA patient SMC (5 out of 21) exhibited lower contractility (median 32%, range 26-39%, Figure 4b). The other SMC from the majority of AAA patients contracted in the same range as the controls, with a mean response of 57% (42-75%; $n=15$) and maximum response of 70% (59-83%). The patients with cells with low contractility belonged to both the ruptured and non-ruptured AAA groups.

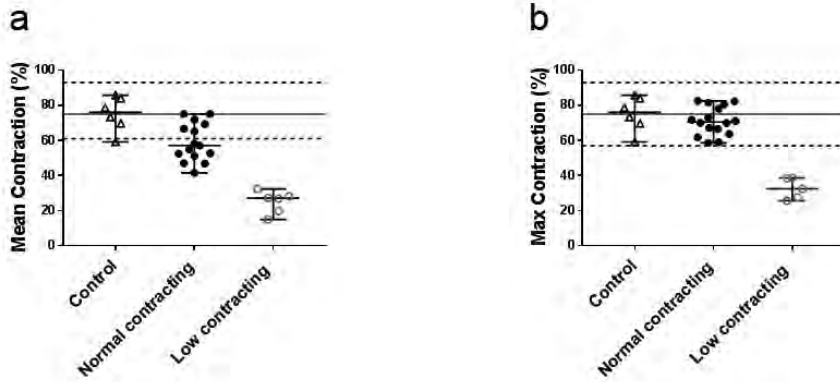


Figure 4. Contractile response of control and AAA patients' SMC a) Mean contractile response of Control (\blacktriangle ; $n=6$), Normal contracting (\bullet ; $n=15$) and Low contracting (\circ ; $n=6$) AAA patients' SMC derived from multiple experiments. b) Maximum contractile response of Control (\blacktriangle ; $n=6$), Normal contracting (\bullet ; $n=16$) and Low contracting (\circ ; $n=5$) AAA patients' SMC. Black horizontal line marks the mean of contraction of the control group. Dotted horizontal lines mark two SD higher and lower than the mean of the control group. Low contracting group is defined as contraction lower than two SD below the mean of the control group. Contraction is expressed in percentages of decrease compared to baseline value. Boxplot is shown as median with range.

Contraction of cells from AAA patients and SMC phenotype

To compare the phenotypic state of Control vs. Normal and Low contracting SMC, changes in SMC specific marker gene expression were studied using qPCR. Firstly, we compared the protein expression of SMC marker proteins α SMA, Calponin and SM22 using western blot (Figure 5a). As shown in the quantification of the blot in Figure 5b, the expression of SMC markers is very heterogeneous in the control as well as both patient contraction groups. Similar trend of variability can be observed on mRNA level, with the expression of the corresponding SMC marker genes, *ACTA2*, *CNN1* and *TAGLN* (Figure 5c).

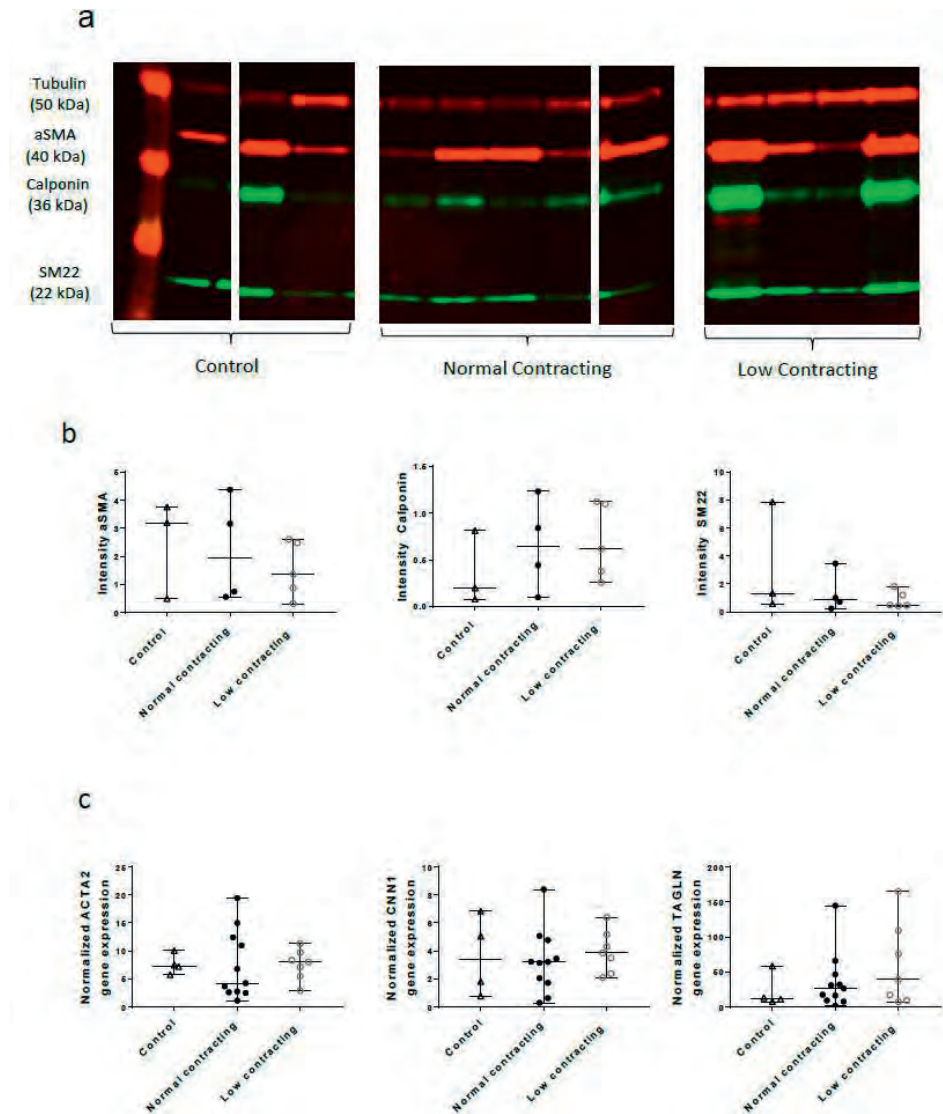


Figure 5. Expression of SMC phenotypic markers a) Western blot analysis of aSMA, Calponin and SM22 in Control (n=3), Normal Contracting (n=5) and Low Contracting (n=4) AAA patients' SMC. Lanes were cropped and grouped from the original image (Supplementary Figure 3), Ladder: lane 0; Control: lanes 1,4 and 5; Normal contracting: lanes 6-9 and 14; Low contracting: lanes 10-13. b) Intensity of aSMA, Calponin and SM22 in Control (n=3), Normal Contracting (n=5) and Low Contracting (n=4) AAA patients' SMC. Intensity red channel (700CW) 5, Intensity green channel (800CW) 3. c) Gene expression of *ACTA2*, *CNN1* and *TAGLN* in mRNA isolated from control (▲; n=4), normal contracting (●; n=13) and low contracting SMC (○; n=5). Boxplots are shown as median with range.

Additionally, no significant differences in gene expression of *SMTN* and *VIM* were observed between cells from controls and Normal and Low contracting patient SMC (Supplementary Figure 2). Furthermore, no significant difference in expression levels of *Mki67* between cells from controls and Normal and Low contracting patient SMC (Supplementary Figure 2) was found, indicating no difference in proliferative capacity. In addition, no differences were found between marker expressions in controls and all patients or controls and sub-groups of non-ruptured and ruptured AAA patient SMC.

To examine overall cell morphology and cytoskeletal properties, as well as expression of the contractile phenotype, immunostaining for smoothelin and F-actin (Supplementary Figure 1) was performed in fixed cells of two controls and three patients. We observed spindle shaped, adherent SMC with long actin fibers and consistent expression of smoothelin, confirming that both control and patient cell lines express this marker of mature SMC. Cell morphology and marker expression do not seem to indicate a phenotypic defect linked to SMC contraction.

Contraction of cells from AAA patients vs. clinical characteristics

To further analyze the link between contractility of SMC from AAA patients with AAA pathology, clinical characteristics (Table 1) were correlated with contractile output. No correlations were found between contraction of all control and patient SMC and gender and age. No correlation between contraction and patient gender or age, maximum aneurysm size, diabetes, hypertension, hyperlipidemia and pre-surgery statin use was found. With the critical value adjusted from 0.05 to 0.006 upon performing the Bonferroni correction, none of the parameters was significantly correlated with contraction. We compared the contractility of SMC which were obtained during open repair after earlier EVAR because of persisting endoleak (n=4) to contractility of control SMC (n=6) and SMC obtained during primary aneurysm open repair (n=17). SMC isolated from reintervention surgery (post-endoleak) demonstrated a trend of lower maximum contraction vs. control, which was not statistically significant ($p=0.050$) based on the small group sizes. Additionally, no significant difference was detected vs. primary aneurysm repair (Figure 6b). A similar trend could be observed in case of mean contraction, with an overall trend of lower contraction in the post-EVAR group (Figure 6a). Furthermore, patients who declared themselves as current smokers (n=5/21) exhibited lower maximum contraction compared to the control group ($p=0.030$) whereas the SMC of patients who currently do not smoke showed no difference vs. control group (Figure 6d). No significant differences in mean contraction were found between the control and current smokers group. (Figure 6c).

Table 1. Clinical characteristics of controls and patients. Age and gender are shown for all controls and patients. Aneurysm related characteristics are shown for patients when available: Aneurysm size (mm), known genetic causes of aneurysm, smoking history, diabetes mellitus, hypertension, hyperlipidemia and statin use pre surgery. Patients are coded RAAA 1-8 if the tissue derived from a ruptured aneurysm, and NRAAA1-13 in case of elective aneurysm repair. Patients whose tissue was collected during open repair post-EVAR are marked with an additional +. Patient whose tissue was collected after a suprarenal repair following an infrarenal repair is marked with #.

Type of biopsy donor	Patient code	Age at time of biopsy	Gender	Aneurysm size (mm)	Genetic cause	Smoking	Diabetes Mellitus	Hypertension	Hyperlipidemia	Statin use pre
Ruptured abdominal aortic aneurysm	RAAA1	72	Female	60	None	Less than 1 package/day	No	Yes	Yes	Yes
Ruptured abdominal aortic aneurysm	RAAA2	60	Male	100	None	Stopped less than 10 years ago	No	Unknown	Yes	Yes
Ruptured abdominal aortic aneurysm	RAAA3	65	Male	83	None	More than 1 package/day	Yes; adult	Yes	Yes	Yes
Ruptured abdominal aortic aneurysm	RAAA4	79	Male	72	None	Stopped more than 10 years ago	No	No	Yes	Yes
Ruptured abdominal aortic aneurysm	RAAA5	67	Male	71	None	No	No	No	Yes	No
Ruptured abdominal aortic aneurysm	RAAA6	70	Male	55	None	No	No	Yes	No	Yes
Ruptured abdominal aortic aneurysm	RAAA7	88	Female	79	None	No	Yes; adult	Yes	No	Yes
Ruptured abdominal aortic aneurysm	RAAA8	83	Female	100	None	More than 1 package/day	No	Yes	No	No
Non-ruptured abdominal aortic aneurysm	NRAAA1+	69	Male	88	None	No	No	Yes	Yes	Yes
Non-ruptured abdominal aortic aneurysm	NRAAA2#	73	Male	86	None	No	No	Yes	No	No
Non-ruptured abdominal aortic aneurysm	NRAAA3†	72	Male	90	None	No	No	No	No	Yes
Non-ruptured abdominal aortic aneurysm	NRAAA4	75	Female	63	None	Less than 1 package/day	No	No	Yes	Yes
Non-ruptured abdominal aortic aneurysm	NRAAA5	58	Female	58	None	Less than 1 package/day	No	Yes	Yes	Yes

Non-ruptured abdominal aortic aneurysm	NRAAA6	71	Male	41	None	No	Yes; adult	Yes	Yes	Yes
Non-ruptured abdominal aortic aneurysm	NRAAA7	64	Male	63	None	Stopped more than 10 years ago	No	No	No	Yes
Non-ruptured abdominal aortic aneurysm	NRAAA8	72	Female	71	None	No	No	No	No	Yes
Non-ruptured abdominal aortic aneurysm	NRAAA9	74	Male	45	None	No	Yes; adult	Yes	Yes	Yes
Non-ruptured abdominal aortic aneurysm	NRAAA10#	76	Male	77	None	Stopped less than 10 years ago	No	Yes	No	No
Non-ruptured abdominal aortic aneurysm	NRAAA11	60	Male	56	None	stopped more than 10 years ago	Unknown	Yes	Yes	No
Non-ruptured abdominal aortic aneurysm	NRAAA12	65	Male	94	None	stopped more than 10 years ago	Unknown	Yes	No	Yes
Non-ruptured abdominal aortic aneurysm	NRAAA13	68	Male	55	None	No	Unknown	Yes	No	No
Control	C1	30	Male	N/A	N/A	N/A	N/A	N/A	N/A	N/A
Control	C2	44	Female	N/A	N/A	N/A	N/A	N/A	N/A	N/A
Control	C3	45	Male	N/A	N/A	N/A	N/A	N/A	N/A	N/A
Control	C4	59	Male	N/A	N/A	N/A	N/A	N/A	N/A	N/A
Control	C5	35	Male	N/A	N/A	N/A	N/A	N/A	N/A	N/A
Control	C6	22	Male	N/A	N/A	N/A	N/A	N/A	N/A	N/A

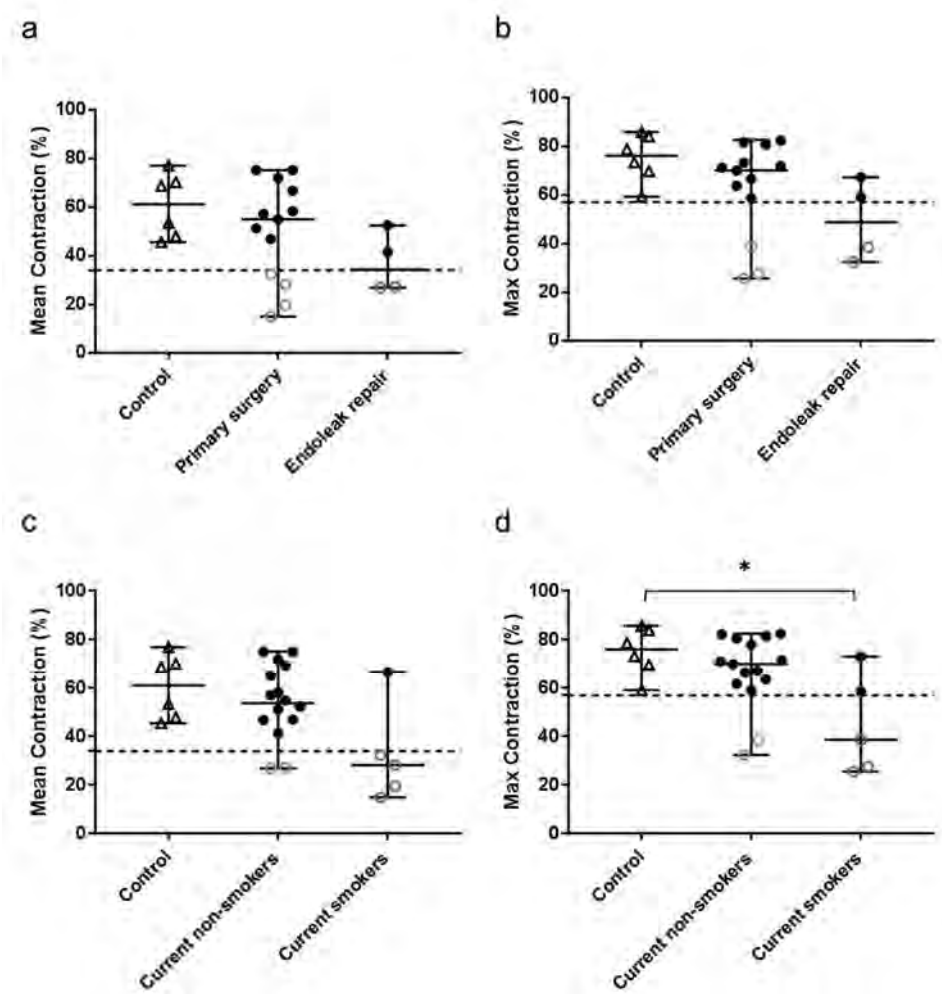


Figure 6. Correlation between impaired contraction of AAA patient SMC and clinical characteristics. a) Mean contractile response of Control (▲; n=6), patients who underwent primary aneurysm repair (Primary surgery; n=17) and patients who underwent secondary surgery for endoleak repair (Endoleak repair; n=4) derived from multiple experiments. b) Maximum contractile response of Control (▲; n=6), patients who underwent primary aneurysm repair (Primary surgery; n=17) and patients who underwent secondary surgery for endoleak repair (Endoleak repair; n=4). SMC obtained during endoleak repair exhibit a trend of lower contractility compared to control group (p=0.050). c) Mean contractile response of Control (▲; n=6), Current non-smokers; n=16 and Current smokers; n=5 derived from multiple experiments. d) Maximum contractile response of Control (▲; n=6), Current non-smokers; n=16 and Current smokers; n=5. Patients with normal contraction are marked with ● and patients with low contraction (more than 2SD below the mean of the control group) are marked with ○. SMC of patients who currently smoke exhibit impaired contractility compared to the

control group ($p=0.030$). Boxplots are shown as median with range and tested with Mann-Whitney U test.

DISCUSSION

Genetic dysfunctions in SMC contractile proteins and their devastating consequences for the aortic wall have been shown in cases of familial thoracic aneurysms ^{5,6}. Although SMCs are implicated in the pathogenesis of AAA, due to their decreased density in the aortic media ³ and pathological apoptosis ²⁰, little is known of their contractile function in the context of sporadic AAA pathogenesis. To investigate the role of SMC in AAA pathology, we employed ECIS to perform a real time screen of control and patient SMC contractility *in vitro*. Using novel methodology, we measured low SMC contraction *in vitro* in a sub-group of included patients with sporadic AAA. In addition, we show a link between impaired contractility of SMCs of AAA patients and current tobacco smoking, suggesting a possible link between the effects of present-day smoking and SMC dysfunction.

Our findings on SMC contractility *in vitro* provide the first evidence of SMC contractile dysfunction in sporadic AAA patients. In comparison to the hereditary aneurysms, both thoracic and abdominal sporadic aortic aneurysms have a broader spectrum of potential causes ³, making AAA more difficult to study and to use in the design of future molecular therapies. Furthermore, AAA is considered to be caused by a combination of lifestyle, gender, age or other cardiovascular disorders ³. SMC function in the aorta is mostly studied or explained through analysis of what happens during dysfunction ¹². Current literature proposes many hypotheses regarding the relevance of SMC contractility for aortic function and structure ⁵⁻⁸, and the severe consequences if that function becomes impaired. However, little experimental work has been published to prove this concept and to address how and why these defects have such disruptive effects on aortic wall structure.

We investigated this concept using a novel assay to measure cell contraction based on the use of ECIS to study SMC contraction in the context of AAA. SMC contractility was previously studied by various *in vitro* methods, focusing on elucidating the *in vitro* contractile mechanisms in physiological ⁹⁻¹¹ and pathophysiological settings ¹². If we compare ECIS to other contraction assays, we note that other available contraction assays such as traction force microscopy are more single cell oriented and require extensive optimization and technical possibilities. More importantly, the time of contraction cannot be predicted beforehand, making filming the contraction with the traction force microscopy difficult to perform. Additionally, since the assays focus on single or a small number of cells, it cannot not certain that they could be used to extrapolate larger-scale screening data of patient material. A previous *ex vivo* study of tensile forces demonstrate that healthy abdominal aortic samples exhibit higher tensile strength than *ex vivo* samples obtained during AAA open repair

²¹. Their study indicates the important role of tensile strength in the aorta, and the consequences of stiffness and elasticity disbalance in individual aneurysm pathology. Moreover, SMC contractility has been investigated in thoracic aorta SMC from Marfan mice. Marfan syndrome is a connective tissue disorder caused by mutations in *FBN1*, and the most severe clinical manifestations include aortic aneurysms and dissections ²². Thoracic aortas of Marfan mice exhibited a reduction of 64 to 81% reduced contraction upon KCl and phenylephrine compared to age matched control mice ²³. This data is in good agreement with our current findings using patient SMC. On a molecular level, it has been published that inflammasome activity leads to the degradation of SMC specific proteins in aortas from patients with sporadic thoracic aortic aneurysm ¹². Using a collagen-wrinkling assay, these authors showed that the activity of the inflammasome leads to reduced SMC contraction *in vitro*. Taken together, literature indicates a link between SMC dysfunction, in particular reduced contractility, and AAA pathology.

Previous studies investigated the link between aneurysm wall stress and risk of rupture, demonstrating a link between increased wall stress and risk of rupture in risk prediction models ^{24,25}. Strikingly, in our assay the clinically distinct groups do not differ in heterogeneity nor in median contractile response. This indicates that the reduced contractility is neither a cause nor a consequence of AAA rupture.

One limitation of this study is the relatively small patient sample and the discrepancy in size between the patient and control groups. However, due to the homogeneity of the control contractile responses in our assay, we present the findings within the current sample size. The small group sizes might account for the lack of correlation between contraction and important clinical parameters, such as age and aneurysm size. An additional limitation is the use of cells obtained through an explant protocol. This means that the cells used in the experiments proliferated from the aortic biopsy which might influence their properties or decrease the effects present in the same cells *in vivo*. Moreover, the contractile division into high and low contracting patient cells might be affected by the anatomical region of the aneurysmal sack from which the biopsy was derived. In addition, the growth rates of 10/18 AAA patients were not available, partially due to rupture (5/10). As non-ruptured aneurysms are mostly asymptomatic, they are often diagnosed incidentally ³, which accounts for the other unavailable growth rates due to short follow up time until surgery (5/10). Potential selection bias could have occurred in our study, as we have included all aneurysm patients, who underwent open AAA surgery at the time of the conduction of the study consecutively. However, there were no additional criteria or patient selection, which prevented selection bias. As we cannot regulate the site of aortic biopsies, variation of aortic tissue could cause a bias in the results. The site could not be strictly defined upfront as it was secondary to patient safety. However, all the biopsies came from the abdominal region of the aorta and from a part which belonged to the aneurysmal

sac, thus from a diseased, dilated region. Most biopsies were taken from the ventral site of the aneurysm.

We initially hypothesized that SMC contraction *in vitro* might be linked to the degeneration or decrease of SMC specific markers as result of a phenotypic switch²⁶. SMC phenotypes have been functionally classified into “synthetic” and “contractile”, characterized by high expression levels of SMC specific contractile proteins; especially smoothelin²⁷. The SMC phenotypic switch might also play an important role in AAA formation, due to the loss of the SMC contractile properties, as indicated by findings in a rat animal model of thoracic aortic aneurysms²⁸. However, no differences in SMC marker expression or proliferation have been found on mRNA level between patients and controls in our study. Additionally, our results show no correlation between SMC contractility and SMC marker expression. In accordance to our findings, it has been reported that lower contractility of Marfan mice thoracic aortas was not accompanied by a reduction in alpha smooth muscle actin expression²³. Remarkably, the variability in SMC marker expression is equally present in the control as well as in the patient group. This indicates that SMC contractility *in vitro* is not solely defined by the contractile state of the SMC phenotype.

Endoleaks are defined as a post-operative complication following endovascular graft placement, which is characterized by persistent blood flow into the aneurysmal sac around the graft²⁹. Endoleaks can be associated with progressive aneurysm growth and risk of secondary aneurysm rupture³⁰. As hinted by previous research³¹, the secondary aneurysm might grow around the positioned graft due to endotension and pressurization by the thrombus surrounding the graft. Based on our findings (Figure 6b), we speculate that secondary aneurysm growth might be associated with SMC contractile dysfunction. Conversely, progressive aneurysm growth and medial degradation could lead to SMC atrophy, which further weakens the wall in a negative feedback loop and the endograft placed against the aortic wall could cause an inflammation process locally, which affect the SMC as well. It is, however, unclear to which extent these processes are related, and larger scale studies are required to elucidate their connection in the context of AAA pathophysiology.

Tobacco smoking is one of the most important risk for developing AAA, illustrated by four times higher prevalence of AAA in life long non-smokers compared to smokers³. Furthermore, it has been shown that smoking increases aneurysm growth rate by 15-20%³². However, no causal link between AAA pathogenesis and smoking has been shown in terms of molecular mechanisms³³. We demonstrate impaired contractility in a group of current smokers compared to the contractility of control SMC. The patients grouped into current non-smokers consists of patient who never smoked and have stopped smoking prior to their inclusion in our study. The link between current and past smoking was examined in detail in a study by Vardulaki et

al³⁴. Based on their findings, levels of exposure to tobacco smoking caused a higher risk of AAA than duration of exposure. They demonstrated a decrease in risk of AAA formation in people who stopped smoking compared to current smokers. As indicated by our findings, current tobacco smoking is associated with impaired contraction compared to control SMC. Taking into account that the contractility of the current smoking group has a lower median compared to the current non-smoker group, we speculate that current smoking might have a negative effect on aortic SMC function. Furthermore, and in accordance to the previous study³⁴, we reason that the pathological effect of smoking on SMC dysfunction might be reversible in AAA patients, indicating potential treatment targets. The association of smoking and potential contractile problems in AAA patients is an interesting finding, however the latter needs further investigation in a larger cohort and additional molecular experiments to elucidate a potential mechanistic link.

In conclusion, we provide the first proof of impaired SMC contractility in patients with sporadic AAA. We describe a novel application of ECIS, which can be further used as a medium-throughput screening assay for translational studies. Our current results suggest that more than one third of AAA patients had impaired contractility in the heterogeneous population of sporadic AAA patients. This study indicates an association between decreased contractility and current smoking in AAA patients. Taken together, our findings might lead to better understanding of the dilation processes in the aortic wall and new therapeutic targets. Further research is needed to clarify the role of SMC contractility in AAA and identify new therapeutic targets in AAA treatment.

Data availability

The datasets generated during and analyzed during the current study are available from the corresponding author on reasonable request.

ACKNOWLEDGEMENTS

We gratefully acknowledge Arjan Hoksbergen, Hilian Nederhoed, Maarten Truijers, Vincent Jongkind and Willem Wisselink for providing the aortic material during surgery. We wish to thank Jeroen Kole and Rene Musters for their help with confocal microscopy. This work was supported by the ICar-AiO grant of the Amsterdam Cardiovascular Science Institute [grant number ICAR-VU AIO 2015], within Amsterdam University Medical Centers, Amsterdam, the Netherlands.

AUTHOR CONTRIBUTIONS

N.B. designed and planned the study, performed the experiments, analyzed the data and wrote the manuscript. J.P.M. performed the experiments, analyzed the data and revised the manuscript. P.L.H., D.M. and J.D.B. helped with the research

design, advised and assisted on the experiments and revised the manuscript. K.K.Y. designed and planned the study, performed the experiments, analyzed the data and revised the manuscript. All authors reviewed the manuscript.

COMPETING INTERESTS

The authors declare no competing interests.

REFERENCES

- 1 Assar, A. N. & Zarins, C. K. Ruptured abdominal aortic aneurysm: a surgical emergency with many clinical presentations. *Postgrad Med J* 85, 268-273, doi:10.1136/pgmj.2008.074666 (2009).
- 2 Chang, J. B., Stein, T. A., Liu, J. P. & Dunn, M. E. Risk factors associated with rapid growth of small abdominal aortic aneurysms. *Surgery* 121, 117-122, doi:10.1016/S0039-6060(97)90279-8.
- 3 Sakalihasan, N., Limet, R. & Defawe, O. D. Abdominal aortic aneurysm. *The Lancet* 365, 1577-1589, doi:10.1016/s0140-6736(05)66459-8 (2005).
- 4 Meital, L. T., Sandow, S. L., Calder, P. C. & Russell, F. D. Abdominal aortic aneurysm and omega-3 polyunsaturated fatty acids: Mechanisms, animal models, and potential treatment. *Prostaglandins Leukot Essent Fatty Acids* 118, 1-9, doi:10.1016/j.plefa.2017.02.001 (2017).
- 5 Milewicz, D. M. et al. Genetic basis of thoracic aortic aneurysms and dissections: focus on smooth muscle cell contractile dysfunction. *Annu Rev Genomics Hum Genet* 9, 283-302, doi:10.1146/annurev.genom.8.080706.092303 (2008).
- 6 Milewicz, D. M. et al. Altered Smooth Muscle Cell Force Generation as a Driver of Thoracic Aortic Aneurysms and Dissections. *Arterioscler Thromb Vasc Biol* 37, 26-34, doi:10.1161/ATVBAHA.116.303229 (2017).
- 7 Zhu, L. et al. Mutations in myosin heavy chain 11 cause a syndrome associating thoracic aortic aneurysm/aortic dissection and patent ductus arteriosus. *Nat Genet* 38, 343-349, doi:10.1038/ng1721 (2006).
- 8 Guo, D. C. et al. Mutations in smooth muscle alpha-actin (ACTA2) lead to thoracic aortic aneurysms and dissections. *Nat Genet* 39, 1488-1493, doi:10.1038/ng.2007.6 (2007).
- 9 Chen, J., Li, H., SundarRaj, N. & Wang, J. H. Alpha-smooth muscle actin expression enhances cell traction force. *Cell Motil Cytoskeleton* 64, 248-257, doi:10.1002/cm.20178 (2007).
- 10 Peyton, S. R. & Putnam, A. J. Extracellular matrix rigidity governs smooth muscle cell motility in a biphasic fashion. *J Cell Physiol* 204, 198-209, doi:10.1002/jcp.20274 (2005).
- 11 Williams, D. A., Fogarty, K. E., Tsien, R. Y. & Fay, F. S. Calcium gradients in single smooth muscle cells revealed by the digital imaging microscope using Fura-2. *Nature* 318, 558, doi:10.1038/318558a0 (1985).
- 12 Wu, D. et al. NLRP3 (Nucleotide Oligomerization Domain-Like Receptor Family, Pyrin Domain Containing 3)-Caspase-1 Inflammasome Degrades Contractile Proteins: Implications for Aortic Biomechanical Dysfunction and Aneurysm and Dissection Formation. *Arterioscler Thromb Vasc Biol* 37, 694-706, doi:10.1161/ATVBAHA.116.307648 (2017).
- 13 Hurst, V., Goldberg, P. L., Minnear, F. L., Heimark, R. L. & Vincent, P. A. Rearrangement of adherens junctions by transforming growth factor- β 1: role of contraction. *American Journal of Physiology-Lung Cellular and Molecular Physiology* 276, L582-L595, doi:10.1152/ajplung.1999.276.4.L582 (1999).
- 14 Szulcek, R., Bogaard, H. J. & van Nieuw Amerongen, G. P. Electric cell-substrate impedance sensing for the quantification of endothelial proliferation, barrier function, and motility. *J Vis Exp*, doi:10.3791/51300 (2014).
- 15 Hu, N. et al. Comparison between ECIS and LAPS for establishing a cardiomyocyte-based biosensor. *Sensors and Actuators B: Chemical* 185, 238-244, doi:https://doi.org/10.1016/j.snb.2013.04.093 (2013).
- 16 Peters, M. F., Lamore, S. D., Guo, L., Scott, C. W. & Kolaja, K. L. Human Stem Cell-Derived Cardiomyocytes in Cellular Impedance Assays: Bringing Cardiotoxicity Screening to the Front Line. *Cardiovascular Toxicology* 15, 127-139, doi:10.1007/s12012-014-9268-9 (2015).
- 17 Zhang, S. Insulin-Stimulated Cyclic Guanosine Monophosphate Inhibits Vascular Smooth Muscle Cell Migration by Inhibiting Ca/Calmodulin-Dependent Protein Kinase II. *Circulation* 107, 1539-1544, doi:10.1161/01.cir.0000056766.45109.c1 (2003).
- 18 Halterman, J. A., Kwon, H. M., Zargham, R., Bortz, P. D. & Wamhoff, B. R. Nuclear factor of activated T cells 5 regulates vascular smooth muscle cell phenotypic modulation. *Arterioscler Thromb Vasc Biol* 31, 2287-2296, doi:10.1161/ATVBAHA.111.232165 (2011).

- 19 Bass, H. M., Beard, R. S., Jr., Cha, B. J., Yuan, S. Y. & Nelson, P. R. Thrombomodulin Induces a Quiescent Phenotype and Inhibits Migration in Vascular Smooth Muscle Cells In Vitro. *Ann Vasc Surg* 30, 149-156, doi:10.1016/j.avsg.2015.10.002 (2016).
- 20 Henderson, E. L. et al. Death of Smooth Muscle Cells and Expression of Mediators of Apoptosis by T Lymphocytes in Human Abdominal Aortic Aneurysms. *Circulation* 99, 96-104, doi:10.1161/01.cir.99.1.96 (1999).
- 21 Raghavan, M. L., Webster, M. W. & Vorp, D. A. Ex vivo biomechanical behavior of abdominal aortic aneurysm: Assessment using a new mathematical model. *Annals of Biomedical Engineering* 24, 573-582, doi:10.1007/bf02684226 (1996).
- 22 Habashi, J. P. et al. Losartan, an AT1 Antagonist, Prevents Aortic Aneurysm in a Mouse Model of Marfan Syndrome. *Science* 312, 117 (2006).
- 23 Chung, A. W. et al. Loss of elastic fiber integrity and reduction of vascular smooth muscle contraction resulting from the upregulated activities of matrix metalloproteinase-2 and -9 in the thoracic aortic aneurysm in Marfan syndrome. *Circ Res* 101, 512-522, doi:10.1161/CIRCRESAHA.107.157776 (2007).
- 24 Maier, A. et al. A Comparison of Diameter, Wall Stress, and Rupture Potential Index for Abdominal Aortic Aneurysm Rupture Risk Prediction. *Annals of Biomedical Engineering* 38, 3124-3134, doi:10.1007/s10439-010-0067-6 (2010).
- 25 Fillinger, M. F., Raghavan, M. L., Marra, S. P., Cronenwett, J. L. & Kennedy, F. E. In vivo analysis of mechanical wall stress and abdominal aortic aneurysm rupture risk. *Journal of Vascular Surgery* 36, 589-597, doi:10.1067/mva.2002.125478 (2002).
- 26 Bennett, M. R., Sinha, S. & Owens, G. K. Vascular Smooth Muscle Cells in Atherosclerosis. *Circ Res* 118, 692-702, doi:10.1161/CIRCRESAHA.115.306361 (2016).
- 27 van der Loop, F. T. L., Gabbiani, G., Kohnen, G., Ramaekers, F. C. S. & van Eys, G. J. J. M. Differentiation of Smooth Muscle Cells in Human Blood Vessels as Defined by Smoothelin, a Novel Marker for the Contractile Phenotype. *Arteriosclerosis, Thrombosis, and Vascular Biology* 17, 665-671, doi:10.1161/01.atv.17.4.665 (1997).
- 28 Mao, N. et al. Phenotypic switching of vascular smooth muscle cells in animal model of rat thoracic aortic aneurysm. *Interact Cardiovasc Thorac Surg* 21, 62-70, doi:10.1093/icvts/ivv074 (2015).
- 29 White, G. H., Yu, W., May, J., Chaufour, X. & Stephen, M. S. Endoleak as a Complication of Endoluminal Grafting of Abdominal Aortic Aneurysms: Classification, Incidence, Diagnosis, and Management. *Journal of Endovascular Therapy* 4, 152-168, doi:10.1177/152660289700400207 (1997).
- 30 Chuter, T. A. M. et al. Endoleak after endovascular repair of abdominal aortic aneurysm. *Journal of Vascular Surgery* 34, 98-105, doi:10.1067/mva.2001.111487 (2001).
- 31 White, G. H. et al. Endotension: An Explanation for Continued AAA Growth after Successful Endoluminal Repair. *Journal of Endovascular Therapy* 6, 308-315, doi:10.1177/152660289900600402 (1999).
- 32 Brady, A. R., Thompson, S. G., Fowkes, F. G. R., Greenhalgh, R. M. & Powell, J. T. Abdominal Aortic Aneurysm Expansion. *Circulation* 110, 16 (2004).
- 33 Nordon, I. M., Hinchliffe, R. J., Loftus, I. M. & Thompson, M. M. Pathophysiology and epidemiology of abdominal aortic aneurysms. *Nature Reviews Cardiology* 8, 92, doi:10.1038/nrcardio.2010.180 (2010).
- 34 Vardulaki, K. A. et al. Quantifying the risks of hypertension, age, sex and smoking in patients with abdominal aortic aneurysm. *BJS* 87, 195-200, doi:10.1046/j.1365-2168.2000.01353.x (2002).
- 35 Wegener, J., Keese, C. R. & Giaever, I. Electric cell-substrate impedance sensing (ECIS) as a noninvasive means to monitor the kinetics of cell spreading to artificial surfaces. *Exp Cell Res* 259, 158-166, doi:10.1006/excr.2000.4919 (2000).
- 36 Kataoka, N. et al. Measurements of endothelial cell-to-cell and cell-to-substrate gaps and micromechanical properties of endothelial cells during monocyte adhesion. *Proceedings of the National Academy of Sciences* 99, 15638 (2002).
- 37 Bland, J. M. & Altman, D. G. Measuring agreement in method comparison studies. *Statistical Methods in Medical Research* 8, 135-160, doi:10.1177/096228029900800204 (1999).
- 38 Yeung, K. K. et al. Transdifferentiation of Human Dermal Fibroblasts to Smooth Muscle-Like Cells to Study the Effect of MYH11 and ACTA2 Mutations in Aortic Aneurysms. *Hum Mutat* 38, 439-450, doi:10.1002/humu.23174 (2017).
- 39 Schindelin, J. et al. Fiji: an open-source platform for biological-image analysis. *Nat Methods* 9, 676-682, doi:10.1038/nmeth.2019 (2012).

Impaired smooth muscle cell contractility as a novel concept of abdominal aortic aneurysm pathophysiology.

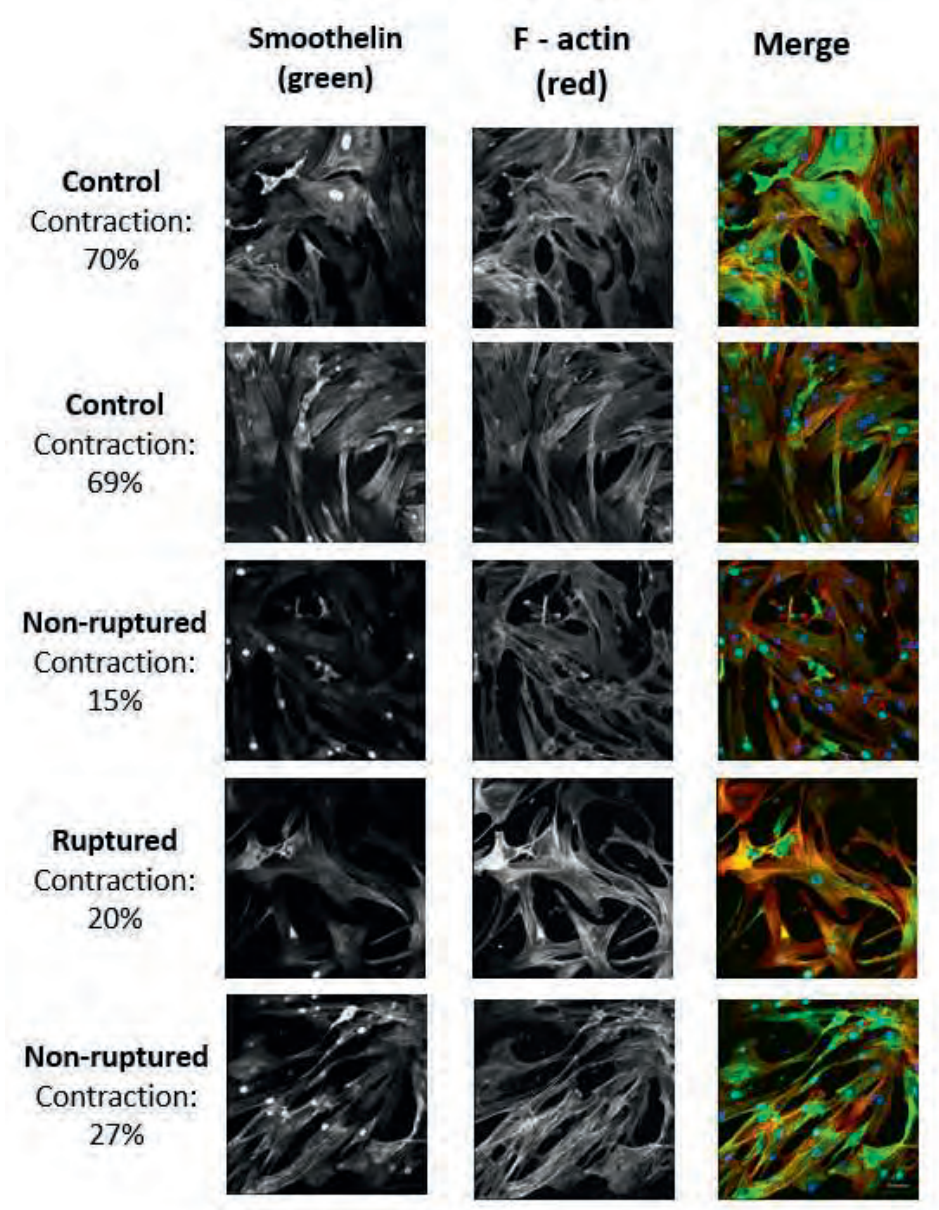
Supplementary information.

Scientific reports; 2019; 9(1), 6837.

Natalija Bogunovic, Jorn P. Meekel, Dimitra Micha, Jan D. Blankensteijn, Peter L. Hordijk, Kak K. Yeung

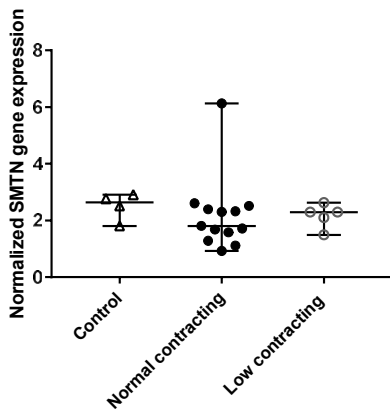
Supplementary Table S1. qPCR primer information GeneBank sequences and forward and reverse qPCR primer sequences of analyzed housekeeping, SMC marker and SMC regulatory genes.

Gene code	RefSeq sequence	Forward and reverse primer sequence
<i>YWHAZ</i>	NM_145690	GATGAAGCCATTGCTGAACTTG CTATTTGTGGGACAGCATGGA
<i>TBP</i>	NM_003194	AGTTCTGGGATTGTACCGCA TCCTCATGATTACCGCAGCA
<i>VIM</i>	NM_003380	AGATGGCCCTTGACATTGAG CGTGATGCTGAGAAGTTTCG
<i>MKI67</i>	NM_002417	AGCACCAGAGGAAATTGTGG TTTTCAAGGACCGAGTCTTG
<i>AIM2</i>	NM_004833	GCTGCACCAAAAGTCTCTCC ATCTCCTGCTTGCCTTCTTG
<i>ACTA2</i>	NM_001141945	ACTGGGACGACATGGAAAAG CATACTGGCTGGGACATTG
<i>CNN1</i>	NM_001308341	GCCCAGAAGTATGACCACCA TGATGAAGTTGCCGATGTTT
<i>SMTN</i>	NM_001207018	TGGAGGAATTGACTGCACTG GAAACCTCTGCCTGCTGTTT
<i>TAGLN</i>	NM_001001522	AAGAATGATGGGCACTACCG AGCCCTCTCCGCTCTAACTG

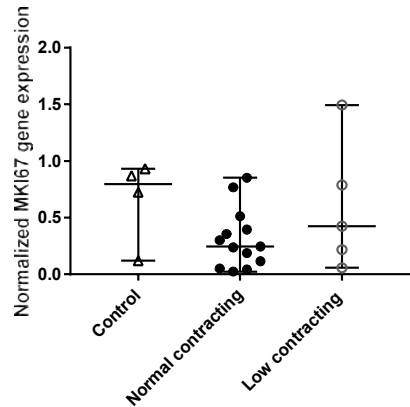


Supplementary Figure 1. Representative images of Smoothelin and F-actin immunostaining in control and patient SMC. Column A: Smoothelin immunostaining depicted in green on the merged image. Column B: F-actin immunostaining depicted in red on the merged image. Column C: merged image of smoothelin, F-actin and DAPI. Scale bar: 50µm.

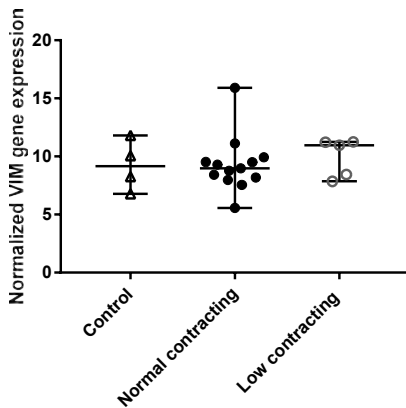
a



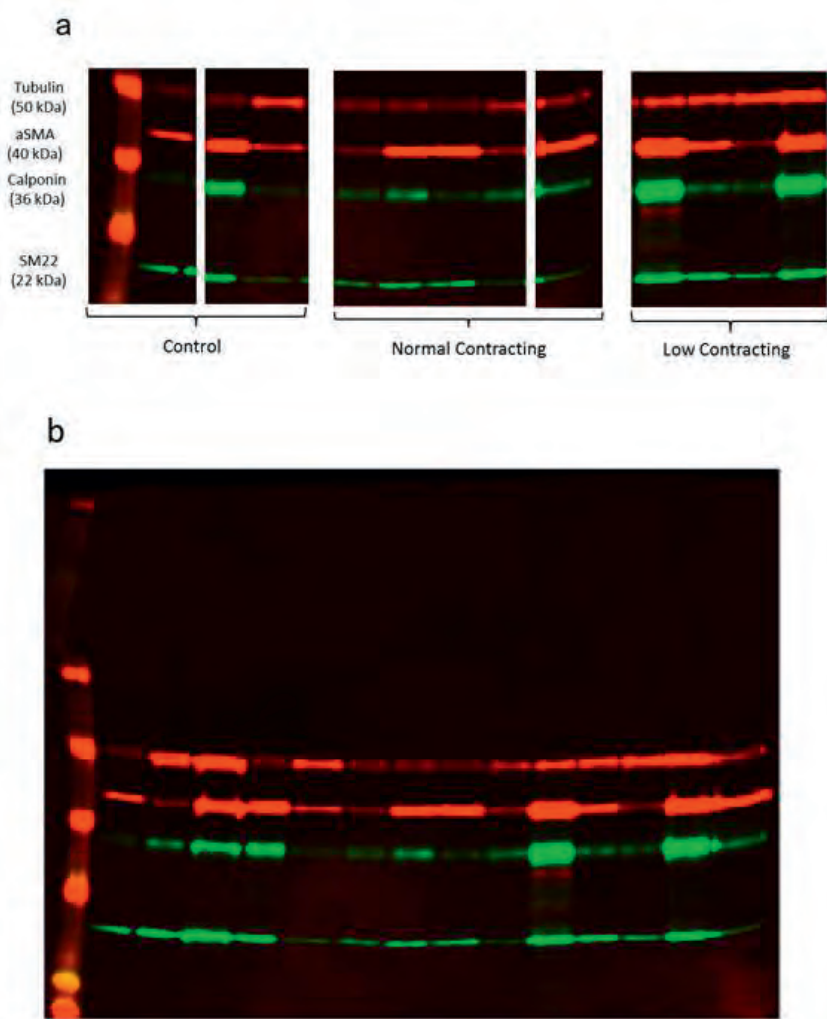
b



c



Supplementary Figure 2. SMC marker gene expression in control and AAA patient SMC. Panels a-c: Gene expression of *SMTN*, *VIM* and *MKI67* in mRNA isolated from control (▲; n=4), normal contracting (●; n=13) and low contracting SMC (○; n=5). Boxplots are shown as median with range.



Supplementary Figure 3. Cropped and full-length western blot used in Figure 5. a) Figure 5a, cropped and grouped lanes from a full western blot. Legend Figure 5a: a) Western blot analysis of aSMA, Calponin and SM22 in Control (n=3), Normal Contracting (n=5) and Low Contracting (n=4) AAA patient SMC. Lanes were cropped and grouped from the original image (Supplementary Figure 3), Ladder: lane 0; Control: lanes 1,4 and 5; Normal contracting: lanes 6-9 and 14; Low contracting: lanes 10-13. b) Intensity of aSMA, Calponin and SM22 in Control (n=3), Normal Contracting (n=5) and Low Contracting (n=4) AAA patient SMC. Intensity red channel (700CW) 5, Intensity green channel (800CW) 3. b) Full-length blot. Intensity red channel (700CW) 5, Intensity green channel (800CW) 3.

Supplementary Video 1. Time-lapse recording of SMC contraction. SMC were seeded in a 25mm dish and stimulated with ionomycin. The cells were recorded for 1h and the video was fast-forwarded 900x. Scale bar: 50µm.

Available online at:

<https://www.nature.com/articles/s41598-019-43322-3#Sec17>



6

An in vitro method to keep human aortic tissue sections functionally and structurally intact.

Jorn P. Meekel, Menno E. Groeneveld, Natalija Bogunovic, Niels Keekstra, René J.P. Musters, Behrouz Zandieh-Doulabi, Gerard Pals, Dimitra Micha, Hans W.M. Niessen, Arno M. Wiersema, Jur K. Kievit, Arjan W.J. Hoksbergen, Willem Wisselink, Jan D. Blankensteijn, Kak K. Yeung

Scientific reports; 2018; 8(1), 8094.

ABSTRACT

The pathophysiology of aortic aneurysms (AA) is far from being understood. One reason for this lack of understanding is basic research being constrained to fixated cells or isolated cell cultures, by which cell-to-cell and cell-to-matrix communications are missed. We present a new, in vitro method for extended preservation of aortic wall sections to study pathophysiological processes.

Intraoperatively harvested, live aortic specimens were cut into 150µm sections and cultured. Viability was quantified up to 92 days using immunofluorescence. Cell types were characterized using immunostaining. After 14 days, individual cells of enzymatically digested tissues were examined for cell type and viability.

Analysis of AA sections (N=8) showed a viability of 40% at 7 days and smooth muscle cells, leukocytes, and macrophages were observed. Protocol optimization (N=4) showed higher stable viability at day 62 and proliferation of new cells at day 92. Digested tissues showed different cell types and a viability up to 75% at day 14.

Aortic tissue viability can be preserved until at least 62 days after harvesting. Cultured tissues can be digested into viable single cells for additional techniques. Present protocol provides an appropriate ex vivo setting to discover and study pathways and mechanisms in cultured human aneurysmal aortic tissue.

The pathophysiology of aortic aneurysms (AA) is far from being understood. One reason for this lack of understanding is basic research being constrained to fixated cells or isolated cell cultures, by which cell-to-cell and cell-to-matrix communications are missed. We present a new, in vitro method for extended preservation of aortic wall sections to study pathophysiological processes.

Intraoperatively harvested, live aortic specimens were cut into 150µm sections and cultured. Viability was quantified up to 92 days using immunofluorescence. Cell types were characterized using immunostaining. After 14 days, individual cells of enzymatically digested tissues were examined for cell type and viability.

Analysis of AA sections (N=8) showed a viability of 40% at 7 days and smooth muscle cells, leukocytes, and macrophages were observed. Protocol optimization (N=4) showed higher stable viability at day 62 and proliferation of new cells at day 92. Digested tissues showed different cell types and a viability up to 75% at day 14.

Aortic tissue viability can be preserved until at least 62 days after harvesting. Cultured tissues can be digested into viable single cells for additional techniques. Present protocol provides an appropriate ex vivo setting to discover and study pathways and mechanisms in cultured human aneurysmal aortic tissue.

INTRODUCTION

Aortic aneurysm (AA) is a common health problem, which is associated with high mortality rates in the event of a rupture. This unpredictable life-threatening rupture leads to rapid aortic exsanguination into thorax, abdominal cavity or retroperitoneum.¹⁻³ To date, studies investigating the pathophysiology of AA have produced inconclusive results concerning the underlying mechanisms. Although different meaningful disease models exist, the lack of a functionally and structurally intact live aortic human tissue model which can bioactively be stimulated *ex vivo*, has posed severe limitations to the study of AA in understanding the pathophysiological mechanism which has restricted the identification of therapeutic targets and the development of efficient therapy.⁴

It has been observed previously that an increase of AA diameter occurs in relation to the transformation of the aortic vessel wall composition. Part of this transformation is a combination of vascular smooth muscle cell (SMC) loss and inflammation and degeneration of extracellular matrix (ECM). These changes are suggested to play a role in the pathogenesis of AA, but mechanisms contributing to these processes, are still poorly understood.^{5, 6}

Although numerous *in vivo* animal models to study AA exist, investigation of human material is limited to the use of fixated tissue or isolated cell cultures.⁷⁻¹² Such approaches, however, have failed to retain the complex organ function of the aorta, which is based on cell-cell interactions, communication with ECM, immune cell infiltration and constant tissue remodelling.¹³⁻¹⁶

Unfortunately, fixated aortic tissue only provides a snapshot into the microstructural characteristics of the diseased tissue, and isolated cultured aortic cells cannot reproduce the complexity of cell-ECM interactions and live pathways. Additionally, usage of animal models is costly, ethically and technically challenging and animal models do not completely resemble the human conditions, as the aortic aneurysms need to be created in the animal model.

Hence, there is a need to provide a new *in vitro* model to study the pathophysiological processes, which are involved human AA. Live sectioning and preservation of human (aneurysmal) aortic tissue can lead to improvement of the understanding of AA pathogenesis. In this study, we present an innovative method for the investigation of human AA pathophysiology by preserving tissue viability and cellular organization of human aneurysmal tissue *ex vivo* for several weeks.

METHODS

Human tissues

The present study was approved by the Medical Ethical Committee of the VU University Medical Center (VUmc) Amsterdam. Informed consent files were signed prior to surgery. In case of acute surgery for ruptured aneurysm repair, delayed informed consent was received in the postoperative period as soon as permitted by the health situation of the patients. All experiments were performed in accordance with relevant guidelines and regulations.

Human aortic tissue was collected from the operating theatre in two hospitals (VUmc, Amsterdam, the Netherlands and Westfriesgasthuis, Hoorn, the Netherlands) during open abdominal AA (AAA) surgery (N=9). Additional vascular tissues were harvested from human non-aortic anatomical sites (N=4): external iliac artery punch and renal artery. Using nine consecutively harvested human vascular tissues (N[AAA]=5 and N[additional vascular tissues]=4), a pilot study with primary viability analysis until 14 days was performed. These results were evaluated to further develop the protocol with minor improvements. Subsequently, new AAA tissue (N=4) was harvested and subjected to the new protocol to evaluate the maximum life span of human AAA tissue sections *ex vivo* (figure 1A).

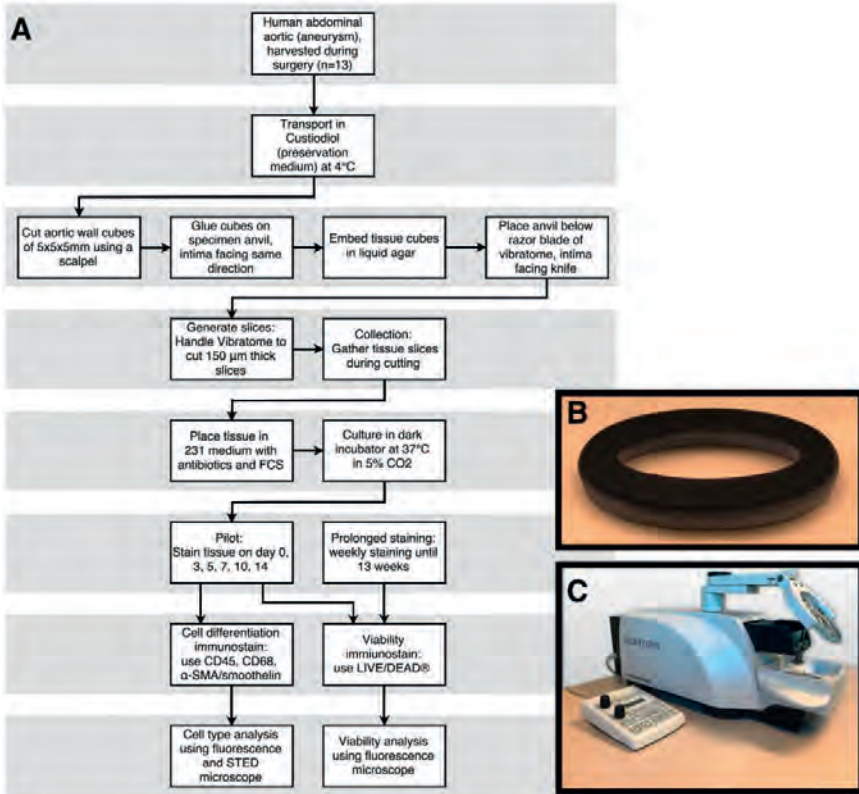


Figure 1. Overview of experimental setup. A: Flow chart of protocol: vascular tissue cubes were cut into sections using a vibrating blade microtome (Leica VT1200 S). Tissue sections were cultured in supplemented culture medium in 24-well plates in a dark humidified atmosphere at 37°C in 5% CO₂. B: Photograph of self-designed 3D-printed mould in which tissue cubes are fixed in agarose. C: Photograph of vibratome Leica VT1200S, used for tissue sectioning. α -SMA indicates alpha smooth muscle actin; FCS, fetal calf serum and STED, stimulated emission depletion.

Transport and vascular section preparation

Directly after harvesting tissue at the operating theatre, the vascular tissue was submerged in Custodiol (Dr. Franz Köhler Chemie GmbH, Bensheim, Germany) at 4°Celsius. The tubes containing tissue were transported on ice to the vibratome (Leica VT1200 S, Leica Biosystems, Nussloch, Germany). Vascular cubes of 5x5x5 mm were cut using a scalpel. These cubes contained intima, media and adventitia. Cubes were then glued on a specimen anvil using Roti Coll superglue (Carl Roth GmbH + Co. KG, Karlsruhe, Germany). The intimal layer of the cubes was facing the knife of the vibratome, to ensure that after cutting, aortic sections were containing all layers. Fixed cubes were embedded in agarose gel solution (1 g agarose in 50 mL

0.5x TAE buffer, UltraPure™ Agarose, Thermo Fisher Scientific Inc., Waltham, MA, USA) using a self-designed 3D-printed mould (figure 1B).

After cooling down and thereby stiffening of agarose gel, the mould was removed. The entirety of anvil, tissue and agarose was immersed in a small reservoir filled with Custodiol at 4° Celsius. The reservoir was placed under the razor blade (Croma Stabil, Feintechnik GmbH, Eisfeld, Germany) of the vibratome (figure 1C). Cutting of sections containing intima, media and adventitia was performed. The first three consecutive sliced sections were discarded, since these often macroscopically did not contain all layers of the vascular wall and lower viability in these sections was to be expected. From earlier (unpublished) pilot experiments, we determined that the best viability results were acquired by cutting 150-µm-thick sections with the vibratome at a speed of 0.08 mm/s with a horizontal amplitude of the razor blade fixed at 2.65 mm. For the development of the present protocol, live bovine tissues were firstly used to set up the optimum settings for the vibratome. Abdominal bovine aorta was obtained from an abattoir (Abattoir Amsterdam B.V, Amsterdam, the Netherlands) directly after euthanization.

Tissue preservation

Immediately after sectioning with the vibratome, tissue sections were transferred in culture medium. Tissue sections were conserved in 24 wells plates, each well filled with 500µl of one of two different media; either Ham's F10 (Ham's F10 Nutrient Mix, Gibco, Life Technologies, Carlsbad, CA, USA) supplemented with Penicillin-Streptomycin (PS, 25,000 U, Gibco, Life Technologies, Carlsbad, CA, USA) and 10% Fetal Bovine Serum (FBS, Gibco, Life Technologies, Carlsbad, CA, USA) or M231 (Medium 231, Smooth Muscle Cell medium, Gibco, Life Technologies, Carlsbad, CA, USA) supplemented with PS (25,000 U) and 5% Smooth Muscle Growth Supplement (SMGS, Gibco, Life Technologies, Carlsbad, CA, USA). Both supplemented culture media (Ham's F10 and M231) of the first 4 consecutively harvested tissues were compared to determine best outcome on tissue viability. Sections were cultured in wells plates in a dark humidified atmosphere at 37°Celsius in 5% CO₂ and culture media were replaced daily.

Immunofluorescence staining: viability and characterization of cell types

Viability was examined by immunofluorescence staining at day 0, 3, 5, 7, 10 and 14 for primary analysis (N=9). After protocol optimization, the newly harvested tissues (N=4) were kept viable as long as possible and were examined monthly by the immunostaining for viability. For analysis, tissues were removed from the culture medium and washed in PBS solution for two minutes. Subsequently, the tissue was incubated in chamber slides for 30 minutes in 300µl of 0.04% calcein acetoxymethyl (calcein AM) and 0.16% ethidium homodimer-1 (EthD-1) solution (LIVE/DEAD® Viability/Cytotoxicity Kit and PBS solution, Life Technologies, Carlsbad, CA, USA).

LIVE/DEAD® Kit stains live and dead cells by accordingly indicating intracellular esterase activity or loss of plasma membrane integrity. Cell-permeant nonfluorescent calcein AM is enzymatically converted to intensely fluorescent calcein (green) by live cell intracellular esterases, which hydrolyse acetoxymethyl ester. EthD-1 becomes fluorescent (red) in cell nuclei upon binding to nucleic acids after entering through the damaged cell membrane of dead cells. Given that live cells have intact cell membranes, transmembrane passage of EthD-1 in live cells does not take place.

Earlier, in feasibility tissues, staining with anthracycline derivative 1% DRAQ7 dye (DRAQ7™, Cell Signaling Technology, Inc., Danvers, MA, USA) in combination with 1% Hoechst (Hoechst 33342™, Cell Signaling Technology, Inc., Danvers, MA, USA) and DNA dye 1% DRAQ5™ (DRAQ5™, Cell Signaling Technology, Inc., Danvers, MA, USA) were used to monitor cell death. However, the latter stained only the upper layer of the tissue, while LIVE/DEAD® Kit stained through the whole thickness of the aortic tissue; making quantification of the live and dead cells possible. In order to characterise cell type composition of the tissue, SMC, leukocytes and macrophages were subjected to immunofluorescence staining against α -SMA/smoothelin, CD45, CD68 respectively. First, tissue was washed twice with 300 μ l of PBS and fixated in 300 μ l of 4% formaldehyde solution (Sigma-Aldrich, St. Louis, MO, USA) for 20 minutes. Fixated tissue was subsequently washed three times for five minutes in 300 μ l of 0.05% PBST (Tween and PBS solution, Sigma-Aldrich, St. Louis, MO, USA) and submerged in a 0.2% solution of Triton (Triton x-100 and PBS solution, Sigma-Aldrich, St. Louis, MO, USA) for twenty minutes and rinsed with a 1.0% BSA solution (Bovine Serum Albumine and PBS solution, Vector Laboratories, Inc, Burlingame, CA, USA). After three PBST washing steps of five minutes, the tissue was incubated overnight in 2% Monoclonal Mouse Anti-Human Smooth Muscle Actin solution at dilution; (DAKO, Glostrup, Denmark). Hereafter, five washing steps of five minutes using PBST, were followed by one hour incubation of 1% Anti-Mouse Alexa Fluor 647 secondary antibody (Thermo Fisher Scientific Inc.). After five PBST washing steps, overnight incubation using 2% Polyclonal Rabbit Anti-Human Primary Smoothelin Antibody (H-300, Santa Cruz Biotechnology, Dallas, TX, USA) was performed. Five PBST washing steps were then followed by incubation of one hour using 1% Anti-Rabbit Alexa Fluor 488 secondary antibody (Thermo Fisher Scientific Inc.).

In additional slides, leukocytes were stained with 2% Monoclonal Mouse Anti-human CD45 (N=1, DAKO, Glostrup, Denmark) and macrophages were stained with 2% Monoclonal Mouse Anti-human CD68 (N=1, DAKO, Glostrup, Denmark) in fixated coupes and after washing with PBST (five steps) followed by incubation of one hour using 1% Anti-Mouse Alexa Fluor 647 secondary antibody (Thermo Fisher Scientific Inc.). Where overnight staining was done at 4° Celsius, the remainder steps were performed at room temperature. Aforementioned α -SMA/smoothelin, CD45 and

CD68 stainings were followed by 15 minutes staining for 2% DAPI (4',6-Diamidino-2-Phenylindole, Dihydrochloride, Thermo Fisher Scientific Inc.) to show cell nuclei and tissue was washed with PBST twice and once with PBS solution at room temperature. Slides with tissue were mounted with VECTASHIELD® Antifade Mounting Medium (Vector Laboratories, Inc, Burlingame, CA, USA) and closed using coverslips. As negative controls for α -SMA/Smoothelin, CD45 and CD68, tissue sections were used in which the primary antibody was omitted from the staining procedure.

In order to assess wall composition over time, aortic tissue sections of one AAA patient were cultured until 14 days in daily replaced supplemented M231 culture medium. After 0, 7 and 14 days, different tissue sections were removed from the culture medium and snap-frozen for analysis. Therefore, the sections were immunostained for smoothelin, as a marker of mature SMC, and DAPI according to above described protocol. Additionally, phalloidin (Rhodamine-phalloidin, Thermo Fisher Scientific Inc.) immunostaining was performed simultaneously with DAPI immunostaining, to present all aortic wall cells and their relation within the tissue sections. Again, after immunostaining, tissues were washed, mounted with VECTASHIELD® and slides were closed using coverslips.

Vascular enzymatic tissue digestion for analysis with individual cells

Multiple tissue sections of two AAA patients were separately submerged in 1 mg/ml collagenase type II (Worthington, Lakewood, NJ, USA) and M231 in tubes. These were placed in a rotator in a dark atmosphere at 37°Celsius for 3 hours. The mixture was then filtrated through a 100 μ M gauze and centrifuged at 300g for 10 minutes. Supernatant was removed and cell pallet was resuspended in 500 μ L of M231. These cells were used for further qualitative immunofluorescence analysis and count and viability assay.

Immunofluorescence staining in digested cells

After primary analysis at day 0, tissues were digested at day 7 and 14 as described above, to quantitatively analyze cell viability and qualitatively analyze characteristics in individual cells. Cells were stained with LIVE/DEAD® Kit, using the same staining protocol as for tissues.

Analysis of immunofluorescence staining

Viability examination of sections was performed using Zeiss Axiovert 200M Marianas™ digital imaging inverted microscope system. The set-up was provided with a non-stepper-motor (z-axis increments: 0.1 μ m) and a filter turret with individual filter blocks for fluorescein isothiocyanate (FITC), a pair of cyanine dyes (CY5 and CY3), aminomethylcoumarin acetate (AMCA) and a differential interference contrast

(DIC) brightfield cube. FITC and CY3 were handled to respectively demonstrate live (calcein) and dead (EthD-1) cells. Imaging was performed using a 16-bit, cooled charge-coupled device camera (Cooke Sensicam SVGA, Cooke Co., Tonawanda, NY, USA). Aforementioned set-up was connected to Slidebook™ (Slidebook v. 5.5 software, Intelligent Imaging Innovations, Inc., Denver, CO, USA) to control hardware and to view and process images. Zeiss air objective lenses at magnifications of 2.5X (for quantitative overview images), 10X and 40X (for detailed higher resolution images and 3D stacks) and 63X (oil objective lens to study individual cells) were used to obtain images. Unspecific background and disproportional intensity staining was corrected for by Slidebook software. The viability proportion of tissue sections was calculated by dividing calcein intensity in square micron by the sum of calcein and EthD-1 in square micron.

Analysis of different cell types was again performed using Zeiss Axiovert 200M Marianas™. Depending on choice of different secondary antibodies CY5, CY3, FITC and DAPI were utilized. Magnifications of 2.5X, 10X and 40X were used for analysis. For characterization of cell type, shutter speeds were based on primary antibody positive stained tissues, while use of Renormalize Button in Slidebook™ was based on negative controls (without primary antibody). To obtain super resolution images a Confocal Laser Scanning Microscope Leica TCS SP8 (Leica Microsystems, Mannheim, Germany) was used. Regions of interest in images previously captured with fluorescence microscope were reviewed using 40X and 63X Leica oil-immersion lenses. Unfortunately, photo bleaching of calcein interfered with visualization of live cells. Therefore, for live and dead quantification solely fluorescence microscopy was used. LAS-X software was used to analyse images of cell type differentiation. Excitation/emission spectra used for secondary antibodies (Alexa Fluor 488, Alexa Fluor 555, Alexa Fluor 647) were chosen out of identically named pre-set excitation/emission spectra in Leica LAS-X.

Aortic wall composition analysis was performed using Nikon A1R (Nikon Instruments, Tokyo, Japan) confocal microscope with 40 X oil objective. Using NIS-Elements C Software (Nikon Instruments), super high-resolution (5120x5120 pixels) intima-to-adventitia stitched images of 5x5 fields of view. Excitation/emission spectra used to capture fluorescent signal of phalloidin (Alexa Fluor 546), and secondary antibody of smoothelin (Alexa Fluor 647) were chosen out of pre-set excitation/emission spectra in NIS-Elements C. Fluorescence levels of smoothelin and phalloidin were quantified using FIJI/ImageJ (v1.0. National Institutes of Health, Bethesda, MD, USA). Following background subtraction, masks of selected tissue areas were created and quantified. Outcomes were corrected for number of cells using DAPI count.

Count and viability assay following tissue digestion

On day 14, individual cell viability assay was performed by the Muse Count & Viability reagent (Millipore, Billerica, MA, USA) following the manufacturer's protocols. Harvested cells in M231 (50 μ L) were added to 450 μ L Count & Viability reagent (Millipore). The system was gated for viability and exclusion of both cellular debris and cell clusters, which was based on cultured commercially available smooth muscle cells of a 31-year old healthy male (Thermo Fisher Scientific Inc., Waltham, MA, USA). The results were analyzed with Muse Count & Viability software module.

Proof of concept: *ex vivo* tissue stimulation and quantification of gene expression by qPCR

Live aortic tissues of AAA patients (N=8) were sectioned according to above described protocol. Complete M231 culture medium (including PS and SMGS) was supplemented with TGF- β (5 ng/ml, BioVision, Milpitas, CA) to stimulate the tissue sections, since dysregulation of TGF- β is often described in literature, as a key player in the development and progression of AAA. Culturing of sections was performed in complete M231 medium with (stimulated) and without TGF- β (non-stimulated) supplement in a dark humidified atmosphere at 37°Celsius in 5% CO₂. Culture medium was replaced daily to ensure constant TGF- β stimulation. After 7 days, both stimulated and non-stimulated tissues were rinsed in PBS and directly snap-frozen. Tissue pieces were stored at -80°Celsius until analysis.

AAA patient pooled (N=8) stimulated and non-stimulated, tissue sections were homogenized apart from each other in two 2.0 mL eppendorfs in 300 μ L lysis buffer (Zymo Research, Irvine, CA, U.S.A.). Total RNA of both eppendorfs was isolated using Quick-RNA™ MiniPrep kit (Zymo Research). Synthesis of complementary DNA was performed in a reverse transcription reaction using VILO kit (Thermo Fisher Scientific Inc.). Quantitative PCR (qPCR) was performed to analyze gene expression. *YWHAZ* was used as housekeeping gene. By use of LightCycler® SYBR Green I Master (Roche Applied Science, Penzberg, Germany) gene expression was analyzed by the LightCycler® 480 Instrument II (Roche Applied Science). Potential differences in expression of interleukin 6 (*IL6*), calponin 1 (*CNN1*), transforming growth factor beta 1 (*TGFB1*), monocyte chemotactic protein 1 (*MCP1*), transforming growth factor beta receptor 1 (*TGFB1*), smoothelin (*SMTN*), intercellular adhesion molecule 3 (*ICAM3*), matrix metalloproteinase-2 (*MMP2*), alpha smooth muscle actin 2 (*ACTA2*), tumor necrosis factor (*TNF*), protein tyrosine phosphatase, receptor type, C (*PTPRC*), antigen Ki-67 (*Ki67*), intercellular adhesion molecule 1 (*ICAM1*), interleukin 8 (*IL8* or *CXCL8*) and matrix metalloproteinase-9 (*MMP9*) in stimulated and non-stimulated AAA tissue sections were evaluated (the entire list of corresponding NCBI Reference Sequence Database codes and forward and reverse primer sequences can be found as Supplementary Table S1 online). RNA

expression was shown as a ratio; relative expressions based on non-stimulated tissue sections was calculated after seven days culturing *ex vivo*.

Statistical analysis

The data was analyzed with SPSS Statistics 22.0 (IBM Corporation, Armonk, NY, USA). Measurements of viability are shown in box-plots. Wilcoxon signed-rank test was performed to compare viability of corresponding tissue cultured in different media (Ham's F10 and M231). Comparisons of viability in the first nine consecutive patient sample on multiple time points were made by repeated measures of analysis of variance (one-way Anova) using the Bonferroni correction for multiple-comparison testing. P-value of < 0.05 is considered statistically significant. Muse Count & Viability software module showed percentage of viable single cells of enzymatically digested tissues.

Data Availability

The datasets generated during and analyzed during the current study are available from the corresponding author on reasonable request.

RESULTS

Primary viability analysis was performed in 9 vascular specimens. After a few adjustments of the protocol (i.e. life-span optimization during sectioning and culturing of the tissues), maximum life endurance of live aortic *ex vivo* tissues was examined in 4 additional aortic tissues. Viability staining showed no difference in viability between cultured tissues (N=4) in Ham's F10 or M231 culture media ($\alpha=0.465$). Since no significant difference was observed between tissue viability cultured in different media, the mean outcomes of tissues in either Ham's F10 or M231 per day per corresponding donor were used for further analysis.

Qualitative evaluation of all images of the first 9 vascular tissues showed that dead cells were located mostly on the surface of the tissue, while live cells were mainly localized in the center of vascular tissue sections (figure 2A-F). Figure 2G shows tissue viability during the experiments; human tissues at day 0 showed a mean viability proportion of 0.42 (N=9, SD: 0.16). Consecutively, mean viability proportion was 0.38 (SD: 0.15) for day 3; 0.43 (SD: 0.12) for day 5; 0.38 (SD: 0.13) for day 7; 0.27 (SD: 0.17) for day 10; and 0.18 (SD: 0.15) for day 14. There was a significant difference in viability proportion between day 0 and day 14 ($P=0.026$) and between day 5 and day 14 ($P=0.015$). AAA tissue viability at day 0 was 0.42 (N=5, SD: 0.2), which was almost similar to the non-aortic-tissue viability at day 0, being 0.41 (N=4, SD: 0.14). Small protocol adjustments were implemented, including pre-sectioning removal of calcium depositions, warmed (37°Celsius) tissue section transport, immunostaining within culture medium and shorter tissue-out-of-incubator times.

After implementing the new protocol, an improved tissue viability proportion of 0.58 after 62 days was observed (figure 3A) in AAA tissue. After 92 culturing days (viability proportion: 0.85), outgrowth of many new cells around the initial tissue was observed, but no viability in the original tissue was seen (figure 3B,C).

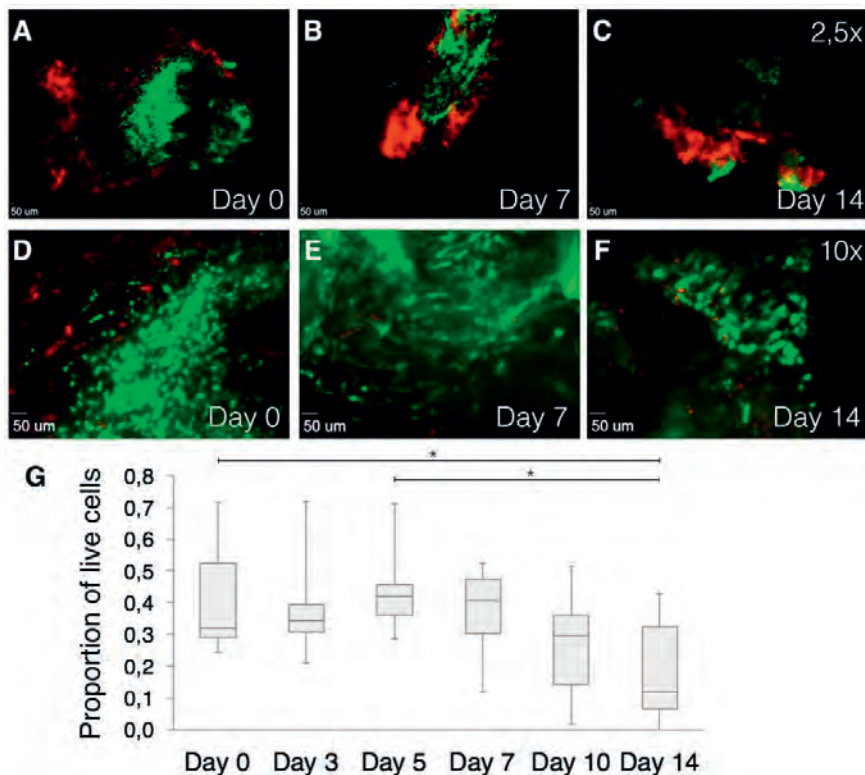


Figure 2. Immunofluorescence images using Zeiss Axiovert 200M Marianas™ Microscope. Cells stained with LIVE/DEAD® Viability/Cytotoxicity Kit. A, B and C: 2.5x magnification of cultured tissues at day 0, 7 and 14, respectively. D, E and F: 10x magnification of cultured tissues at day 0, 7 and 14, respectively. Green fluorescence shows live cells, while red fluorescence indicates dead nuclei. Live cells are mainly located central to tissue. G: Quantification of live human cells in harvested vascular tissues of distinct patients (n=9). Box plots show proportions of square micron of green fluorescence divided by the sum of green and red fluorescence. *p<0.05 compared with other time points using ANOVA with Bonferroni test.

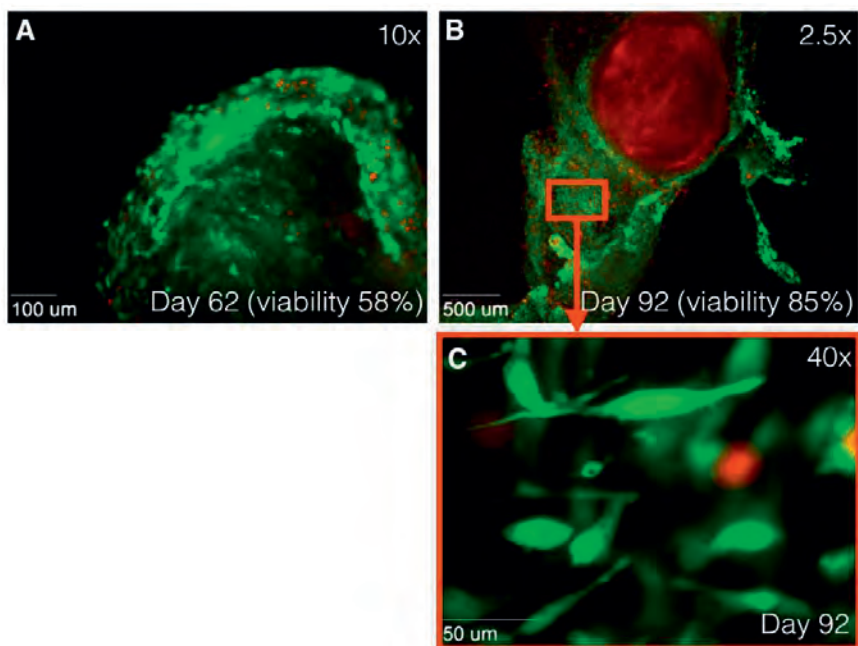


Figure 3. Immunofluorescence images at 10x magnification using Zeiss Axiovert 200M Marianas™ Microscope. Human tissue stained with LIVE/DEAD® Viability/Cytotoxicity Kit. Green fluorescence shows live cells, while red fluorescence indicates dead nuclei. A: Alive tissue at day 62 after harvesting. Tissue viability of 58%. B: Alive tissue at day 62 after harvesting at 2.5x magnification and C: at 40x magnification. Outgrowth of new cells is observed after 92 days, while original tissue shows only staining of EthD-1 (dead cells). Tissue viability of 85%. EthD-1 indicates ethidium homodimer-1.

Immunofluorescence: smooth muscle cells, leucocytes and macrophages, and aortic wall composition

Given that primary analysis showed best viability outcomes on day 5 and 7, these days were designated to perform further experiments. Cells with a similar shape to SMC were observed during analysis of viability images using LIVE/DEAD® Kit (figure 3C). Digital imaging microscope analysis of immunofluorescence staining showed cells with colocalized α -SMA and smoothelin, early and late SMC marker, respectively (figure 4A-C), again with aforementioned characteristic SMC shape. Additionally, confocal scanning laser microscopy was utilized to gain high quality images, which confirmed the presence smooth muscle cells (figure 4D-F). Moreover, fixated immunostaining for CD45 and CD68 showed leucocytes and macrophages, respectively (figure 5A-D). By retrospectively analyzing the images of tissues immunostained with LIVE/DEAD® Kit, the morphological form of live leucocytes could be recognized.

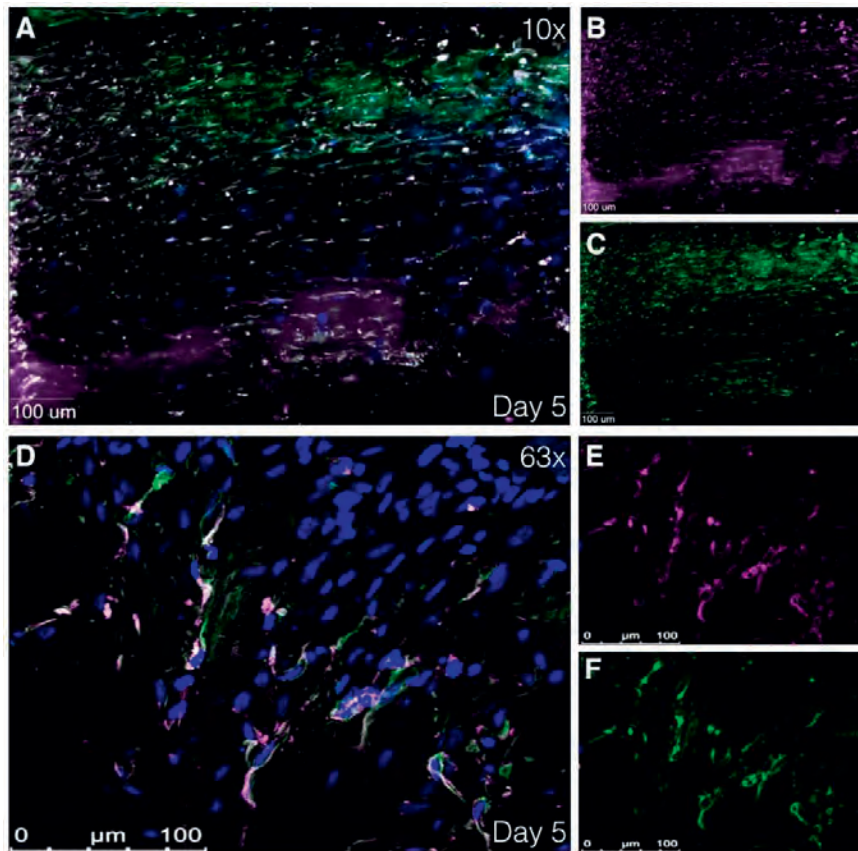


Figure 4. Immunofluorescence images showing smooth muscle cells. A-C: Immunofluorescence images at 40x magnification using using Zeiss Axiovert 200M Marianas™ Microscope at day 5 after harvesting. D-F: Immunofluorescence image at 63x magnification using super resolution Confocal Laser Scanning Microscope Leica TCS SP8.

Human tissue stained with α -SMA and smoothelin (smooth muscle cell markers) at day 5 after harvesting. A,D: Merged image of α -SMA (purple), smoothelin (green) and DAPI (blue). B,E: Isolated α -SMA staining. C,F: Isolated smoothelin staining. α -SMA indicates alpha smooth muscle actin and DAPI, 4',6-diamidino-2-phenylindole.

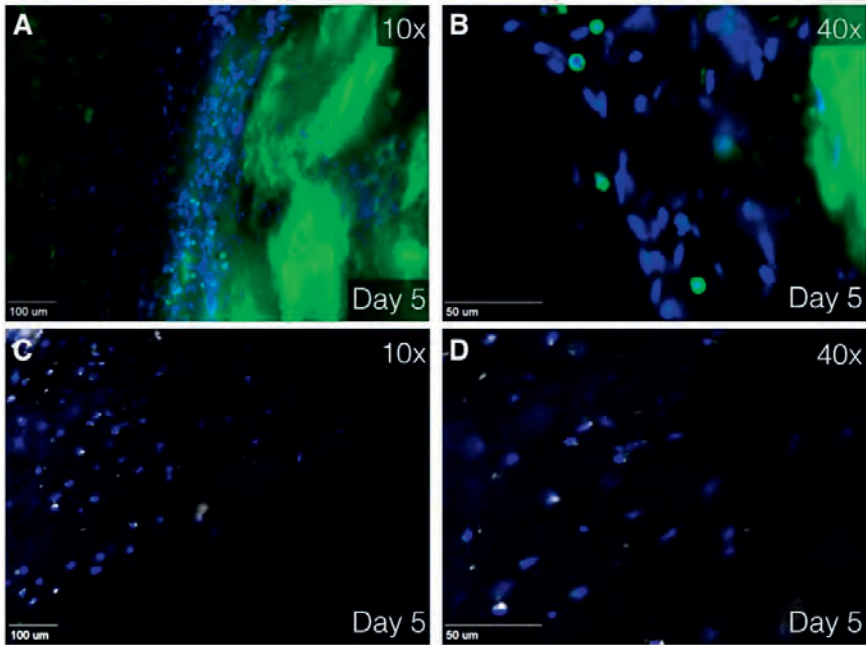


Figure 5. Immunofluorescence image at 10x (A,C) and 40x (B,D) magnification using Zeiss Axiovert 200M Marianas™ Microscope. Human tissue stained with DAPI (blue), CD45 (green, A,B) and CD68 (white, C,D) Green staining at the right side (A,B) is due to unintentional fluorescence of elastin. CD indicates cluster of differentiation and DAPI, 4',6-diamidino-2-phenylindole.

Stitched overview images of the aneurysmal aortic wall show smooth muscle cells (immunostained by smoothelin) in the upper part of the tissues at day 0, 7 and 14 after culturing (figure 6). Phalloidin immunostaining shows all cells of the aortic wall. Thereby, co-staining of both smoothelin and phalloidin indicates the tunica media (mainly consisting of smooth muscle cells), while in underlying tissue only expression of phalloidin is observed, indicating the tunica adventitia (mainly consisting of fibroblasts). This distinction between tunica media and tunica adventitia is observed at day 0, 7 and 14. Fluorescence quantification of smoothelin per nucleus shows a fold increase of 1.6 and 2.3 for day 7 and day 14, respectively. Fluorescence quantification of phalloidin per nucleus shows a fold increase of 4.8 and 5.5 for day 7 and day 14, respectively.

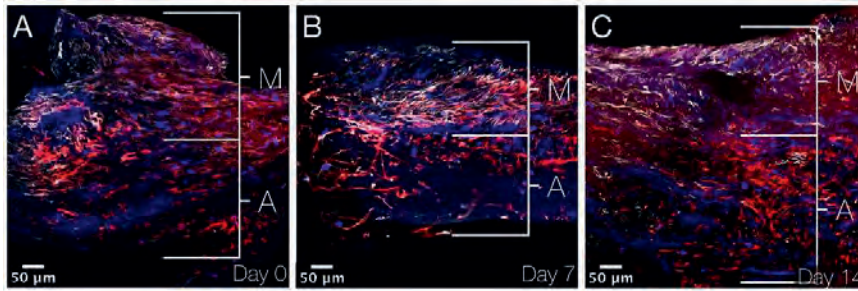


Figure 6. Immunofluorescence images showing aneurysmal aortic wall sections. A-C: XY stitched images at 40x magnification using Nikon A1R confocal microscope on day 0, 7 and 14 after culturing. Smooth muscle cells are immunostained by smoothelin (white), actin (found in practically all eukaryotic cells) by phalloidin (red) and cell nuclei by DAPI (blue). Smooth muscle cells are found in the media and other cells (mainly fibroblasts) in the adventitia. M indicates media; A, adventitia and DAPI, 4',6-diamidino-2-phenylindole.

Outcome of enzymatic digestion of the aortic tissue: individual cell analysis

Tissues of AAA patients (N=2) at day 14 in culture were enzymatically digested. Fluorescent calcein was observed in cytoplasm of enzymatically-digested cells, surrounding the nucleus. Separate cells attached to the slide after enzymatic digestion with collagenase. Different cell shapes and nuclei were observed in the individual cells (figure 7). Digested tissue sections showed viability of 0.75 (in 950.000 cells) in one patient and viability of 0.83 (in 800.000 cells) in the other patient.

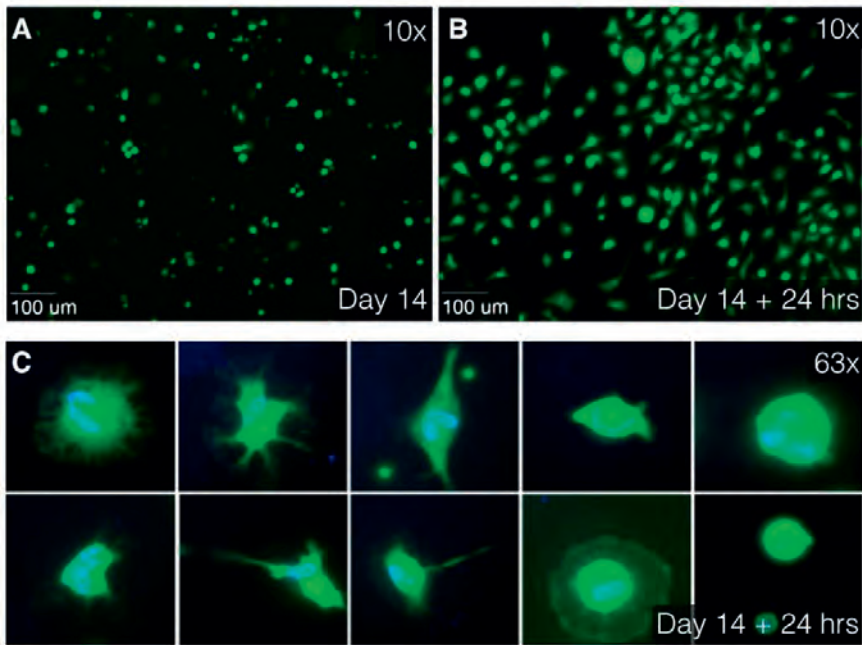


Figure 7. Immunofluorescence images at 10x (A,B) and 63x oil (C) magnification using Zeiss Axiovert 200M Marianas™ Microscope. A: After 14 days of culturing, tissues were enzymatically digested using collagenase. Live separate cells, stained with Calcein AM (green), float as round cells in culture medium. B: After 24 hours of additional culturing, the cells were attached to the slide. C: Different cell type characteristics and differences in cell nuclei are observed in attached cells. Live cytoplasm is stained with Calcein AM (green) and cell nuclei are stained with DAPI (blue). AM indicates acetoxymethyl and DAPI, 4',6-diamidino-2-phenylindole.

RNA expression results of stimulated and non-stimulated aortic tissue sections.

Tissue sections of eight AAA patients were subjected to stimulation with TGF- β for 7 days. Control tissue sections of the same patients were cultured without TGF- β stimulation. Pooled RNA analysis of stimulated tissue sections was relatively related to non-stimulated tissue sections. In this feasibility analysis, elevated relative expression of interleukin 6 (*IL6*), calponin 1 (*CNN1*) and transforming growth factor beta 1 (*TGFB1*) was observed in the pool of TGF- β stimulated tissue sections, while the remainder of the studied genes showed a decrease in expression (figure 8).

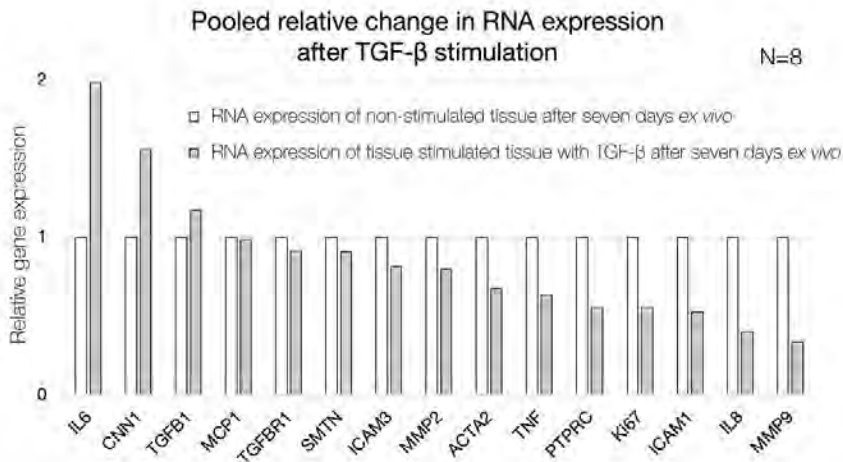


Figure 8. Quantification of gene expression of pooled non-stimulated (white) and TGF- β -stimulated (grey) AAA patient tissue sections after seven days ex vivo. Relative expression is shown as ratio based on non-stimulated tissue sections. IL6 indicates interleukin 6; CNN1, calponin 1; TGF β 1, transforming growth factor beta 1; MCP1, monocyte chemotactic protein 1; TGF β R1, transforming growth factor beta receptor 1; SMTN, smoothelin; ICAM3, intercellular adhesion molecule 3; MMP2, matrix metalloproteinase-2; ACTA2, alpha smooth muscle actin 2; TNF, tumor necrosis factor; PTPRC, protein tyrosine phosphatase, receptor type, C; Ki67, antigen KI-67; ICAM1, intercellular adhesion molecule 1; IL8 (or CXCL8), interleukin 8 and MMP9, matrix metalloproteinase-9.

DISCUSSION

The underlying mechanisms of the development, progression, and rupture of AA are still poorly understood. Prior studies on AA were performed in animal models, fixated human tissue, or isolated human cell cultures. An *in vitro* human model to study pathophysiological processes involved in human AA is lacking. For this reason, we developed a method to obtain vital, ex vivo human vascular tissue. In these cultured aneurysmal and non-aneurysmal vascular specimens, evaluation of viability showed that the larger part of human vascular tissue sections can be kept alive in culture for up to 62 days, while maintaining microstructural organisation of the vascular wall. The live cells were mainly observed in the centre of human tissue. As expected, dead cells were mainly located at the edges of the tissue, which were subjected to cutting trauma. After optimization of the protocol, we attained even higher proportions of surviving tissue.

Interestingly, viability proportion outcomes increased after day 3 compared to day 0. These results are strengthened by not only the significant difference in mean viability of tissue sections between day 0 and day 14, but also between day 5 and day 14.

Cells might go through an early phase of apoptosis due to stress factors arising from physical trauma. Initially, these mechanisms might still be reversible,^{17, 18} with subsequent recovery as of day 3. Another possible explanation for the observed increase of live cells is cell proliferation. This theory is supported by the development and expansion of live cells, observed in the tissues cultured over 60 and 90 days and the growth of new cells at the intimal side.

Another important finding was that we achieved to preserve tissue architecture and infiltrating cells *ex vivo*. In this composition, we found many live smooth muscle cells as the main cell type, but we also observed leucocytes and macrophages involved in the occurrence and aggravation of AA.¹⁹⁻²¹ Based on our composition staining using smoothelin and phalloidin, we provide support for our hypothesis that both tunica media and tunica adventitia are preserved after 14 days. Phalloidin is not specific for fibroblasts. However, phalloidin staining in spindle shaped cells combined with lack of smoothelin staining in the lower layer of the tissue sections, strongly indicates fibroblasts, which are generally known to be in the tunica adventitia. Quantification results showed an increase in fluorescence per nucleus in both smoothelin and phalloidin. This might implicate, that although over time the viability diminishes, the actual cell size, or expression of cell markers increases over time. However, based on the results of one study patient, caution must be applied, as the findings might not be representative for other patients. Unfortunately, the friable tunica intima is frequently damaged due to vibratome sectioning. Preservation of the AA tissue composition in *ex vivo* tissues facilitates the study of cell behaviour and interaction between different cell types, and provides the opportunity to investigate the effects of pharmacological substances on tissue composition or in organ on a chip models.

Analysis of digested tissue sections showed a high viability of single cells, even after treatment with collagenase. Furthermore, again different cell types could be morphologically distinguished, supporting the purpose of this protocol; creating an *ex vivo* arterial environment, which mimics the *in vivo* interaction of different cell types and extracellular matrix. The ability to digest the tissue sections greatly broadens the possibilities of this protocol. For example, FACS, MACS and traction force microscopy are examples of downstream applications that can be performed to expand the characterisation of cells which have been cultured and potentially stimulated in an *ex vivo* aortic microenvironment.²²⁻²⁴

To evaluate the feasibility of live aortic tissue section stimulation and RNA expression analysis, we stimulated aortic vibratome tissue sections with TGF- β , since prior studies have provided paradoxical hypotheses on the role of TGF- β (and thereby stimulation by angiotensin II) in the development and progression of AAA.^{25,26} In this pooled stimulated versus non-stimulated analysis, we found elevated RNA expression of interleukin 6 (*IL6*), calponin 1 (*CNN1*) and transforming growth

factor beta 1 (*TGFB1*), in the stimulated tissue sections. Interestingly, TGF- β has previously been reported to elevate expression of interleukin 6 in different types of fibroblasts, which is in line with our results.^{27,28} Simultaneously, it has been previously observed, that TGF- β overexpression in animal models decreases MMP2, MMP9 and lymphocytes (PTPRC), consistent with our findings in human tissue sections.²⁹ However, with a small sample size and pooled patient data, caution must be applied, as the findings might not be representative for all AAA patients. Future studies with the current method are therefore recommended.

The results of this study meet the need for a new *in vitro* model in which the pathophysiological processes involved in human AA can be studied. In our protocol, sectioning is performed using the vibratome, which has been successfully used for the live cutting and *ex vivo* preservation of cardiac mouse tissues and human salivary gland and tumour sections of breast and parathyroid for a maximum of two weeks.^{14, 30-33} However, this is the first report of a protocol demonstrating over 60 days *ex vivo* viability in vibratome sectioned aortic tissue.

It can be argued that cells with a short lifespan or cells vulnerable to culturing will not survive for a long period in the *ex vivo* tissue sections. Nevertheless, during the first days of culturing we can study the individual cells, interactions between cells and ECM, behavior of immune cells and remodelling of the tissue as seen in other specialist fields using vibratome sections.²⁵ Subsequently, we have successfully stimulated the live tissue sections and the live tissue can serve as a patient specific scaffold on which new cells can be seeded and pharmacological experiments can be performed.

To the best of our knowledge, we are the first to present a method to keep entire aortic tissue sections alive *in vitro*. This method may be applicable also to other human (cardiovascular) tissue. We achieved slicing, preservation, proliferation, and analysis of live aortic tissues for at least 60 days after harvesting. Diverse cell types (including smooth muscle cells and white blood cells) and intracellular characteristics of live tissues were presented. Besides well-known fluorescence imaging, FACS, MACS and traction force microscopy, we are currently investigating the use of these tissue sections in new techniques in which we study elastic properties, aortic wall secretome, and pathways by additional inhibition/stimulation tests. By having established a method for extended *in vitro* preservation of functionally and structurally intact vascular tissue sections, research on the etiopathophysiology of AA and possibly other vascular diseases may have entered a new era.

ACKNOWLEDGEMENTS

We are grateful to all the patients (and their family members) who donated vascular tissue. The authors thank Hilian Nederhoed, Hans Coveliers, Maarten Truijers and Vincent Jongkind for providing the vascular specimens during surgery. We also thank Erik van Tol, Theodorus van Schaik, Harm Ebben, Jacqueline Hoozemans, Josje Evers, Orkun Doganer and Adriaan Beunders for collecting tissue and preparing the experiments. Furthermore, Frank Hoexum, Thomas Koedam, and Dieuwertje van Dam are thanked for their support in retrieving tissue and informed consents, Elisa Meinster is thanked for her support during the experiments, Jeroen Kole is thanked for his assistance in the use of different microscopes and Arie de Boer is thanked for providing abdominal bovine aorta.

AUTHOR CONTRIBUTION STATEMENT

J.P.M. performed the research design, planned the study, performed the experiments, analyzed the data and wrote the manuscript. M.E.G. and N.B. performed the research design, performed the experiments, analyzed the data and revised the manuscript. N.K. performed the experiments. R.J.P.M., G.P., A.M.W., J.K.K., A.W.J.H., advised and assisted on the experiments. B.Z.-D., D.M., H.W.M.N. advised and assisted on the experiments and revised the manuscript. W.W. and J.D.B. performed the research design, advised and assisted on the experiments and revised the manuscript. K.K.Y. performed the research design, planned the study, performed the experiments, analyzed the data and revised the manuscript. All authors reviewed the manuscript.

COMPETING FINANCIAL INTERESTS

The research leading to present results has received funding from Atrium, Endologix, WL Gore & associates, Bracco, Medac, BTG, Cook and institutional grants ICAR-AIO, ACS MD-postdoc, VUmc fund and Dutch national van Walree fund. Funding was received by K.K.Y. (all funding stated above) and J.D.B. (Cook). The authors declare no non-financial competing interests.

REFERENCES

1. Dua, A., Kuy, S., Lee, C. J., Upchurch, G. R. & Desai, S. S. Epidemiology of aortic aneurysm repair in the United States from 2000 to 2010. *J. Vasc. Surg.* 59, 1512–1517 (2014).
2. Sidloff, D. et al. Aneurysm global epidemiology study public health measures can further reduce abdominal aortic aneurysm mortality. *Circulation* 129, 747–753 (2014).
3. Lozano, R. et al. Global and regional mortality from 235 causes of death for 20 age groups in 1990 and 2010: A systematic analysis for the Global Burden of Disease Study 2010. *Lancet* 380, 2095–2128 (2012).
4. Davis, F. M., Rateri, D. L. & Daugherty, A. Mechanisms of aortic aneurysm formation: translating preclinical studies into clinical therapies. *Heart (British Cardiac Society)* 100, 1498–1505 (2014).
5. Hellenthal, F. A. M. V. I., Buurman, W. A., Wodzig, W. K. W. H. & Schurink, G. W. H. Biomarkers of AAA progression. Part 1: Extracellular matrix degeneration. *Nature Reviews Cardiology* 6, 464–474 (2009).
6. Hellenthal, F. A. M. V. I., Buurman, W. A., Wodzig, W. K. W. H. & Schurink, G. W. H. Biomarkers of abdominal aortic aneurysm progression. Part 2: Inflammation. *Nat. Rev. Cardiol.* 6, 543–552 (2009).
7. Cherifi, H. et al. Comparative study of abdominal and thoracic aortic aneurysms: their pathogenesis and a gingival fibroblasts-based ex vivo treatment. *Springerplus* 4, (2015).
8. Wang, Q. et al. Monocyte Chemoattractant Protein-1 (MCP-1) regulates macrophage cytotoxicity in abdominal aortic aneurysm. *PLoS One* 9, (2014).
9. Airhart, N. et al. Smooth muscle cells from abdominal aortic aneurysms are unique and can independently and synergistically degrade insoluble elastin. *J. Vasc. Surg.* 60, 1033–1042.e5 (2014).
10. Xiong, F. et al. Inhibition of AAA in a rat model by treatment with ACEI perindopril. *J. Surg. Res.* 189, 166–173 (2014).
11. Liu, Z. et al. Murine abdominal aortic aneurysm model by orthotopic allograft transplantation of elastase-treated abdominal aorta. *J. Vasc. Surg.* 62, 1607–1614.e2 (2015).
12. Kloster, B. O., Lund, L. & Lindholt, J. S. Inhibition of early AAA formation by aortic intraluminal pentagalloyl glucose (PGG) infusion in a novel porcine AAA model. *Ann. Med. Surg.* 7, 65–70 (2016).
13. Sasai, Y. Cytosystems dynamics in self-organization of tissue architecture. *Nature* 493, 318–326 (2013).
14. Pillekamp, F. et al. Establishment and characterization of a mouse embryonic heart slice preparation. *Cell. Physiol. Biochem.* 16, 127–132 (2005).

15. Ghosh, A., Pechota, L. V. T. A., Upchurch, G. R. & Eliason, J. L. Cross-talk between macrophages, smooth muscle cells, and endothelial cells in response to cigarette smoke: the effects on MMP2 and 9. *Mol. Cell. Biochem.* 410, 75–84 (2015).
16. Vorkapic, E., Lundberg, A. M., Mäyränpää, M. I., Eriksson, P. & Wågsäter, D. TRIF adaptor signaling is important in abdominal aortic aneurysm formation. *Atherosclerosis* 241, 561–568 (2015).
17. Seye, C. I. et al. 7-Ketocholesterol induces reversible cytochrome c release in smooth muscle cells in absence of mitochondrial swelling. *Cardiovasc. Res.* 64, 144–153 (2004).
18. Kumar, V., Abbas, A. K. & Aster, J. C. *Robbins Basic Pathology Ninth Edition*. Elsevier Saunders (2013).
19. Middleton, R. K. et al. The pro-inflammatory and chemotactic cytokine microenvironment of the abdominal aortic aneurysm wall: A protein array study. *J. Vasc. Surg.* 45, 574–580 (2007).
20. Samadzadeh, K. M. et al. Monocyte activity is linked with abdominal aortic aneurysm diameter. *J. Surg. Res.* 190, 328–334 (2014).
21. Tsuruda, T. et al. Adventitial mast cells contribute to pathogenesis in the progression of abdominal aortic aneurysm. *Circ. Res.* 102, 1368–1377 (2008).
22. Kennedy, E. et al. Embryonic rat vascular smooth muscle cells revisited - A model for neonatal, neointimal SMC or differentiated vascular stem cells? *Vasc. Cell* 6, (2014).
23. Levenberg, S., Ferreira, L. S., Chen-Konak, L., Kraehenbuehl, T. P. & Langer, R. Isolation, differentiation and characterization of vascular cells derived from human embryonic stem cells. *Nat. Protoc.* 5, 1115–1126 (2010).
24. Adhikari, N. et al. Guidelines for the Isolation and Characterization of Murine Vascular Smooth Muscle Cells. A Report from the International Society of Cardiovascular Translational Research. *J. Cardiovasc. Transl. Res.* 8, 158–163 (2015).
25. Lin, F. & Yang, X. TGF- β signaling in aortic aneurysm: Another round of controversy. *J. Genet. Genomics* 37, 583–591 (2010).
26. Chen, X., Lu, H., Rateri, D. L., Cassis, L. A. & Daugherty, A. Conundrum of angiotensin II and TGF- β interactions in aortic aneurysms. *Current Opinion in Pharmacology* 13, 180–185 (2013).
27. Seong, G. J. et al. TGF- β -induced interleukin-6 participates in transdifferentiation of human Tenon's fibroblasts to myofibroblasts. *Mol. Vis.* 15, 2123–2128 (2009).
28. Eickelberg, O. et al. Transforming growth factor- β 1 induces interleukin-6 expression via activating protein-1 consisting of JunD homodimers in primary human lung fibroblasts. *J. Biol. Chem.* 274, 12933–12938 (1999).
29. Dai, J. et al. Overexpression of transforming growth factor- β 1 stabilizes already-formed aortic aneurysms: A first approach to induction of functional healing by endovascular gene therapy. *Circulation* 112, 1008–1015 (2005).

30. Riegler, J., Gillich, A., Shen, Q., Gold, J. D. & Wu, J. C. Cardiac tissue slice transplantation as a model to assess tissue-engineered graft thickness, survival, and function. *Circulation* 130, S77–S86 (2014).
31. Su, X. et al. Three-dimensional organotypic culture of human salivary glands: the slice culture model. *Oral Dis.* 22, 639–648 (2016).
32. Holliday, D. L. et al. The practicalities of using tissue slices as preclinical organotypic breast cancer models. *J. Clin. Pathol.* 66, 253–255 (2013).
33. Koh, J., Hogue, J. A. & Sosa, J. A. A novel ex vivo method for visualizing live-cell calcium response behavior in intact human tumors. *PLoS One* 11, (2016).

An in vitro method to keep human aortic tissue sections functionally and structurally intact.

Supplementary information.

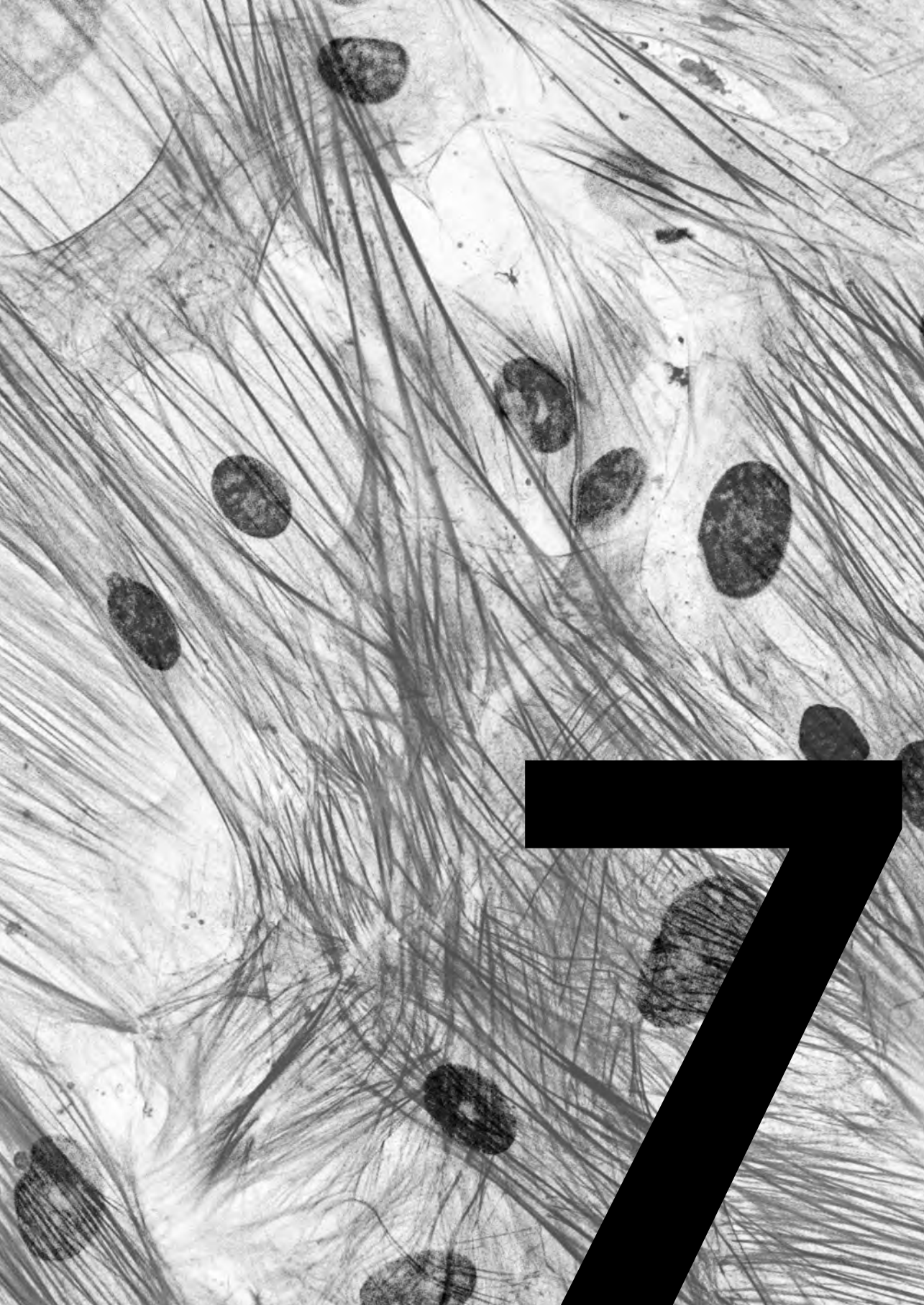
Scientific reports; 2018; 8(1), 8094.

Jorn P. Meekel, Menno E. Groeneveld, [Natalija Bogunovic](#), Niels Keekstra, René J.P. Musters, Behrouz Zandieh-Doulabi, Gerard Pals, Dimitra Micha, Hans W.M. Niessen, Arno M. Wiersema, Jur K. Kievit, Arjan W.J. Hoksbergen, Willem Wisselink, Jan D. Blankensteijn, Kak K. Yeung

Supplementary Table S1. RefSeq codes and primer sequences

RefSeq code and forward and reverse primer sequences per corresponding gene. RefSeq indicates NCBI Reference Sequence Database code.

Gene name	RefSeq	Forward and reverse primer sequence
<i>YWHAZ</i>	NM_145690	GATGAAGCCATTGCTGAACTTG CTATTTGTGGGACAGCATGGA
<i>IL6</i>	NM_000600	ACAGCCACTCACCTCTTCA ACCAGGCAAGTCTCCTCAT
<i>CNN1</i>	NM_001308341	GCCCAGAAGTATGACCACCA TGATGAAGTTGCCGATGTTC
<i>TGFB1</i>	NM_000660	CCGACTACTACGCCAAGGAG GGTATCGCCAGGAATTGTTG
<i>MCP1</i>	NM_002982	CACTCTCGCCTCCAGCATGA ATCTCCTTGGCCACAATGGT
<i>TGFB1</i>	NM_001306210	ACAACCGCACTGTCAATCAC TCTCCAAACTTCTCCAAATCG
<i>SMTN</i>	NM_001207018	TGGAGGAATTGACTGCACTG GAAACCTCTGCCTGCTGTTG
<i>ICAM3</i>	NM_001320605	TGTTTGAAGGAAGGCTCCAG AGTAACACCGCCACGAAGAC
<i>MMP2</i>	NM_004530	CCGTGGTGAGATCTTCTTCTTC GCTGGTCAGTGGCTTGGGGTA
<i>ACTA2</i>	NM_001141945	ACTGGGACGACATGGAAAAG CATACATGGCTGGGACATTG
<i>TNF</i>	NM_000594	TCAACCTCCTCTCTGCCATC AGTAGACCTGCCCAGACTCG
<i>PTPRC</i>	NM_080921	AGTATCCCCGGA CTCTTTGG AGGGTTGAGTTTGCATTGG
<i>Ki67</i>	NM_002417	AGCACCAGAGGAAATTGTGG TTTTCAGGGACCGAGTCTTG
<i>ICAM1</i>	NM_000201	GGCTGGAGCTGTTTGAGAAC AGGAGTCGTTGCCATAGGTG
<i>IL8 (CXCL8)</i>	NM_000584	GTGTGAAGGTGCAGTTTTC CCTTGGGGTCCAGACAGAG
<i>MMP9</i>	NM_004994	ACAGGCAGCTGGCAGAGGA CGCGGCAAGTCTTCCGAGTA



Bioengineered Patient-Specific 3D Vascular Scaffolds for the Investigation of Smooth Muscle Cell and Extracellular Matrix Dysfunction in Aortic Aneurysms.

Natalija Bogunovic, Jorn P. Meekel, Jisca Majolée, Marije Hekhuis,
Jakob Pyszkowski, Stefan Jockenhövel, Magnus Kruse,
Elise Rieseboos, Dimitra Micha, Jan D. Blankensteijn,
Peter L. Hordijk, Samaneh Ghazanfari*, Kak K. Yeung*

* These authors have contributed equally.

ABSTRACT

Abdominal aortic aneurysms (AAA) are associated with overall high mortality in case of rupture. The pathophysiology is unclear, but smooth muscle cells (SMC) dysfunction and extracellular matrix (ECM) degradation have been proposed as underlying causes. We aim to create a patient-specific 3D vascular model for translational studies of SMC-ECM interactions and their role in AAA pathophysiology.

SMC isolated from the aortic wall of controls and AAA patients are seeded on electrospun poly-lactide-co-glycolide scaffolds and cultured for five weeks, after which endothelial cells are added. Cell morphology, orientation, mechanical properties and ECM production are quantified for validation and comparison between controls and patients.

We show that cultured SMC proliferated into multiple layers after five weeks in culture and produced ECM proteins. Endothelial cells attach to multilayered SMC, mimicking layer interactions. The bioengineered scaffolds exhibit visco-elastic properties comparable to biological vessels; cytoskeletal organization increases during the five weeks in culture; increased cytoskeletal alignment and decreased ECM production indicate different organization of AAA patients' cells compared to control.

In conclusion, our 3D bioengineered scaffolds are robust, patient-specific models of SMC-endothelial cell organization and ECM production. We demonstrate a valuable preclinical model of AAA with applications in both translational research and therapeutic developments.

INTRODUCTION

Abdominal aortic aneurysms (AAA) are pathological dilations of the aorta. AAA typically remain asymptomatic until the aortic wall is weakened to the extent of rupture, in which case AAA develops into a surgical emergency associated with a mortality rate of up to 90%.^[1] The pathophysiology behind these severe alterations in the aortic wall remains elusive.^[2] Earlier studies implicate defects in medial smooth muscle cells (SMC)^[3-6] and extracellular matrix (ECM) remodeling^[7-9] as key factors in the pathogenesis. Given that the exact causal process is unclear, the only available treatment for AAA is invasive surgical repair.

The elastic aortic medial layer is composed of circumferentially oriented SMC, ECM fibers and microfibrils^[10]. As the predominant cell type in the media, SMC are the main producers of ECM components^[7, 8]. ECM remodeling in aortic aneurysms is characterized by degradation of fibers and the elastic laminae.^[7] Due to the action of proteolytic enzymes, such as matrix metalloproteinases (MMPs)^[7, 11] and altered ECM protein secretion by SMC^[12], the pathological change surmounts the productive capabilities of SMC and the overall ECM quantity is decreased.^[7]

SMC and the ECM are functionally linked through the mechanotransduction complex consisting of extracellular microfibrils (largely fibrillin-1), which connect with intracellular actomyosin filaments through heterodimeric transmembrane complexes (integrins).^[3, 13, 14] Disruption of the components of the mechanotransduction complex has severe consequences on the strength of the aortic wall, increasing its tendency to dilate and eventually rupture^[13]. Therefore, patients with an AA show divergent force transmission, tensile strengths and stiffness of the whole aorta.^[15]

Research and therapy development are hindered by the difficulty of recreating the complex micro-environment of the aorta and constructing a relevant disease model. To investigate the pathophysiology of vascular diseases on cellular level, the use of vascular scaffolds is on the rise.^[16, 17] In addition, vascular scaffolds are being developed for therapeutic use to replace prosthetic vascular grafts.^[18-20] Significant steps have been made in the development of bioengineered grafts mimicking small vessels with biodegradable scaffolds^[21, 22] and decellularized patient materials.^[23] However, bioengineered grafts to study large vessel diseases such as AAA pathophysiology are not available.

We aspired to create 3D cell cultures on patterned scaffolds, seeded with patient-specific AAA cells. These novel 3D cultures were compared to existing 2D models to demonstrate increased robustness and complexity. Mechanical properties, fiber orientation and ECM secretion were assessed to characterize the scaffolds and compare them to biological vessels. Scaffolds seeded with healthy SMC were compared to scaffolds seeded with SMC of AAA patients to potentially uncover AAA-related molecular defects. Our preclinical model provides unique insight into the

patient-specific cellular dysfunctions which contribute to the progressive pathological dilation of the aortic wall.

MATERIALS AND METHODS

Patient population

AAA biopsies were collected during open aneurysm repair in Amsterdam University Medical Centers, location VU Medical Center (Amsterdam, the Netherlands). Control biopsies were collected from non-dilated aortas of heart-beating donors during organ harvesting procedures for post-mortem renal transplantation. All patients signed an informed consent to participate in the study. Material from control biopsies was collected anonymously with only age and gender available. All material was collected in accordance with regulations of the WMA Declaration of Helsinki and institutional guidelines of the Medical Ethical Committee of the Amsterdam UMC, location VU Medical Center. Patient and control clinical information is shown in **Table 1**.

Aortic biopsy explant protocol

Primary aortic SMC were isolated from aortic biopsies of healthy controls and AAA patients according to our previously described protocol^[24]. The aortic medial layer was isolated from the biopsies and using explant protocol, patient-specific cell lines were obtained within a month. SMC of controls (n=7) and AAA-patients (n=8) were used in the experiments. All SMC cell lines were cultured in 231 medium (Thermo Fisher Scientific, Waltham, MA, USA), supplemented with Smooth Muscle Growth Supplement (Thermo Fisher Scientific), and 100 units/ml penicillin and 100 µg/ml streptomycin (Thermo Fischer Scientific) to provide optimal vascular SMC growth. Cells were cultured in a humidified incubator at 37 °C, 5% CO₂.

Table 1. Clinical characteristics of controls and AAA patients. Age and gender are shown for all controls and patients. Aneurysm diameter and indication of rupture are shown for the patients.

Cell line	Age (years)	Gender	Aneurysm diameter (cm)	Rupture
<i>Control 1</i>	69	M	N/A	N/A
<i>Control 2</i>	59	M	N/A	N/A
<i>Control 3</i>	44	F	N/A	N/A
<i>Control 4</i>	50	M	N/A	N/A
<i>Control 5</i>	68	M	N/A	N/A
<i>Control 6</i>	59	M	N/A	N/A
<i>Control 7</i>	50	M	N/A	N/A
<i>AAA patient 1</i>	68	M	55	No
<i>AAA patient 2</i>	64	M	63	No
<i>AAA patient 3</i>	75	F	70	Yes
<i>AAA patient 4</i>	63	F	63	No
<i>AAA patient 5</i>	74	F	55	No
<i>AAA patient 6</i>	74	M	100	Yes
<i>AAA patient 7</i>	60	M	56	No
<i>AAA patient 8</i>	65	M	94	No

Fabrication of scaffolds

The membranes were prepared by electrospinning process, using a Fluidnatek LE500 (Bioinicia SL, Valencia, Spain provided by IuL Biosystems, Königwinter, Germany). Fibers made of poly-lactide-co-glycolide (PLGA; Purasorb PLG 8523, Corbion, Gorinchem, Netherlands), a biocompatible and biodegradable polymer^[25], were spun from a solution with a mass concentration of 5 wt% PLGA in 75 % chloroform (CHCl₃, Carl Roth GmbH, Karlsruhe, Germany) and 25 % methanol (MeOH, neoLab Migge Laborbedarf - Vertriebs GmbH, Heidelberg, Germany). All chemicals were used as delivered, without further purification^[26].

PLGA was dried in a vacuum at 40 °C for 12 h before dissolution under continuous stirring for 12 h in the mentioned solvents. In preparation of the spinning process, the spinning solution was filled into a 5 mL syringe (B. Braun Melsungen AG, Melsungen, Germany), which was connected to a multi nozzle spinneret with 24 nozzles. The polymer solution was extruded using the syringe pump at a flow rate of

25 mL/h through a hollow needle with a diameter of 0.4 mm (B. Braun Melsungen AG, Melsungen, Germany). At a voltage of ± 25 kV, the polymer solution is stretched into fibers. The fibers are collected on a rotating mandrel ($\varnothing = 200$ mm) at a rotational speed of 100 rpm. The nonwoven thickness was 250-300 μm . The spinning process was carried out at 23 °C and a humidity of 30 % R.H. The morphology of the scaffold was examined using scanning electron microscopy (SEM; Leo 1450 VP, Zeiss, Germany; **Figure 1a**).

The pore size distribution of three different samples was measured with a capillary flow pore size meter (PSM 165, Topas GmbH, Dresden, Germany). An adapter with a flow cross-section of 2.01 cm^2 and a test fluid (Topor, Topas GmbH, Dresden, Germany) with a surface tension of 16.0 mN/m were used^[26].

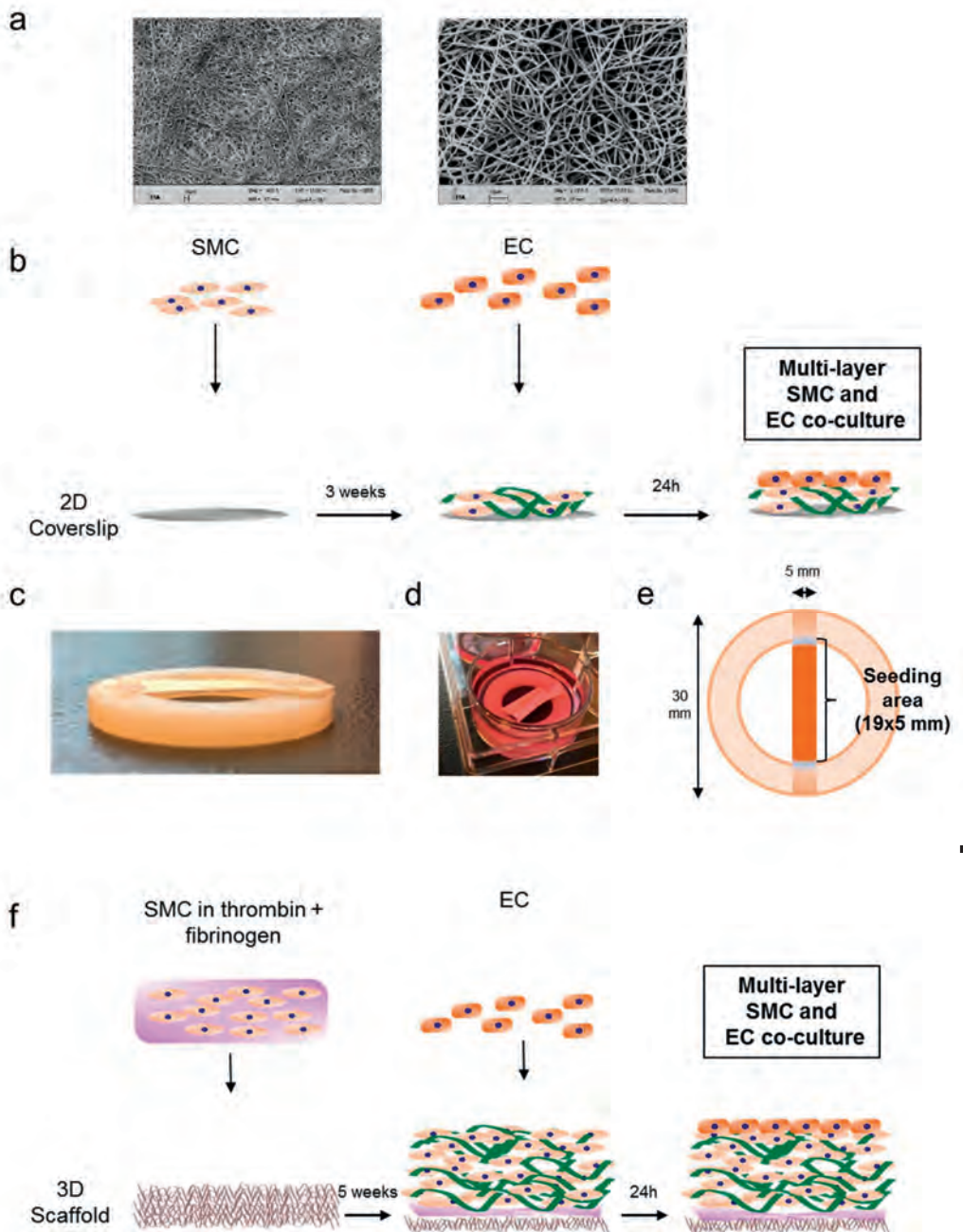


Figure 1. 2D and 3D SMC cultures. SEM images of 3D electrospun, patterned poly-lactide-co-glycolide scaffold (left panel: 500x magnification; right panel: 2000x magnification; scale bar: 10µm). b) Schematic of the 2D co-culture experiment with SMC and EC seeded on glass coverslips during a three week time course. c) PLGA scaffold ribbon mounted on the silicone ring. d) 3D scaffold incubated in cell culture medium. e) Schematic representation of centralized SMC seeding area on the 3D scaffold (19 x 5 mm). f) Schematic of the 3D co-culture experiment with SMC and EC seeded on PLGA scaffolds during a five week time course.

Seeding SMC and EC in 2D cultures

SMC of controls and AAA patients were seeded on round glass coverslips in 6 well plates (13mm,#1; Thermo Fischer Scientific) in a seeding density of 100,000 cells/well in complete SMC medium, as depicted in Figure 1b. Medium was refreshed two times per week during the three weeks of culturing. Samples were fixated in 4% paraformaldehyde after one, two and three weeks and consecutively immunostained for further qualitative and quantitative analysis.

After three weeks of culturing, endothelial cells (EC; Human Umbilical Vein Endothelial Cells (HUVEC); Lonza, Basel, Switzerland) were added on top of the established multilayer of SMC and ECM (Figure 1b). Two days prior to EC seeding, complete 231 SMC culture medium was exchanged for endothelial cell medium (Sanbio, Uden, the Netherlands) to ensure SMC adjustment to a different culture medium. Afterwards, 300,000 EC were seeded per well on top of the SMC. Medium was aspirated from the wells and EC were carefully pipetted on top of the seeding surface in complete endothelial cell medium. Medium was refreshed the next day. Two days after seeding, samples were fixated in 4% paraformaldehyde and immunostained for the morphological studies.

Seeding SMC and EC in 3D cultures on scaffolds

As cultures on plastic or glass can be maintained for a shorter period of time, due to cell detachment in overgrown layers, patterned scaffolds employed as an advanced alternative. The PLGA scaffold sheet was UV sterilized on each side for 30 min and cut into ribbons of 30x5 mm in the direction parallel to the scaffold patterning. Nylon rings (OD: 30 mm, ID: 19 mm, Praxis, Diemen, the Netherlands) were sterilized in ethanol overnight and subsequently using UV light for 30min on each side. The ribbons were mounted onto the nylon rings using super glue (Secondelijm, Pattex, Henkel, Amsterdam, the Netherlands; Figure 1c). Upon gluing, the scaffolds were dried at room temperature for 24h and then UV sterilized. Consequently, the scaffolds were incubated in complete medium overnight to dampen them medium prior to cell seeding (Figure 1d).

The next day, complete medium was removed from the scaffolds. Powder thrombin (Sigma-Aldrich) was diluted in non-supplemented medium into a final concentration

of 10 IU/ml, filter sterilized and kept on ice prior to seeding. Powder fibrinogen (Sigma) was diluted in non-supplemented medium to a final concentration of 10 mg/ml, filter sterilized and kept on ice prior to seeding. SMC of controls and AAA patients were counted and centrifuged. Per scaffold, 450,000 cells were resuspended in 20 μ l of ice-cold thrombin solution. In the following step, 20 μ l fibrinogen was added to the mixture. Cells were then seeded onto the scaffold ribbons in the inner ring centralized seeding area (19x5 mm; Figure 1e). After roughly 30s, the mixture rigidified due to thrombin and fibrinogen reaction ensuring that the cells remain attached in the seeding area (Figure 1f). The scaffolds were placed in an incubator for 30 minutes, allowing further gel stiffening and cell attachment upon which complete medium was added. Medium was refreshed 2 times per week during five weeks of culturing. Samples were fixated in 4% paraformaldehyde after one, three and five weeks and consecutively immunostained for further qualitative and quantitative analysis.

After five weeks of culturing, EC were added on top of the multilayer of SMC and ECM (Figure 1f). For 2D and 3D cultures alike, SMC were incubated in EC medium for 2 days prior to seeding. EC were pipetted on top of the seeding surface and medium was refreshed the next day. Two days after seeding, samples were fixated in 4% paraformaldehyde and immunostained for the morphological studies.

Immunostaining and confocal microscopy

After fixation in 4% paraformaldehyde, samples were washed 3x with PBS-Tween (PBST) and the cells were subsequently permeabilized for 10 min in 0.2% Triton in PBST. Samples were incubated in blocking solution, consisting of 1% BSA solution in PBST for 1h at room temperature. Primary rabbit monoclonal antibody against VE-cadherin was used to visualize the endothelial barrier (D87F2, Cell Signaling, Danvers, MA, USA) and primary mouse monoclonal antibody against fibrillin-1 was used to visualize the fibrillin-1 fibers in the ECM (MAB2502, Merck, Kenilworth, NJ, USA). Both primary antibodies were incubated overnight at 4 °C in 1:400 dilution. Samples were washed 5x in PBST. Secondary antibodies Alexa Fluor® 488 Goat Anti-Mouse (IgG) and Alexa Fluor® 546 Goat Anti-Rabbit (IgG) (1:100; Thermo Fisher Scientific), DAPI to label cell nuclei (1:200; Thermo Fisher Scientific), and Alexa Fluor 647 Phalloidin to label F-actin (1:200; Thermo Fisher Scientific), were incubated for 1h at room temperature in the dark. Scaffold samples were sealed with Mowiol mounting medium containing Diazabicyclo-octane (Dabco, Sigma-Aldrich) in glass bottom 35mm dishes. Coverslips were sealed with Mowiol on glass slides. Images were acquired using the Nikon A1R (Nikon, Tokyo, Japan) microscope and the corresponding Nis-Elements C Software (Nikon). Representative images were taken from samples fixated at day 1, week 1, 2 and 3 for 2D cultures, and week 1, 3 and 5 for 3D cultures in different experiments. Representative images were analyzed

and separate channel images were created using Fiji (v.152, National Institutes of Health, Bethesda, MD, USA)^[27].

Measuring scaffold stiffness using nanoindentation

Micromechanical properties of scaffolds without cells and scaffolds seeded with control SMC were measured after five weeks. Scaffolds in complete cell culture medium were measured with the Piuma Nanoindenter instrument (Optics11, Amsterdam, the Netherlands). The surface of the scaffold was indented with a spherical indentation probe with a spring constant and tip radius of approximately 0.04 N/m and 61 μm , respectively (Figure 3a). The indentation probe is part of a unique opto-mechanical ferrule-top cantilever force transducer, operated by a z-axis piezoelectric motor^[28]. A controlled piezo displacement rate of 5 $\mu\text{m/s}$ was set to move the glass tip into the sample surface. The resulting force was measured through cantilever displacement.

The elastic properties of the scaffolds were given by the effective (or reduced, plain strain) Young's Modulus, which does not include any assumption for the Poisson ratio of the scaffolds. The effective Young's Modulus was modelled within the linear elastic regime, up to an indentation depth of 1 μm for the scaffolds without cells, and 2 μm for the cell-containing scaffolds. For both samples, 25 measurements were taken from a grid scan with an area of 400 $\mu\text{m} \times 400 \mu\text{m}$. Hertz contact model was applied to the loading curve, as suggested for measuring viscoelastic materials, and denotes the effective Young's Modulus as shown in **Equation 1**, with R as indenter tip radius, h as indentation depth and P as load.^[29, 30]

Equation 1:

$$E_{eff} = \frac{3}{\sqrt{4PR} * \sqrt[3/2]{h}}$$

SMC F-actin alignment in multilayers

Organization of the F-actin fibers was characterized by anisotropy measurements using FibrilTool plug-in in Fiji ^[31]. Values of the anisotropy index range from zero to one, where parallel lines result in an anisotropy index close to one, and structures lacking parallel organization result in values closer to zero. F-actin alignment was measured in acquired images of SMC derived from controls and AAA patients in 2D and 3D cultures. Following the published protocol, X-Y fields of view were marked as regions of interest (ROI). Using FibrilTool, anisotropy was quantified within these ROI. For 2D cultures, anisotropy was measured on single focal plane images in two control and two patient cell lines. For 3D cultures seeded on scaffolds, anisotropy

was measured on 15 optical slices throughout the Z stack with a step size 0.5 μm in two control and two patient cell lines.

Fibrilin-1 production by SMC

Fibrilin-1 production by SMC was semi-quantitatively assessed using the acquired immunostaining images. The area of fibrilin-1 fibers in each field of view ROI was masked by adjusting the threshold for the 488-fluorescent channel. Acquired area values in the ROI were normalized by dividing the area value by the number of nuclei per image. Fibrilin-1 production was compared between two control and two patient cell lines in 2D cultures after one, two and three weeks and in 3D cultures after five weeks.

Mechanical properties and tensile strength

Tensile stress and elastic modulus were compared between control ($n=5$) and patient ($n=5$) cell lines in 3D scaffolds after 5 weeks of cultures. Means of three individual scaffolds per cell line were used to calculate the final data points. Uniaxial tensile tests on the samples were performed using a mechanical tester (Zwick, Ulm, Germany) at a strain rate of 3 mm/min with a 10 N load cell. The dimensions of the samples were measured using a digital caliper before each test. Ultimate tensile stress and the elastic modulus (E) were calculated from the stress-strain curve of each measurement. The elastic modulus was determined via linear regression of the slope of the curve.

Statistical Analysis

Data were analyzed with SPSS (v22.0, IBM, Armonk, NY, USA). Two groups were compared using the non-parametric Mann-Whitney U test and multiple groups were compared using Kruskal-Wallis test and using the Mann-Whitney U test for post-hoc analysis. Correlations were tested with Spearman's Rank correlations. Multiple related samples were tested with Friedman's ANOVA. Data are presented as box plots with median and range. Tests were considered statistically significant at $p<0.05$. Boxplots and scatterplots were made using GraphPad Prism7 (GraphPad software Inc., San Diego, CA, USA). If the number of samples was low, individual data was presented.

RESULTS

Morphological characterization of 2D and 3D co-cultures

As shown in **Figure 2a**, SMC seeded in 2D cultures on glass coverslips adhered throughout the surface of the glass coverslip after one week. The cells formed a semi-confluent monolayer and occasional cell-cell contact. SMC continued to proliferate, as was observed after two and three weeks of culturing, noticeable by the formation of multiple layers of SMC.

SMC were seeded on the scaffolds to establish a vascular system of increased complexity, as described in the methods. Representative confocal images of SMC proliferation in three time-points were shown in Figure 2b; each image represents an optical slice extracted from a Z-stack. After one week in culture, SMC growth on the scaffold was observed in the form of multiple sparse layers on the scaffold. The observed organization hints the initial formation of a multi-layer mimicking the media. After three weeks, SMC multi-layer organization developed further into confluent monolayers stacked on top of each other. The same trend can be observed after five weeks of culturing.

EC were seeded on top of the multi-layered SMC in 2D and 3D cultures after three and five weeks, respectively. As depicted in Figure 2c, EC form a confluent monolayer on the SMC 2D culture, characterized by VE-cadherin staining. Immunofluorescent staining revealed the presence of the characteristic endothelial barrier with intercellular junctions. EC seeded on 3D scaffolds, and thus more layers of SMC, exhibit diverse morphologies in different regions. In some regions of the scaffolds, EC grew on top of the SMC multilayers, forming tube-like structures. These structures were partially overgrown by other layers of SMC forming on top of them (Figure 2d). Oppositely, some regions on the scaffolds were distinguishable by a confluent monolayer of EC representing the endothelial barrier (Figure 2e).



c

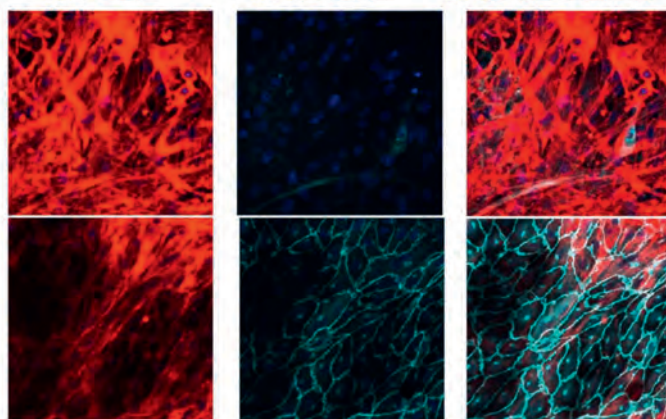
2D
Coverslip

Week 3

DAPI/F-actin

DAPI/VE-cadherin

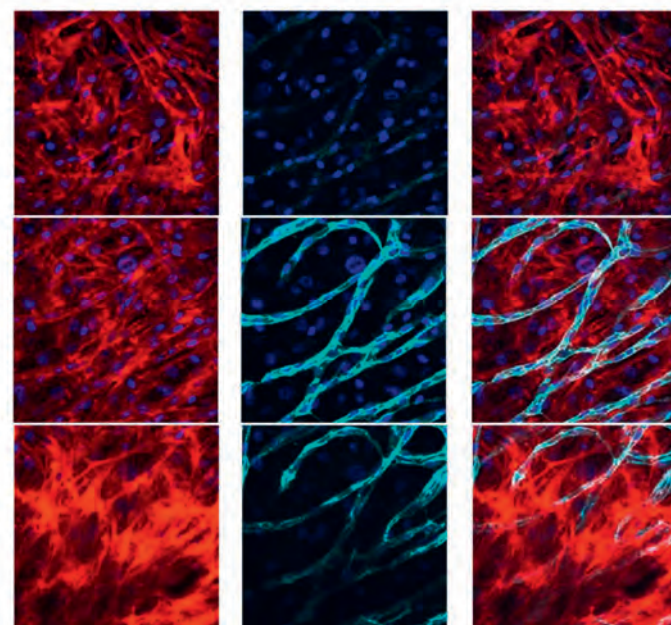
DAPI/F-actin/VE-cadherin



d

3D
Scaffold

Week 5



e

3D
Scaffold

Week 5

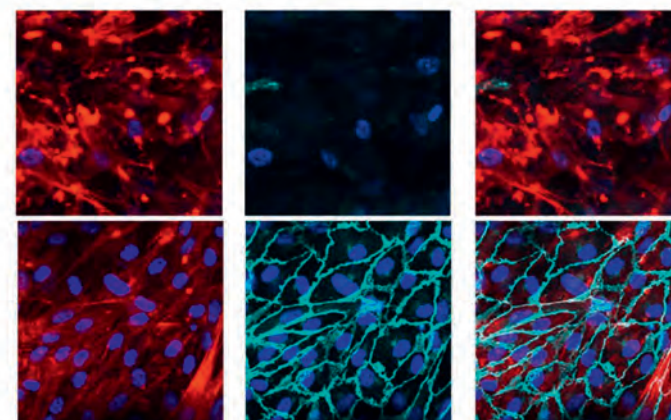


Figure 2. Formation of SMC multilayers and EC layers in 2D and 3D cultures. Cells were immunostained for F-actin (red) and DAPI (blue) and EC were stained for VE-cadherin (cyan). a) Representative images of SMC proliferation on glass coverslips over time (Left to right: one, two and three weeks after seeding). b) Representative images of SMC proliferation on 3D scaffold in time (Left to right: one, three and five weeks after seeding). c) Representative images of a co-culture of multilayered SMC and a monolayer of EC on top of them, seeded on a glass coverslip (middle and top layer, merge F-actin and DAPI, VE-Cadherin and DAPI and merge tricolor). d) Representative images of a co-culture of multilayered SMC and EC forming tube-like structures on a 3D scaffold (two middle layers and top layer, merge F-actin and DAPI, VE-Cadherin and DAPI and merge tricolor). e) Representative images of a co-culture of multilayered SMC and a monolayer of EC on top of them, seeded on a 3D scaffold (middle and top layer, merge F-actin and DAPI, VE-Cadherin and DAPI and merge tricolor). Scale bar: 50µm.

Stiffness and visco-elastic behavior

Micromechanical properties of scaffolds without cells and scaffolds seeded with SMC were measured using nano-indentation. Visco-elastic properties of the scaffold were assessed by applying longer constant pressure with the tip of the nano-indenter, as depicted on the schematic in **Figure 3a**. The mechanical load of the sample decreased in time under constant pressure, exhibiting visco-elastic behavior, characteristic for biological tissues^[32] (Figure 3b; stress-relaxation curve). Furthermore, scaffold stiffness was assessed by indenting samples with and without SMC, as depicted in the schematic in Figure 3c. Median stiffness of the scaffold without cells (19.8, range 10.5-54.3 kPa) was almost 20 fold increased compared to the median stiffness of the scaffold seeded with SMC (1.3 kPa; range 0.5-2.1 kPa; $p=0.004$, Figure 3d). Unlike the stiffness of the scaffold without cells, the stiffness of the scaffold with SMC was in the range of stiffness values of normal biological tissues^[33].

Mechanical properties of the scaffolds

Mechanical properties of the scaffolds were assessed after five weeks of culturing SMC on the 3D scaffold and ultimate tensile stress was compared between samples seeded with control and patient SMC. Similar tensile stress was observed in the patient group, with a median response of 460 kPa (380 - 550 kPa) as in the control group, median 400 kPa (range 280 - 440 kPa, Figure 3e). The elastic modulus was presented as the recorded median elasticity of the AAA patient group: 442 kPa (range 306 - 664 kPa) versus controls median 376 (range 289 – 420; Figure 3f).

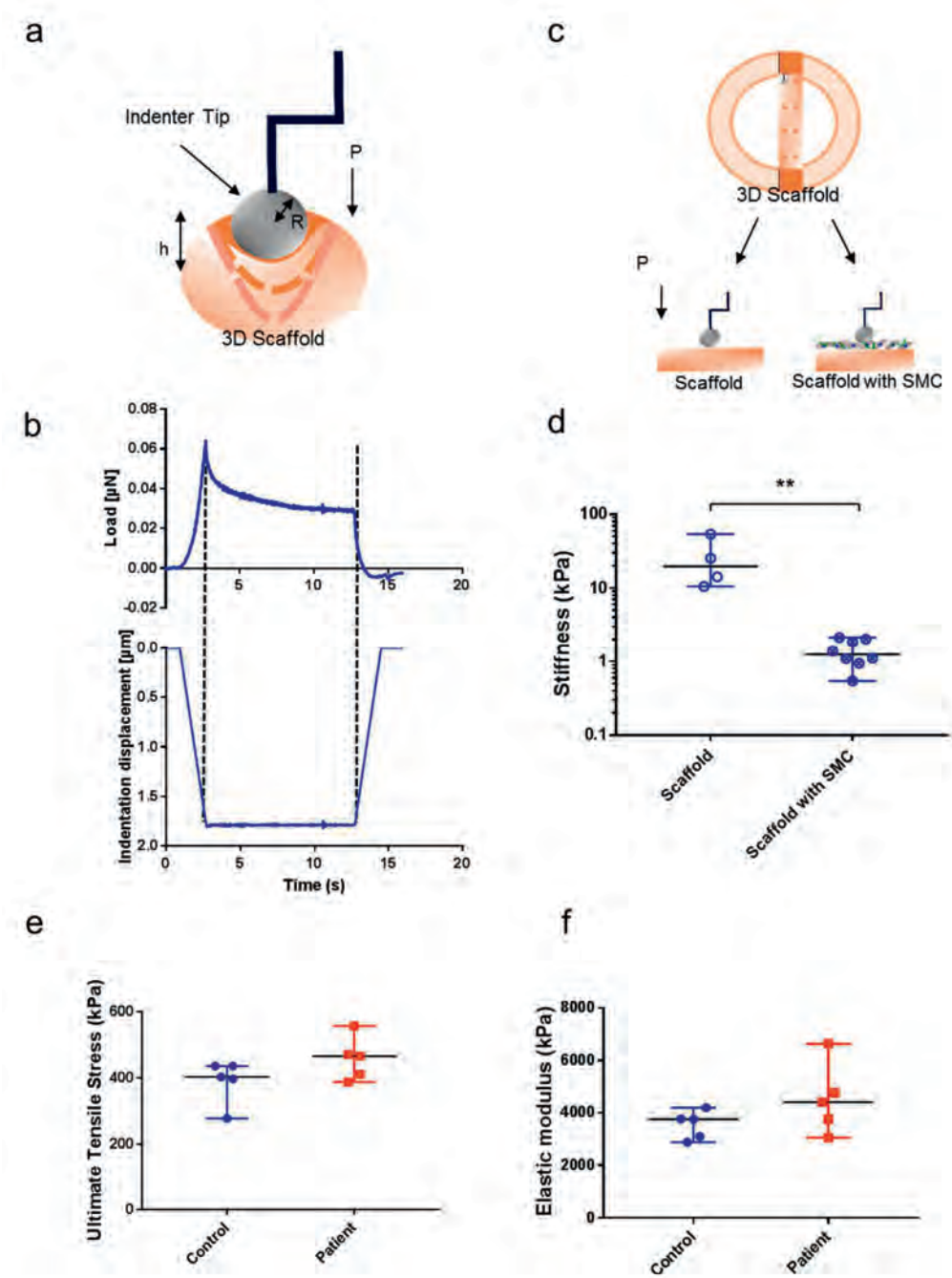


Figure 3. Mechanical properties and stiffness of the vascular construct. a) Schematic representation of a spherical tip indenting the surface of the vascular scaffold with constant pressure. b) Stress-relaxation curve of constant pressure indentation of a scaffold with cells. Upper graph represents the force loading curve (μN), lower graph represents the constant indentation depth applied to the sample (μm). c) Schematic representation of scaffold stiffness assessment using nanoindentation and recorded diverse response from scaffolds with and without SMC. d) Differences in stiffness of scaffold with and without cells (Pa, $p < 0.004$) measured by nano-indentation. Each data point represents one measurement, obtained by indenting the surface. e) Differences in tensile stress between scaffolds seeded with control and AAA patient SMC, measured by uniaxial tensile test (kPa). f) Differences in elastic modulus between scaffolds seeded with control and AAA patient SMC, measured by uniaxial tensile test (kPa). Each data point represents the mean of measurements performed in three scaffolds.

F-actin alignment and parallel organization in time

Changes in F-actin alignment over time were quantified using anisotropy measurements. Anisotropy of individual slices of a Z-reconstruction was measured in SMC which were seeded on glass coverslips in two control cell lines and immunostained after one, two and three weeks. SMC show random F-actin alignment on the coverslip after one week (**Figure 4a**). After two and three weeks, the confluency increased without a significant change in parallel organization. F-actin parallel organization did not increase significantly in week two and three compared to week one in SMC cultures on glass coverslips (Figure 4a). Same can be observed in a larger number of cells after three weeks of culturing on glass coverslips (Figure 4c).

Anisotropy of individual slices of a Z stack was measured in scaffolds which were immunostained after one, three and five weeks. SMC showed random F-actin alignment on the scaffold one week after seeding. Multiple confluent monolayers of cells with parallel F-actin organization were observed after three weeks. A similar level of F-actin organization was observed after five weeks. F-actin parallel organization progressively increased in time: week one showed a mean anisotropy of 0.02 versus week three 0.17 ($p < 0.001$) versus week five 0.20 ($p < 0.001$; Figure 4b). After week three however, the anisotropy did not further change. Same can be observed in a larger number of cells after 5 weeks of culturing on 3D scaffolds (Figure 4d).

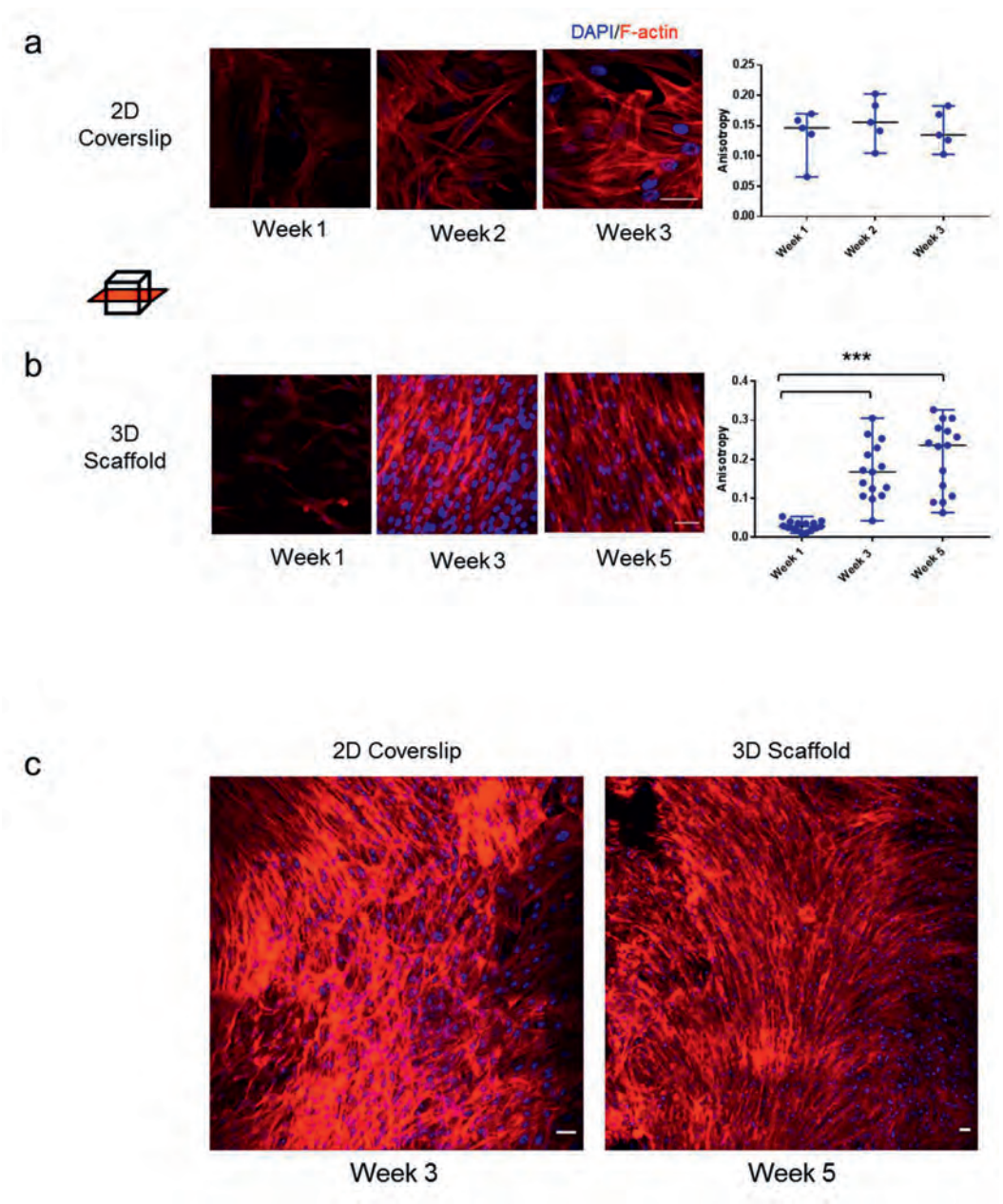


Figure 4. Changes of SMC F-actin alignment in time. Samples were immunostained for F-actin (red) and DAPI (blue). a) Images left to right: representative images of a control SMC F-actin alignment on glass coverslips in week one, two and three. Boxplot shows anisotropy measurements of SMC F-actin alignment in time. Data points represent individual measurements in one representative control cell line per time point. b) Images left to right: representative images of a control SMC F-actin alignment on 3D scaffold at week one, three and five. Boxplot shows anisotropy measurements of SMC F-actin alignment in time. Data points represent individual measurements in one representative control cell line per time point (** $p < 0.001$ vs week three; vs week five). c) Stitched images of SMC F-actin alignment on scaffold (left) and coverslip (right). Graphs are shown as median with range. Scale bar: 50 μm .

Differential F-actin alignment in SMC derived from AAA patients compared to controls

F-actin alignment was measured in cells seeded in 2D cultures on glass coverslips, after one, two and three weeks. At each time point, a trend of higher anisotropy was measured in the samples with patient cells ($n=2$) compared to controls ($n=2$, **Figure 5a**). For anisotropy measurements in the 3D scaffold samples, Individual optical slices of a Z-stack were marked as regions of interest and F-actin anisotropy was quantified (Figure 5b). A trend of higher F-actin alignment was again present in samples of both patients ($n=2$) compared to both controls ($n=2$) after 5 weeks in culture. Furthermore, low variability between the two controls and two patients was observed (Figure 5c).

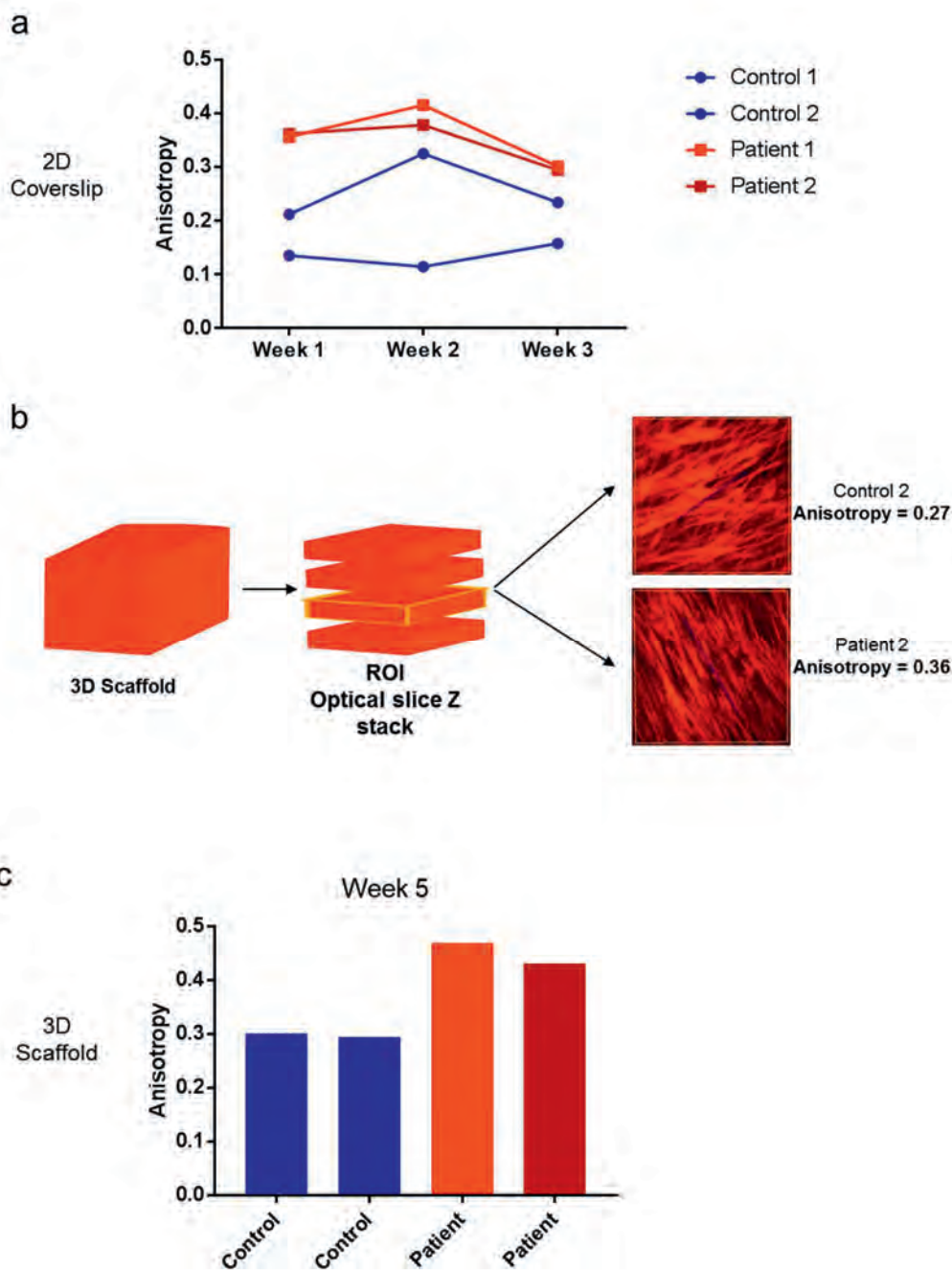


Figure 5. Differential F-actin alignment in SMC derived from AAA patients compared to controls. Samples were immunostained for F-actin (red) and DAPI (blue). a) Boxplots show anisotropy measurements of SMC F-actin alignment on glass coverslips during the course of three weeks. F-actin in patient cell lines (n=2, red) shows a trend of higher alignment compared to controls (n=2, blue) in every time point. Data points represent mean of three measurements in each cell line per time point. b) Schematic representation of anisotropy measurements in Z-stacks imaged on 3D scaffold samples. An individual optical slice was marked as the region of interest, and F-actin anisotropy was quantified. Representative images and measurement outcomes of control 2 and patient 2 are shown. c) Boxplots depict anisotropy measurements of SMC F-actin alignment on the scaffold after 5 weeks of culturing. F-actin in patient cell lines (n=2, red) shows a trend of higher alignment compared to controls (n=2, blue). Data points represent mean measurements in each cell line. Bar graph represents the mean per cell line.

Control SMC produce more Fibrillin-1 networks compared to AAA patients

Fibrillin-1 production was observed in SMC of controls (n=2) and AAA patients (n=2) which were grown for 3 weeks as 2D cultures on glass coverslips. Fibrillin-1 production levels in controls and patients did not differ after one and two weeks; however, the control group showed a trend of higher fibrillin-1 production after three weeks of culturing compared to patients (**Figure 6a**), accompanied by low intragroup variability. Representative images of differences in fibrillin-1 production are shown in Figure 6b. Fibrillin-1 production was also quantified in controls (n=2) and AAA patients (n=2) after 5 weeks of culturing on 3D scaffolds. Again, a trend of higher Fibrillin-1 production is present in the control group (as shown on Figure 6c and representative images in Figure 6d; representative 3D structures of control and patients SMC and ECM are shown in video 1 and video 2, respectively).

DISCUSSION

Defects in SMC and elastic fibers of the ECM, which consequentially lead to altered cell-matrix connections, play an important role in AAA formation.^[34] However, identifying the mechanisms behind these defects and designing corresponding therapies is hindered by the lack of relevant bioengineered models. In the present study, we created a 3D vascular scaffold to study SMC and ECM organization and interaction. Our scaffolds demonstrate morphological and mechanical properties similar to those of biological vascular tissues and mimic interaction between the media and intima layer. Using patient-specific cultures biological scaffolds with multilayered SMC from controls and AAA patients, we found changes in cytoskeleton alignment and ECM production between aneurysm derived SMC compared to the control.

Current bioengineering innovations in 3D printing are not progressive enough to print highly complex and accurate models of the aneurysmal aortic wall.^[35] As our construct represents a novel model, we compared our findings regarding SMC

behavior with known and well established 2D cultures for validation. Culturing cells on a scaffold allows for a more robust construction, consisting of more successive layers of SMC which closely resembles the aorta, and isn't threatened by cell detachment like 2D cultures. Therefore, we opted to use PLGA, a biodegradable material which was previously known as suitable material for vascular scaffolding using SMC.^[36] To our best knowledge, this is the first model which is bioengineered with patient specific SMC of both healthy individuals and AAA patients, and thus provides a unique possibility to study patient-specific physiological processes in AAA involving SMC.

As opposed to the 2D cultures where we observed a monolayer of EC, the co-culture on the 3D scaffolds appeared to be less uniform. The EC possibly filled the gaps in between the SMC layers, forming this distinct morphology. Similar structures were observed in the presence of fibroblast-conditioned medium, indicating that the tube-like cell could also be a product of the signaling molecules excreted by the larger number of SMC on the scaffold.^[37] Another explanation could be that the multilayered SMC provide a substrate of different stiffness than the few layers of SMC on the stiff glass coverslip; similar tube-like structures were observed in lower percentage collagen gels.^[38]

Aortic stiffening occurs primarily in regions of the aorta which are prone to aneurysmal dilation^[39] as a pathological characteristic of the aortic wall^[40]; it has been previously published that there is an increase in stiffness of 30% in human ascending aneurysmal tissue compared to controls.^[41] This literature supports our findings that vascular scaffolds seeded with SMC derived from AAA patients demonstrate a trend of increased stiffness compared controls. The trend was however not statistically significant, possibly due to small group sizes. The stiffness measurements performed to characterize the scaffold revealed stiffness ranges which are common for biological *ex vivo* vessels and visco-elastic properties typical for living tissue.^[32, 33] Moreno-Flores et al. measured stress-relaxation as parameters of cellular viscoelasticity using atomic force microscopy. Our data is entirely in line with their published data, as we demonstrate the same threefold decrease in force, as shown by the stress-relaxation curve (Figure 3b).^[42] As discussed by the authors, such behavior indicates visco-elastic properties of the living cells and ECM.^[42]

Aortic SMC and the ECM are circumferentially oriented in the medial layer.^[43] SMC alignment is an important factor in aortic function and structure, as SMC contraction regulates blood flow and pulse pressure.^[44] We assessed that SMC *in vitro* align more parallel in time and we showed a trend of increase in F-actin alignment in SMC derived from AAA patients compared to controls. Increased mechanical stress results in increased stiffness and cytoskeletal reorganization in bronchial SMC.^[45] As the aorta is exposed to increased mechanical wall stress^[46], a similar pathological mechanism could be in place, which would account for the increases in stiffness and

anisotropic behavior measured in our patient 3D cultures compared to control. We thus speculate that the pathological mechanical wall stress in the aneurysm affected the stiffness and alignment of patient SMC, even in *in vitro* cultures derived from the original tissue.

Mutations in the *FBN1* gene encoding fibrillin-1 are often the cause for aneurysm repair in young patients, even in their thirties^[47]. Fibrillin-1 is a protein found in the elastic fiber microfibrils in the extracellular matrix of the aorta^[47], where it performs its biological role in TGF- β binding and activation.^[48] Our results confirm the decrease in fibrillin-1 in AAA patients compared to controls in our setup. These results could shed a light on the role of fibrillin-1 and pathological ECM remodeling in the pathophysiology of non-syndromic AAA without a known genetic cause.

A shortcoming of this study is the small group size and low number of SMC donors used per experiment. However, as the primary goal was to share our design of 3D vascular scaffolds and hint the prospective applications for discriminating between controls and AAA patients, we present the findings within the current group sizes. An additional word of caution: as the biopsies were obtained during open aneurysm repair, we did not have control over the aortic site from which the biopsy derived due to prioritizing patient safety. Yet we can confidently state that all the patient biopsies are derived from the abdominal region of the aorta belonging to the dilated and diseased region of the aneurysmal sac, in most cases from the ventral side.

CONCLUSION

In conclusion, we demonstrate the feasibility of constructing a 3D vascular scaffold consisting of patient-specific SMC and the ECM they produced. We measured mechanical and biological properties comparable to the aortic wall and we have showed the possibility to co-culture SMC and EC in our setup. We further find a tendency of increased stiffness and F-actin alignment in the 3D-scaffolds seeded with AAA patients' SMC. Furthermore, fibrillin-1 production was decreased in AAA patients, suggesting that SMC derived from AAA patients show defective production of the ECM, even *in vitro*. Although future investigation is needed to perfect the scaffold design and increase its size and complexity, we believe that our scaffolds represent a valuable preclinical model of AAA with applications in both translational research and therapy developments.

ACKNOWLEDGMENTS

We gratefully acknowledge Arjan Hoksbergen, Hilian Nederhoed, Maarten Truijers, Vincent Scholtes and Willem Wisselink for providing the aortic material during surgery. We wish to thank Jeroen Kole and Rene Musters for their help with confocal microscopy.

This work was supported by the ICaR-AiO grant of the Amsterdam Cardiovascular Science Institute [grant number ICAR-VU AIO 2015], within Amsterdam University Medical Centers, Amsterdam, the Netherlands. Kak Khee Yeung was supported by W. L. Gore & Associates through an unrestricted research grant.

REFERENCES

1. Assar, A.N.,C.K. Zarins, Ruptured abdominal aortic aneurysm: a surgical emergency with many clinical presentations. *Postgraduate medical journal*, 2009. 85(1003): p. 268-273.
2. Sakalihasan, N., R. Limet,O.D. Defawe, Abdominal aortic aneurysm. *The Lancet*, 2005. 365(9470): p. 1577-1589.
3. Milewicz, D.M., D.C. Guo, V. Tran-Fadulu, A.L. Lafont, C.L. Papke, S. Inamoto, C.S. Kwartler,H. Pannu, Genetic basis of thoracic aortic aneurysms and dissections: focus on smooth muscle cell contractile dysfunction. *Annu Rev Genomics Hum Genet*, 2008. 9: p. 283-302.
4. Milewicz, D.M., K.M. Trybus, D.C. Guo, H.L. Sweeney, E. Regalado, K. Kamm,J.T. Stull, Altered Smooth Muscle Cell Force Generation as a Driver of Thoracic Aortic Aneurysms and Dissections. *Arterioscler Thromb Vasc Biol*, 2017. 37(1): p. 26-34.
5. Morisaki, H., K. Akutsu, H. Ogino, N. Kondo, I. Yamanaka, Y. Tsutsumi, T. Yoshimuta, T. Okajima, H. Matsuda, K. Minatoya, H. Sasaki, H. Tanaka, H. Ishibashi-Ueda,T. Morisaki, Mutation of ACTA2 gene as an important cause of familial and nonfamilial nonsyndromatic thoracic aortic aneurysm and/or dissection (TAAD). *Human Mutation*, 2009. 30(10): p. 1406-1411.
6. Renard, M., B. Callewaert, M. Baetens, L. Campens, K. MacDermot, J.-P. Fryns, M. Bonduelle, H.C. Dietz, I.M. Gaspar, D. Cavaco, E.-L. Stattin, C. Schrandt-Stumpel, P. Coucke, B. Loeys, A. De Paepe,J. De Backer, Novel MYH11 and ACTA2 mutations reveal a role for enhanced TGF β signaling in FTAAD. *International Journal of Cardiology*, 2013. 165(2): p. 314-321.
7. Jacob, M.P., Extracellular matrix remodeling and matrix metalloproteinases in the vascular wall during aging and in pathological conditions. *Biomedicine & Pharmacotherapy*, 2003. 57(5): p. 195-202.
8. Jacob, M.P., C. Badier-Commander, V. Fontaine, Y. Benazzoug, L. Feldman,J.B. Michel, Extracellular matrix remodeling in the vascular wall. *Pathologie Biologie*, 2001. 49(4): p. 326-332.
9. Sakalihasan, N., A. Heyeres, B.V. Nusgens, R. Limet,C.M. Lapière, Modifications of the extracellular matrix of aneurysmal abdominal aorta as a function of their size. *European Journal of Vascular Surgery*, 1993. 7(6): p. 633-637.
10. Dingemans, K.P., P. Teeling, J.H. Lagendijk,A.E. Becker, Extracellular matrix of the human aortic media: An ultrastructural histochemical and immunohistochemical study of the adult aortic media. *The Anatomical Record*, 2000. 258(1): p. 1-14.
11. Longo, G.M., W. Xiong, T.C. Greiner, Y. Zhao, N. Fiotti,B.T. Baxter, Matrix metalloproteinases 2 and 9 work in concert to produce aortic aneurysms. *The Journal of Clinical Investigation*, 2002. 110(5): p. 625-632.
12. Nataatmadja, M., M. West, J. West, K. Summers, P. Walker, M. Nagata,T. Watanabe, Abnormal extracellular matrix protein transport associated with increased apoptosis of vascular smooth muscle cells in Marfan syndrome and bicuspid aortic valve thoracic aortic aneurysm. *Circulation*, 2003. 108(10 suppl 1): p. II-329.
13. Fedak, P.W.M., M.P.L. de Sa, S. Verma, N. Nili, P. Kazemian, J. Butany, B.H. Strauss, R.D. Weisel,T.E. David, Vascular matrix remodeling in patients with bicuspid aortic valve malformations: implications for aortic dilatation. *The Journal of Thoracic and Cardiovascular Surgery*, 2003. 126(3): p. 797-805.
14. Humphrey Jay, D., A. Schwartz Martin, G. Tellides,M. Milewicz Dianna, Role of Mechanotransduction in Vascular Biology. *Circulation Research*, 2015. 116(8): p. 1448-1461.

15. Vorp, D.A., B.J. Schiro, M.P. Ehrlich, T.S. Juvonen, M.A. Ergin, B.P. Griffith, Effect of aneurysm on the tensile strength and biomechanical behavior of the ascending thoracic aorta. The Annals of Thoracic Surgery, 2003. 75(4): p. 1210-1214.
16. Jeong, S.I., J.H. Kwon, J.I. Lim, S.-W. Cho, Y. Jung, W.J. Sung, S.H. Kim, Y.H. Kim, Y.M. Lee, B.-S. Kim, C.Y. Choi, S.-J. Kim, Mechano-active tissue engineering of vascular smooth muscle using pulsatile perfusion bioreactors and elastic PLCL scaffolds. Biomaterials, 2005. 26(12): p. 1405-1411.
17. Mann, B.K., R.H. Schmedlen, J.L. West, Tethered-TGF- β increases extracellular matrix production of vascular smooth muscle cells. Biomaterials, 2001. 22(5): p. 439-444.
18. Tillman, B.W., S.K. Yazdani, S.J. Lee, R.L. Geary, A. Atala, J.J. Yoo, The in vivo stability of electrospun polycaprolactone-collagen scaffolds in vascular reconstruction. Biomaterials, 2009. 30(4): p. 583-588.
19. Nieponice, A., L. Soletti, J. Guan, Y. Hong, B. Gharaibeh, T.M. Maul, J. Huard, W.R. Wagner, D.A. Vorp, In Vivo Assessment of a Tissue-Engineered Vascular Graft Combining a Biodegradable Elastomeric Scaffold and Muscle-Derived Stem Cells in a Rat Model. Tissue Engineering Part A, 2009. 16(4): p. 1215-1223.
20. Ghazanfari, S., K.A. Alberti, Q. Xu, A. Khademhosseini, Evaluation of an elastic decellularized tendon-derived scaffold for the vascular tissue engineering application. Journal of Biomedical Materials Research Part A, 2019. 107(6): p. 1225-1234.
21. Williamson, M.R., R. Black, C. Kielty, PCL-PU composite vascular scaffold production for vascular tissue engineering: Attachment, proliferation and bioactivity of human vascular endothelial cells. Biomaterials, 2006. 27(19): p. 3608-3616.
22. Jessup, D.B., M.M. Grove, S. Marks, A. Kirby, Planned use of GP IIb/IIIa inhibitors is safe and effective during implantation of the Absorb Bioresorbable Vascular Scaffold. Cardiovascular Revascularization Medicine, 2018. 19(8): p. 956-959.
23. Gao, L.-P., M.-J. Du, J.-J. Lv, S. Schmall, R.-T. Huang, J. Li, Use of human aortic extracellular matrix as a scaffold for construction of a patient-specific tissue engineered vascular patch. Biomedical Materials, 2017. 12(6): p. 065006.
24. Bogunovic, N., J.P. Meekel, D. Micha, J.D. Blankensteijn, P.L. Hordijk, K.K. Yeung, Impaired smooth muscle cell contractility as a novel concept of abdominal aortic aneurysm pathophysiology. Scientific Reports, 2019. 9(1): p. 6837.
25. Makadia, H.K., S.J. Siegel, Poly lactic-co-glycolic acid (PLGA) as biodegradable controlled drug delivery carrier. Polymers, 2011. 3(3): p. 1377-1397.
26. Kruse, M., P. Walter, B. Bauer, S. Rütten, K. Schaefer, N. Plange, T. Gries, S. Jockenhoevel, M. Fuest, Electro-spun membranes as scaffolds for human corneal endothelial cells. Current eye research, 2018. 43(1): p. 1-11.
27. Schindelin, J., I. Arganda-Carreras, E. Frise, V. Kaynig, M. Longair, T. Pietzsch, S. Preibisch, C. Rueden, S. Saalfeld, B. Schmid, J.-Y. Tinevez, D.J. White, V. Hartenstein, K. Eliceiri, P. Tomancak, A. Cardona, Fiji: an open-source platform for biological-image analysis. Nature Methods, 2012. 9: p. 676.
28. Mattei, G., L. Cacopardo, A. Ahluwalia, Micro-Mechanical Viscoelastic Properties of Crosslinked Hydrogels Using the Nano-Epsilon Dot Method. Materials (Basel, Switzerland), 2017. 10(8): p. 889.
29. Mattei, G., G. Gruca, N. Rijnveld, A. Ahluwalia, The nano-epsilon dot method for strain rate viscoelastic characterisation of soft biomaterials by spherical nano-indentation. Journal of the Mechanical Behavior of Biomedical Materials, 2015. 50: p. 150-159.

30. Field, J.S.,M.V. Swain, Determining the mechanical properties of small volumes of material from submicrometer spherical indentations. *Journal of Materials Research*, 2011. 10(1): p. 101-112.
31. Boudaoud, A., A. Burian, D. Borowska-Wykręt, M. Uyttewaal, R. Wrzalik, D. Kwiatkowska,O. Hamant, FibrilTool, an ImageJ plug-in to quantify fibrillar structures in raw microscopy images. *Nature Protocols*, 2014. 9: p. 457.
32. Maccabi, A., A. Shin, N.K. Namiri, N. Bajwa, M. St. John, Z.D. Taylor, W. Grundfest,G.N. Saddik, Quantitative characterization of viscoelastic behavior in tissue-mimicking phantoms and ex vivo animal tissues. *PLOS ONE*, 2018. 13(1): p. e0191919.
33. van Disseldorp, E.M.J., N.J. Petterson, F.N. van de Vosse, M.R.H.M. van Sambeek,R.G.P. Lopata, Quantification of aortic stiffness and wall stress in healthy volunteers and abdominal aortic aneurysm patients using time-resolved 3D ultrasound: a comparison study. *European Heart Journal-Cardiovascular Imaging*, 2018. 20(2): p. 185-191.
34. Humphrey, J.D., M.A. Schwartz, G. Tellides,D.M. Milewicz, Role of mechanotransduction in vascular biology: focus on thoracic aortic aneurysms and dissections. *Circulation research*, 2015. 116(8): p. 1448-1461.
35. Garreta, E., R. Oria, C. Tarantino, M. Pla-Roca, P. Prado, F. Fernández-Avilés, J.M. Campistol, J. Samitier,N. Montserrat, Tissue engineering by decellularization and 3D bioprinting. *Materials Today*, 2017. 20(4): p. 166-178.
36. In Jeong, S., S.Y. Kim, S.K. Cho, M.S. Chong, K.S. Kim, H. Kim, S.B. Lee,Y.M. Lee, Tissue-engineered vascular grafts composed of marine collagen and PLGA fibers using pulsatile perfusion bioreactors. *Biomaterials*, 2007. 28(6): p. 1115-1122.
37. Newman, A.C., M.N. Nakatsu, W. Chou, P.D. Gershon,C.C.W. Hughes, The requirement for fibroblasts in angiogenesis: fibroblast-derived matrix proteins are essential for endothelial cell lumen formation. *Molecular Biology of the Cell*, 2011. 22(20): p. 3791-3800.
38. Sieminski, A.L., R.P. Hebbel,K.J. Gooch, The relative magnitudes of endothelial force generation and matrix stiffness modulate capillary morphogenesis in vitro. *Experimental Cell Research*, 2004. 297(2): p. 574-584.
39. Akhtar, R., M.J. Sherratt, J.K. Cruickshank,B. Derby, Characterizing the elastic properties of tissues. *Materials Today*, 2011. 14(3): p. 96-105.
40. Kadoglou, N.P.E., I. Papadakis, K.G. Moulakakis, I. Ikonomidis, M. Alepaki, P. Moustardas, S. Lampropoulos, P. Karakitsos, J. Lekakis,C.D. Liapis, Arterial stiffness and novel biomarkers in patients with abdominal aortic aneurysms. *Regulatory Peptides*, 2012. 179(1): p. 50-54.
41. García-Herrera, C.M., J.M. Atienza, F.J. Rojo, E. Claes, G.V. Guinea, D.J. Celentano, C. García-Montero,R.L. Burgos, Mechanical behaviour and rupture of normal and pathological human ascending aortic wall. *Medical & Biological Engineering & Computing*, 2012. 50(6): p. 559-566.
42. Moreno-Flores, S., R. Benitez, M.d. Vivanco,J.L. Toca-Herrera, Stress relaxation and creep on living cells with the atomic force microscope: a means to calculate elastic moduli and viscosities of cell components. *Nanotechnology*, 2010. 21(44): p. 445101.
43. Ghazanfari, S., A. Driessen-Mol, S.P. Hoerstrup, F.P.T. Baaijens,C.V.C. Bouten, Collagen matrix remodeling in stented pulmonary arteries after transapical heart valve replacement. *Cells Tissues Organs*, 2016. 201(3): p. 159-169.
44. Milewicz, D.M., D.-C. Guo, V. Tran-Fadulu, A.L. Lafont, C.L. Papke, S. Inamoto, C.S. Kwartler,H. Pannu, Genetic basis of thoracic aortic aneurysms and dissections: focus on smooth muscle cell contractile dysfunction. *Annu. Rev. Genomics Hum. Genet.*, 2008. 9: p. 283-302.

45. Smith, P.G., L. Deng, J.J. Fredberg, G.N. Maksym, Mechanical strain increases cell stiffness through cytoskeletal filament reorganization. *American Journal of Physiology-Lung Cellular and Molecular Physiology*, 2003. 285(2): p. L456-L463.
46. Vorp, D.A., M.L. Raghavan, M.W. Webster, Mechanical wall stress in abdominal aortic aneurysm: Influence of diameter and asymmetry. *Journal of Vascular Surgery*, 1998. 27(4): p. 632-639.
47. Milewicz Dianna, M., K. Michael, N. Fisher, S. Coselli Joseph, T. Markello, A. Biddinger, Fibrillin-1 (FBN1) Mutations in Patients With Thoracic Aortic Aneurysms. *Circulation*, 1996. 94(11): p. 2708-2711.
48. Hynes, R.O., The Extracellular Matrix: Not Just Pretty Fibrils. *Science*, 2009. 326(5957): p. 1216.



Summary and Discussion

SUMMARY AND DISCUSSION

Aortic aneurysms (AA) are pathological dilations of the aorta. Various risk factors¹ have been associated with this multifactorial disease, but the molecular mechanism behind the changes leading to the dilation of the aortic wall remain elusive. Smooth muscle cells (SMC) are the predominant cell type in the aorta; they reside in the aortic media - providing structural support to the vessel, regulating blood flow with their contractile ability - and produce components of the matrix which surrounds them. SMC dysfunction was previously implicated in AA formation; it has been shown that SMC apoptosis² and phenotypic switch³ occur during the pathogenesis, and that mutations in SMC specific genes lead to aneurysm formation. Previous research did not elucidate the pathological mechanisms behind the changes in the aortic wall, partially due to inadequate *in vitro* disease models. The aim of this thesis was to further explore the role SMC play in AA pathophysiology, and renovate the field of AA research by developing novel models and methods that pave the path to future AA research.

In the present work we tackled various aspects of SMC involvement in AA pathophysiology: we developed a new method to directly convert skin fibroblasts into SMC-like cells to study the effects of mutations in SMC specific genes and their effects on splicing which cannot be studied in cell that do not express the genes (**Chapter 2**); we used that method to study the consequences of these mutations on SMC contractile and migratory functions (**Chapter 3**); we showed differences in TGF β signaling in relation to betaglycan in patients with dominant-negative, compared to haplo-insufficient mutations in *FBN1* which causes Marfan syndrome (**Chapter 4**); we developed a new method to measure SMC contraction *in vitro* and proved that SMC of patients with AAA show impaired contraction, correlating to secondary surgery and current smoking (**Chapter 5**); we developed a new method to preserve aortic sections alive for 90 days *in vitro*, whilst maintaining their original microenvironment (**Chapter 6**); we developed a new *in vitro* model of aortic aneurysms by using patient-specific SMC which produced their own extracellular matrix and 3D structure, which differed between patients and controls (**Chapter 7**).

The research topics elaborated in these chapters are grouped into three sections based on the similar topics they report on. Section I (Chapters 2, 3 and 4) provide insight into the genetic aspects of aneurysms: mutations in SMC specific and relevant genes and our attempts to elucidate the functional aspects of these mutations and develop new, improved ways to study them. Section II (Chapter 5) is focused on developing a new method to measure SMC contraction *in vitro*, and the application of that method to compare contraction of AA patient's SMC and healthy control SMC, and subsequently link them to clinical characteristics of these patients. Section III (Chapters 6 and 7) is devoted to novel models of AA which consist out of multiple cell type and have a complex 3D structure. Both Chapters introduce new

aspects of studying cells and matrix in an attempt to elucidate the processes happening in the aneurysmal wall.

I. Mutations in aortic aneurysm related genes lead to altered transdifferentiation potential, splicing errors, impaired smooth muscle cell functionality and TGF β signaling

Mutations in SMC-specific genes have been associated with familial thoracic aortic aneurysms and dissections⁴⁻⁶. Mutations in genes encoding proteins of the SMC contractile apparatus, such as *ACTA2*⁴ (encodes alpha-smooth muscle actin 2, aSMA) and *MYH11*⁷ (encodes myosin heavy chain 11) appear to play a causal role in aortic pathology, hinting at the importance of SMC contraction in maintaining the aortic balance. Mutations in *FBN1*⁸ (encodes fibrillin-1) are causal for the development of Marfan syndrome, and mutations in genes involved in TGF β signaling lead to syndromic manifestations of aortic aneurysms (*SMAD3*⁹, encodes SMAD3; *TGFBR2*¹⁰, encodes TGF β receptor type 2), causing other connective tissue syndromes with systemic manifestation. These connective tissue syndromes all have cardiovascular manifestations, of which most severe and life-threatening aortic aneurysms and dissections. The influence of these mutations on the aortic phenotype is known, but the genotype to phenotype relationship is mostly unclear.

To study SMC specific genes (and the proteins they encode) SMC are needed in laboratory conditions. The only currently available options are invasive aortic biopsies or induced pluripotent stem cells (iPSC), generated from other cell types, which is costly and complex. To tackle the gap in current knowledge, we developed a transdifferentiation (direct conversion of one mature cell type into another) protocol, described in **Chapter 2**, proposing a way to create SMC-like cells from dermal fibroblasts. This transdifferentiation can be achieved within two weeks, using a culture medium containing TGF β 1, a cytokine which modulates SMC phenotype *in vivo*, and matrigel, a scaffold containing collagen and elastin which mimics the aortic microenvironment in which SMC are embedded. Our protocol is in accordance with previous work, utilizing TGF β 1 *in vitro* to induce aSMA expression¹¹ in human fibroblasts. To validate the transdifferentiation protocol, we quantified the contraction of the scaffold (as an indication of the seeded cells gaining SMC-typical contractile abilities), SMC specific mRNA and protein expression, and compared these to scaffolds seeded with dermal fibroblasts which were not treated with transdifferentiation medium. We showed an increase in expression of SMC markers, comparable to those of primary SMC isolated from aortic biopsies.

We further used this protocol in **Chapters 2 and 3** to investigate individual mutations and their pathogenicity through their effects on splicing, transdifferentiation efficiency and effects on SMC function. To examine transdifferentiation efficiency, we compared the de novo expression of SMC markers between cells of patients with a

mutation and cells of healthy controls, and the effects of the mutation on SMC function.

Mutations leading to alternative splicing of *FBN1* and *COL3A1* have been implicated in aneurysm formation in earlier literature^{12,13}. In **Chapter 2**, we demonstrated an application of our method to detect the effects on splicing: splicing errors can only be detected once the transcript is present, meaning only in cells that express these genes. We demonstrate that mutations located in introns of *ACTA2* and *MYH11* genes lead to alternative splicing (presence of alternative transcripts) in certain patient cell lines we examined. Detecting these alternative transcripts would not be possible in dermal fibroblasts, since they do not express these SMC specific genes. Using this method, we are able to predict the effects of the mutation on SMC without obtaining them from the patients post-operatively.

In **Chapter 3**, we expanded the study to include functional testing, trying to uncover the consequences of the mutations on SMC functions such as contraction and migration. We detected that the SMC-like cells of a patient with an *ACTA2* mutation contract less, compared to controls. As alpha smooth muscle actin (aSMA, encoded by *ACTA2*) is paramount for SMC contraction^{14,15}, it comes as no surprise that this mutation in *ACTA2* has a negative effect on the contractile function. In addition, *ACTA2* is involved in myofibroblast (an intermediate cell type between fibroblasts and SMC) motility¹⁵, which might explain why SMC-like cells of a patient with an *ACTA2* mutation migrate less than the control group. Migration of SMC-like cells of a patient with an *MYH11* mutation was also decreased in the same assay, possibly affecting the same contraction and migration abilities as the *ACTA2* mutations. SMC-like cells of a patient with a *TGFBR2* mutation also migrated slower compared to control. The link between *TGFBR2* and migration is unclear, but mutations in *TGFBR2* have previously been shown to inhibit SMC-mediated vascular remodeling¹⁶, and it is known that TGF β signaling is promoting SMC migration¹⁶, underscoring the relevance of this pathway in SMC migration, and the potential consequences of its disruption. Taken together, these results indicate that aneurysm causing mutations affect SMC function, which could be an indication of how these mutations lead to aortic wall dilation.

In **Chapter 4**, we examine the link between betaglycan, also known as TGF β receptor type 3, and TGF β signaling in Marfan syndrome using dermal fibroblasts of Marfan patients. The Marfan causing *FBN1* mutations can be subdivided in haploinsufficient (HI), causing the absence of the fibrillin-1 protein, and dominant-negative (DN), causing the presence of a malformed fibrillin-1 protein¹⁷. We demonstrate an increase in the expression of several TGF β target genes (*COL1A1*, *FN1* and *TGF β 1* itself) in patients with DN mutations, indicating an increase in TGF β signaling, compared to patients with HI mutations. The increase in signaling was consistent with the increased expression of the betaglycan protein, possibly

indicating a role of betaglycan in facilitating the increase in downstream signaling by aiding TGF β binding on the cell membrane. It is known that betaglycan can repress or increase TGF β signaling¹⁸. Since TGF β signaling is severely altered in patients with DN Marfan syndrome due to a malformed fibrillin-1 protein, we speculate that betaglycan signaling changes accordingly, as opposed to HI where no fibrillin-1 is present. Betaglycan might be an additional relevant player in Marfan altered TGF β signaling.

II. SMC contraction is disrupted in patients with AAA: results from a novel method and implications of associated clinical factors

Mutations in SMC specific genes, such as *ACTA2* and *MYH11*, have been implicated in cases of familial thoracic aneurysms^{4,6,7,19}. However, little was known regarding the contribution of disturbed SMC contraction in cases of non-hereditary sporadic aneurysms. In **Chapter 5** we explore the concept that disturbed SMC contractility is a broadly present phenomenon in sporadic AAA formation and that it is not exclusively present in patients with mutations. To obtain data from a larger group of sporadic patients, we firstly needed to optimize the currently available techniques for contraction measurements.

Current techniques for measuring *in vitro* SMC contractility are traction force microscopy^{20,21}, quantification of Fura-2 fluorescence intracellular calcium fluxes²² as an indirect indicator of contraction and collagen wrinkling assays²³. Traction force microscopy is highly quantitative^{20,21}, but limited to measuring single cells, making it difficult to analyze larger cohorts of cells from different patients. Collagen wrinkling assays are, in contrast, appropriate for measurements of a population of cells²³, but the contraction data are obtained by quantification of large-scale images which are not obtained in real time, making it unsuitable to capture subtle differences. In **Chapter 5**, we provided an alternative by repurposing ECIS, a real-time assay which is largely used to quantify cell adhesion and migration²⁴⁻²⁷. ECIS has previously been used to investigate SMC migration in wound-healing assays²⁸⁻³⁰. We utilize the rapid measurement properties of ECIS and a strong contraction stimulus (ionomycin) to induce immediate maximum contraction.

We challenged the concept that SMC contraction is “one-on-one” dependent on SMC phenotype. We hypothesized that normal SMC contraction correlated with the contractile phenotype, characterized by expression of contractile marker proteins, such as alpha smooth muscle actin and smoothelin³¹. On the contrary, we found no correlation between SMC markers and contractility. Similar findings were reported in an animal model, where an induced aneurysm was not accompanied by a reduction in α SMA³². It was speculated that contraction could be impaired in a phenotype-independent manner, possibly through the degradation of ECM which inhibits KCl

influx and consequential contraction³³⁻³⁵. Controversially, phenotypic variability was also perceived in the control group in our study. Our results indicate that there is no clear difference between controls and patients as to marker expression, but also that both groups express intragroup variability in markers, and thus a phenotype which is not uniform. Based on the differences we measure, we presume that the cells retain traits of the tissue they belong to, indicating another mechanism could be in place, such as epigenetics^{36,37} or disturbed signaling pathways.

Tobacco smoking is one of the most prominent risk factors both for developing AA and for an increase in AA growth rate³⁸⁻⁴⁰. However, the mechanism by which tobacco consumption contributes to aneurysm formation is unknown. It is considered that the mechanism is unrelated to those involved in atherosclerotic plaque formation, and that it might affect collagen synthesis, MMPs and oxidative stress⁴⁰. In **Chapter 5**, we show an association between SMC contraction and current smoking. The group of patients who are current non-smokers also includes past smokers. This is in accordance with literature which emphasizes a link between current smoking^{40,41}, rather than chronic smoking in general as the key pathology driving factor. This could signify that, in case that smoking does disturb SMC contraction, this effect could be reversible and that patients who would stop smoking would benefit from improvement of their SMC function.

Endoleaks are post-operative complications after endovascular aneurysm repair. They manifest as persistent blood flow into the aneurysmal sac surrounding the inserted endograft⁴². This complication was not the topic of extensive molecular research, but previous clinical studies link endoleaks with developing aneurysm growth and risk of secondary aneurysm rupture⁴³. Decreased contraction in patients who underwent secondary surgery as a treatment for their endoleaks could indicate a link between SMC contractile dysfunction and the occurrence of endoleaks. It has been reported that in cases of secondary surgery for endoleak treatment, more unorganized thrombus was found attached to the endograft in than SMC and ECM which are normally present in a healthy wall, and are both necessary for the incorporation of the graft into the aortic wall post-operation⁴⁴. However, as endoleaks are multifactorial, they may not be always associated with a defect in SMC. We hypothesize, based on our findings, that impaired SMC contractility disables the aortic wall from fully incorporate the endograft prothesis, leading to incomplete endograft implementation into the wall and consequential endoleaks or vice versa. Another possible explanation could be that SMC dedifferentiated and lost some of their contractile function, as they were not subjected to direct blood pressure. Endograft implementation could also cause inflammation of the vessel, further worsening SMC function.

Our findings of impaired contraction of SMC isolated from biopsies of a sub-group of patients led us to propose the following concept for AA development (Figure 1). Impaired contraction decreases the SMC's ability to resist blood flow and to perform both vasoconstriction and vasodilation. The vessel wall becomes gradually damaged over time and becomes increasingly strained since it needs to resist the same flow and pressure with decreased capacity. The balance between SMC and ECM becomes disrupted: since the SMC contraction is reduced, the ECM fibers receive more load, causing elastin and collagen damage. This disbalance also damages the mechanotransduction complex of the SMC, altering the transmission of force from the cytoskeleton and contractile machinery onto the ECM fibers. This cascade leads to the weakening of the aortic wall and consequential aneurysmal dilation.

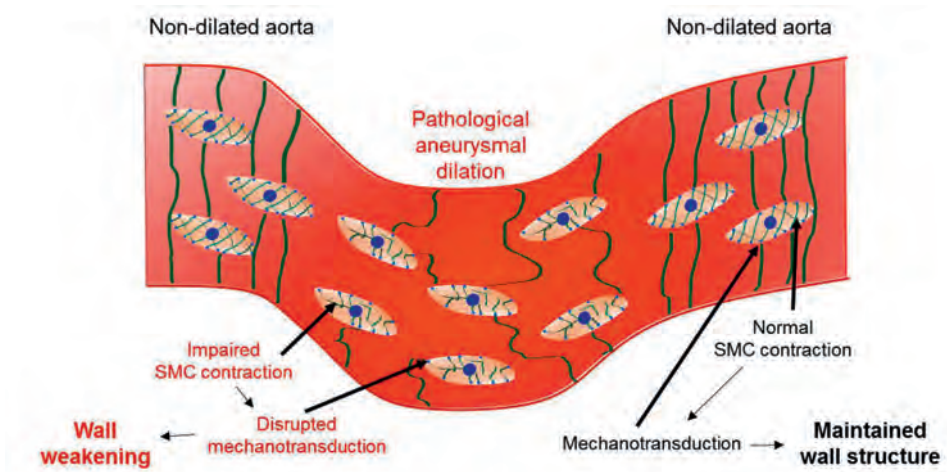


Figure 1. **Impaired smooth muscle cell contraction leads to aneurysm formation.** Impaired smooth muscle cell contraction generates less force within the cell. The reduction in force is then transmitted from the cytoskeleton onto the fibers of the extracellular matrix through adhesion molecules on the cell membrane. Due to the decreased force in the smooth muscle cells, the extracellular matrix endures more of the pressure, leading to disruption and damage to the fibers. The general disbalance in the vessel wall leads to weakening and eventually dilation, causing the formation of an aneurysm.

III. Ex vivo aneurysm sections and a reverse engineered aneurysm wall as novel models for translational research

Translational research into AA is significantly hindered by the lack of appropriate models. *In vivo* models are created by inducing targeted mutations or deficiencies, which, however, fail to capture the multifactorial character nature of pathogenesis human AA⁴⁵⁻⁴⁷. In research utilizing *in vitro* models, most of the data was obtained from single cells or fixed tissue samples, used to investigate marker expression or ECM degradation, which often obviously simplifies the disease picture since many

wall components are not observed^{33,34}. In **Chapters 6 and 7**, we aimed to create better models to study not only SMC, but also their interaction with other wall components that are affected by AA.

In **Chapter 6**, we developed a method to keep aortic tissue sections alive in culture. Using a vibrating microtome, we sectioned the aortic biopsy into pieces containing all three layers of the aorta, suitable for culturing. Live-dead staining revealed living cells within the sections on day zero, three and fourteen in culture. Interestingly, the percentage of live cells increases after day three, possibly because cells underwent a reversible proapoptotic state during the cutting⁴⁸, or the tissue retained proliferative capacity. Within this *ex vivo* organ, we do not only preserve SMC and other cell types in the vessel wall, but also infiltrating macrophages and leucocytes, which are known to be involved in inflammation in AA^{49,50}. We speculate that the presence of these cells could maintain a proinflammatory state in the sections, which stimulates SMC cytokine and reactive oxygen species production⁵¹. We stimulated the sections with TGF β to mimic the naturally occurring signaling in the aorta which contributes to aneurysm formation^{52,53}. In our model, this led to increases in gene expression of *IL6*, *CNN1* and *TGFB1* itself, in accordance with earlier studies, indicating that our model can be used for stimulation studies to investigate aneurysm related signaling^{54,55}.

In **Chapter 7**, we used an opposite approach and attempted to reverse engineer the tissue from patient-specific SMC which produce their own ECM. We aspired to develop a model where the differences we measure could only be attributed to the SMC and the traits they retained from the original tissue from which they were isolated. Using patient-specific SMC and bioengineered PLGA scaffolds, we created a 3D model of the aortic media to mimic the SMC's natural environment and SMC-ECM contact, which is highly relevant for AAA formation⁵⁶. We opted for PLGA which was previously tested and approved as a material for vascular scaffolding⁵⁷. Using a biodegradable material which is safe for use in humans is also beneficial for potential future stent-graft applications of our research⁵⁸. We also mimicked the interaction between the media and intima in AA by adding endothelial cells (EC) to the model, as it is known that they produce proteases and recruit macrophages into the medial layer⁵⁹. More importantly, studies have shown that targeting the endothelium could have a preventive effect on AAA: reestablishing the endothelium led to prevention of AAA formation, stabilizing already formed AAA through secreting paracrine mechanisms involved in recruiting other vascular cells and to the re-formation of SMC and ECM⁶⁰. For this reason, exploring the link between SMC, ECM and EC is a valuable part of our model, which may well lead to novel mechanistic insights.

We tested stiffness and elasticity of the SMC and ECM and found that the stiffness of our model was comparable to that of biological vessels, exhibiting a similar visco-elastic response⁶¹. SMC orientation in the aorta is imperative for their function. SMC

and encompassing ECM are circumferentially oriented in the medial layer⁶², which allows them to contract and relax uniformly, regulating blood flow and pulse pressure⁵. We measured anisotropy of F-actin, as a proxy for cell directionality and observed that this parameter increases in time during culturing, possibly due to the larger number of layers that are being formed. It is known that SMC reorientate themselves in response to flow^{63,64}, but it was striking that they reoriented without any additional stimuli in our model. On the other hand, cyclic stretching and flow might have been present in the aorta and stayed imprinted in the cells which now exhibit these changes *in vitro*, since cyclic stretching was associated with SMC apoptosis and aneurysm formation⁶⁵⁻⁶⁷.

Bioengineering a novel system allowed us to follow the synthesis of its components in time. We quantified ECM production, in particular fibrillin-1 fibers. Fibrillin-1 is found in the elastic fiber microfibrils in the extracellular matrix of the aorta⁶⁸, where it is involved in TGF β binding and activation⁶⁹. Mutations in *FBN1* cause aortic aneurysms as severe cardiovascular symptoms as part of Marfan syndrome^{8,68}. In the aorta itself, fibrillin-1 is affected by the overall ECM remodeling, facilitated by matrix metalloproteinase enzymes⁷⁰. In **Chapter 7**, we provide novel evidence that fibrillin-1 in the abdominal aneurysmal aorta might also be decreased due to its decreased production by SMC. These results might underscore the importance of fibrillin-1 in cases of non-syndromic AAA without a known genetic cause. The reduction of fibrillin-1 might lead to an increase TGF β signaling, as fibrillin-1 keeps TGF β latent in a complex in the ECM.

If we compare the models in **Chapters 6 and 7**, the main similarities between the two models are that they are both robust, involve multiple cell types and include ECM, as compared to 2D cell culture. In comparison to animal models, they retain the specificity of the original patient material, making them more suitable for the investigation of the multifactorial human AA than animal models which are induced by a single targeted alteration. Due to the increased complexity, compared to cell culture, they allow a larger number of readouts and the investigation of a broader spectrum of processes involved in AA pathology. The main difference is that in the sections, as in original tissue, we can also study immune cell infiltration. Since the sections derive from the original aneurysm tissue, there could be more systemic effects that are still present, such as wall stretching from hypertension or damage from rupture in the case of rupture. However, the 3D scaffold gives us a controlled model with a strong focus on SMC, where we can examine the differences in the cells and the AA effects imprinted in them.

Future perspectives

The efforts invested in aneurysm research during the past decades did not bring us much closer to answering the fundamental question: “why does the aorta dilate?”. Answering this question and pinpointing the underlying mechanisms that lead to this pathological phenomenon are the first and essential steps to revolutionize the way we perceive and consequently treat aortic aneurysms.

Within the patient population, there are patients who are not aware that they have an aneurysm until it is discovered accidentally or until it ruptures. Some patients already have a diagnosed aneurysm, affected relatives or know that they are carrying an aneurysm causing mutation. These patients are affected by the burden of being sick or the prospect of becoming sick, which influences their quality of life. Since no pharmaceutical option is available, they can only wait to become a candidate for surgery. Patient-specific research into their SMC defects can only be done retrospectively, once these patients already underwent the invasive surgical procedure, during which researchers can obtain samples of the aortic wall which contains the SMC. The transdifferentiation method we developed in **Chapter 2** opens new possibilities: we could research SMC related pathologies before the patient undergoes surgery. In the future, when we would also have a working pharmaceutical therapy, diagnosing molecular issues prospectively would help improve patient outcomes and quality of life. Our method could become a standardized screening test, available alongside other diagnostics at outpatient clinics for patients with a known aneurysm containing mutation who have not undergone surgery.

The newly discovered contraction impairment (**Chapter 5**) could turn out to be a unifying factor between molecular and mechanical issues that occur in the aorta during AA formation^{71,72}. This defect might be targeted in future clinical trials with medications which improves contraction, like in the case of improved cardiomyocyte contraction in relation to heart failure with a medication that stabilizes the cytoskeleton⁷³. Larger scale studies should also be conducted to confirm the correlation between impaired SMC contraction and comorbidities, such as current smoking and secondary surgery to treat endoleaks. Using impaired contraction as a selection factor for affected patients, a more in-depth and larger scale study can be performed to not only investigate the mechanism behind contractile dysfunction, but possibly also the mechanism in which smoking leads to aneurysm growth and the reason for which some patients require secondary surgery.

The unique, preserved microenvironment of the tissue sections (**Chapter 6**) could be used for future drug testing. Stimulating affected tissue originating from patients could be used for screening pharmacological agents for aneurysm treatment. Upscaling the scaffold we developed (**Chapter 7**) into a tubular model which mimics

the aorta could provide more insight into the organization of SMC in a vessel and its flow dynamics, and how that is disturbed in an aneurysm. By testing burst pressure, we could reveal the breaking point or durability of aneurysms of some people, which could, in relation to the clinical picture and molecular analysis reveal possible rupture prediction factors. We could combine the transdifferentiated cells from the fibroblasts of the patient and the future tubular scaffold, and repair aneurysms with an ex vivo grown aorta of the same patient. These cells could also be used as coating for sutures or grafts, improving the healing process. This could also be relevant for future clinical trials of pharmaceutical products, since it also might relieve the burden which is currently being placed on animal work.

On a general note, all the methods and models developed during this thesis research could be used to further investigate the role of SMC in AA pathogenesis with additional research questions. They could be utilized to compare subpopulations of patients with potentially specific pathological mechanisms and risk factors, such as gender specific studies, patients with diabetes, current and past smokers etc. and improve current genetic testing. The opportunities created by these novel methods also allow us to investigate potential therapeutics and their effects on SMC function. To conclude, the work presented in this thesis has made a step in the direction of reclassifying aortic aneurysms into severe multifactorial cardiovascular disease with known causes. We anticipate that the legacy of our work will lead towards better understanding of why aortas dilate and subsequent development of new, improved future therapeutic prospects.

REFERENCES

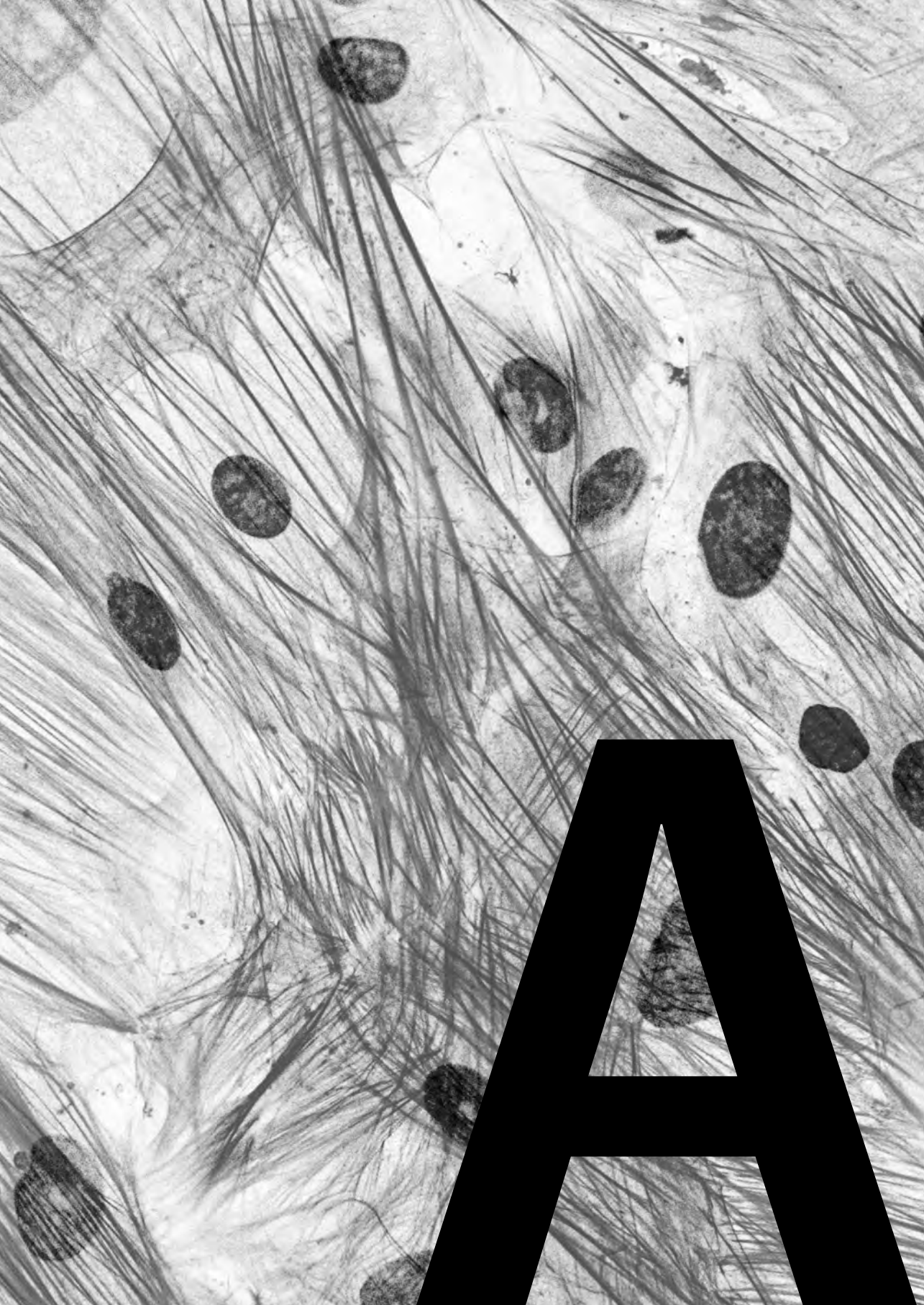
- 1 Forsdahl, S. H., Singh, K., Solberg, S. & Jacobsen, B. K. Risk factors for abdominal aortic aneurysms. *Circulation* 119, 2202-2208 (2009).
- 2 Thompson, R. W., Liao, S. & Curci, J. A. Vascular smooth muscle cell apoptosis in abdominal aortic aneurysms. *Coronary artery disease* 8, 623-631 (1997).
- 3 Ailawadi, G. et al. Smooth muscle phenotypic modulation is an early event in aortic aneurysms. *The Journal of thoracic and cardiovascular surgery* 138, 1392-1399 (2009).
- 4 Guo, D.-C. et al. Mutations in smooth muscle α -actin (ACTA2) lead to thoracic aortic aneurysms and dissections. *Nature Genetics* 39, 1488, doi:10.1038/ng.2007.6 (2007).
- 5 Milewicz, D. M. et al. Genetic basis of thoracic aortic aneurysms and dissections: focus on smooth muscle cell contractile dysfunction. *Annu. Rev. Genomics Hum. Genet.* 9, 283-302 (2008).
- 6 Milewicz, D. M. et al. Altered Smooth Muscle Cell Force Generation as a Driver of Thoracic Aortic Aneurysms and Dissections. *Arterioscler Thromb Vasc Biol* 37, 26-34, doi:10.1161/ATVBAHA.116.303229 (2017).
- 7 Takeda, N. et al. A deleterious MYH11 mutation causing familial thoracic aortic dissection. *Human Genome Variation* 2, 15028, doi:10.1038/hgv.2015.28 (2015).
- 8 Dietz, H. C. & Pyeritz, R. E. Mutations in the human gene for fibrillin-1 (FBN1) in the Marfan syndrome and related disorders. *Human Molecular Genetics* 4, 1799-1809, doi:10.1093/hmg/4.suppl_1.1799 (1995).
- 9 van de Laar, I. M. B. H. et al. Mutations in SMAD3 cause a syndromic form of aortic aneurysms and dissections with early-onset osteoarthritis. *Nature Genetics* 43, 121-126, doi:10.1038/ng.744 (2011).
- 10 Tran-Fadulu, V. et al. Analysis of multigenerational families with thoracic aortic aneurysms and dissections due to TGFB1 or TGFB2 mutations. *Journal of Medical Genetics* 46, 607, doi:10.1136/jmg.2008.062844 (2009).
- 11 Rønnev-Jessen, L. & Petersen, O. W. Induction of alpha-smooth muscle actin by transforming growth factor-beta 1 in quiescent human breast gland fibroblasts. Implications for myofibroblast generation in breast neoplasia. *Laboratory investigation; a journal of technical methods and pathology* 68, 696-707 (1993).
- 12 Guo, D., Tan, F. K., Cantu, A., Plon, S. E. & Milewicz, D. M. FBN1 exon 2 splicing error in a patient with Marfan syndrome. *American journal of medical genetics* 101, 130-134 (2001).
- 13 Kuivaniemi, H. et al. Identical G+ 1 to A mutations in three different introns of the type III procollagen gene (COL3A1) produce different patterns of RNA splicing in three variants of Ehlers-Danlos syndrome. IV. An explanation for exon skipping some mutations and not others. *Journal of Biological Chemistry* 265, 12067-12074 (1990).
- 14 Guo, D.-C. et al. Mutations in smooth muscle α -actin (ACTA2) lead to thoracic aortic aneurysms and dissections. *Nature Genetics* 39, 1488-1493, doi:10.1038/ng.2007.6 (2007).
- 15 Rockey, D. C., Weymouth, N. & Shi, Z. Smooth muscle α actin (Acta2) and myofibroblast function during hepatic wound healing. *PLoS One* 8, e77166 (2013).
- 16 Gao, F. et al. Disruption of TGF- β signaling in smooth muscle cell prevents flow-induced vascular remodeling. *Biochemical and Biophysical Research Communications* 454, 245-250, (2014).
- 17 den Hartog, A. W. et al. The effect of losartan therapy on ventricular function in Marfan patients with haploinsufficient or dominant negative FBN1 mutations. *Netherlands Heart Journal* 24, 675-681, doi:10.1007/s12471-016-0905-8 (2016).

- 18 Ruiz-Ortega, M., Rodríguez-Vita, J., Sanchez-Lopez, E., Carvajal, G. & Egido, J. TGF- β signaling in vascular fibrosis. *Cardiovascular Research* 74, 196-206, doi:10.1016/j.cardiores.2007.02.008 (2007).
- 19 Milewicz, D. M. et al. Genetic basis of thoracic aortic aneurysms and dissections: focus on smooth muscle cell contractile dysfunction. *Annu Rev Genomics Hum Genet* 9, 283-302, doi:10.1146/annurev.genom.8.080706.092303 (2008).
- 20 Chen, J., Li, H., SundarRaj, N. & Wang, J. H. Alpha-smooth muscle actin expression enhances cell traction force. *Cell Motil Cytoskeleton* 64, 248-257, doi:10.1002/cm.20178 (2007).
- 21 Peyton, S. R. & Putnam, A. J. Extracellular matrix rigidity governs smooth muscle cell motility in a biphasic fashion. *J Cell Physiol* 204, 198-209, doi:10.1002/jcp.20274 (2005).
- 22 Williams, D. A., Fogarty, K. E., Tsien, R. Y. & Fay, F. S. Calcium gradients in single smooth muscle cells revealed by the digital imaging microscope using Fura-2. *Nature* 318, 558, doi:10.1038/318558a0 (1985).
- 23 Wu, D. et al. NLRP3 (Nucleotide Oligomerization Domain-Like Receptor Family, Pyrin Domain Containing 3)-Caspase-1 Inflammasome Degrades Contractile Proteins: Implications for Aortic Biomechanical Dysfunction and Aneurysm and Dissection Formation. *Arterioscler Thromb Vasc Biol* 37, 694-706, doi:10.1161/ATVBAHA.116.307648 (2017).
- 24 Hurst, V., Goldberg, P. L., Minnear, F. L., Heimark, R. L. & Vincent, P. A. Rearrangement of adherens junctions by transforming growth factor- β 1: role of contraction. *American Journal of Physiology-Lung Cellular and Molecular Physiology* 276, L582-L595, doi:10.1152/ajplung.1999.276.4.L582 (1999).
- 25 Szulcek, R., Bogaard, H. J. & van Nieuw Amerongen, G. P. Electric cell-substrate impedance sensing for the quantification of endothelial proliferation, barrier function, and motility. *J Vis Exp*, doi:10.3791/51300 (2014).
- 26 Hu, N. et al. Comparison between ECIS and LAPS for establishing a cardiomyocyte-based biosensor. *Sensors and Actuators B: Chemical* 185, 238-244, (2013).
- 27 Peters, M. F., Lamore, S. D., Guo, L., Scott, C. W. & Kolaja, K. L. Human Stem Cell-Derived Cardiomyocytes in Cellular Impedance Assays: Bringing Cardiotoxicity Screening to the Front Line. *Cardiovascular Toxicology* 15, 127-139, doi:10.1007/s12012-014-9268-9 (2015).
- 28 Zhang, S. Insulin-Stimulated Cyclic Guanosine Monophosphate Inhibits Vascular Smooth Muscle Cell Migration by Inhibiting Ca/Calmodulin-Dependent Protein Kinase II. *Circulation* 107, 1539-1544, doi:10.1161/01.cir.0000056766.45109.c1 (2003).
- 29 Halterman, J. A., Kwon, H. M., Zargham, R., Bortz, P. D. & Wamhoff, B. R. Nuclear factor of activated T cells 5 regulates vascular smooth muscle cell phenotypic modulation. *Arterioscler Thromb Vasc Biol* 31, 2287-2296, doi:10.1161/ATVBAHA.111.232165 (2011).
- 30 Bass, H. M., Beard, R. S., Jr., Cha, B. J., Yuan, S. Y. & Nelson, P. R. Thrombomodulin Induces a Quiescent Phenotype and Inhibits Migration in Vascular Smooth Muscle Cells In Vitro. *Ann Vasc Surg* 30, 149-156, doi:10.1016/j.avsg.2015.10.002 (2016).
- 31 van der Loop, F. T. L., Gabbiani, G., Kohnen, G., Ramaekers, F. C. S. & van Eys, G. J. J. M. Differentiation of Smooth Muscle Cells in Human Blood Vessels as Defined by Smoothelin, a Novel Marker for the Contractile Phenotype. *Arteriosclerosis, Thrombosis, and Vascular Biology* 17, 665-671, doi:10.1161/01.atv.17.4.665 (1997).
- 32 Chung, A. W. et al. Loss of elastic fiber integrity and reduction of vascular smooth muscle contraction resulting from the upregulated activities of matrix metalloproteinase-2 and -9 in the thoracic aortic aneurysm in Marfan syndrome. *Circ Res* 101, 512-522, doi:10.1161/CIRCRESAHA.107.157776 (2007).
- 33 Chung Ada, W. Y. et al. Loss of Elastic Fiber Integrity and Reduction of Vascular Smooth Muscle Contraction Resulting From the Upregulated Activities of Matrix

- Metalloproteinase-2 and -9 in the Thoracic Aortic Aneurysm in Marfan Syndrome. *Circulation Research* 101, 512-522, doi:10.1161/CIRCRESAHA.107.157776 (2007).
- 34 Chew, D. K. W., Conte, M. S. & Khalil, R. A. Matrix metalloproteinase-specific inhibition of Ca²⁺ entry mechanisms of vascular contraction. *Journal of Vascular Surgery* 40, 1001-1010, (2004).
- 35 Chen, E., Larson, J. D. & Ekker, S. C. Functional analysis of zebrafish microfibril-associated glycoprotein-1 (Magp1) in vivo reveals roles for microfibrils in vascular development and function. *Blood* 107, 4364-4374 (2006).
- 36 Clifford, R. L., Singer, C. A. & John, A. E. Epigenetics and miRNA emerge as key regulators of smooth muscle cell phenotype and function. *Pulmonary Pharmacology & Therapeutics* 26, 75-85, (2013).
- 37 Villeneuve, L. M. et al. Epigenetic histone H3 lysine 9 methylation in metabolic memory and inflammatory phenotype of vascular smooth muscle cells in diabetes. *Proceedings of the National Academy of Sciences* 105, 9047, doi:10.1073/pnas.0803623105 (2008).
- 38 Brady Anthony, R., Thompson Simon, G., Fowkes, F. G. R., Greenhalgh Roger, M. & Powell Janet, T. Abdominal Aortic Aneurysm Expansion. *Circulation* 110, 16-21, doi:10.1161/01.CIR.0000133279.07468.9F (2004).
- 39 Sakalihasan, N., Limet, R. & Defawe, O. D. Abdominal aortic aneurysm. *The Lancet* 365, 1577-1589, doi:10.1016/s0140-6736(05)66459-8 (2005).
- 40 Nordon, I. M., Hinchliffe, R. J., Loftus, I. M. & Thompson, M. M. Pathophysiology and epidemiology of abdominal aortic aneurysms. *Nature Reviews Cardiology* 8, 92, doi:10.1038/nrcardio.2010.180 (2010).
- 41 Vardulaki, K. A. et al. Quantifying the risks of hypertension, age, sex and smoking in patients with abdominal aortic aneurysm. *BJS* 87, 195-200, doi:10.1046/j.1365-2168.2000.01353.x (2000).
- 42 White, G. H., Yu, W., May, J., Chaufour, X. & Stephen, M. S. Endoleak as a Complication of Endoluminal Grafting of Abdominal Aortic Aneurysms: Classification, Incidence, Diagnosis, and Management. *Journal of Endovascular Therapy* 4, 152-168, doi:10.1177/152660289700400207 (1997).
- 43 Chuter, T. A. M. et al. Endoleak after endovascular repair of abdominal aortic aneurysm. *Journal of Vascular Surgery* 34, 98-105, doi:10.1067/mva.2001.111487 (2001).
- 44 Major, A. et al. Implant Degradation and Poor Healing after Endovascular Repair of Abdominal Aortic Aneurysms: An Analysis of Explanted Stent-Grafts. *Journal of Endovascular Therapy* 13, 457-467, doi:10.1583/06-1812MR.1 (2006).
- 45 Cheng, J., Zhou, X., Jiang, X. & Sun, T. Deletion of ACTA2 in mice promotes angiotensin II induced pathogenesis of thoracic aortic aneurysms and dissections. *Journal of thoracic disease* 10, 4733-4740, doi:10.21037/jtd.2018.07.75 (2018).
- 46 Habashi, J. P. et al. Losartan, an AT1 Antagonist, Prevents Aortic Aneurysm in a Mouse Model of Marfan Syndrome. *Science* 312, 117, doi:10.1126/science.1124287 (2006).
- 47 Silence, J., Lupu, F., Collen, D. & Lijnen, H. R. Persistence of atherosclerotic plaque but reduced aneurysm formation in mice with stromelysin-1 (MMP-3) gene inactivation. *Arteriosclerosis, thrombosis, and vascular biology* 21, 1440-1445 (2001).
- 48 Seye, C. I. et al. 7-Ketocholesterol induces reversible cytochrome c release in smooth muscle cells in absence of mitochondrial swelling. *Cardiovasc Res* 64, 144-153, doi:10.1016/j.cardiores.2004.05.016 (2004).
- 49 Middleton, R. K. et al. The pro-inflammatory and chemotactic cytokine microenvironment of the abdominal aortic aneurysm wall: a protein array study. *Journal of vascular surgery* 45, 574-580 (2007).
- 50 Tsuruda, T. et al. Adventitial mast cells contribute to pathogenesis in the progression of abdominal aortic aneurysm. *Circulation research* 102, 1368-1377 (2008).

- 51 Shimizu, K., Mitchell Richard, N. & Libby, P. Inflammation and Cellular Immune Responses in Abdominal Aortic Aneurysms. *Arteriosclerosis, Thrombosis, and Vascular Biology* 26, 987-994, doi:10.1161/01.ATV.0000214999.12921.4f (2006).
- 52 Lin, F. & Yang, X. TGF- β signaling in aortic aneurysm: another round of controversy. *Journal of Genetics and Genomics* 37, 583-591 (2010).
- 53 Chen, X., Lu, H., Rateri, D. L., Cassis, L. A. & Daugherty, A. Conundrum of angiotensin II and TGF- β interactions in aortic aneurysms. *Current opinion in pharmacology* 13, 180-185 (2013).
- 54 Seong, G. J. et al. TGF- β -induced interleukin-6 participates in transdifferentiation of human Tenon's fibroblasts to myofibroblasts. *Molecular vision* 15, 2123 (2009).
- 55 Kurpinski, K. et al. Transforming growth factor- β and notch signaling mediate stem cell differentiation into smooth muscle cells. *Stem cells* 28, 734-742 (2010).
- 56 Humphrey, J. D., Schwartz, M. A., Tellides, G. & Milewicz, D. M. Role of mechanotransduction in vascular biology: focus on thoracic aortic aneurysms and dissections. *Circulation research* 116, 1448-1461, doi:10.1161/CIRCRESAHA.114.304936 (2015).
- 57 In Jeong, S. et al. Tissue-engineered vascular grafts composed of marine collagen and PLGA fibers using pulsatile perfusion bioreactors. *Biomaterials* 28, 1115-1122, (2007).
- 58 Iwai, S. et al. Biodegradable polymer with collagen microsphere serves as a new bioengineered cardiovascular prosthesis. *The Journal of Thoracic and Cardiovascular Surgery* 128, 472-479, (2004).
- 59 Sun, J., Deng, H., Zhou, Z., Xiong, X. & Gao, L. Endothelium as a Potential Target for Treatment of Abdominal Aortic Aneurysm. *Oxid Med Cell Longev* 2018, 6306542-6306542, doi:10.1155/2018/6306542 (2018).
- 60 Franck, G. et al. Reestablishment of the Endothelial Lining by Endothelial Cell Therapy Stabilizes Experimental Abdominal Aortic Aneurysms. *Circulation* 127, 1877-1887, doi:10.1161/CIRCULATIONAHA.113.001677 (2013).
- 61 Moreno-Flores, S., Benitez, R., Vivanco, M. d. & Toca-Herrera, J. L. Stress relaxation and creep on living cells with the atomic force microscope: a means to calculate elastic moduli and viscosities of cell components. *Nanotechnology* 21, 445101, doi:10.1088/0957-4484/21/44/445101 (2010).
- 62 Ghazanfari, S., Driessen-Mol, A., Hoerstrup, S. P., Baaijens, F. P. T. & Bouten, C. V. C. Collagen matrix remodeling in stented pulmonary arteries after transapical heart valve replacement. *Cells Tissues Organs* 201, 159-169 (2016).
- 63 Dartsch, P. C., Hämmerle, H. & Betz, E. Orientation of Cultured Arterial Smooth Muscle Cells Growing on Cyclically Stretched Substrates. *Cells Tissues Organs* 125, 108-113, doi:10.1159/000146146 (1986).
- 64 Kanda, K. & Matsuda, T. Mechanical Stress-Induced Orientation and Ultrastructural Change of Smooth Muscle Cells Cultured in Three-Dimensional Collagen Lattices. *Cell Transplantation* 3, 481-492, doi:10.1177/096368979400300605 (1994).
- 65 Dartsch, P. C. & Hämmerle, H. Orientation response of arterial smooth muscle cells to mechanical stimulation. *Eur J Cell Biol* 41, 339-346 (1986).
- 66 Ghazanfari, S. et al. Analysis of alterations in morphologic characteristics of mesenchymal stem cells by mechanical stimulation during differentiation into smooth muscle cells. (2010).
- 67 Jia, L.-X. et al. Mechanical stretch-induced endoplasmic reticulum stress, apoptosis and inflammation contribute to thoracic aortic aneurysm and dissection. *The Journal of Pathology* 236, 373-383, doi:10.1002/path.4534 (2015).
- 68 Milewicz Dianna, M. et al. Fibrillin-1 (FBN1) Mutations in Patients With Thoracic Aortic Aneurysms. *Circulation* 94, 2708-2711, doi:10.1161/01.CIR.94.11.2708 (1996).
- 69 Hynes, R. O. The Extracellular Matrix: Not Just Pretty Fibrils. *Science* 326, 1216, doi:10.1126/science.1176009 (2009).

- 70 Fedak, P. W. M. et al. Vascular matrix remodeling in patients with bicuspid aortic valve malformations: implications for aortic dilatation. *The Journal of Thoracic and Cardiovascular Surgery* 126, 797-805, (2003).
- 71 Annambhotla, S. et al. Recent Advances in Molecular Mechanisms of Abdominal Aortic Aneurysm Formation. *World Journal of Surgery* 32, 976-986, doi:10.1007/s00268-007-9456-x (2008).
- 72 Vorp, D. A., Raghavan, M. L. & Webster, M. W. Mechanical wall stress in abdominal aortic aneurysm: Influence of diameter and asymmetry. *Journal of Vascular Surgery* 27, 632-639, (1998).
- 73 Crunkhorn, S. Improving cardiomyocyte contractility. *Nature Reviews Drug Discovery* 17, 546-546, doi:10.1038/nrd.2018.117 (2018).



APPENDICES

English summary
Dutch summary
List of publications
Acknowledgements

ENGLISH SUMMARY

Aortic aneurysms (AA) are pathological dilations of the aorta. They usually occur in the abdomen (Abdominal Aortic Aneurysm: AAA) and have a prevalence of 2-8% in men (>60 years) and 2% in women. As the disease progresses, aneurysms tend to grow and even rupture. In most cases, AA patients have no symptoms, so many of them are unaware that they have an aneurysm. Ruptured aneurysms are associated with a mortality rate of up to 80%, due to severe bleeding complications and sudden rupture. AA are currently treated by open or endovascular surgery. However, both carry certain risks; open aortic surgery is a major, complex procedure with risk of complications, and endovascular surgery has a significant risk for reintervention. Ideally, a pharmaceutical therapy would be available as a non-invasive alternative to surgery. However, no such therapy is currently available because we do not understand the molecular causes of the disease. If we understood which cells, proteins and genes are involved, we could design medication to target these specific molecules and processes.

The aorta consists out of three layers, the outer layer (tunica adventitia, consisting mostly out of collagen fibers and fibroblasts), the middle layer (tunica media, consisting mostly out of smooth muscle cells and elastin fibers) and the inner layer (tunica intima, consisting out of a single layer of endothelial cells). Smooth muscle cells are the predominant cell type in the aorta. Their role is to maintain the structure of the aortic wall with their contractile properties, and produce the matrix that surrounds them. It has been shown that smooth muscle cells play a role in aneurysm formation. Loss of smooth muscle cell contractile proteins and smooth muscle cell programmed cell death have been shown to happen early on during aneurysm development, indicating that smooth muscle cell dysfunction plays a role in aneurysm formation.

The aim of this thesis is to investigate the role of smooth muscle cell dysfunction in aneurysm formation, and identify key smooth muscle cell specific processes, genes and proteins that are involved. For this purpose, we developed new models and methods to study aortic aneurysms and smooth muscle cell dysfunction *in vitro*, and gain valuable insights which can later be translated for the benefit of the patients. The research topics we worked on are divided into three major sections: I. is focused on the genetic defects in smooth muscle cell specific genes which are involved in aneurysm formation, and a new method we invented and applied to study these defects. II. is focused on a new method for measuring smooth muscle cell contraction *in vitro* and the new conclusions we made using that method. III. is focused on novel 3D models we developed to study AA in the lab. Using these models, we were able to recreate a piece of the aorta, giving us valuable information about the structure and processes that occur.

I. Genetic mutations affecting smooth muscle cell function leading to aortic aneurysm formation

Mutations in smooth muscle cell specific genes lead to aneurysm formation. These genes encode for proteins, which are in the case of mutations either missing or malformed, meaning that they cannot perform their normal function. Since they cannot perform their function, the balance in the aortic wall is shifted, making it more unstable and prone to dilation. To study these proteins, we need access to smooth muscle cells, which we can only get through surgery, or by making them from stem cells, which takes a very long time and it is very expensive.

For this reason, we developed a method to directly convert fibroblasts, cells obtained from a skin biopsy into smooth muscle like cells in 14 days in **Chapter 2**. Skin biopsies are taken from patients with an aneurysm and transformed into smooth muscle cells, imitating the original smooth muscle cells in the aorta of the same patient. We used a scaffold which contains collagen and elastin, imitating the fibers in the aortic wall and a protein which stimulates smooth muscle cell development in the body. The fibroblasts from the skin started expressing smooth muscle cell genes and proteins which are normally not present in skin. We can now use this method to discover defects in the smooth muscle cell proteins, which we wouldn't be able to predict in skin cells. This is especially useful for patients who have a genetic mutation, but have not yet developed an aneurysm. We can use this method to predict what the effect on the mutation will have on their proteins, and consequentially on the aortic wall and aneurysm formation process. Using the cells, we converted with our new method, we further developed techniques to look at the functions of these cell and if these functions are changed as a consequence of the mutations. We can check how much smooth muscle like cells contract or migrate, allowing us to better understand the effects of these mutations (**Chapter 3**). In **Chapter 4** we further investigated aneurysm related signaling, particularly TGF β signaling. TGF β is a protein which controls vital processes regarding smooth muscle cell function by binding to receptor complexes at the smooth muscle cell membrane. We identified that TGF β receptor type 3 also plays a role in aneurysm related signaling, and not only types 1 and 2, as it was previously believed.

II. Impaired smooth muscle cell contraction in patients with abdominal aortic aneurysms

It was previously published by multiple authors that smooth muscle cell contraction is important for maintaining the structure of the aortic wall, and that its loss contributes to aortic aneurysm formation. One of the foundations for this claim is that mutations in genes which make proteins of the contractile machinery lead to aneurysm formation (Chapter 2). However, loss of smooth muscle cell contraction in

AA patients was never measured in these smooth muscle cells *in vitro*. One of the reasons is the lack of suitable method for screening larger numbers of patient cells, which is needed to identify patterns in disturbed contraction. To uncover this, we worked on building a biobank of control and patient smooth muscle cells which were isolated from aortic biopsies during surgery. Patient biopsies were taken during open aneurysm repair and control biopsies were taken from non-dilated aortas of post-mortem kidney donors. In **Chapter 5** we developed a new method to measure contraction of live smooth muscle cells from healthy controls and aneurysm patients after stimulation. Using this new method, we could get a quantitative numeric output and detect which patient cells have weaker contraction compared to healthy control smooth muscle cells. We investigated cells of patients with no genetic mutation, meaning that this is the first time that it is experimentally proven that smooth muscle cells of sporadic aneurysm patients have contractile dysfunction. In addition, we showed that these are mostly patients who currently smoke and who had complications after their endovascular repair and had to have a second surgery. This also indicates a link between certain complications or risk factors for AA and decreased contraction, which can help further investigation into the molecular mechanism.

III. 3D *in vitro* models of the aneurysmal wall: interaction between different cell types and extracellular matrix in aneurysm pathology

The aorta is a complex system consisting of three layers and multiple cell types and a network of fibers between them. During aneurysm development, the structure of the aortic wall is disintegrating, due to smooth muscle cell death and elastin and collagen fiber degradation. It is difficult to study these complex intertwined processes if we only observe one isolated cell type, or a sample which is fixated in formaldehyde since it paints only a part of the picture. To better understand the live, dynamic processes that occur in the aortic wall during aneurysm formation, we developed two new models to study the 3D structure of the aortic wall and how it is disturbed in aneurysms (**Chapter 6**). First, we managed to cut a section of the aortic biopsy obtained during surgery using a special cutting mechanism, with a vibrating blade, which ensures that the section contains all three layers with preserved living cells inside. We can then keep this tissue alive in the lab for up to 62 days. It also contains immune cells which infiltrated the aortic wall during the inflammation in the aneurysm tissue. Using this new model, we can compare preserved tissue pieces of healthy individuals and aneurysm patients, and study all the involved components. We can in this way compare sections of a healthy aortic wall to an aneurysmal, and study what happens with all the components in a live aortic section. We can also use these pieces to stimulate different signaling processes and see how the live aneurysmal wall reacts, or test pharmacological compounds as part of the search for medication of aortic aneurysms.

In **Chapter 7** we took a different approach and designed a new model as a reconstruction of the 3D structure of the aorta. Smooth muscle cells produce the matrix fibers which surround them in the aorta, for example elastin fibers. We used a 3D printed material that is suitable for cells and added smooth muscle cells from healthy controls and aneurysm patients, making a patient-specific model for each cell line. We observed these cells for multiple weeks, as they grew and made their own matrix fibers. In this way, we could recreate a small piece of the aorta. On top of it, we added endothelial cells, which are located on top of the smooth muscle cells in the aorta, on the very inside of the blood vessel. This part of our model imitates the communication between these two cell types. The patient-specific cell carries the individual hallmarks of aneurysm pathology, so we are able to measure these differences in the 3D model we created and use it to better understand why aneurysms occur.

The models and methods we developed for this thesis can be further used to uncover the pathological mechanisms of smooth muscle cell dysfunction in aortic aneurysm formation. The method of converting skin fibroblasts into smooth muscle-like cells can be used to predict defects in patients with a mutation in smooth muscle cell specific genes before they undergo surgery. The contraction method can be used to expand on the findings regarding the link about contraction and smoking, and examine if other known risk factors influence smooth muscle cell contraction. The 3D models can be used to gain better understanding about the crosstalk between different components of the aneurysm wall, and how it contributes to aneurysm formation. We anticipate that the legacy of our work will lead towards better understanding of why aortas dilate and subsequent development of new, improved future therapeutic prospects.

NEDERLANDSE SAMENVATTING

Een aorta-aneurysma (AA) is een pathologische verwijding van de aorta. In westerse landen komt deze aandoening voornamelijk voor in de buik (abdominaal aorta-aneurysma: AAA), met een prevalentie van 2-8% bij mannen >60 jaar en 2% bij vrouwen. Tijdens het verloop van de ziekte kunnen aneurysma's groeien en uiteindelijk zelfs scheuren. De meeste AA-patiënten hebben geen symptomen, waardoor ze niet weten dat ze een aneurysma hebben. Het plotseling scheuren van aneurysma's kan leiden tot ernstige inwendige bloedingen, en dit wordt geassocieerd met een sterftcijfer van 80%. Momenteel worden AA's behandeld door middel van open of endovasculaire chirurgische ingrepen. Beide behandelingen brengen bepaalde risico's met zich mee; een open aorta operatie is een complexe procedure met risico op complicaties, en een endovasculaire operatie heeft een aanzienlijk risico op her-interventie. Als alternatief voor deze invasieve chirurgische ingrepen zou behandeling met een farmaceutische therapie een goede optie zijn. Op dit moment is er echter nog geen medicatie beschikbaar, omdat er nog weinig bekend is over het onderliggende moleculaire mechanisme van het ontstaan en verloop van AA. Meer inzicht in welke cellen, eiwitten en genen betrokken zijn bij het verloop van deze ziekte zou bij kunnen dragen aan de ontwikkeling van medicatie.

De aorta bestaat uit drie lagen, de buitenste laag (tunica adventitia, bestaande uit voornamelijk collageenvezels en fibroblasten), de middelste laag (tunica media, bestaande uit voornamelijk gladde spiercellen en elastinevezels) en de binnenste laag (tunica intima, bestaande uit een enkele laag endotheelcellen). Gladde spiercellen zijn het meeste voorkomende celtype in de aorta. Deze cellen zijn belangrijk voor het behoud van de structuur van de aortawand met contractiele eigenschappen, en voor de productie van de omringende matrix. Het is al eerder aangetoond dat gladde spiercellen een belangrijke rol spelen bij de vorming van aneurysma's. Tijdens de vroege ontwikkeling van aneurysma's is te zien dat gladde spiercellen contractiele eiwitten verliezen en dat er geprogrammeerde celdood optreedt in deze cellen. Deze processen laten zien dat dysfunctie van gladde spiercellen kan bijdragen aan de vorming van aneurysma's.

Dit proefschrift heeft als doel om de rol van gladde spierceldysfunctie op de vorming van aneurysma's te onderzoeken, en om de belangrijkste gladde spiercel-specifieke processen, genen en eiwitten die hierbij zijn betrokken te identificeren. We hebben nieuwe modellen en methoden ontwikkeld om aorta-aneurysma's en gladde spierceldysfunctie *in vitro* te kunnen bestuderen. De nieuwe inzichten die verkregen kunnen worden door het toepassen van deze nieuw methoden kunnen bijdragen aan de behandeling van AA patiënten. De onderzoeksthema's die beschreven worden in dit proefschrift zijn onderverdeeld in drie secties: I. is gericht op de genetische defecten in specifieke genen voor gladde spiercellen die betrokken zijn bij de

vorming van aneurysma's, en op een nieuwe methode die we hebben ontwikkeld en toegepast om deze defecten te bestuderen. II. is gericht op een nieuwe methode om contractie van gladde spiercellen *in vitro* te meten en de nieuwe bevindingen die met deze methode gevonden zijn. III. is gericht op nieuwe 3D-modellen die we hebben ontwikkeld om AA in het laboratorium te bestuderen. Het nabootsen van een stuk van de aorta met deze 3D-modellen, heeft waardevolle informatie gegeven over de structuur en processen die plaatsvinden in dit weefsel.

I. Genetische mutaties die de functie van gladde spiercellen beïnvloeden, wat leidt tot aorta-aneurysma vorming

Mutaties in specifieke genen, die coderen voor gladde spiercel specifieke eiwitten, leiden tot aneurysma vorming. Mutaties in deze genen kunnen zorgen voor het compleet ontbreken of misvorming van deze eiwitten, die daardoor hun normale functie niet kunnen uitoefenen. Een tekort aan functionele eiwitten in de aortawand zorgt ervoor de balans wordt verschoven, waardoor de aorta onstabiel en vatbaarder wordt voor verwijding. Om deze eiwitten te bestuderen zijn gladde spiercellen nodig, die verkregen kunnen worden van de patiënt tijdens een operatie, of door ze te maken van stamcellen, wat een lang en kostbaar proces is.

Om deze redenen hebben we in **Hoofdstuk 2** een methode ontwikkeld om fibroblasten, die verkregen zijn uit huidbiopten, in 14 dagen direct om te zetten in gladde spierachtige cellen. Huidbiopten werden afgenomen bij aneurysma patiënten en omgezet in gladde spierachtige cellen, om hiermee originele gladde spiercellen van de aorta van dezelfde patiënt na te bootsen. Hiervoor werd gebruikt gemaakt van een scaffold met collageen en elastine, als imitatie van de vezels in de aortawand, en een eiwit dat de vorming van gladde spiercellen in het lichaam stimuleert. Genen en eiwitten van gladde spiercellen kwamen tot expressie in deze fibroblasten afgenomen van de huid, terwijl deze genen en eiwitten normaal niet voorkomen in fibroblasten. Het gebruik van deze methode kan er voor zorgen dat we defecten in eiwitten van gladde spiercellen kunnen ontdekken, die we niet zouden kunnen vinden in normale huidcellen. Dit kan worden toegepast bij patiënten met een genetische mutatie, die nog geen aneurysma ontwikkeld hebben. We kunnen hiermee voorspellen wat het effect van de mutatie zal zijn op de eiwitten, en vervolgens op de aortawand en aneurysma ontwikkeling bij deze patiënten.

Met behulp van de cellen die zijn omgezet naar gladde spierachtige cellen, hebben we ook technieken ontwikkeld om functionele eigenschappen van deze cellen en veranderingen hierin als gevolg van mutaties te meten. We kunnen controleren in welke mate gladde spierachtige cellen samentrekken of migreren, waardoor we de effecten van mutaties beter kunnen begrijpen (**Hoofdstuk 3**). In **Hoofdstuk 4** hebben we vervolgens onderzoek gedaan naar aneurysma-gerelateerde signalering, voornamelijk gericht op TGFβ signalering. TGFβ is een eiwit dat betrokken is bij het reguleren van vitale gladde spiercel functies, door zich te binden

aan receptorcomplexen op het gladde spiercelmembraan. We hebben ontdekt dat TGF β -receptor type 3 ook een rol speelt bij aneurysma-gerelateerde signalering, in plaats van alleen type 1 en 2, zoals eerder werd aangenomen.

II. Verminderde contractie van gladde spiercellen bij patiënten met abdominale aorta-aneurysma's

Meerdere auteurs hebben eerder gepubliceerd dat contractie van gladde spiercellen belangrijk is voor het behoud van de structuur van de aortawand en dat het verlies hiervan bijdraagt aan de vorming van aorta-aneurysma. Deze bewering is voornamelijk gebaseerd op de bevinding dat mutaties in genen coderend voor contractiele eiwitten leiden tot aneurysma-vorming (**Hoofdstuk 2**). Het verlies van contractie van gladde spiercellen bij AA-patiënten werd *in vitro* echter nooit gemeten. Een van de redenen hiervan is het ontbreken van een geschikte screeningsmethode waarmee grote aantallen patiënten cellen, die nodig zijn om verstoorde contractie te identificeren, onderzocht kunnen worden. Daarom hebben we een biobank opgezet van gladde spiercellen van gezonde controles en aneurysma patiënten. Gladde spiercellen werden geïsoleerd uit aortabiopten, die zijn verkregen tijdens operaties. Patiëntbiopten werden afgenomen tijdens open aneurysma operaties en controle biopten werden afgenomen van niet-verwijde aorta's van postmortale nierdonoren. In **Hoofdstuk 5** hebben we een nieuwe methode ontwikkeld om de contractie van levende gladde spiercellen van gezonde controles en aneurysmapatiënten na stimulatie te meten. Met deze nieuwe methode kregen we een kwantitatieve numerieke output en konden we detecteren welke patiëntencellen een zwakkere contractie hadden in vergelijking met gezonde controle gladde spiercellen. We hebben hierbij cellen van patiënten zonder genetische mutatie onderzocht, wat betekent dat dit de eerste keer was dat experimenteel werd bewezen dat gladde spiercellen van patiënten met sporadisch aneurysma verminderde contractie hebben. Daarnaast lieten we zien dat verminderde gladde spiercel contractie vooral voorkomt in patiënten die momenteel roken en die complicaties hadden na hun endovasculaire operatie, waardoor ze een tweede operatie moesten ondergaan. Deze resultaten tonen aan dat er een verband is tussen verminderde gladde spiercel contractie en bepaalde complicaties of risicofactoren voor AA, wat kan bijdragen aan verder onderzoek naar het moleculaire mechanisme.

III. 3D *in vitro* modellen van de aneurysmale aortawand: interactie tussen verschillende celtypes en extracellulaire matrix in aneurysma pathologie

De aorta is een complex systeem dat bestaat uit drie lagen met meerdere celtypes, omringd met een netwerk van vezels. Tijdens de ontwikkeling van een aneurysma wordt de structuur van de aortawand afgebroken door de dood van gladde spiercellen en de afbraak van elastine en collageenvezels. Dit complexe ziektebeeld, waarin meerdere processen tegelijkertijd plaatsvinden, is moeilijk te bestuderen. Het

onderzoeken van slechts één geïsoleerd celtype, of gefixeerd weefsel in formaldehyde, geeft maar een klein deel weer van het complete proces. Om de levende, dynamische processen die optreden in de aortawand tijdens aneurysmavorming beter te begrijpen, hebben we twee nieuwe modellen ontwikkeld. Hiermee kunnen we de 3D-structuur van de aortawand bestuderen en bekijken hoe deze structuur wordt verstoord in aneurysma's (**Hoofdstuk 6**). We hebben een techniek ontwikkeld om een deel van een aortabiopt, dat verkregen is tijdens een operatie, te snijden op een speciale manier met een vibrerend mes. Hierdoor ontstond een stuk weefsel, bestaande uit alle drie de lagen van de aortawand met daarin geconserveerde levende cellen, wat vervolgens maximaal 62 dagen in leven gehouden kon worden in het laboratorium. In dit stuk weefsel waren ook immuuncellen aanwezig, die tijdens de ontsteking van het aneurysma in de aortawand zijn gefiltreerd. Met behulp van dit nieuwe model kunnen we levend weefsel van gezonde individuen en aneurysma-patiënten vergelijken, en verschillende processen die betrokken zijn in AA vorming bestuderen. Daarnaast kunnen deze stukjes weefsel gebruikt worden om de reactie van de levende aneurysmale wand na stimulatie van specifieke signaalprocessen te bestuderen, of om medicatie voor aorta-aneurysma's te testen.

In **Hoofdstuk 7** hebben we een andere benadering gekozen om een nieuw model te ontwerpen waarin de 3D-structuur van de aorta werd gereconstrueerd. Gladde spiercellen produceren matrixvezels, zoals elastinevezels, waardoor ze omringt worden. Patiënt specifieke modellen werden gemaakt door meerdere gladde spiercellijnen van gezonde controles en aneurysma-patiënten te kweken op een 3D-geprint materiaal. We observeerden deze cellen gedurende meerdere weken, waarin ze groeiden en hun eigen matrixvezels produceerden. Op deze manier konden we een klein stukje van de aorta nabootsen. Daarnaast hebben we ook endotheelcellen toegevoegd aan de binnenkant van het bloedvat, bovenop de gladde spiercellen, waardoor de communicatie tussen deze twee celtypes werd geïmiteerd. Het gebruik van patiënt specifieke cellen draagt bij aan de individuele kenmerken van de aneurysma-pathologie, die we door middel van dit 3D-model kunnen meten en gebruiken om aneurysma vorming beter te begrijpen.

De modellen en methoden die we voor dit proefschrift hebben ontwikkeld, kunnen bijdragen aan meer inzicht in de pathologische mechanismen waarop gladde spiercel dysfunctie zorgt voor de vorming van aorta-aneurysma. De methode waarin huidfibroblasten worden omgezet in gladde spierachtige cellen kan worden gebruikt om defecten te voorspellen bij patiënten met een mutatie in specifieke genen voor gladde spiercellen, al voordat ze een operatie ondergaan. De methode om gladde spiercel contractie te meten laat zien dat verminderde contractie is gelinkt aan roken. Dit onderzoek kan worden uitgebreid door te kijken naar de invloed van andere bekende risicofactoren voor AA op de contractie van gladde spiercellen. De 3D-modellen kunnen worden gebruikt om meer kennis te krijgen over de communicatie

tussen verschillende celtypes en componenten van de aneurysmawand en de rol hiervan op de vorming van aneurysma's. We verwachten dat dit proefschrift zal bijdragen aan meer kennis over aorta aneurysma's en dat dit kan leiden tot de ontwikkeling van nieuwe, verbeterde therapeutische behandelingen.

LIST OF PUBLICATIONS

Impaired smooth muscle cell contractility as a novel concept of abdominal aortic aneurysm pathophysiology.

Bogunovic, N., Meekel, J. P., Micha, D., Blankensteijn, J. D., Hordijk, P. L. & Yeung, K. K. (2019). *Scientific reports*, 9(1), 1-14.

Pathogenic effect of a TGFB1 mutation in a family with Loeys–Dietz syndrome.

Cozijnsen, L., Plomp, A. S., Post, J. G., Pals, G., **Bogunovic, N.**, Yeung, K. K., Niessen, H.W.M., Gouman, M.J.T.J., Barge-Schaapveld, D.Q.C.M & Micha, D. (2019). *Molecular Genetics & Genomic Medicine*, 7(10), e00943.

Betaglycan (TGFB3) up-regulation correlates with increased TGF- β signaling in Marfan patient fibroblasts in vitro.

Bogunovic, N.*, Groeneveld, M.E.*, Musters, R. J. P., Tangelder, G. J., Pals, G., Wisselink, W., Micha, D. & Yeung, K. K. (2018). *Cardiovascular Pathology*, 32, 44-49

**authors contributed equally.*

An in vitro method to keep human aortic tissue sections functionally and structurally intact.

Meekel, J. P., Groeneveld, M. E., **Bogunovic, N.**, Keekstra, N., Musters, R. J., Zandieh-Doulabi, B., Pals, G., Micha, D., Niessen, H.W.M., Wiersema, A.M., Kievit, J.K., Hoksbergen, A.W.J., Wisselink, W., Blankensteijn, J.D. & Yeung, K. K. (2018). *Scientific reports*, 8(1), 1-12.

Transdifferentiation of human dermal fibroblasts to smooth muscle-like cells to study the effect of MYH11 and ACTA2 mutations in aortic aneurysms.

Yeung, K. K., **Bogunovic, N.**, Keekstra, N., Beunders, A. A., Pals, J., van der Kuij, K., Overwater, E., Wisselink, W., Blankensteijn, J.D., van Hinsbergh, V.W.M., Musters, R. J.P., Pals, G., Micha, D. & Zandieh-Doulabi, B. (2017). *Human mutation*, 38(4), 439-450.

Mutations in PIH1D3 cause X-linked primary ciliary dyskinesia with outer and inner dynein arm defects.

Paff, T., Loges, N. T., Aprea, I., Wu, K., Bakey, Z., Haarman, E. G., Daniels, J.M.A., Sijstermans, E. **Bogunovic, N.**, Dougherty, H.W., Höben, I. M., Grosse-Onnebrink, J., Matter, A., Olbrich, H., Werner, C., Pals, G., Schmidts, M., Omran, H. & Micha, D. (2017). *The American Journal of Human Genetics*, 100(1), 160-168.

The effects of acute administration of losartan, angiotensin II type-1 receptor antagonist, on hemodynamics and oxidative stress parameters in malignant hypertensive rats.

Bogunovic, N., Miloradović, Z., Jovović, Đ., Mihailović-Stanojević, N., Ivanov, M., Vajić, U. J., Karanović, D. & Grujić-Milanović, J. (2015). *Veterinarski glasnik*, 69(5-6), 323-335.

Submitted manuscripts:

Bioengineered Patient-Specific 3D Vascular Scaffolds for the Investigation of Smooth Muscle Cell and Extracellular Matrix Dysfunction in Aortic Aneurysms.

Bogunovic, N., Meekel, J.P., Majolee, J., Hekhuis, M., Pyszkowski, J., Jockenhövel, S., Kruse, M., Riesebo, E., Micha, D., Blankensteijn, J.D., Hordijk, P.L., Ghazanfari, S. & Yeung, K. K. (2020).

Inflammatory Activity of Human Perivascular Adipose Tissue in Abdominal Aortic Aneurysms.

Meekel, J. P.* , Dias-Neto, M.*, **Bogunovic, N.**, Hoozemans, J.B., Conceição, G., Mendes, C., Eringa, E.C., Balm, R., Blankensteijn, J.D. & Yeung K.K. (2020).

*authors contributed equally.

Manuscripts in preparation:

The role of vascular smooth muscle cells in the development and progression of aortic aneurysms and aortic dissections.

Rombouts, K., van Merrienboer, T., **Bogunovic, N.**, van der Velden, J., Yeung, K.K.

Molecular phenotyping and functional assessment of smooth muscle like-cells with pathogenic variants in aneurysm genes ACTA2, MYH11, SMAD3 and FBN1.

Bogunovic, N.*, Burger, J.*, Liu, H., van Vliet, N., IJpma A., Maugeri, A., Micha, D., ten Hagen, T.L.M., Majoer-Krakauer, D., van der Pluijm, I., Essers, J., Yeung, K.K.

*authors contributed equally.

ACKNOWLEDGEMENTS

My PhD time was an incredible adventure! I moved from Serbia to my dream city, Amsterdam, to start an important research project that would forever change the way we perceive aortic aneurysms. A couple of years later, Amsterdam stayed my dream city, and I hope I managed to leave at least a small, but permanent mark in the world of aneurysm research. Little did I know that my PhD would make me a part of three departments, working with four supervisors, countless wonderful colleagues, many sleepless nights at the OR or at the lab and not fewer sleepless nights on many exciting conference trips! I am truly grateful for all of you for making my journey colorful, exciting and meaningful. I surely made both friendships and memories for life.

First of all, **Kakkhee**, thank you for bringing me here! We had a very exciting journey together these five years in our joint vision and passion about smooth muscle cells. Just look how far we have come! Thank you for giving me this opportunity to kick start my scientific career and inspiring me to always strive for more. On a non-scientific note, thank you for always listening to me and being there for me in hard times. No other supervisor would be cool enough to party around the world, watch Netflix together at 5am or wait up for me when I got lost on a night out.

Dear **prof. Hordijk, Peter**: I couldn't have done it without you! Thank you for supporting me, guiding me and teaching me from the very start. You showed me all the basics and gave me the foundation to develop my own ideas, and I wouldn't be the scientist I am today without you. Thank you for always listening to me in tough times. Also, very important, thank you for always putting up with me being stubborn and letting me try my way, before I most of the time, still admitted you were right.

Dear **prof. Blankensteijn, Jan**: Thank you for our chocolate meetings! They did not only inspire me to question everything and everyone in my research, but also to always look at the bigger picture and ask myself (and others) good challenging questions. Thank you for your life and scientific advice, although I think I in the end always focused on the wrong one. Thank you for being a great mentor and taking the time to have great philosophical conversations with me that always left me inspired!

Thank you, **Dimitra**, for teaching me the magic of cells and molecular biology! Thank you for all your support throughout the years in life and science. Also, thank you for inspiring me to want to have my own group, and fight to develop it in the competitive world of academia. I admire your passion and conviction for research! I will always fondly remember the time we had with Ferdy and building everything up.

I would like to thank my **reading committee**: prof. Reinier Boon, prof. Ron Balm, prof. Dianna Milewicz, prof. Clark Zeebregts, dr. Vivian de Waard and dr. Caroline Cheng for taking the time and effort to review my thesis.

To the amazing colleagues of the **Department of Surgery** of both the VUmc and AMC: thank you for accepting a lab person among your medical midst. I am so proud and impressed by all of you and the effort and conviction you put into doing research and never keeping your eyes off the prize-all of you one day walking in the blue scrubs and saving lives! To start with the VUmc: **Jorn**, thank you for all the dynamic and exciting years we worked side by side, and for always taking the effort to push me to do and be better. I had amazing fun with you all these years and I definitely became a more persistent researcher! **Ted**, thank you for all the nice times at conferences as for improving my Dutch, a skill not to be overlooked. **Harm and Menno**-guys, thank you for paving the path for all of us, and motivating us by giving us such big shoes to fill. Thank you for showing us how to do our PhDs, but also, how to enjoy life to the max in the meantime. To **Orkun, Stefan and Sabrina**-I'm super proud of you guys finding your way as the third generation of our research group. Thank you for all the fun times and keep up the great work! To **Tijs, Jacqueline and Jan**-thank you for at least temporarily being in our group and making the experience memorable! Thank you **Marina** for all our nice times together!

To **prof. Wisselink**-thank you for all of your input and help, you are the gold standard for us all! To **Hoks, Maarten, Hillian, Vincent, other Vincent** -thank you for all of your help and kindness! Thank you for always thinking of me for tissue, and even more thank you for leaving it at the receptionist in the small hours of the night. ☺ To **prof. Bonjer**-thank you for all your help and support! To **Ron**-thank you for being such a life saver many times! You always managed to help me in time for each of my complicated situation, which I enormously appreciate!

And to the AMCCers: Thank you **Hamid, Sylvana, Reza, Nick, Victoria and Anna** for complementing our VUmc group. I enjoyed working with you in Amsterdam, but also the very memorable times of "working" in Liege and London. We conquered the world together. ☺ To **Vivian**, thank you for always suggesting fun new research ideas and inspiring me by your never-ending curiosity about SMC and research. To **prof. Balm**- thank you for your input and always witty remarks, it was a pleasure working with you!

Thank you smooth muscle cell squad (I can already hear the song), **Albert, Karlijn and Tara**! Working with our precious cells became so much more gezellig with you there, and all of our laughing in the lab, from the Nein Man, to all the dances we invented and you will hopefully recreate upon reading this book (yes pressure). To **Albert**-thank you for being such a kind and caring person, and always making sure everyone has a smile on their face! That is a truly rare trait and you are a gem of the

lab and the department. To **Karlijn and Tara**, I cannot wait to see you develop your projects and write a booklet similar to this-I am already upfront proud of you. **Karlijn**, I am already amazed by your skill and research mind. I'm looking forward to seeing you take this project to places and directions I never thought of. **Tara**, you are truly one of a kind! I have no doubt that you will achieve your surgical, research or whichever other goals with that level of passion and enthusiasm!

To previous and current members of the Hordijk group: **Jan**, thank you for all of your help from the very beginning! To **Manon, Joanna, Eric and Mark**-it was great to overlap a bit with you guys, thank you for all the nice times! To **Igor** – for making a Dutch lab gezellig with Balkan fun, and always having an emergency rakija at hand. **Vanessa**, thank you for all the nice time, I wish you the best of luck at the AMC and with wrapping up your project! **Fabienne**, it was a pleasure having our PhDs overlap a bit. I already look forward to the weekly quesadillas in the future. To all the wonderful people of the **Physiology Department**, thank you for being such a delight to work with both at the old days at the MF, as well as in the location with the best view in Amsterdam, O2. I am grateful to be part of such a nice mix of interesting people, who can at the same time provide expertise on unknown proteins or rare cell culture techniques, and go for fun drinks after work, or have crazy adventures on TPO. To the great crowd of the 10th floor: **Phat, Veerle, Laura, Reinier, Ed, Pieter, Xue, Rio, Diewertje**-I enjoyed running into you and chatting next to the coffee machine about everything and nothing. Thank you **Jeroen, Sylvia and Rene** for introducing me to the world of wave lengths, photons and other little understandable things that lead to beautiful cell pictures. Thank you **Jolanda and Isabelle** for all of your help and support during my PhD and development into postdoc, it is all much appreciated! Thank you, Aimee and Jessica, for helping that everything always goes so smooth.

Jisca and Liza, thank you for being such great friends! I enjoyed immensely that we did our PhDs together side by side and that we could share the good and the bad, the fun and the frustrating, the swimming and the dancing, the parties and the babies and to make so many important memories in and out of the lab. I'm looking forward to share our personal and professional milestones for many years in the future! **Finn and Richard**, thank you for being great friends and for all the nice moments and meals we had. Same story, hope that many more will come in the coming years. ☺

To the department of **Clinical Genetics**: Thank you **Ferdy** for all the great times we had as officemates, and for introducing me to the wonderful world of Pathé! Thank you, Gerard, for your support, for the Christmas dinners and summer BBQs, and for all the stories of women in trains. ;) Thank you, **Alessandra**, for all your help! Thank you, **Behrouz**, for your support! Thank you **Samaneh** for our great collaboration! Thank you **Lauria** for all the great times and laughs, and for always being there for me when I saw a new series and movie I really needed to discuss, but the non-

visionary people haven't seen it yet. I would like to especially thank the many, many **interns of the Department of Clinical Genetics** who I had the pleasure of working with during these five years: thank you for all the fun times in the lab and nice lunches we shared! To my former students, **Zuzana, Marije, Leah, Fatimah and Lotte**: thank you for contributing to the work in this thesis, couldn't have done it without you! To **Ian and Sejla**: hvala balkanske zene na svim lepim vremenima uz Cecu, nasu majku! I wish you both a lot of success in developing your careers! **Tosca** I am so proud to see you develop in every way and persistently going after your goals. Thank you for being such a good friend and keep up the good work, you are awesome! Thank you **Lisanne** for all the nice times and being such a lovely new addition to the group! Thank you, **Nathalie**, for your witty comments, insightful questions and your friendly support, as well as the coffee and lunch meetings. Thank you **Huib and Chen** for all your help and for being such a nice addition to our group. I would also like to thank all of the colleagues from **Diagnostics** for always being so friendly and helpful, and for all the nice borrels you organized throughout the years!

Thank you, Joyce, for our collaboration and our very nice long phone calls. We made a great team to not let the project do us. To **Jeroen, Ingrid and Danielle**-thank you for your input and pleasant meetings.

Elise, thank you first of all for collecting me as a friend to start it all, that is in itself a rare achievement. ;) We had such an incredible time being desk neighbors for a few years while our friendship grew, peaking over each other's shoulders to comment on all things work and life related. Thank you for being a great friend, supporting me, making me laugh, and explaining the simple things about humanity that I somehow missed. **Antonio and Gerardo**, muchas gracias for being such awesome friends. In case of a zombie apocalypse, we meet at the cheese shop. **Josje**, thank you for being such a great friend, during our collegial time and after. Thank you for the analytical talks, unconditional support and crazy parties. You always bring a smile on my face!

Lana, as we recently recapped, it's wonderful how we were a stožer from the very beginning. Thank you for introducing me to our beloved Amsterdam and all the exciting parties and festivals which I enjoyed enormously, even though I always left early. I have limitless appreciation for our friendship and our never-ending voice messages, as well as the useful and useless topics we daily debate on. Thank you for being there with me throughout my entire scientific adventure and in what's to come. To **Renato, Karina, Pieter, Bastien and Karlien**: thank you for being such an awesome friend group and kind people! I think it's super special how we came from different sides of the world and with different personalities, and always had so much fun, support and joy with each other, even with my shocking lack of understanding of music! Thank you for your friendship that made my PhD time and

life in Amsterdam much more fun! To the chicas, thank you for the psychoanalysis, self-care homework, Balkan music and headstand tutorials.

Hvala **Jelici, Zoranu, Milanu, Neveni Uni i Danijeli** na prvom poglavlju mog naucnog putovanja I podrsci. Jako sam uzivala u radu sa vama, i vreme koje sam provela kod vas je definitivno bio jak podsticaj da nastavim svoju naucnu karijeru.

Hvala mojim divnim drugaricama na svoj podrsci poslednjih deceniju i po, a pogotovo tokom ovog perioda. Prosto je neverovatno da je proslo vec 15ak godina, i koliko smo se sve promenile I napredovale za ovo vreme, a opet nekako ostale iste. ☺ Iako smo razdvojene, neke stvari se nikad ne menjaju, i jako cenim nasa prijateljstva. **Jovana, Irena, Dragana, Tijana, Anja i Ana**, hvala na svemu! Hvala **Dunja i Stanko** hvala na uvek dobroj hrani I jos boljem druzenju! Hvala **Miko** sto si uvek tako gotivan ortak, and **Jacob**, for teaching me how to play the game of life. **Taca, Joona and Rein**, thank you for inviting me to Hel in the winter to see the supreme moose, which obviously strengthened my character enough to be able to complete a PhD.

Hvala **Mama, Milena and Jan** for a lifelong support and belief in me that got me where I am now. To my **grandparents Drago and Marija**, thank you for helping shape the person I am today. Big thank you to my African/Canadian family branch, **Goran, Violeta, Marko and Luka**: thank you for your long-distance support! Thank you van Muilekom family (I promise to one day switch to Dutch. That day just always seems to be not this day. ☺) To **Rob, Lizbeth, Doret, Ludo, Erik, Mijke, Manoek, Erik, Henk, onsJo, Maud, Milou, Pieter, Maarten and Philip**-thank you for adopting me and giving me a family so far from my Serbian home! Thank you, **Amoy and Dolf**, for taking me in and always being so great to me.

Leon, I know you showed up a bit late in the making of this book, but I'm looking forward to writing the next chapters of my life with you. Thank you for always pushing me to achieve my goals and being who I truly am.

Natalija Bogunović was born on February 23rd, 1991 in Belgrade, Serbia. She received her Bachelor's degree in Biology from the University of Belgrade in 2013. Since she developed an interest in translational research, she continued her studies in the Master's program Experimental Physiology in 2013 at the University of Belgrade. Her interest in cardiovascular diseases spiked during her Master thesis research which she performed at the Institute for Medical Research in Belgrade, where she worked on malignant hypertension. Afterward, she decided to move abroad and continue to pursue her passion for research in cardiovascular diseases by starting her PhD at the VUmc in Amsterdam, as a collaboration between the departments of Vascular Surgery, Physiology, and Clinical Genetics. Natalija's PhD research was focused on the role of smooth muscle cells in the pathophysiology of aortic aneurysms and the results of that research are presented in this thesis. She is currently working as a postdoc at the Amsterdam UMC, location VUmc and continuing her research into the pathophysiology of aortic aneurysms with a focus on transcriptional regulation.



Amsterdam Cardiovascular Sciences



 Amsterdam UMC
University Medical Center

